Basin analysis of the Katangan Basin of Zambia: subsidence mechanisms, dynamic stratigraphy, and mineral systems



Martin Purkiss
Linacre College
University of Oxford

A thesis submitted for the degree of
Doctor of Philosophy
Trinity 2023

Contents

1 Introduction **6**

2 Background **10**

2.1 Tectonic evolution 10

2.1.1 Cratonic basement and pre-Katangan deformation 10

2.1.2 Neoproterozoic extension and basin formation 13

2.1.3 Basin inversion 16

2.2 Stratigraphy 19

2.2.1 Lower Roan Group 21

2.2.2 Upper Roan Group 23

2.2.3 Mwashia Group 24

2.2.4 Nguba Group 24

2.2.5 Kundelungu Group 25

2.2.6 Comparison to stratigraphy in the D.R.C. 25

2.2.7 Breccias 27

2.3 Glaciation 28

2.4 Mafic magmatism 30

2.5 Basin forming mechanisms 32

2.6 Mineralisation history 33

3 Application of facies analysis in the Zambian Copperbelt and its stratigraphic implications for the Katangan basin **37**

3.1 Introduction 37

3.2 Methodology . . . 39
3.3 Facies scheme . . . 41
3.4 Facies associations . . . 49
3.4.1 Proximal alluvial fan facies association . . . 49
3.4.2 Distal alluvial fan facies association . . . 50
3.4.3 Fluvial facies association . . . 51
3.4.4 Glaciofluvial facies association . . . 52
3.4.5 Fan-delta facies association . . . 54
3.4.6 Delta plain facies association . . . 55
3.4.7 Delta slope facies association . . . 56
3.4.8 Prodelta facies association . . . 58
3.4.9 Intertidal facies association . . . 59
3.4.10 Sabkha facies association . . . 61
3.4.11 Microbial facies association . . . 62
3.4.12 Foreshore - shoreface facies association . . . 64
3.4.13 Carbonate ramp facies association . . . 66
3.4.14 Glaciomarine facies association . . . 68
3.4.15 Transition zone facies association . . . 70
3.4.16 Deep water facies association . . . 71
3.4.17 Subaqueous slope facies association . . . 72
3.5 Type examples of facies successions . . . 74
3.6 Stratigraphic evolution . . . 79
3.7 Discussion . . . 88
3.8 Conclusions . . . 90

4 Sequence stratigraphic correlations for the Katangan basin of Zambia, and their uncertainties and implications 91

4.1 Introduction . . . 91
4.2 Methodology . . . 94
4.3 Results . . . 98

4.3.1 Solwezi 98
4.3.2 Lubambe/Konkola North 100
4.3.3 Chambishi 104
4.3.4 Mufulira 107
4.3.5 Ndola 112
4.3.6 Mansa 115
4.3.7 Chilonga 118
4.3.8 Sequence stratigraphic correlation 1: synchronous terrestrial rifting across the Kafue anticline 120
4.3.9 Sequence stratigraphic correlation 2: diachronous terrestrial rifting across the Kafue anticline 128
4.4 Discussion 134
4.4.1 Sequence hierarchies 134
4.4.2 Comparison to previous sequence stratigraphic interpretations 134
4.4.3 Diachronous rifting 136
4.4.4 The 'ore shale' 137
4.4.5 Neoproterozoic glaciations as time lines 138
4.5 Conclusions 140

5 Quantifying the subsidence history of the Katangan basin and its Tonian rift episodes 142

5.1 Introduction 142
5.2 Methodology 144
5.2.1 Type logs 144
5.2.2 Decompaction 144
5.2.3 Backstripping 145
5.2.4 Palaeobathymetry 148
5.2.5 Eustasy 148
5.2.6 Ages 150

5.2.7 Uniform extension model 151
5.3 Results 154
5.3.1 1D burial history 154
5.3.2 Backstripping and rift signatures 157
5.4 Discussion 163
5.5 Conclusion 166

6 The mineralisation factor:
remarks on quantifying mineralisation potential in sediment-hosted Cu systems 168
6.1 Introduction 168
6.2 Methodology 169
6.3 Results 173
6.4 Discussion 174
6.5 Conclusions 175

7 Discussion 177
7.1 A dynamic stratigraphic perspective of the Katangan basin 177
7.1.1 Lower Roan Group 177
7.1.2 Upper Roan Group 180
7.1.3 Mwashia Group 182
7.1.4 Nguba 185
7.2 Kundelungu 187
7.3 Mineralisation in a dynamic stratigraphic context 190

8 Conclusions 201

9 Appendix I – facies descriptions 205

Bibliography 282

List of Figures

1.1 Generalised map of the Katangan basin, showing its position between the Congo, Bangweulu, and Kalahari cratons, and the Irumide belt. Major settlements are marked, as well as the three main Cu-deposit hosting regions (Zambian Copperbelt, Domes Region, Congolese Copperbelt) highlighted. The Congo craton marks the northwest margin of the basin, the Bangweulu craton its northeast margin, and the Mwembeshi shear zone its southern margin. The basin's SE margin is not formally defined, and inferred here. 7

2.1 Map of major cratons, belts, and structures adjoining the Katangan basin; map and abbreviations from Xu et al. (2022): BB, Bangweulu Block; CFB, Cape Fold Belt; CKB, Choma-Kalomo Block; DB, Damara Belt; GB, Garip Belt; GCB, Ghanzi-Chobe Belt; IB, Irumide Belt; KB, Kaoko Belt; KbB, Kibaran Belt; KhB, Kheis Belt; LB, Lufilian Belt; LmB, Limpopo Belt; MozB, Mozambique Belt; NaqB, Namaqua Belt; NB, Natal Belt; Ri, Richtersveld Terrane; UB, Ubendian Belt; UsB, Usagaran Belt; WCB, West Congo Belt; ZB, Zambezi Belt; ZC, Zimbabwe Craton; I-External Fold and Thrust Belt; II-Domes Region; III-Synclinorial Belt; IV-Kantanga High; V-Foreland Basin. 11

2.2 Map of South-West Gondwana, showing major cratons, fold belts and arcs, as well as approximate dates for extensional and compressional regimes in each belt; map and abbreviations from Frimmel et al. (2011): CDPT Cuchilla Dionsio-Pelotas Terrane, CFT Cabo Frí Terrane, CT Coastal Terrane, CUT Curitiba Terrane, LAT Luis Alves Terrane, MT Marmora Terrane, SM/OT Serra do Mar-Oriental Terrane, PSZ Purros Shear Zone, SBSZ Sierra Ballena Shear Zone, CSZ Colenso Shear Zone. . . 14

2.3 Simplified map of major structures and displacements in southern Africa, showing the Mwembeshi Shear Zone separating the Lufilian Arc in the North from the Zambezi Belt to the South (Daly et al., 1984). 17
2.4 Conceptual evolution of the Lufilian Arc - Zambezi Belt orogen, from initial extension post-∼880 Ma to postulated ocean crust development, and subsequent compression and uplift (John et al., 2004). 18
2.5 Locations of drill cores used in this thesis, and supplementary data from literature across the basin. Note the paucity of data in the central and SW part of the basin, covered by Kalahari sand. Locations are generalised, as some previous studies refer to areas without specifying exact localities. Exact locations, where provided, are found in the following: Lwawu Mission (Key et al., 2001); Mwinilunga, Lufunfu, Makonga, Kibambale, Mansa (Master and Wendorff, 2011); Chambeshi sub-basin (Bull et al., 2011); Fishtie (Hendrickson et al., 2015); Kamoa (Kennedy et al., 2019); Tenke-Fungurume (Mambwe et al., 2020). 19
2.6 Table from Selley et al. (2005) summarising several mine-specific lithostratigraphic schemes, and comparing them to a lithostratigraphy of the D.R.C. 20
2.7 Lithostratigraphic log showing a generalised stratigraphy of the Zambian Copperbelt (Selley et al., 2005). 21
2.8 Lithostratigraphic correlation of units across the western Zambian Copperbelt along the 'ore shale' unit and its equivalents (Binda and Mulgrew, 1974). 22
2.9 Lithostratigraphic correlation of units across the Zambian and Congolese (formerly Shaba Province, Zaire) Copperbelts (Cailteux et al., 1994). 26
2.10 The most recent and complete lithostratigraphic classification to-date for the D.R.C. from (Cailteux and De Putter, 2019). 27
2.11 Mafic samples from the Domes region plotted on a Zr/Y versus Zr/Nb tectonic discrimination diagram, showing clear geochemical similarities to modern early rift and proto-oceanic rift settings in Africa (Kampunzu et al., 2000). 31

2.12 An idealised model of the sediment-hosted Cu-deposits, showing fluid circulation through red bed clastics as the Cu-source, evaporites providing a seal and source for saline brines, and faults that provide a fluid pathway towards reductants and Cu-pricipitation sites (Hitzman et al., 2010). 34

2.13 Stratigraphic distribution of mineralised horizons in the Zambian Copperbelt (vertical scale approximate), showing mineralisation existing predominantly in the Copperbelt Orebody Member, but also occurring much higher in the stratigraphy (Selley et al., 2005). 35

3.1 Geological map of the Zambian Copperbelt, showing core distribution. Collar codes and locations: KRX082 (Solwezi), KN192 (Lubambe, Konkola sub-basin), RCB2 (Chambishi sub-basin), L83 (Mufulira), IT26 (Ndola), KADD04 (Lusale), ZMSDD003 (Mansa), and CHLDD001 (Chilonga). 39

3.2 Type log for the alluvial fan facies associations, showing a 120 m logged section of the RCB2 core. Conglomerate and sand facies form a broad fining-up succession, transitioning from proximal to distal alluvial fan facies associations. Blue arrows indicate fining trends and sediment sources becoming more distal. 50

3.3 25 m long type log for the fluvial facies association, showing a section of the KRX082 core in Solwezi. Stratified conglomerate facies punctuate sandy facies that fine upwards and are punctuated by thin mud units. 52

3.4 6 m long log for the glaciofluvial facies association in the ZMSDD003 core. Fluvial conglomerate and sand facies with internal erosion surfaces are sharply overlain by a clast-poor diamictite, interpreted as glacial, forming a deepening succession. Blue arrows represent deepening-upwards, and red arrows shallowing-up trends. 53

3.5 30 m long type log for the fan-delta facies association in the KN192 core in which proximal fan or talus slope conglomerates shallow up from, and are bounded at their top by, wackes deposited by subaqueous sediment gravity flows. 55

3.6 8 m long log of the delta plain facies association in the KN192 core, showing clean structured sandstones interbedded with muddy siltstones. They are separated by sandy mudstones which are interpreted to form part of the delta slope facies association, supporting a broadly deltaic interpretation. 56

3.7 15 m long type log for the delta slope facies association, showing a section of the KN192 core. Sandy mudstones with an abundance of primary structures predominate, punctuated by conglomerate and lenses of coarse sand units that stack aggradationally. 58

3.8 Type log for the prodelta facies association in the KN192 core, comprising repeated fining-up sandstone beds interspersed with laminated silts and mudstones. Facies show an overall progradational trend over the whole section. 59

3.9 20 m long type log of the intertidal facies association in the KN192 core. Heterolithic and carbonate-bearing heterolithic facies predominate, generally aggrading or prograding, separated by emergent surfaces showing dissolution textures (Rk facies). 61

3.10 12 m long type log of the sabkha facies association, showing a section of the L83 core. Facies variation is high, comprising predominantly dolomitic carbonate units, often containing abundant primary and secondary anhydrite, punctuated by carbonate-bearing sandstone units with sharp or erosive bases. The succession aggrades on a scale of 10's m. 62

3.11 12 m long type log of the microbial facies association, showing a section of the KN192 core in which domal and curved vertical and sub-vertical laminated structures are observable. 63

3.12 The AnCa facies in the L83 core, characteristic of the sabkha facies association. Nodular anhydrite and enterolithic structures (circled red) embedded in grey silty dolomite are abundant. Arrows indicate way-up for the three cores, the bottom of the core is lower left. 64

3.13 The StMic facies in the IT26 core, showing microbially induced sedimentary structures that characterise the facies (circled red), which are interpreted as domal and columnar stromatolites. Arrows indicate way-up for the three cores, the bottom of the core is lower left. 64
3.14 18 m long type log for the shoreface facies association, showing a section of the IT26 core. Well-sorted and cross-stratified sandstones gently deepen into carbonate-bearing sandstone units. Planar and ripple lamination is abundant, with the lower parts of the facies association showing well-developed trough cross-beds. 65
3.15 20 m long type log for the carbonate ramp facies association in the IT26 core, showing laminated carbonates, sometimes with enigmatic serrated textures and thin interstitial mudstones and siltstones, shallow upwards into coarse sandy carbonate facies. 67
3.16 Clast counts for the crDia sub-facies in the ZMSDD003 core, measured at 0.5 m intervals, showing higher clast proportion and tendency for upwards clast quantity reduction. 68
3.17 Clast counts for the cpDia sub-facies in the ZMSDD003 core, measured at 0.5 m intervals, showing significantly lower clast counts ($<$ 10 clasts / 0.5 m). 68
3.18 24 m long type log for the glaciomarine facies association, showing a section of the ZMSDD003 core. Clast-poor diamictite facies, interpreted to be of glacial origin, are sharply overlain by planar laminated carbonates, followed by laminated silty carbonates. 69
3.19 10 m long type log for the transition zone facies association in the CHLDD001 core. Laminated mudstones and siltstones with thin intercalated sandy beds show abundant lamination, and soft-sediment deformation, forming part of an overall aggradational facies package. 70
3.20 25 m long type log for the deep water facies association, showing a section of the ZMSDD003 core. Laminated carbonate-bearing mudstone facies are overlain by planar-laminated dark mudstones. A possible cm-scale slump structure occurs at the base of the dark mudstone succession. 71

3.21 55 m long type log for the subaqueous slope facies association in the L83 core. Clast-rich diamictite facies sharply overlie silty mudstones, forming a deepening succession, which shallows up into carbonate-bearing mudstone and laminated carbonate facies. 72
3.22 120 m long succession of fan-delta and delta slope to intertidal facies associations in core KN192. Note upwards thinning and fining of conglomerate units, and subsequent thickening of carbonate units, as the succession switches from overall retrogradational to overall progradational. 75
3.23 100 m long deep carbonate ramp to slope facies association succession in core KN192. Note possible stromatolitic textures just underneath the carbonate diamictite, possibly representing a source for the carbonate clasts in the overlying diamictite. 77
3.24 40 m long succession of deep water to glaciofluvial and glaciomarine facies associations in core ZMSDD003, initially shallowing up, then deepening. Note the erosional contact at the base of the glaciofluvial facies association. 78
3.25 Facies occurrence counts (i.e. number of separate countable facies units) in the Lower Roan Group showing clear preponderance of clastic facies. Carbonate-bearing facies represent the transition towards the Upper Roan Group. 81
3.26 A schematic block diagram showing conceptual succession and distribution of gross depositional environments the Zambian Copperbelt during the syn-rift stage of basin evolution. Terrestrial deposition predominates, with prevalent facies associations marked. The block diagram does not represent a specific location, but is an amalgamation of depositional system trends observed throughout the Zambian Copperbelt stratigraphy. 81
3.27 Facies counts in the Upper Roan Group showing a clear reversal of facies trends compared to the Lower Roan, with clastic facies being almost absent and carbonate facies predominating. 83
3.28 A schematic block diagram of the Zambian Copperbelt during Upper Roan Group times, showing a more connected basin with abundant carbonate facies as part of an epicontinental sea. 83

3.29 Facies counts in the Mwashia Group. Fine-grained facies with some carbonate content predominate, as do microbial facies. Diamictites are also introduced (towards the top of the Mwashia in core KN192). 84

3.30 A schematic block diagram of the Zambian Copperbelt during renewed rifting in Mwashia times. Deep carbonate ramps predominated, with biotically mediated carbonates at the basin's margins. The basin began to widen and deepen, with renewed extension resulting in emplacement of mafic suites. 85

3.31 Facies counts in the Nguba Group showing an abundance of diamictites representing the Grand Conglomerat, and a preponderance of finer facies with carbonates. Note the paucity of microbial facies. 86

3.32 A schematic block diagram of the basin during Nguba times showing laterally extensive diamictites, both debris flow and glacially derived, representing the Grand Conglomerat, and a preponderance of finer facies as the basin remained deep following Mwashia rifting. 87

3.33 Facies counts in the Kundelungu. Note that the facies distribution changes as a result of the ZMSDD003 core being situated on the basin edge, introducing coarser clastic facies (XSst, CCgm). In the deeper portions of the basin, finer clastic and mixed clastic-carbonate facies predominate. 88

4.1 A comparison of different nomenclature, timings, and definitions used for different depositional sequence models from Catuneanu et al. (2009). LST: lowstand systems tract; TST: transgressive systems tract; HST: highstand systems tract; FSST: falling-stage systems tract; RST: regressive systems tract; TR: transgressive–regressive; CC: correlative conformity; MFS: maximum flooding surface; MRS: maximum regressive surface. A detailed exposition of the various models can be found in Catuneanu et al. (2009). 93

4.2 Map showing the line of section across cores logged across the Domes region, classical Copperbelt, and eastern part of the Katangan basin: KRX082 (Solwezi), KN192 (Lubambe), RCB2 (Chambishi), L83 (Mufulira), IT26 (Ndola), ZMSDD003 (Mansa), CHLDD001 (Chilonga). Dashed red lines represent inferred normal faults. 95

4.3 A stratigraphic log of the lower half of the KRX082 core in Solwezi underneath the metamorphic thrust sheet, showing a thick transgressive systems tract (TST), with a MFS1 interpreted at the top of the succession. MOD1, 2 refers to interpretations for sequence stratigraphic correlations 1 and 2; which in this core are identical. Asterisks denote confidence in the stratigraphic surface. 99

4.4 A stratigraphic log of the KN192 core in Lubambe showing a section through the siliciclastic Lower Roan, and more carbonate-dominated Upper Roan, Mwashia, and Nguba Groups. MOD1, 2 refers to interpretations for sequence stratigraphic correlations 1 and 2; which in this core are identical. 101

4.5 Log and core photographs of the Lower to Upper Roan transition section of core KN192 in Lubambe. The interpreted unconformity or correlative conformity (SB2) separates the delta slope facies below with the predominantly intertidal facies above. The core photograph shows this section with red emergent surface sharply juxtaposed with deeper water facies below (red line shows the SB2 surface). Cores young from bottom right to top left, with depths marked on the core. 103

4.6 A stratigraphic log of the RCB2 core in Chambishi, showing Lower and Upper Roan sections forming a type example of Zambian Copperbelt stratigraphy. MOD1, 2 refers to interpretations for sequence stratigraphic correlations 1 and 2; which in this core are identical. 105

4.7 A stratigraphic log of the L83 core in Mufulira, showing Upper Roan, Mwashia, Nguba, and Kundelungu Groups. MOD1, 2 refers to sequence stratigraphic correlations 1 and 2. Note that the brecciated interval and overlying karst facies shown in figure 4.8 allow for two viable sequence stratigraphic arrangements. 108

4.8 Log and core photographs of the surfaces assumed in correlation 2 to be unconformities or correlative conformities in core L83. They show the brecciated section, comprising highly altered carbonates and mafic suites, sharply leading into a thin oxidised Rk facies unit, an unoxidised dolomite unit, and a thicker oxidised Rk facies unit. Cores young from bottom right to top left. 111

4.9 A stratigraphic log of the IT26 core in Ndola. MOD1, 2 refers to sequence stratigraphic correlations 1 and 2. Depending on the interpretation of key surfaces, the core shows the complete Katangan stratigraphy (Lower Roan to Kundelungu Groups), or only half of it (Mwashia, Nguba, Kundelungu Groups). 113

4.10 A stratigraphic log of the ZMSDD003 core near Mansa, showing the Kundelungu Group overlying the Nguba Group which unconformably lies on basement. Note the high-confidence erosional SB4 truncating mudstones of the underlying Nguba HST. MOD1, 2 refers to interpretations for sequence stratigraphic correlations 1 and 2; which in this core are identical. 115

4.11 Log and core photographs of the base-Kundelungu unconformity in the ZMSDD003 core. The interpreted unconformity surface is marked by a red line. Coarse fluvial or glaciofluvial facies erode into shelf mudstones and are overlain by diamictite facies (cpDia). Cores young from bottom right to top left. 117

4.12 A stratigraphic log of the interpreted Mwashia and Nguba Groups in the CHLDD001 core near Chilonga. MOD1, 2 refers to interpretations for sequence stratigraphic correlations 1 and 2; which in this core are identical. 118

4.13 Sequence stratigraphic correlation 1 framework along the line of section shownin figure 4.2, showing logged cores and key stratigraphic surfaces that bound the Lower Roan, Upper Roan, Mwashia, Nguba and Kundelungu Groups. 120

4.14 Sequence stratigraphic section across the Kafue anticline, Bangweulu block and eastern part of the basin during the Lower Roan TST, with low-order cyclicity, proximal terrestrial sedimentation predominating in disconnected sub-basins. Vertical lines represent core constraints 121

4.15 Sequence stratigraphic cross-section showing widespread intertidal and sabkha successions forming the Upper Roan LST. 123

4.16 Sequence stratigraphic cross section showing the Upper Roan TST and Mwashia HST marking a pronounced deepening and expansion of the basin. 125

4.17 Sequence stratigraphic cross section showing deposition being initiated in Chilonga during the Mwashia TST, and the basin remaining deep during the long-lived Nguba HST, comprising the Grand Conglomerat diamictites. 125

4.18 Sequence stratigraphic section showing the high-order base-Kundelungu erosional unconformity, SB4, that marks a significant basinward facies shift. 126
4.19 Sequence stratigraphic section showing Petit Conglomerat diamictites forming part of the Kundelungu TST. 127
4.20 Sequence stratigraphic correlation 2 framework, showing key stratigraphic surfaces that bound each stratigraphic Group. In contrast to sequence stratigraphic correlation 1, basal clastics in Ndola are assigned to the Mwashia Group. 128
4.21 Sequence stratigraphic section showing a narrower Lower Roan rift, filled with low-order cycles of proximally derived clastic facies. 129
4.22 Sequence stratigraphic section showing the Upper Roan LST prograding and aggrading above disconnected or partially connected Lower Roan sub-basins. 130
4.23 Sequence stratigraphic section showing the Upper Roan TST and westwards retrograding paralic facies culminating in the high-order Mwashia flooding surface. . . 131
4.24 Sequence stratigraphic section showing the Mwashia Group overstepping the Roan basin margins and Mwashia-age clastics being deposited in Ndola. Deposition is initiated in Chilonga during this time. 132
4.25 Sequence stratigraphic section showing the high-order Nguba MFS3 and long-lived HST stepping over the margins of the Bangweulu block in Mansa. 133
4.26 Sequence stratigraphic section showing the high-order base-Kundelungu unconformity SB4 and associated basinward facies shift, and Petit Conglomerat diamictite deposition initiating the subsequent TST. 133
4.27 A comparison of sequence stratigraphic interpretations of the IT26 core from Bull et al. (2011) (left) and this work (right). Note the dilation of sequence thickness as facies resolution attenuates, and parasequences being mistaken for sequences in Bull et al.'s (2011) interpretation. The complete stratigraphic log for IT26, including key, is provided in Appendix 2. 135
4.28 A comparison of sequence stratigraphic interpretations of the RCB2 core from Bull et al. (2011) (left) and this work (right). Note the three sequences in Bull et al.'s (2011) interpretation fitting into the Lower Roan HST proposed in this work. The complete stratigraphic log for RCB2, including key, is provided in Appendix 2. . . 136

5.1 Schematic showing the process of backstripping, partioning the total (water-loaded) basement subsidence into its principal components of sediment loading and tectonic subsidence. With increasing sediment load, the mantle is displaced, and previously deposited sediment layers are compacted. 146

5.2 A selection of passive margin tectonic subsidence curves. The dashed line represents the seafloor thermal decay curve (shallowed by 500m). Curves 1-5 represent the Paleozoic Miogeocline, Moroccan Basin, Campos Basin, Gippsland Basin, and Gulf of Lion, respectively (Xie and Heller, 2009). 147

5.3 The uniform extension model as a schematic diagram, showing crust, lithospheric mantle and asthenosphere, with densities ρ_c, ρ_m, ρ_a. The crust has a thickness of y_c and the lithosphere a thickness of y_L. The crust is thinned by a stretch factor, β to y_c/β, the lithosphere to y_L/β, with the initial width of extension zone x_0 being stretched to $x_0\beta$, forming a sedimentary basin of thickness y_s with a fill density of ρ_s. Figure adapted from Allen and Allen (2013). 152

5.4 1D burial histories for Solwezi, Konkola, Chambishi, and Mufulira. 155

5.5 1D burial histories for Ndola, Lusale, Mansa, and Chilonga. 156

5.6 1D burial histories across the Katangan basin, showing the basin deepening to the north-west, and in the eastern arm of the basin. 157

5.7 Tectonic subsidence profiles for Solwezi, Konkola, Chambishi, and Mufulira, showing clear Lower Roan, and less pronounced Mwashia, rift signatures. Red bars represent tectonic subsidence (area represents age and depth error), grey bars the water-loaded basement subsidence. Kundelungu subsidence bars are unfilled to indicate their uncertainty. 158

5.8 Tectonic subsidence profiles and for Ndola, Lusale, Mansa, and Chilonga. Chilonga shows a subtle rift subsidence profile. Red bars represent tectonic subsidence (area represents age and depth error), grey bars the water-loaded basement subsidence. Kundelungu subsidence bars are unfilled to indicate their uncertainty. 159

5.9 Tectonic subsidence profiles and β values for Solwezi, Konkola, Chambishi, and Mufulira. The black line represents the uniform extension model calibrated by tectonic subsidence constraints and stratigraphy, showing two phases of extension. Red bars show tectonic subsidence (area represents age and depth error), grey bars are water-loaded basement subsidence. 160

5.10 Tectonic subsidence profiles and β values for Ndola, Lusale, Mansa, and Chilonga. The black line represents the uniform extension model calibrated by tectonic subsidence constraints and stratigraphy. Only Chilonga shows a clear fit of the forward model with the backstripped tectonic subsidence. Red bars show tectonic subsidence (area represents age and depth error), grey bars are water-loaded basement subsidence. 161

5.11 Partitioning of β-factors, tectonic subsidence and syn-rift sediment thickness into the two extensional phases in the Katangan basin. Mwashia rift signatures for syn-rift sediment thickness, tectonic subsidence, and lithospheric stretching are generally subdued. 162

5.12 Cumulative stretching factor cross-section across the Katangan basin, showing highest stretching in the Domes region. The Zambian Copperbelt shows moderately stretched lithosphere, reducing towards the basin margins near Lusale and Mansa. Towards the eastern margin of the basin, the lithosphere was stretched again. 164

6.1 A schematic illustration of the components comprising the mineralisation factor (m) in green: a clastic source of thickness S, reduction potential (E_S), and permeability (k_S), underlying a reductant of reduction potential (E_R) and permeability (k_R). Both experience a heat flux (Q), which drives fluid convection. 170

6.2 The mineralisation factor ranges for Kamoa, Lubambe (core KN192), Chambishi (core RCB2), Ndola (core IT26), and Chilonga (core CHLDD001). An arbitrary $\pm$5 uncertainty envelope is added to partially account for uncertainties in inputs. In this model, mineralisation appears most likely where $m >$15. 173

7.1 Palaeogeographic reconstruction of early-mid Lower Roan time, showing major normal faults (centre panel); chronostratigraphy and general stratigraphic trends (left panel); backstripped subsidence plot, using the Konkola type section as an illustrative example (right panel). Modified after Daly et al., (2024) [in prep.] The highly extended central rift zone is shown in orange against a backdrop of terrestrial Lower Roan deposition in yellow. 178

7.2 Palaeogeographic reconstruction of Upper Roan time, showing an extensive epicontinental sea and evaporitic basins covering the Lower Roan rift fill and onlapping basement as the basin thermally subsides (centre panel); chronostratigraphy and general stratigraphic trends (left panel); backstripped subsidence plot, using the Konkola type section as an illustrative example (right panel). Modified after Daly et al., (2024) 181

7.3 Tentative and simplified reconstruction of the two generations of rift systems forming the Katangan basin along the margins of the Congo, Bangweulu and Kalahari cratons: an arcuate Lower Roan rift, and a $\sim$ SE-NW trending sub-parallel Mwashia rifts. The Bangweulu craton underlying the traditional Zambian and Congolese Copperbelts is based on Bangweulu-age ($\sim$1.8 Ga) basement extending from the Kafue anticline westwards across the Domes region to the Kabompo Dome (De Waele, Liégeois, Nemchin and Tembo, 2006). Modified after Daly et al. (2024) 184

7.4 Palaeogeographic reconstruction of early to mid-Nguba time, showing major Mwashia normal faults and reactivated Lower Roan fault networks; the subaqueous slope deposits were likely much more numerous and widespread than illustrated on the map (centre panel); chronostratigraphy and general stratigraphic trends (left panel); backstripped subsidence plot, using Konkola type section as an illustrative example (right panel). Modified after Daly et al. (2024). 187

7.5 Chronostratigraphic log showing general stratigraphic evolution, depositional settings and tectonic processes operating in the katangan basin in Zambia and the D.R.C., based on facies analysis in this work as well as work by [1] Armstrong et al. (2005), [2] Selley et al. (2018), [3] Cahen et al. (1970), [4] Selley et al. (2005), [5] Muchez et al. (2015), [6] Binda (1994), [7] Key et al. (2001), [8] Kampunzu et al. (2000), [9] Rooney et al. (2015), [10] Halverson et al. (2020), [11] John et al. (2004), [12] Daly et al. (2020) *unpublished*, [13] Torrealday et al. (2000). 190

7.6 Heat flux at the basement-sediment interface over the course of Roan rifting and thermal subsidence, based on the McKenzie uniform extension model (McKenzie, 1978) in different parts of the basin. Though the absolute values come with significant uncertainty, the trend of increasing syn-rift heat flux with increasing stretching is evident. Dashed lines represent the fault-controlled subsidence phase. 196

7.7 1D burial-temperature plot of the Solwezi type log, derived from core KRX082, showing ranges of temperatures the Lower Roan could have achieved during Roan rifting, with a stretching factor of 1.5 198

7.8 Composite lifetime burial-temperature plot for Solwezi showing burial and Roan temperature estimates prior to basin inversion, followed by a cooling/uplift model based on apatite and zircon fission track thermochronometry. The two main mineralisation events, Roan diagenetic, and Lufilian syn- to post-orogenic, are shown. The two lines in the thermal model are based on apatite fission tracks at a 95% confidence interval; the higher temperature bound is seen as a more reliable estimate of thermal evolution on account of being constrained by zircon fission tracks. 199

9.1 The dMs facies in the ZMSDD003 core, showing dark grey, fissile mudstone units with faint thin planar lamination. Arrows indicate way-up for the three cores. . . . 206

9.2 The SlMs facies in the CHLDD001 core. Laminites comprise thin planar laminated silts and mudstones. Arrow indicates way-up; mm-scale QP card for scale. 206

9.3 The LSl facies in the ZMSDD003 core, showing abundant laminites and thin graded beds. Some of the beds are grey and reduced; the majority are oxidised to a reddish-brown. 208

9.4 The SstMs facies in the KN192 core, showing wavy and lenticular arkose beds in laminated silt and mudstone. Small sand dikes are also visible. Arrows indicate way-up for the three cores. 212
9.5 The Wck facies in the KN192 core, showing poor sorting, trough cross-lamination, granular outsized clasts and poorly developed structures. Arrows indicate way-up for the three cores. Mm-scale QP card for scale. 212
9.6 The MsgSst sub-facies in the KN192 core, showing sandstones grading into planar laminated siltstone and mudstones. Arrows indicate way-up for the four cores. . . . 215
9.7 The tMsSst sub-facies in the KN192 core showing sharp interbedding of thinly bedded laminated mud- and siltstone units with arkosic sandstones. 215
9.8 The MscSst sub-facies in the KN192 core, showing subarkosic units crudely interbedded with siltstones. Soft-sediment deformation is visible, as are abundant scattered granules. Arrows indicate way-up for the three cores. 218
9.9 The pLSst sub-facies in the IT26 core displaying characteristic poor sorting, with granule-sized feldspar clasts dispersed in a poorly laminated arkose. Arrows indicate way-up. 223
9.10 The XSst facies in the IT26 core showing trough cross-stratification, with silty laminae delineating foresets. Arrow indicates the way up. 223
9.11 The fCCgm sub-facies in the KN192 core, showing clear cross-stratification. Arrows indicate way-up for the cores. Mm-scale QP card for scale. 226
9.12 Sub-facies dCCgm in the KN192 core. Note the range of clast angularity and sphericity. Arrows indicate way-up for the cores. Mm-scale QP card for scale. . . . 226
9.13 Clast counts for the crDia sub-facies in the ZMSDD003 core, measured at 0.5 m intervals, showing higher clast proportion and tendency for upwards clast quantity reduction. 227
9.14 Clast counts for the cpDia sub-facies in the ZMSDD003 core, measured at 0.5 m intervals, showing significantly lower clast counts ($<$ 10 clasts / 0.5 m). 227
9.15 The crDia sub-facies in the ZMSDD003 core, showing variation in clast size and composition (e.g. andesite, mica schist). Arrows indicate way-up for the two cores. 229

9.16 The cpDia sub-facies in the ZMSDD003 core, showing a lower clast count and average size. Grey patches are reduction spots. Arrows indicate way-up for the three cores. 229
9.17 The CaDia sub-facies in the KN192 core with variably angular, mostly low sphericity, clasts embedded in a dolomitic, silty matrix. Arrow indicates the way up for both cores. 231
9.18 The CaMs facies in the ZMSDD003 core, showing planar lamination, shear structures, and thin carbonate beds. Arrows indicate way-up for the three cores. 235
9.19 The lSlCa facies in the ZMSDD003 core, showing abundant rhythmic graded laminites in carbonate and siltstone. The arrow indicates way-up for the two cores. 235
9.20 The CaHet facies in the KN192 core, showing discontinuous wavy sand laminae interbedded with silty, carbonate-bearing mudstone and carbonate. Arrow indicates way-up. 237
9.21 Facies CaSst in the IT26 core with very coarse to fine gravel-sized sub-litharenite with dolomitic matrix. The arrow indicates way-up. 237
9.22 Facies CaCgm in the KN192 core, showing poor sorting and clast-supported texture with minor sulphide mineralisation. The arrow indicates way-up for both cores. . . 241
9.23 The pLCa sub-facies in the ZMSDD003 core, showing ubiquitous parallel planar lamination and low silt-content. The arrow indicates way-up for both cores. 241
9.24 The AnCa facies in the L83 core, characteristic of the sabkha facies association. Nodular anhydrite and enterolithic structures (circled red) embedded in grey silty dolomite are abundant. Arrows indicate way-up for the three cores. The core begins in the lower left-hand corner. 244
9.25 The StMic facies in the IT26 core, showing microbially induced sedimentary structures that characterise the facies (circled red), which are interpreted as domal and columnar stromatolites. Arrows indicate way-up for the three cores. The core begins in the lower left-hand corner. 244
9.26 KRX082 (Solwezi) stratigraphic log 246
9.27 KRX082 (Solwezi) stratigraphic log, continued 247
9.28 KRX082 (Solwezi) stratigraphic log, continued 248

9.29 KN192 (Lubambe) stratigraphic log 249
9.30 KN192 (Lubambe) stratigraphic log, continued 250
9.31 RCB2 (Chambishi) stratigraphic log 251
9.32 RCB2 (Chambishi) stratigraphic log, continued 252
9.33 L83 (Mufulira) stratigraphic log 253
9.34 L83 (Mufulira) stratigraphic log, continued 254
9.35 IT26 (Ndola) stratigraphic log, continued 255
9.36 CHLDD001 (Chilonga) stratigraphic log 256
9.37 CHLDD001 (Chilonga) stratigraphic log, continued 257
9.38 KADD04 (Lusale) stratigraphic log 258
9.39 KADD04 (Lusale) stratigraphic log, continued 259
9.40 KADD04 (Lusale) stratigraphic log, continued 260
9.41 ZMSDD003 (Mansa) stratigraphic log 261
9.42 265
9.43 Example of two columns in isostatic balance assuming Airy isostasy, the left being loaded with a thickness of sediment (decompacted), the right backstripped showing commensurate isostatic adjustment, after Allen and Allen (2013). 271
9.44 Radial plots of apatite fission-track ages for KRX082 (left) and KN192 (right), with central ages of 454 $\pm$ 48 Ma, and 443 $\pm$39 Ma, respectively. 279
9.45 Radial plots of zircon fission-track ages for KRX082 (left) and KN192 (right), showing considerable dispersion in sample ages, with central ages of 461 $\pm$ 71 Ma, and 414 $\pm$72 Ma, respectively. 281
9.46 Preliminary thermal model for samples at a depth of 2204 m in the KRX082 core, with pink lines indicating a 95% confidence interval, and box showing zircon fission track constraints. 281

Abstract

The Neoproterozoic Katangan basin of Central Africa represents the largest sediment-hosted copper province on Earth, recording ∼300 Myr of sedimentation. This work applies a basin analysis approach to understanding the basin's evolution in Zambia, combining facies analysis, sequence stratigraphy, and subsidence analysis.

The Katangan basin shows two phases of rifting and thermal subsidence, punctuated by two major glacial events. The Lower Roan Group comprises the proximally deposited terrestrial syn-rift fill of the initial amagmatic rift, reaching decompacted thicknesses of ∼2.6 km in Solwezi. The overlying Upper Roan Group shows a sharp transition to carbonate-dominated facies and evaporite successions deposited in an epicontinental sea with extensive paralic zones as the basin transitioned from fault-controlled to predominantly thermally controlled subsidence.

The Mwashia Group represents a second, magmatic, phase of rifting between ∼765 and ∼735 Ma. It is expressed in the Zambian Copperbelt predominantly as distal facies, starved of coarse sediment, recording the basin deepening and expanding beyond the initial Lower Roan rift. The base of the Nguba is traditionally demarkated by diamictites at its base and was accommodated via post-rift thermal subsidence. The Kundelungu is demarkated at its base by a regionally correlatable sea level lowstand and glacial diamictites. It represents an initially quiescent tectonic regime prior to flexure and basin inversion.

Backstripped subsidence profiles support a diachronous rift origin for the basin. The Lower Roan central rift zone is interpreted to have been situated south of the Domes region in Zambia, with crustal stretching exceeding 50%. It likely accommodated $>$ 8 km Katangan stratigraphy prior to basin inversion during the Lufilian orogeny.

Facies analysis, sequence stratigraphy, and quantitative subsidence analysis can inform understand-

ing of the Katangan's mineral systems, emphasising the importance of rapid retrogradational successions in forming potential mineralisation sites and possible diachroneity of mineralised units. When combined, they can form the foundation of quantitative estimates of mineralisation potential.

To my grandfather, Joachim:

Thank you for telling me *"Aus Dir wird mal was!"*.

I hope I'm on my way there.

Acknowledgements

I would like to express my sincere gratitude to my supervisors, Mike Daly and Bruce Levell. I am very fortunate to have been able to benefit from your experience, instruction, insights and guidance. The many hours spent discussing the Katangan were a pleasure. Your perspectives on geology, work, and life in general are much appreciated. Learning from you has been as enjoyable as it has been edifying. I have grown as a geologist, and as a person, thanks to both of you.

This work is the result of a NERC CASE studentship with the Oxford Doctoral Training Partnership in Environmental Research. I am therefore very grateful to First Quantum Minerals for funding this project, for their support and generosity throughout. Thank you to Munshya Zimba, Jon Stacey, and many others for the discussions and feedback; exchanging ideas with you has been insightful, and has significantly improved this work. My gratitude is also extended to the Lubambe Copper Mine and KoBold Metals for their support.

Andy Carter, I am much obliged to you for your time and guidance through the AFTA preparation, and your contributions. Victoria Forth, Martha Brundin, and Claire Rylatt, your help in navigating the meanders of the University's administrative channels has been invaluable.

My time in Oxford has been a pleasure, and without Jake Ciborowski and Laurence Hopkinson accommodating my curiosity and encouraging me during my undergraduate degree, I likely wouldn't have ended up here; thank you both.

Carmen, your unyielding support and encouragement have been wonderful. If quantum gravity ever makes you feel detached from reality, the Earth Sciences would welcome you. To my dear friend Ryan, thank you for your company throughout this journey, it's been a joy. I have learnt a lot from your sense of humour and approach to life. Toby, Nathan, Bubile, Veronica, and all the friends whose company I've been fortunate to enjoy over the last four years, I am deeply grateful to you.

Statement of originality

Chapter 3 of this thesis forms a paper submitted to the Journal of African Earth sciences: Purkiss, M. (2024), *Application of facies analysis in the Zambian Copperbelt and its stratigraphic implica-tions for the Katangan basin*.

This thesis also contains work done in collaboration, to which the author contributed substantially. Specifically, Chapter 7 makes reference to, and contains figures modified after, the following work: Daly, M.C., Zimba, M., Purkiss, M., Chibesakunda, F. (2024), *Lithospheric Thickness, Rift and Inversion Tectonics: The Formation and Deformation of the Neoproterozoic Katangan Basin of Central Africa*. Preliminary fission-track analysis results presented here were collected in collaboration with Andy Carter at University College London.

Chapter 1

Introduction

The Neoproterozoic Katangan basin of Central Africa is a SW-NE trending basin extending from the D.R.C. through Zambia to Angola and Namibia. It contains the Katangan Supergroup, deposited over $\sim$300 Myr, spanning the Tonian, Cryogenian, and Ediacaran periods. The basin hosts the Central African Copperbelt, the world's largest sediment-hosted copper province (Hitzman et al., 2005). It is divided into the Zambian and Congolese Copperbelts, respectively, which together form a 400 km long arc approximately following the Zambian-Congolese border (fig. 1.1).

Mining of outcropping ore bodies by indigenous peoples in the Central African Copperbelt has taken place for over 4000 years (Broughton et al., 2002). Today, the region is of global importance in the supply of metals needed for the transition to a low-carbon future, accounting for approximately 14% of global Cu production in 2022, with the majority being sourced from the D.R.C. (USGS, 2023). It contains more than 10 giant Cu and Co deposits, including Konkola, Nchanga, Nkana, Chambishi, Kamoa, Kolwezi, Tenke, and Fungurume (Selley et al., 2005, 2018).

The Katangan basin has been extensively studied for over a century (Stutzer, 1911; Davidson, 1931; Mendelsohn, 1961; Binda, 1994; Selley et al., 2005; Basson et al., 2023). However, a basin-scale understanding of the Katangan's evolution is generally under-developed compared to detailed studies of its deposits, with several aspects remaining poorly understood or contentious. Poor exposure, and a focus on mine-scale studies, complicated by convoluted lithostratigraphic nomenclature, which varies between mines and countries, have hindered understanding of the basin at a regional scale (Mendelsohn, 1961; Cailteux et al., 1994; Cailteux and De Putter, 2019).

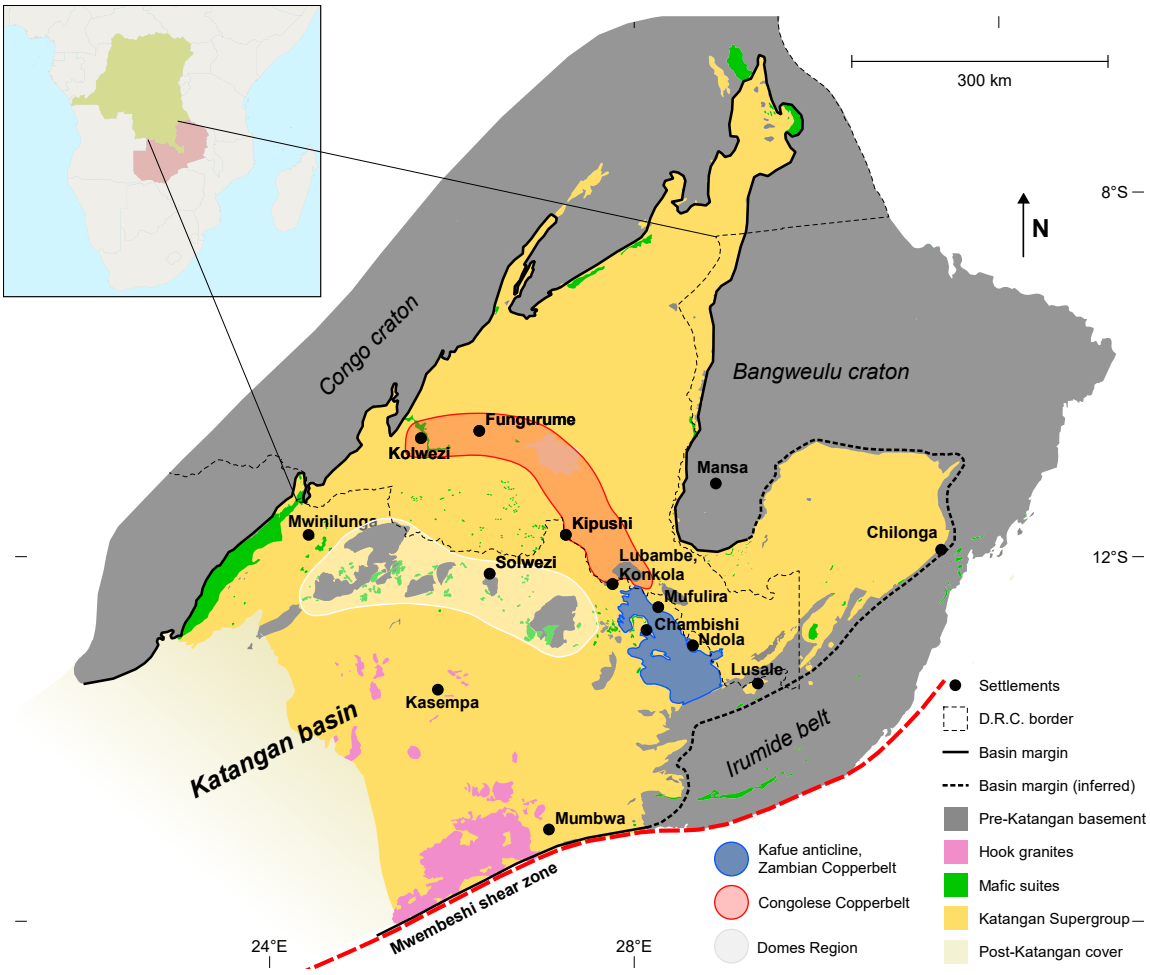

Figure 1.1: Generalised map of the Katangan basin, showing its position between the Congo, Bangweulu, and Kalahari cratons, and the Irumide belt. Major settlements are marked, as well as the three main Cu-deposit hosting regions (Zambian Copperbelt, Domes Region, Congolese Copperbelt) highlighted. The Congo craton marks the northwest margin of the basin, the Bangweulu craton its northeast margin, and the Mwembeshi shear zone its southern margin. The basin's SE margin is not formally defined, and inferred here.

That relationships exist between sedimentary facies and sediment-hosted mineralisation has long been appreciated in the Central African Copperbelt (Mendelsohn, 1961; Garlick, 1964; Eden, 1974; Clemmey, 1976). However, sedimentological analysis performed predominantly on a mine-scale has resulted in conflicting interpretations of, and ambiguity regarding, depositional processes of different facies. Facies analysis has also been limited in its application as part of a broader mineral systems approach (e.g. Hitzman et al. (2005); McCuaig et al. (2018)).

The paucity of age constraints in the Katangan basin limits a precise understanding of basin evolution through time. A relative chronostratigraphic framework driven by sequence stratigraphic

correlations could partially alleviate this problem. Lithostratigraphic correlations are severely limited on account of diachroneity imparted by correlating on the basis of lithology, rather than time. Appreciating possible diachroneity of stratigraphic units allows for different models of tectonostratigraphic evolution to be made and tested. Key stratigraphic surfaces also allow for more reliable correlations to be made where lithologies are repeated or too ambiguous to be correlated lithostratigraphically, particularly as many drill cores don't capture the full stratigraphy.

Basin-forming mechanisms have remained contentious (Binda, 1994; Selley et al., 2005), and sequence stratigraphic correlations in Zambia have not been extended to the basin margins towards the NE, SE, and far East of the basin near Mansa, Lusale, and Chilonga (Bull et al., 2011; Woodhead, 2013). No attempts at quantifying the subsidence history of the Katangan basin have been published thus far.

Appreciating the relevance of sedimentary facies and applying the principles of sequence stratigraphy to contextualise them in space and time should not be limited to the ore deposits in the Katangan basin. These approaches are applicable to, and have shown to be valuable in understanding, other sediment-hosted Cu deposits (e.g. White Pine (Hamilton, 1967)), PGE deposits (e.g. Norilsk (Krivolutskaya et al., 2021)) and has been shown to be of use in sediment-hosted uranium deposits (Hou et al., 2017).

The aim of this project was to generate a more holistic understanding of the Katangan basin's tectonostratigraphic evolution, providing a framework into which mine-scale studies could fit. To achieve this aim, the following objectives were set out:

1.) Create a robust facies scheme to interpret Katangan depositional environments from drill core. This scheme should encompass the majority of Katangan stratigraphy in the Zambian part of the basin, whilst remaining sufficiently flexible to allow for modification and accommodate more facies in future. The purpose of this scheme would be to allow for more consistent and accurate interpretations of the basin's depositional systems to be made, which would have controlled the nature and distribution of siliciclastic Cu-sources, redox and permeability boundaries.

2.) Apply the facies scheme to drill core to identify key stratigraphic surfaces. Key stratigraphic surfaces would then be used to generate sequence stratigraphic correlations to constrain the architecture of the basin fill along and beyond the Kafue anticline. This would allow for relative chronological surfaces to be established in parts of the stratigraphy with no precise chronological constraints.

3.) Generate local type logs (best estimates of the full stratigraphy prior to any erosion or deformation), and general estimates of palaeobathymetry through time, using the facies scheme and sequence stratigraphic correlations.

4.) Decompact and backstrip local type logs to quantify burial history, basin subsidence, and constrain basin forming mechanisms, and apply the McKenzie Uniform Extension Model (McKenzie, 1978) to generate estimates of crustal stretching and heat flow. This would help constrain basin domains with the greatest accommodation potential for siliclastic Cu-sources, and heat flow to drive hydrothermal systems.

5.) Use fission-track thermochronometry to quantify the cooling history of the basin following the onset of basin inversion, when much of the basin's mineralisation formed.

6.) Combine facies analysis, sequence stratigraphy, and subsidence analysis in a dynamic stratigraphic framework and holistically evaluate their impact on the Katangan's mineral systems.

This work is based predominantly on drill core, and extensive use was made of government and industry core facilities in Zambia. The geographic scope of this work predominantly encompasses the Zambian Copperbelt, though basin-scale perspectives are provided where possible. It has been attempted to adapt basin analysis techniques to the common constraints of Neoproterozoic basins (e.g. paucity or lack of palaeontological data), and apply structured, reproducible workflows.

Chapter 2

Background

2.1 Tectonic evolution

2.1.1 Cratonic basement and pre-Katangan deformation

The Katangan basin lies at the juncture of three ancient portions of lithosphere: the Congo, Bangweulu and Kalahari cratons (fig. 2.1). These form Archaean to Mesoproterozoic basement rocks, comprising metagranites, migmatites, metavolcanics and metasediments, which have undergone multiple phases of deformation (Mendelsohn, 1961; Daly et al., 1984; John et al., 2004; Selley et al., 2005; Rainaud et al., 2005). These three cratons are interpreted to have formed the ancient supercontinent Rodinia, though the exact positioning of the Congo and Kalahari cratons in Rodinia is still unclear (De Waele et al., 2008; Jacobs et al., 2008). The cratonic margins are in-part delineated by various orogenic belts, including the Palaeoproterozoic Ubendian and Usagaran Belts, and Mesoproterozoic Kibaran and Irumide Belts (Hanson, 2003).

The Bangweulu block comprises Eburnian schists, felsic metavolcanics and granitoids association with deformation and magmatism between $\sim$ 2000 and 1800 Ma (Andersen and Unrug, 1984). Some mafic suites show TDM model ages of 3200 Ma to 2400 Ma, and form part of an enigmatic Archean core to the Bangweulu Craton (De Waele et al., 2006). The geochemical similarity of the Bangweulu metavolcanics to calc-alkaline magmatic suites associated with modern subduction zones has been used to invoke a compressional regime on the north-western margin of the Bangweulu craton (Andersen and Unrug, 1984). In the classical Zambian Copperbelt, the old-

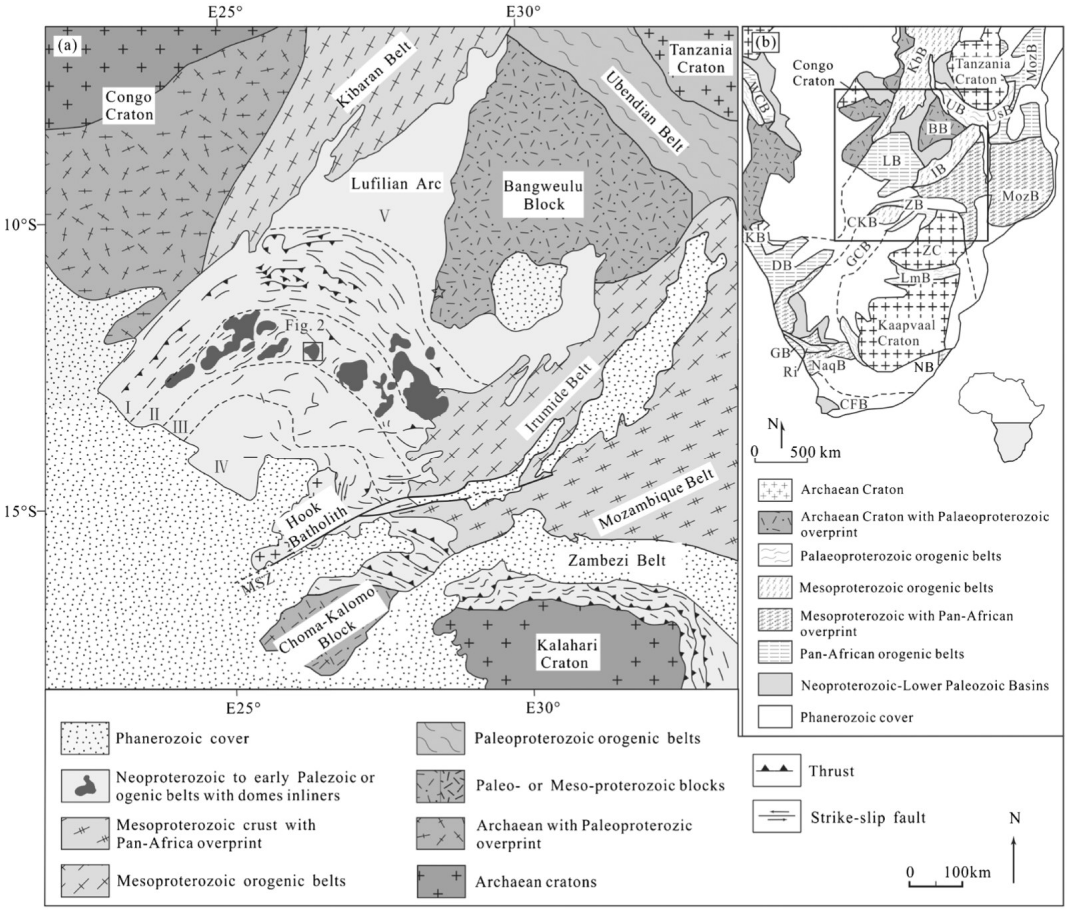

Figure 2.1: Map of major cratons, belts, and structures adjoining the Katangan basin; map and abbreviations from Xu et al. (2022): BB, Bangweulu Block; CFB, Cape Fold Belt; CKB, Choma-Kalomo Block; DB, Damara Belt; GB, Garip Belt; GCB, Ghanzi-Chobe Belt; IB, Irumide Belt; KB, Kaoko Belt; KbB, Kibaran Belt; KhB, Kheis Belt; LB, Lufilian Belt; LmB, Limpopo Belt; MozB, Mozambique Belt; NaqB, Namaqua Belt; NB, Natal Belt; Ri, Richtersveld Terrane; UB, Ubendian Belt; UsB, Usagaran Belt; WCB, West Congo Belt; ZB, Zambezi Belt; ZC, Zimbabwe Craton; I-External Fold and Thrust Belt; II-Domes Region; III-Synclinorial Belt; IV-Kantanga High; V-Foreland Basin.

est basement rocks are the Palaeoproterozoic Lufubu Schists and Gneisses, which form part of the Lufubu Metamorphic Complex (Mendelsohn, 1961; Selley et al., 2005; Rainaud et al., 2005). The Lufubu Metamorphic Complex ranges in age from 1980 $\pm$ 7 to 1874 $\pm$ 8 Ma, with the oldest unit in the Copperbelt being the Mkushi gneisses with an age of 2049 $\pm$ 6 Ma (Rainaud et al., 2005). The precursor to the Lufubu Metamorphic Complex is interpreted to be one or several magmatic arcs that developed between 2000 and 1850 Ma, which formed a terrane that was accreted onto the Tanzanian craton during the Ubendian orogeny (Rainaud et al., 2005).

The Congo craton amalgamated from a series of Mesoproterozoic orogenies, and comprises the Archaean Angola-Kasai Craton, Congo-Uganda craton, and Cameroon-Gabon-S*ão*-Francisco Craton (Hanson, 2003; De Waele et al., 2008). Formation of the Congo craton is inferred to have been completed by the end of the Kibaran orogeny at 1380 Ma (De Waele et al., 2008). The Kalahari Craton, like the Congo craton, amalgamated during the Mesoproterozoic, and together with the Bangwuelu and Congo cratons is interpreted to have formed part of Rodinia (Hanson, 2003). The Kalahari Craton nucleated around an Archaean core during the Palaeoproterozoic along the Magondi-Okwa-Kheis Belt. Between 1750 Ma and 1000 Ma, the Kalahari Craton was surrounded by a series of Mesoproterozoic belts as a result of continent-continent collision and arc accretion, with the Umkondo–Borg large igneous province (LIP) developing at $\sim$1110 Ma (Jacobs et al., 2008).

Two Mesoproterozoic craton-margin belts constrain the Katangan basin: the Irumide and the Kibaran. The NE-SW-striking Irumide Belt shows north-westerly and south-easterly directed thrust sheets emanating from an upright central structural domain; the Irumide Belt terminates against the Ubendian Belt (Daly et al., 1984; De Waele, Liégeois, Nemchin and Tembo, 2006). Isotopic and structural evidence suggests the belt represents the repeatedly reworked margins of the Bangweulu craton (Daly, 1986*a*,*b*; Porada and Berhorst, 2000; John et al., 2004; De Waele, Liégeois, Nemchin and Tembo, 2006). Metamorphic grades range from greenschist to amphibolite facies, along a clockwise medium-P-T-t path; peak metamorphic conditions have been constrained to between 1050 and 1020 Ma (De Waele, Kampunzu, Mapani and Tembo, 2006).

The 1400 to 1000 Ma Kibaran Belt to the West of the basin separates the Bangweulu Craton from the Kasai-Angola portion of the Congo craton. It forms a Northeast to Southwest-oriented domain comprising a metamorphosed supracrustal assemblage of amphibolite-grade metasediments, intrusive granitoids and gneisses (Cahen, 1984; Hanson, 2003; Rainaud et al., 2005; De Waele et al., 2008). Both the Irumide and Kibaran belts are interpreted to represent a prolonged phase of mountain building during the assembly of Rodinia from 1400 to 1000 Ma (Porada and Berhorst, 2000; Hanson, 2003; John et al., 2004).

Parts of the Katangan basement are unconformably overlain by metasediments of the Mesoproterozoic Muva Supergroup (Selley et al., 2005). Muva sediments have been divided into several stratigraphic units, two of which are the Mporokoso Group, and Kasama Formation (Daly and Unrug, 1982). The Mporokoso Group comprises predominantly quartzites and shales, with basal por-

tions being highly immature. Minor intercalated tuffs and ignimbrites suggest coeval magmatism in the Bangweulu Craton during deposition of the Mporokoso Group. The Kasama Formation sits unconformably on the Bangweulu basement. It is significantly more mature than the Mporokoso Group, and becomes more marine in an eastwards direction (Daly and Unrug, 1982). U-Pb analyses of detrital zircons and tuff units in Muva sediments yield ages of $\sim$ 1900 Ma to $\sim$ 1800 Ma, indicating that the Mporokoso Group and its coeval equivalents, the Kanona and Manshya River Groups, are related and sourced from magmatic centres operating in the Bangweulu Craton at that time (De Waele and Fitzsimons, 2007). The younger Kasama Formation was dated at $\sim$ 1430 Ma, supporting Daly and Unrug (1982)'s interpretation of it possibly representing a second reworking of Mporokoso sediments (De Waele and Fitzsimons, 2007).

2.1.2 Neoproterozoic extension and basin formation

The present-day Katangan basin extends from the D.R.C. through Zambia and Angola, and can be interpreted to extend into the Namibian Damara Belt (Daly et al., 1984; Key et al., 2001; De Waele and Fitzsimons, 2007; Kennedy et al., 2019). Its western and northeastern margins are well-defined, following the margins of the Congo and Bangweulu cratons, shown in fig. 1.1 (Daly et al., 1984; Porada and Berhorst, 2000; Key et al., 2001). The southeastern margin of margin of the basin is less well-defined, being considered to be the Mwembeshi Shear Zone and Irumide Belt (Daly et al., 1984; Porada and Berhorst, 2000; De Waele and Fitzsimons, 2007) The eastern arm of the basin wrapping around the southern portion of the exposed Bangweulu craton is poorly defined (Porada and Berhorst, 2000), but may be interpreted to extend to the Mugesse Shear Zone of Tanzania (De Waele and Fitzsimons, 2007). The central and southwestern parts of the basin in Zambia and Angola are covered by Kalahari sands with little outcrop; however, the Mwembeshi Shear Zone is considered as a southern margin of the basin (Daly, 1986*a*, 1988).

Evidence for Neoproterozoic extension and rifting is abundant both in the Katangan basin, and along the margins of the Congo, Bangweulu and Kalahari cratons (fig. 2.2), broadly constrained from $\sim$ 880 Ma to 735 Ma (Key et al., 2001; Hanson, 2003; John et al., 2004; De Waele et al., 2008; Jacobs et al., 2008). The geometry of sub-basins and fault networks, rapid transitions between immature clastic facies, and widespread tholeiitic magmatism later in the Katangan basin's history are characteristics shared with Phanerozoic rift systems (Tembo et al., 1999; Porada and Berhorst,

2000; Key et al., 2001; Armstrong et al., 2005; Selley et al., 2005, 2018).

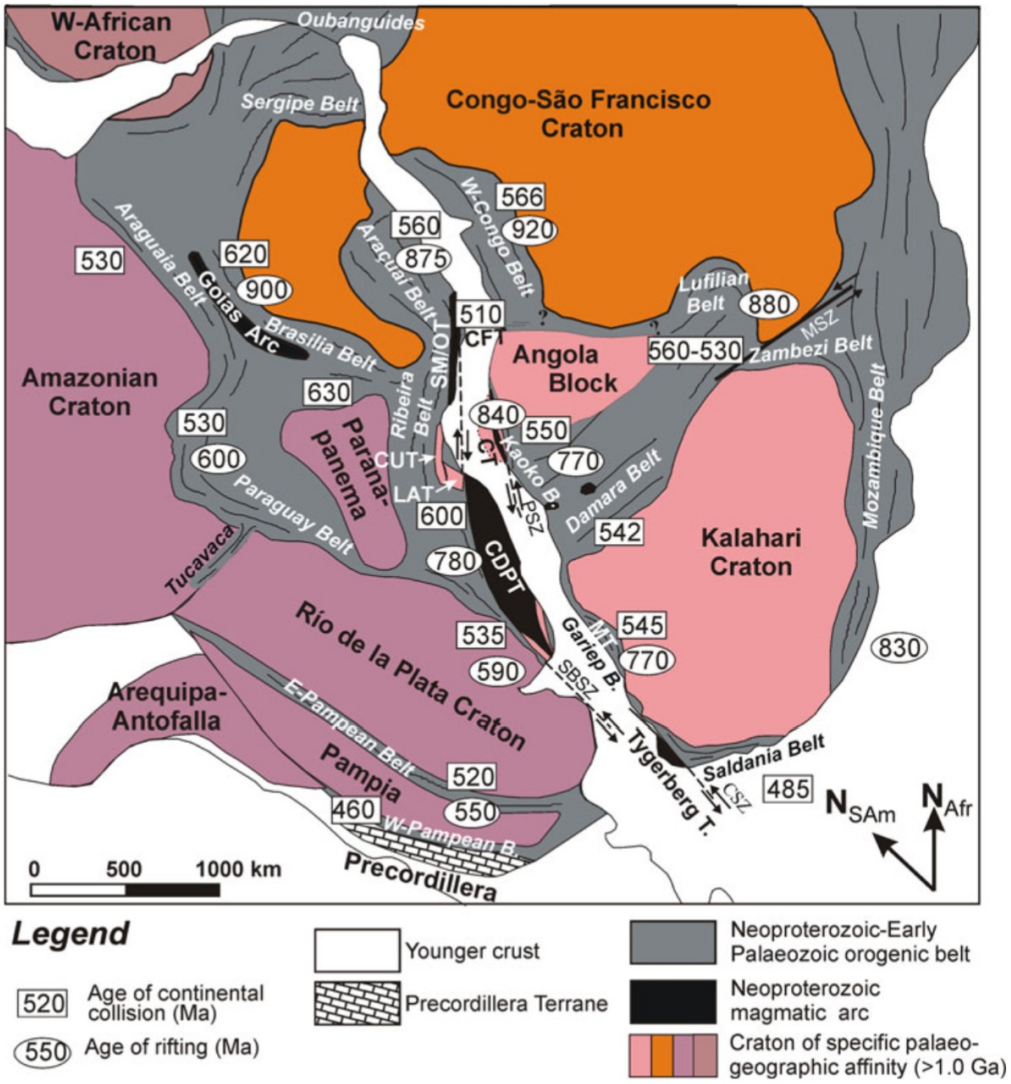

Figure 2.2: Map of South-West Gondwana, showing major cratons, fold belts and arcs, as well as approximate dates for extensional and compressional regimes in each belt; map and abbreviations from Frimmel et al. (2011): CDPT Cuchilla Dionsio-Pelotas Terrane, CFT Cabo Frí Terrane, CT Coastal Terrane, CUT Curitiba Terrane, LAT Luis Alves Terrane, MT Marmora Terrane, SM/OT Serra do Mar-Oriental Terrane, PSZ Purros Shear Zone, SBSZ Sierra Ballena Shear Zone, CSZ Colenso Shear Zone.

Porada and Berhorst (2000) inferred a passive margin developing on the southern portions of the Congo craton during Neoproterozoic continental extension. Continental breakup along the margins of the Congo craton is supported by $\sim$ 760 Ma mafic magmatism in the Damaran orogen in Namibia (Frimmel et al., 1996; McGee et al., 2012).

Evidence of rifting and continental breakup at $\sim$ 800 - 750 Ma on the Kalahari Craton is preserved

along its western margins Jacobs et al. (2008). Similarly, evidence of Neoproterozoic rifting is also preserved along the southern margins of the Congo craton (De Waele et al., 2008). The Zambezi supracrustal sequence contains intrusive and extrusive igneous suites emplaced between $\sim$ 880 Ma and $\sim$ 820 (John et al., 2004; Johnson et al., 2007). U-Pb ages for zircons in the Kafue rhyolites vary from 863 Ma (Barr et al., 1978) to 879 $\pm$ 19 Ma (Hanson et al., 1994) and 876 $\pm$ 10 Ma (Johnson et al., 2007), constraining timing for Zambezi rift development. The Lusaka granite has been U-Pb dated at 821 $\pm$ 9 Ma (Johnson et al., 2007).

Onset of deposition in the Katangan basin commenced following the emplacement of the Nchanga granite at 883 $\pm$ 10 Ma (Armstrong et al., 2005). However, sparse detrital zircon data suggests initial deposition could have taken place after $\sim$ 840 Ma (Selley et al., 2018). Microcline-bearing pegmatite veins at Luanshya and Musoshi show Rb-Sr dates of 840 $\pm$ 42 Ma (Cahen et al., 1970; Armstrong et al., 2005).

Two phases of extension have been inferred for the Katangan basin, the first being a terrestrial rift starting after $\sim$ 880 Ma, followed by thermal subsidence, the second at $\sim$ 765 - 735 Ma resulting in the basin opening to the Southwest and ocean crust developing (Key et al., 2001; Selley et al., 2005). The structural geometry of sub-basins in the Katangan Basin, as well as their gross stratigraphic architecture has previously been used to infer a rift origin for the basal clastics in the basin (Binda, 1994; Selley et al., 2005; John et al., 2003).

Abundant mafic suites across the basin are evidence of a second phase of extension which induced magmatism. Key et al. (2001) invoked the second phase of extension being oriented $\sim$ East-West, the result of reactivated basement structures controlling magmatism in the Western part of the Katangan basin. The geochemical signatures of mafic suites that were emplaced between 765 Ma and 735 Ma show tholeiitic and E-MORB affinities (Kampunzu et al., 1991; Tembo et al., 1999; Kampunzu et al., 2000). This is supported by the occurrence of eclogites in the West Zambezi belt, near Chombwa, and south of Lusaka (John et al., 2003; Goscombe et al., 2020), which show incompatible trace element patterns comparable to those of modern mid-ocean ridge basalts. Sm-Nd analyses of eclogites show eclogitisation ages of $\sim$600 Ma, which have been used to infer the presence of ocean crust in the Southwest of the basin, which was subducted during the subsequent Lufilian orogeny (John et al., 2003, 2004). John et al. (2003) used this to postulate a large ocean basin separating the Congo and Kalahari cratons.

2.1.3 Basin inversion

Following Neoproterozoic extension, the Bangweulu, Congo, Kalahari cratons converged, forming three mobile belts at their margins: the Damaran Belt, Lufilian Arc, and Zambezi Belt (Porada, 1989; Porada and Berhorst, 2000; Hanson, 2003; John et al., 2004; Naydenov et al., 2014).

The intracontinental Damaran Belt formed following the closure of the Adamastor and Khomas oceans along the triple junction of the Congo, Kalahari and Río de la Plata Cratons (Naydenov et al., 2014). This tectonostratigraphically complex region comprises several zones, separated by large-scale structures and lineaments, characterised by significant changes in gross facies assemblages (Frimmel et al., 2011). Peak metamorphic conditions were likely achieved at 535 Ma (Frimmel et al., 2011).

The Zambezi Belt records the collision of the Congo and Kalahari cratons, and forms a fold-and-thrust belt with predominantly South-West and South-South-West vergence (Coward and Daly, 1984; Porada, 1989; John et al., 2004; Naydenov et al., 2014). In its central portions, it contains Mesoproterozoic inliers with crystallisation ages of $\sim$1070 Ma to $\sim$1080 Ma, with a high pressure metamorphic event U-Pb dated at $\sim$526 Ma (Goscombe et al., 2000). The Belt likely experienced Barrovian, predominantly amphibolite-grade, metamorphism, though eclogites in parts have been interpreted to indicate increased crustal thicknesses during orogensis (Hanson et al., 1994). John et al. (2004) argued that 70 Myr after subduction of ocean crust, both the Zambezi Belt and Lufilian arc both experienced contemporaneous crustal thickening, with peak metamorphic conditions recorded by garnet-staurolite-kyanite schists from the Zambezi Belt indicate peak metamorphic conditions of $\sim$700 $\pm$25 degC at 10 $\pm$1 kbar.

The Mwembeshi Shear Zone is a major crustal lineament showing sinistral displacement (fig.2.3).

It has traditionally been interpreted as separating the Zambezi and Lufilian Arc, on account of opposing vergence of structures on either side of the lineament, and lower metamorphic grades being sharply juxtaposed with high metamorphic grades North and South of the shear zone, respectively (Coward and Daly, 1984; Naydenov et al., 2014). Interpretations of its tectonic significance vary (e.g. Daly (1986*a*); Porada and Berhorst (2000); Naydenov et al. (2014)); however, recent magnetotelluric and high-resolution aeromagnetic data show a clear lithospheric-scale discontinu-

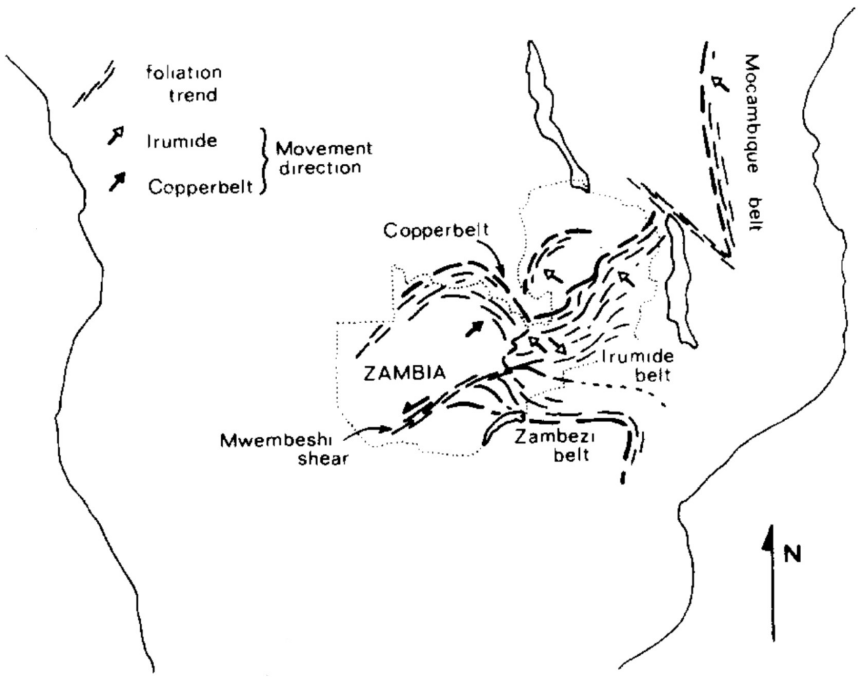

Figure 2.3: Simplified map of major structures and displacements in southern Africa, showing the Mwembeshi Shear Zone separating the Lufilian Arc in the North from the Zambezi Belt to the South (Daly et al., 1984).

ity underneath the Mwembeshi Shear Zone, which has now been interpreted as major suture zone along modified sub-continental lithospheric mantle (Sarafian et al., 2018).

Like the Zambezi Belt, The Lufilian Arc is the result of a collision between the Congo and Kalahari cratons (Porada, 1989; John et al., 2004; Naydenov et al., 2014). It is linked to the Damara Belt of Namibia forming the Damara-Lufilian orogen, and may be linked to the West Congo Belt (Daly, 1986*a*; Porada and Berhorst, 2000; Key et al., 2001). The Lufilian Arc forms an arcuate NE-verging fold-and-thrust belt, with basement thrust over Katangan cover across the traditional Zambian Copperbelt and Domes region (Daly et al., 1984; Cosi et al., 1992; Porada and Berhorst, 2000). Basement rocks in the Lufilian Arc are predominantly exposed in the Domes Region, and are typically of lower metamorphic grade than the Zambezi Belt (Cosi et al., 1992; Porada and Berhorst, 2000). The Lufilian Arc comprises the Katangan Supergroup and Muva sediments, showing varying degrees of deformation throughout the basin (Mendelsohn, 1961; Coward and Daly, 1984; Naydenov et al., 2014). John et al. (2004) determined peak metamorphic conditions of whiteschists in the Lufilian arc at 750 °C $\pm$ 25 and 13 $\pm$ 1 kbar. A simplified geodynamic model is shown in fig. 2.4.

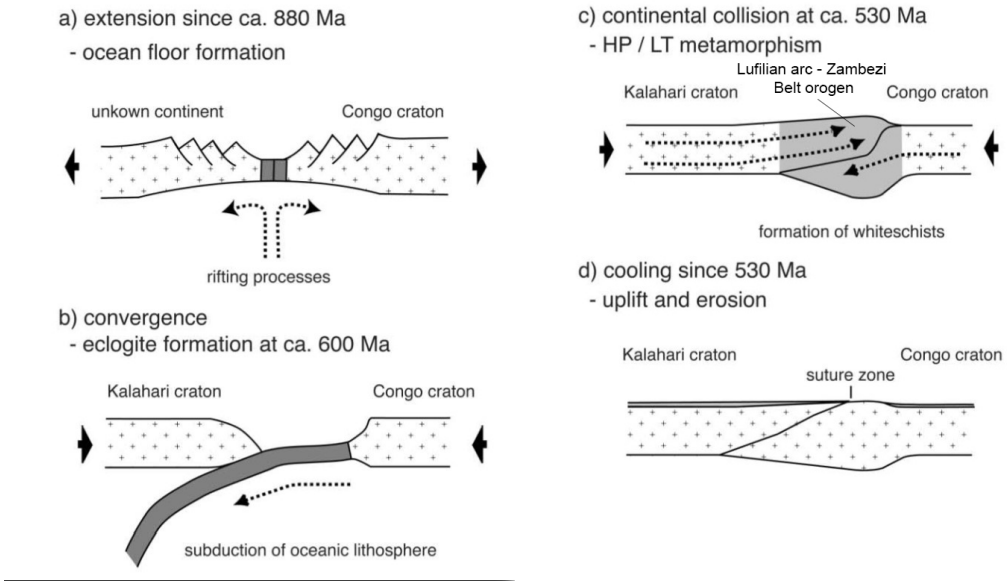

Figure 2.4: Conceptual evolution of the Lufilian Arc - Zambezi Belt orogen, from initial extension post-∼880 Ma to postulated ocean crust development, and subsequent compression and uplift (John et al., 2004).

The Hook Batholith forms an extensive igneous complex South of the Lufilian Arc and has been interpreted to be syn- to post-Lufilian in age, intruding into the uppermost portions of Katangan stratigraphy (Hanson et al., 1993). It represents a calc-alkalic suite, comprising quartz-monzonites, granodiorites, syenites and alkali granites (Naydenov et al., 2014).

2.2 Stratigraphy

The Katangan Supergroup unconformably overlies the Katangan basement, and covers a depositional history of ca. 300 myr (Key et al., 2001; Armstrong et al., 2005; Cailteux and De Putter, 2019). Stratigraphic data is mostly restricted to mines, with only limited work looking at more regional basin architecture (e.g. Porada and Berhorst (2000); Master and Wendorff (2011)). Locations of data used to supplement what is proposed in this thesis are shown in figure 2.5, to illustrate their distribution.

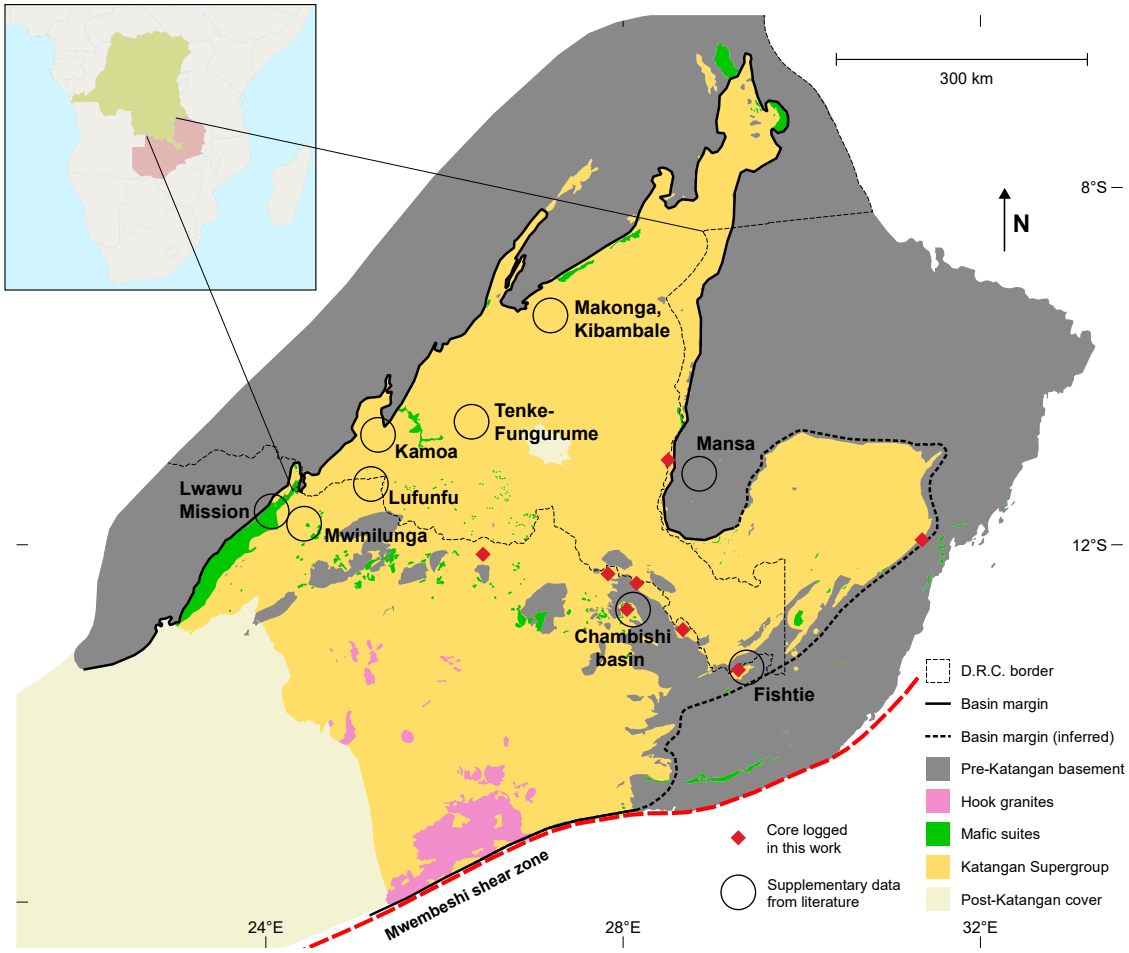

Figure 2.5: Locations of drill cores used in this thesis, and supplementary data from literature across the basin. Note the paucity of data in the central and SW part of the basin, covered by Kalahari sand. Locations are generalised, as some previous studies refer to areas without specifying exact localities. Exact locations, where provided, are found in the following: Lwawu Mission (Key et al., 2001); Mwinilunga, Lufunfu, Makonga, Kibambale, Mansa (Master and Wendorff, 2011); Chambeshi sub-basin (Bull et al., 2011); Fishtie (Hendrickson et al., 2015); Kamoa (Kennedy et al., 2019); Tenke-Fungurume (Mambwe et al., 2020).

Stratigraphic nomenclature for the Katangan Basin has traditionally been derived from local mine stratigraphy, and correlation on the basis of lithostratigraphy. This has lead to a variety of classifications that often differ significantly from one another (Mendelsohn, 1961; Binda and Mulgrew, 1974; Binda, 1994; Cailteux et al., 1994). An example of the variety of lithostratigraphic schemes for the is shown in table 2.6.

Zambian Copperbelt** Group	Formation	Member	Regional (Binda, 1995)	Luanshya*	Nkana-Mindola (Clemmey, 1976)	Nkana-Mindola*	Chambishi*	Nchanga (Binda and Mulgrew, 1974)	Konkola*	Musoshi (Lefebvre, 1989)	Lubembe (Lefebvre, 1989)	Mufulira*	Congolese Copperbelt (Cailteux et al.,1994; Cailteux and Kampunzu, 2002)	
Upper Kundelungu												Mokambo Fm (foreland molasse?)	Kundelungu Group	Plateaux (Ku 3)
												Upper Kundelungu Shales		Kiubo (Ku 2)
														Ku 1.3
														Ku 1.2
	Petite Conglomerate											Petit Conglomerate		Petite Conglomerate (Ku 1.1)
Lower Kundelungu	Kundelungu Shales							Kundelungu Shales				Kundelungu Shales	Nguba Group	Ng 2
														Ng 1.3
	Kakontwe							Kakontwe	Kakontwe	Kakontwe		Kakontwe		Kakontwe (Ng 1.2)
	Grand Conglomerate							Grand Conglomerate	Grand Conglomerate	Grand Conglomerate		Grand Conglomerate		Grand Conglomerate (Ng 1.1)
Mwashia	Upper			Mwashia		Mwashia	Mwashia	Mwashia	Mwashia	Upper Mwashia	Mwashya	Mwashia Shales	Mwashya Group	U. Mwashya (R-4.2)
	Middle							Upper Roan		Lower Mwashia	Mines S.G. R.A.T S.G. (tectonic emplacement?)	U. Dol.		L. Mwashya (R-4.1)
	Lower					Ultra Far Water Formation								
Upper Roan			Carbonate Unit	RU1	Bancroft Fm		Dolomite Formation		Upper Roan	Kanwangungu Fm.		Ibd Shale & Qtzite Inter. Dol.	Roan Group: Dipeta Subgroup	R-3.4/ R-3.3/ R-3.2/ R-3.1 (R.G.S.)
Lower Roan	Kitwe	Antelope	Mixed Unit	RU2; RL3	Antelope Clastics Mbr	Far Water Seds	Sandy Talc Schist	Shale with Grit	Shale with Grit	Kibalongo Fm.	Musoshi Fm.	Glassy Qtzite		
		Chambishi		RL4	Chambishi Dolomites Mbr	Far Water Dol. Dol-Arg Seq.	Cherty Dol. Ibd Arg-Dol.	Chingola Dol. Dol. Schist U. Banded Shale	HW Aquifer	Chingola Fm.	Kitotwe Mbr Kabemba Mbr	U. Arg. Qtzite	Roan Group: Mines Subgroup	Kambove Dolomite (R-2.3)
		Nchanga		RL5	Nchanga Quartzite Mbr	U. Quartzite	U. Quartzite	Feld. Qtzite	HW Qtzite	Pelito-Arkosic Fm.		Marker Grit		
		Rokana			Rokana Evaporites Mbr	Near Water Sediments	Ibd Arg-Dol. Ibd Qtzite-Sh. Ibd Arg Qtzite-Dol. HW Quartzite	Banded Sst U. Pink Quartzite Shale Marker Banded Sst L. Chert Marker				L. Arg. Qtzite A Orebody Inter A/B Formation B Orebody		Dolomitic Shales (R-2.2) Kamoto Dolomite (R-2.1)
		Copperbelt Orebody		RL6	Copperbelt Orebody Mbr	HWArgillite Ore Shale	Ore Shale	L. Banded Shale	Ore Shale	Ore Shale	F.Q.	Inter B/C Formation Mulseam		
	Mindola Clastics	Kafue	Siliciclastic Unit	RL7	Kafue Arenites Mbr	FW Cgl. Arkosic Sst. L. Cgl.	FW Cgl. Ark. and Arg. Cobble Cgl.	Transition Ark. Arkose Conglomerate	FW Cgl. FW Sst. Porous Cgl.	Mutonda Fm.	Sinbi Mbr Lubembe Mbr	C Orebody Sst. Footwall Formation	Roan Group: R.A.T. Subgroup	R.A.T. (R-1)
		Konkola			Basal Quartzites Mbr	FW Transition FW Quartzite Basal Cgl.	FW Quartzite Basal Cgl.		FW Qtzite Pebble Cgl. Basal Cgl.	Kafufya Fm. Chimfunsi Fm.			?	?

Figure 2.6: Table from Selley et al. (2005) summarising several mine-specific lithostratigraphic schemes, and comparing them to a lithostratigraphy of the D.R.C.

The stratigraphy in the Zambian Copperbelt is broadly divided into four lithostratigraphic Groups, from bottom to top: Lower Roan, Upper Roan, Mwashia, Nguba and Kundelungu. These are shown in figure 2.7, and described below. It should be emphasised that throughout this work the stratigraphic Groups being referred to are defined using the sequence stratigraphic correlation 1 proposed in Chapter 4 of the thesis, using the stratigraphic nomenclature from Selley et al. (2005) and Batumike et al. (2007), unless otherwise specified.

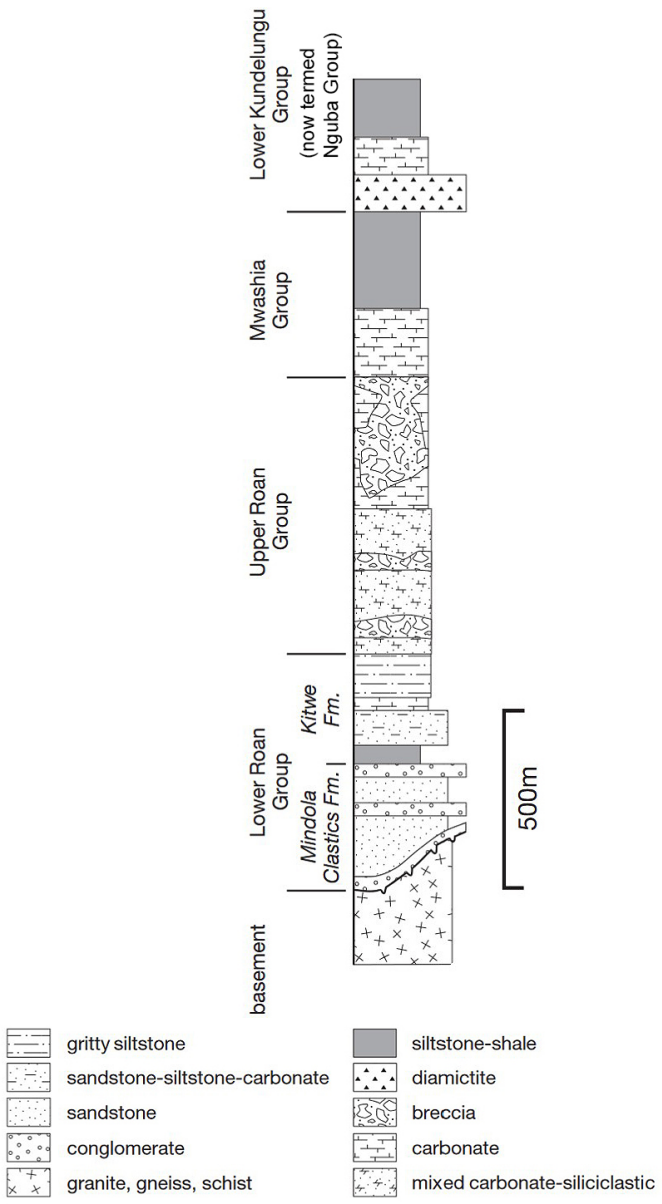

Figure 2.7: Lithostratigraphic log showing a generalised stratigraphy of the Zambian Copperbelt (Selley et al., 2005).

2.2.1 Lower Roan Group

The Lower Roan is traditionally divided into the Mindola Clastics and overlying Kitwe Formations. Binda (1994) proposed the adoption of the term Siliciclastic Unit to describe the Lower Roan and homogenise mine-specific nomenclature. The Mindola Clastics Formation comprises breccias, conglomerates, and texturally immature sandstones of arkosic to arenitic composition (Mendelsohn, 1961; Binda, 1994; Selley et al., 2005). Several conglomerate units may punctuate the Mindola

Clastics Formation, including the 'basal boulder conglomerate', 'second conglomerate' and 'footwall conglomerate', though not all are present throughout the classical Zambian Copperbelt (Binda, 1994). Sandstone units up to hundreds of m's thick may separate individual conglomeratic horizons (Binda, 1994). The Kitwe Formation is traditionally separated from the underlying Mindola Clastics Formation by the Copperbelt Orebody Member (Clemmey, 1976), or Ore Formation (Eden, 1974), containing the ore-bearing horizon locally termed the 'ore shale' on the Western side of the Kafue Anticline (Mendelsohn, 1961; Clemmey, 1976; Eden, 1974). This unit has been lithostratigraphically interpreted to correlated with a mud seam between Formations B and C in the Mufulira deposit on the Eastern side of the Kafue Anticline by Selley et al. (2005). The 'ore shale' varies in composition from wacke, to muddy and often dolomitic siltstone, that may be carbonaceous (Mendelsohn, 1961; Annels, 1974; Eden, 1974; Clemmey, 1974). The remainder of the overlying Kitwe Formation shows a mixed clastic-carbonate composition, resulting in Binda (1994) naming it the 'Mixed Unit'. How these units have traditionally been correlated in the Zambian Copperbelt is shown in fig. 2.8. Carbonate content increases up-section, with interbedded dolomites and silt- or mudstones becoming more laterally extensive (Selley et al., 2005).

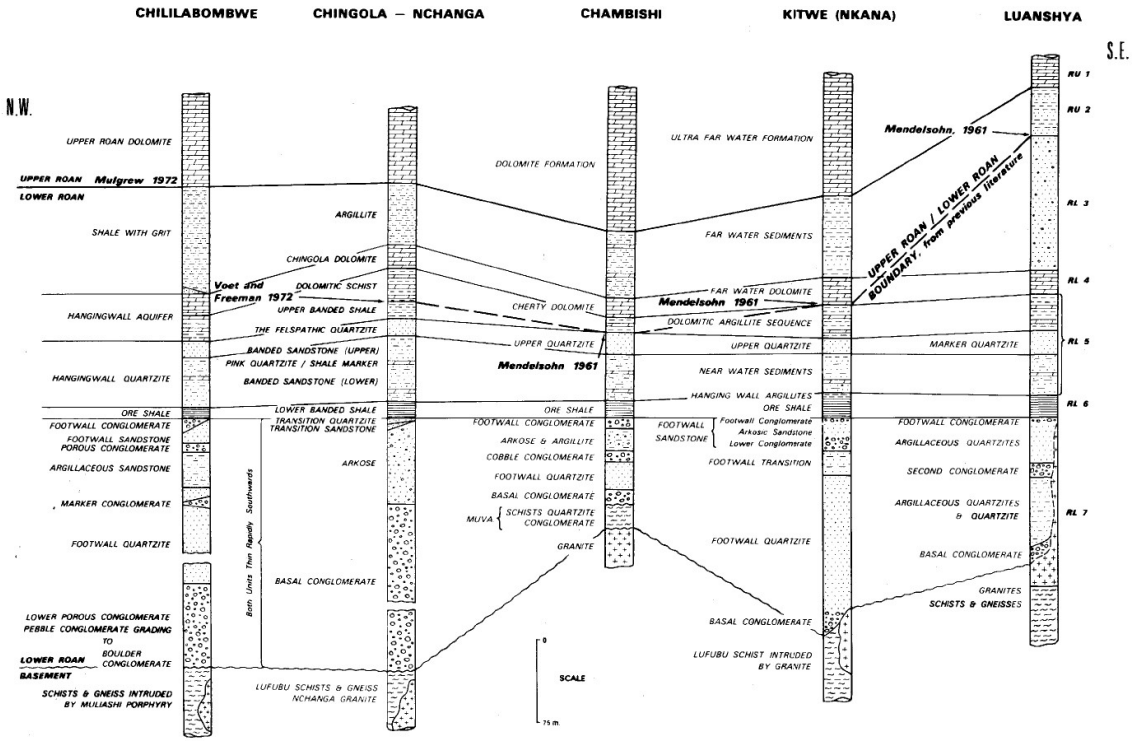

Figure 2.8: Lithostratigraphic correlation of units across the western Zambian Copperbelt along the 'ore shale' unit and its equivalents (Binda and Mulgrew, 1974).

The Mindola Clastics Formation has traditionally been interpreted as representing alluvial fan, fan-delta, and fluvial sedimentation (Sweeney et al., 1986; Binda, 1994; Selley et al., 2005; Bull et al., 2011). Controversy regarding possibly aeolian deposition was outlined by Eden (1974); Binda (1994). Initial syn-rift deposition took place in disconnected troughs and sub-basins (Selley et al., 2005). The introduction of carbonate (predominantly dolomitic) units throughout the Kitwe Formation attests to progressive transgressive conditions (Clemmey, 1976; Selley et al., 2005). However, the general transgressive trend may be punctuated by periods of emergence, with Garlick and Fleischer (1972) describing dessication cracks and replaced anhydrite nodules. These fluctuations, and in parts evaporitic conditions as part of a generally retrogradational trend throughout the upper Lower Roan and into the Upper Roan, have been noted by several authors (Mendelsohn, 1961; Clemmey, 1976; Binda, 1994; Selley et al., 2005; Bull et al., 2011).

The onset of deposition of the Lower Roan Group is poorly temporally constrained. The Nchanga red granite provides an absolute maximum age of 883 $\pm$ 10 Ma (Armstrong et al., 2005). However, a variety of sources point towards a younger, albeit very poorly constrained, age of sedimentation initiation. Cahen et al. (1970) reported Rb/Sr dates for microcline-bearing pegmatite veins of 840 $\pm$ 42 Ma at the Roan Antelope (now Luanshya) and Musoshi mines, and sparse U-Pb dates of detrital zircons at $\sim$840 Ma also suggest deposition significantly post-dates emplacement of the Nchanga granite (Selley et al., 2018).

2.2.2 Upper Roan Group

The Upper Roan Group is characterised by an abundance of carbonates, with minor clastic component and widespread breccias. Its thickness varies, but may be up to 800 m thick (Selley et al., 2005). The interface between Lower and Upper Roan is not formally defined, though the first thick, laterally continuous carbonate unit is classically used as the boundary between the two groups, though its boundary becomes less clear on the Eastern margin of the Kafue anticline, where the 'Glassy Quartzite' unit may be the boundary (Mendelsohn, 1961; Binda, 1994; Selley et al., 2005). Dolomitic carbonates predominate and have been variably classified, often forming part of the Bancroft Formation. They commonly contain nodules of anhydrite and remnant and replaced evaporitic textures (Mendelsohn, 1961; Bull et al., 2011). Lesser quantities of sandstone, siltstone and mud-

stone may be present, and form part of a broad deepening succession (Mendelsohn, 1961; Selley et al., 2005).

Much of the Upper Roan has been interpreted to represent a carbonate platform, with extensive marginal sabkhas and widespread stromatolitic carbonates, possibly as reefs (Clemmey, 1976; Binda, 1994; Bull et al., 2011). Breccia bodies have been variously attributed to tectonism, olistostromes and salt movement (Annels, 1984; Jackson and Warin, 2003; Wendorff, 2005).

2.2.3 Mwashia Group

The Mwashia Group comprises black mudstones, carbonates and silty carbonates. It is a relatively thin unit, characterised by persistently fine grain size, and introduction of mafic bodies; ironstones may also be present (Key et al., 2001; Selley et al., 2005; Master and Wendorff, 2011). The lower boundary of the Mwashia Group is poorly defined; it may be delineated by black mudstones or breccias on a local scale (Selley et al., 2005). It is interpreted as a more regional deepening event, flooding pre-existing carbonate platforms (Selley et al., 2005; Bull et al., 2011). Mafic magmatism is expressed in low-volume, laterally extensive intrusive suites across the traditional Copperbelt, and more voluminous extrusive suites towards the Western part of the basin (Key et al., 2001). The age of the Mwashia is broadly constrained by the ages of mafic extrusive suites at $\sim$765 - $\sim$735 Ma (Key et al., 2001), and Re-Os dating of black shales at $\sim$ 727 Ma (Rooney et al., 2015).

2.2.4 Nguba Group

The Nguba Group comprises a mixed clastic carbonate succession, defined lithostratigraphically by diamictites of the Grand Conglomerat (also referred to as the Mwale Formation sensu (Cailteux and De Putter, 2019)) at its base (Master and Wendorff, 2011; Kennedy et al., 2019). The diamictites are varied in composition and thickness, ranging from 10's m thick in the Zambian Copperbelt to over 1 km thick in the Congolese Copperbelt (Selley et al., 2018; Kennedy et al., 2019). They are frequently overlain by dolomitic mudstones, which, when characteristically striped, are known as the Dolomie Tigrée, and carbonates of the Kakontwe Formation (Batumike et al., 2007). As the Nguba Group is often not well-exposed at-surface and thick (¿1 km) successions have not been intersected in drill core in the Zambian Copperbelt, lithostratigraphic nomenclature (e.g. Dolomie

Tigrée) from the D.R.C. is often borrowed. Much of the upper portions of the group are mixed in composition, but in Zambia tend to comprise fine clastics and carbonate successions (Master and Wendorff, 2011). The Nguba Group has been interpreted to represent a wide, mostly deep basin (Batumike et al., 2007). The age of the basal Nguba has been constrained by contacts with underlying mafic units in the western part of the Zambian Copperbelt at $\sim$ 735 Ma, and is broadly correlated with the Sturtian glaciation (Rooney et al., 2015).

2.2.5 Kundelungu Group

The Kundelungu Group is not well-exposed in Zambia, with lithostratigraphic schemes being predominantly based on the Congolese Copperbelt where it is better preserved. It is lithostratigraphically delineated at its base by a diamictite unit, the Petit Conglomerat, which is generally thinner than the underlying Grand Conglomerat. The Petit Conglomerat is often overlain by the Calcaire Rose, with the rest of the Kundelungu Group comprising generally finer mixed clastic-carbonate successions (Selley et al., 2005; Batumike et al., 2007). The age of the Kundelungu Group is poorly constrained, relying predominantly on the Petit Conglomerat being interpreted to correspond to the Ghaub diamictite in Namibia, and therefore the Marinoan glaciation, broadly dated at 635 ± 1.2 Ma (Hoffmann et al., 2004). The Kundelungu Group is generally interpreted as representing deposition in a quiescent basin, prior to inversion during the Lufilian Orogeny (Batumike et al., 2007; Cailteux and De Putter, 2019).

2.2.6 Comparison to stratigraphy in the D.R.C.

Correlations between stratigraphy in Zambia and the D.R.C. have received attention (Cailteux et al., 1994; Woodhead, 2013), yet the reliance on locality specific lithostratigraphic nomenclature has often hindered a detailed correlation beyond the group-scale. One traditional correlation between the two Copperbelts is shown in figure 2.9, with an up-to-date stratigraphic classification in the D.R.C. being shown in figure 2.10.

A distinction between Lower and Upper Roan has not been adopted for the Congolese Copperbelt stratigraphy. The stratigraphic equivalent to the basal portions of the Lower Roan is not well-expressed in the Congolese part of the basin. The Lower Roan equivalent group and has been traditionally been divided into the 'Roches Argileuses Talqueuses' (commonly abbreviated

<table>
<tr><th colspan="4">ZAMBIA AND MUSOSHI DISTRICT (S. SHABA)</th><th colspan="2">SHABA</th></tr>
<tr><th>UNIT
(Formation)</th><th>MEMBER
(Mine term)</th><th colspan="2">FORMATION</th><th>FORMATION</th><th>GROUP</th></tr>
<tr><td>Mwashia Group

(Mwashia Fm)</td><td></td><td></td><td></td><td>Upper Mwashya
(R-4.2)
Lower Mwashya
(R-4.1)</td><td>Mwashya
(R-4)</td></tr>
<tr><td>Carbonate U.
(Upper Roan ss)
(Bancroft Dol.)</td><td></td><td>Kirilabombwe Group</td><td>Kanwangungu Fm
(RU 1-RU 2)</td><td>(R-3.4)

(R-3.3)</td><td>Dipeta</td></tr>
<tr><td rowspan="5">Mixed Unit

(Kitwe Fm)</td><td>Antelope Clastics
(shale with grit)</td><td></td><td>Kibalongo Fm
(RL 3)</td><td>(R-3.2)
(R-3.1)</td><td>(R-3)</td></tr>
<tr><td>Chambishi Dolomite
(cherty dolomite and dolomitic argillite)</td><td rowspan="4">Musoshi Group</td><td>Chingola Fm
(Chingola Dolomite or RL4 and upper RL5)</td><td>Kambove Dolomite</td><td rowspan="4">Mines

(R-2)</td></tr>
<tr><td>Nchanga Quartzite
(upper quartzite)</td><td>Pelito-arkosic Fm

(RL5)</td><td rowspan="2"></td></tr>
<tr><td>Rokana Evaporites
(hangingwall)</td><td rowspan="2">dolomitic shales (R-2.2.2, R-2.2.3)
S.D.B. (R-2.2.1)
Kamoto Dolomite (R-2.1)</td></tr>
<tr><td>Copperbelt orebody
(ore shale, greywacke)</td><td>Ore Shale Fm
(RL6)</td></tr>
<tr><td rowspan="3">Siliciclastic Unit

'Footwall'
(Mindola Clastics)</td><td>Kafue Arenites
(footwall congl.)</td><td rowspan="3">(RL7)</td><td>Mutonda Fm</td><td>(R-1.3)
(R-1.2)</td><td>R.A.T.
(R-1)</td></tr>
<tr><td rowspan="2"></td><td>Kafufya Fm</td><td rowspan="2">?</td><td rowspan="2">?</td></tr>
<tr><td>Chimfunsi Fm</td></tr>
<tr><td colspan="6">Unconformity
BASEMENT COMPLEX</td></tr>
</table>

Figure 2.9: Lithostratigraphic correlation of units across the Zambian and Congolese (formerly Shaba Province, Zaire) Copperbelts (Cailteux et al., 1994).

to R.A.T.) and Mine Groups, the former more recently being re-named the Musonoï, comprising mixed carbonates and fine-grained clastics (Cailteux and De Putter, 2019).

The Upper Roan in Zambia is broadly equivalent to the Fungurume (formerly Dipeta) Group, comprised of mixed clastics, carbonates and intrusive suites (Cailteux and De Putter, 2019). The Mwashia is common to both the Congolese and Zambian parts of the Katangan basin, but traditionally classified as the Mwashya sub-group, forming part of the Roan Group. In the DRC, the Kamoa sub-basin records terrestrial Mwashia-age units comprising breccias, sandstones, and conglomerates of the 'Poudingue' unit, and sandy turbidites of the Mwashya sub-group (Kennedy et al., 2019). In more basinal settings, the lithology of the Mwashya is broadly similar to that of the Mwashia in Zambia, being shaly and/or dolomitic (Cailteux et al., 1994). The Nguba and Kundelungu Groups broadly lithologically comparable across both sides of the basin, though their thickness, particularly of the Nguba, vary significantly (Selley et al., 2018; Kennedy et al., 2019).

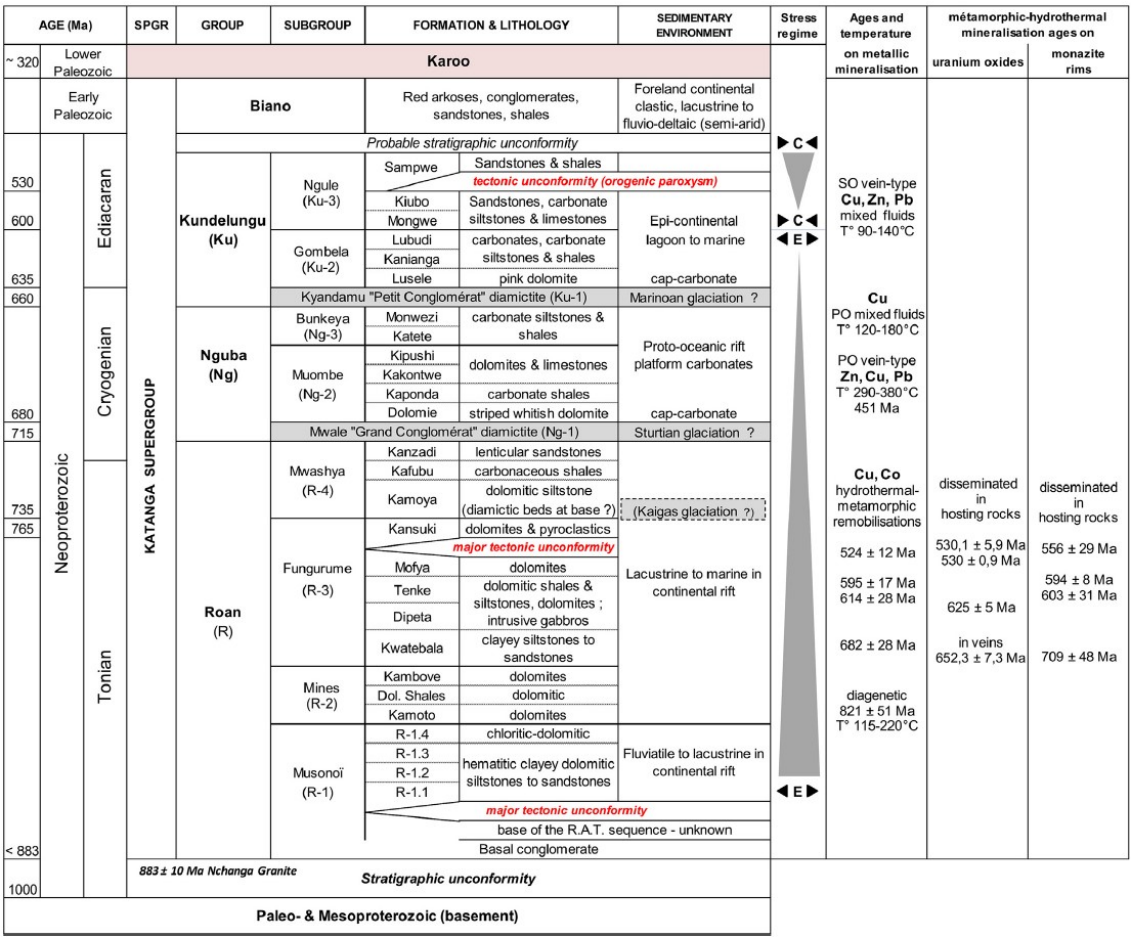

Figure 2.10: The most recent and complete lithostratigraphic classification to-date for the D.R.C. from (Cailteux and De Putter, 2019).

2.2.7 Breccias

Breccias are widespread in the Katangan basin, forming individual horizons or complexes up to 100's thick. They comprise polylithic assemblages of carbonates, mafic clasts and fine clastics, which have undergone significant alteration (Wendorff, 2000; Selley et al., 2005), and are predominantly found in the Upper Roan (and D.R.C. equivalent) units.

Early interpretations of breccias, both in smaller bodies prevalent in the Zambian Copperbelt, and larger ones hosting allochthonous blocks in the Congolese Copperbelt, were predominantly tectonic (Cailteux et al., 1994; Wendorff, 2003, 2005). Wendorff (2003) interpreted some of these breccias as being of sedimentary origin, developed as a result of a compressional regime in the Katangan.

Allochthonous blocks in the D.R.C. were interpreted as having been rafted as part of olistostromes in a northerly advancing foreland succession, and breccia bodies in Mufulira representing syn-rift olistostromes (Wendorff, 2005). This resulted in breccia units being incorporated into contentious alternative lithostratigraphic schemes for the Katangan basin (Wendorff, 2003, 2005).

The currently more accepted view is that Katangan breccias are result of halokinesis and subsequent dissolution (Jackson and Warin, 2003; Selley et al., 2018). Widespread evaporites, thicker in the Congolese Copperbelt than in the Zambian Copperbelt, likely facilitated halokinesis and transport of allochthonous blocks of Katangan stratigraphy prior to, and during, the Lufilian Orogeny (Jackson and Warin, 2003; Selley et al., 2018). No original salt has yet been described in the basin, with most of the evaporite minerals having undergone dissolution, with the resulting breccias representing residual material derived from the surrounding stratigraphy (Jackson and Warin, 2003; Selley et al., 2018; Basson et al., 2023).

2.3 Glaciation

The presence of glaciogenic units in the Katangan basin was first documented by Stutzer (1911), who placed them the Karoo Supergroup and interpreted them as having formed during the Dwyka glaciation. Subsequent regional mapping showed, however, that diamictites in the basin occurred as two laterally extensive units: the Grand Conglomerat, and above it, the Petit Conglomerat (Robert, 1933; **?**, 1940). The Grand and Petit Conglomerat have also been termed the Mwale and Kyandamu Formation, respectively (Batumike et al., 2007). The Grand Conglomerat is sometimes also referred to as the Great Conglomerate (Binda and Van Eden, 1972)

Both the Grand and Petit Conglomerat show varied facies and facies associations. They are predominantly characterised by massive polymict diamictites. Clasts are varied in size, shape and composition, including quartzites, granites and schists (Robert, 1940; Master and Wendorff, 2011). Many of these diamictites show features associated with glaciogenic deposits, with striations, dropstones and lonestones, as well as orthogonal crack networks having been reported, which have been interpreted as patterned ground (Stutzer, 1911; Master and Wendorff, 2011). The majority of the diamictites have classically been interpreted as being deposited in glaciomarine environments (Binda and Van Eden, 1972; Master and Wendorff, 2011). Clast-supported conglomerates and coarse sand-

stones, such as those in the Luapula beds, are interpreted to represent fluvial or glaciofluvial deposits at depocentre margins (Master and Wendorff, 2011).

The Grand Conglomerat forms an extensive marker horizon covering an area in excess of 65000 km^2, in parts being over 1 km thick (Master and Wendorff, 2011). The Petit Conglomerat tends to be thinner, in the order of 10s m thickness, and though less commonly preserved in the Zambian Copperbelt (Selley et al., 2005), appears to be equally laterally extensive (Wendorff and Key, 2009; Master and Wendorff, 2011). Both the Grand and Petit Conglomerat are often overlain by regionally extensive carbonate units. The Grand Conglomerat is overlain by the Kakontwe Limestone, and Petit Conglomerat by the Calcaire Rose (Master and Wendorff, 2011).

Haematitic and jaspilitic banded ironstones and formations have been reported below, and associated with, the diamictites of the Grand Conglomerat in Zambia, in and north of the Domes region as part of the Mwashia (Porada and Berhorst, 2000; Master and Wendorff, 2011; MacIntyre, 2019). They are also known to occur above the Grand Conglomerat in the Nguba Group, and have been inferred to co-occur with glacial successions in the Katangan (Wendorff and Key, 2009).

The Grand Conglomerat and Petit Conglomerat are correlated globally with the Sturtian and Marinoan glaciations, respectively, and more locally with the Chuos and Ghaub diamictites in the Damaran orogenic belt (Hoffmann et al., 2004; Wendorff and Key, 2009). Despite the Katangan diamictites's similarities to their Namibian counterparts (e.g. similar tectonic settings, C-isotope patterns and stratigraphic carbonate-diamictite relationships), age constraints on their formation remain poor (Selley et al., 2005; Master and Wendorff, 2011; Halverson et al., 2020; Xiao and Narbonne, 2020). Altered porphyritic volcanic pods in contact with the Grand Conglomerat in the western part of the basin were dated by Key et al. (2001), providing a maximum age of the Grand Conglomerat sedimentation of 735 Ma. Rooney et al. (2015) used Re-Os geochronology to constrain the Sturtian glaciation globally from 717 - 660 Ma, with shales immediately below the Grand Conglomerat being dated at 727.3 $\pm$ 4.9 Ma. Bodiselitsch et al. (2005) showed that there were pronounced iridium anomalies in carbonates above the Grand and Petit Conglomerat. These were invoked to have been formed by extraterrestrial material, rich in iridium, settling on ice sheets that was incorporated into post-glacial sediments upon melting to generate a positive Ir-excursion. It was estimated that the duration of the Marinoan glaciation was greater than 3 Myr, and most likely 12 Myr (Bodiselitsch et al., 2005).

Though many diamictites in the Katangan basin show evidence of glacial origins, Kennedy et al. (2019) showed that diamictites in the Kamoa sub-basin, and likely many others in the Katangan basin, could only rarely be directly attributed to glacial processes. Instead, many represent debris flow deposits, that could be highly diachronous and that any glacial evidence is often obscured by re-working.

Eyles and Januszczak (2004) suggested that the progressive and diachronous rifting along Congo and Kalahari cratons during the Neoproterozoic generated many of the diamictites that had previously been interpreted as glacial. This would suggest that though glaciation was widespread, the chronostratigraphic relevance of individual diamictite units may be more related to rifting than global glaciation.

2.4 Mafic magmatism

Mafic suites are abundant in the Katangan basin. In the eastern part of the basin, they form abundant low-volume intrusive bodies of mafic to intermediate composition (Mendelsohn, 1961; Kampunzu et al., 1991; Cailteux et al., 1994; Selley et al., 2005). Their distribution in the basin broadly follows the Lufilian arc (Tembo et al., 1999). The western part of the Katangan basin contains pyroclastic units and larger volumes of laterally extensive mafic suites, which can be traced for 150 km into Angola (Unrug, 1983; Key et al., 2001; Kennedy et al., 2019).

Igneous rocks are commonly associated with the Upper Roan and Mwashia Groups; as both intrusive and extrusive bodies. SHRIMP U–Pb dating has constrained their emplacement to $\sim$765 - $\sim$735 Ma (Key et al., 2001) Upper Roan igneous bodies are predominantly intrusive, interpreted as hypabyssals commonly doleritic or gabbroic in composition (Clemmey, 1976; Cailteux et al., 1994; Selley et al., 2005). However, isolated occurrences of lamprophyres intruding Lower Roan sediments have been described in Nkana, where an ilmenite-bearing, biotite-rich intrusion cross-cuts basement schists and the Lower Roan have been described (Jordaan, 1961). So far, no extrusive volcanics have been proven to be of Lower or Upper Roan age in Zambia.

Both extrusive and intrusive suites are more abundant and laterally extensive in the Mwashia Group (Tembo et al., 1999; Kampunzu et al., 1991; Key et al., 2001). In Zambia, the largest volumes of mafic rocks occur in the North-West, comprising volcanic pods, basaltic-andesites and massive and

banded lavas, with amygdaloidal pillow lavas being described at Lwawu Mission (Key et al., 2001). Mwashia extrusives and pyroclastic material has been documented in the D.R.C. at several locations including Shituru and Kambove (**?**Cailteux et al., 1994), with ignimbrites described in Mulungwishi (Lefebvre, 1977).

Mwashia magmatism is seen to record renewed extension of the basin, associated with continental breakup (Cailteux et al., 1994; Key et al., 2001; Selley et al., 2005). Bulk geochemical analysis of Katangan igneous rocks matches that of those in known continental rifts (see fig. 2.11) (Cailteux et al., 1994).

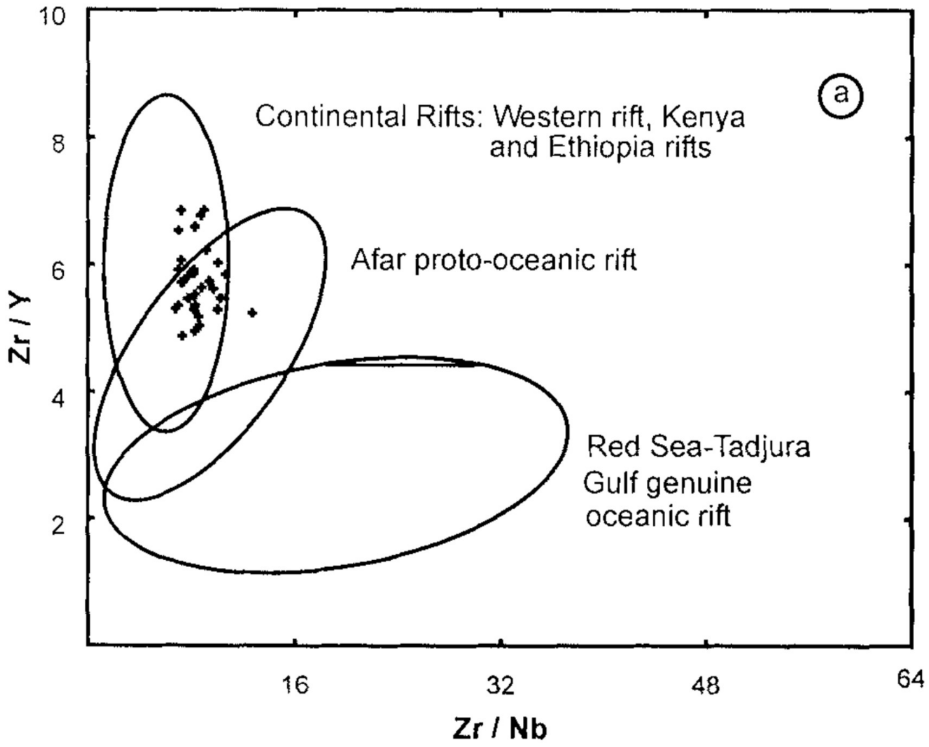

Figure 2.11: Mafic samples from the Domes region plotted on a Zr/Y versus Zr/Nb tectonic discrimination diagram, showing clear geochemical similarities to modern early rift and proto-oceanic rift settings in Africa (Kampunzu et al., 2000).

Mafic rocks appear to be genetically related, having similar geochemical signatures across the basin (Tembo et al., 1999). Enrichment in incompatible elements indicates limited interaction with, and incorporation of, crustal material (Tembo et al., 1999). Mafic suites appear to have been derived from alkaline and tholeiitic magmas (Tembo et al., 1999; Kampunzu et al., 2000), with ferrodiorites and immobile trace element compositions indicating an Ethiopian or Afar type rift basin setting (Kampunzu et al., 2000). This is supported by rift-related stratigraphic architecture during Mwashia

times (Key et al., 2001; Kennedy et al., 2019). Towards the northern portion of the basin, outcrops near Kibambale show enriched mantle (E-MORB) signatures, which have been interpreted to represent a more mature, Red Sea type rift basin (Kampunzu et al., 1991; Tembo et al., 1999; Kampunzu et al., 2000). This is supported by the presence of andesitic volcanics in the Mwashia Group, suggesting the Katangan evolved from a continental rift into a primitive ocean basin (Kampunzu et al., 2000; Key et al., 2001).

Evidence of rifting to the south-west of the Katangan basin is found in igneous rocks of similar ages in the Damara Belt of Namibia. Pegmatite veins and syenites in the Toekems sub-basin yield ages of 763 $\pm$ 5 Ma and 756 $\pm$ 2 Ma, respectively (McGee et al., 2012). Similar ages were also determined from zircons in rhyolites of the Gariep Belt of Namibia (Frimmel et al., 1996). This suggests widespread magmatism and rifting from south-eastern to the south-western margins of the Congo craton (McGee et al., 2012).

2.5 Basin forming mechanisms

Despite detailed deposit studies having been published across the Katangan, basin forming mechanisms have remained contentious (Mendelsohn, 1961; Binda, 1994; Kampunzu and Cailteux, 1999; Selley et al., 2018).

Initial ideas involved gradual infilling of steep Katangan palaeotopography, followed by a marine transgression (Mendelsohn, 1961; Binda, 1994). Evidence included the absence of syn-rift basaltic magmatism, ophilites or development of ocean crust, dyke swarms or magnetic anomalies that would indicate rifting, and apparent paucity of syn-depositional faults (Binda, 1994; Selley et al., 2005).

However, a rift origin for the basin is now generally favoured on account of abundant stratigraphic and structural similarity to modern Phanerozoic rift systems (Kampunzu and Cailteux, 1999; Gawthorpe and Leeder, 2000; Selley et al., 2005, 2018). The geometry of sub-basins and fault networks in the Lower Roan matches that of archetypal rift systems, as does the gross stratigraphic architecture (Selley et al., 2005). Coarse basal clastics, rapid transitions between immature, predominantly clastic, facies in the Lower Roan, followed by submergence and development of extensive carbonate platforms similarly matches that of modern rifts (Kampunzu and Cailteux, 1999; Gawthorpe and

Leeder, 2000; Selley et al., 2018). Further evidence of rifting occurs later in the basin's history during Mwashia times, where tholeiitic magmatism becomes abundant and debris flows indicate renewed topography-generation (Key et al., 2001; Kennedy et al., 2019).

2.6 Mineralisation history

Mineralisation models for the Zambian Copperbelt have evolved over time, from early epigenetic and syngenetic models to diagenetic-hydrothermal. Early epigenetic models invoked hydrothermal fluids circulating through Katangan sediments due to granite-emplacement (Jackson, 1932; Sweeney et al., 1991) These ideas were questioned by Schneiderhöhn (1932), who identified an unconformable contact of the Katangan Supergroup on granitic basement. Subsequent syn-genetic models relied on the distribution of minerals seemingly matching the geometry of palaeoshorelines (Garlick and Fleischer, 1972; Sweeney et al., 1991). However, facies distributions do not clearly align with sulphide zonation, and metasomatic alteration is difficult to explain using syngenetic mineralisation models (Sweeney et al., 1991). Diagenetic-hydrothermal processes are now favoured. These invoke saline fluid flow derived from interaction with evaporites and driven by extension, with metals, sourced from red-beds undergoing diagenesis, being precipitated at reducing horizons (Sweeney et al., 1991; Hitzman et al., 2005; Selley et al., 2005).

This aligns with accepted models of the archetypal sediment-hosted copper system, which involves several key components, including 1. red-bed clastics as a Cu-source, 2. a source of sulphur, commonly evaporitic, 3. low to moderate temperature saline aqueous fluids as a transport medium, 4. focusing of fluid flow to a precipitation site, 5. precipitation of sulphides at a reducing surface (Hitzman et al., 2005, 2010). This is shown in figure 2.12.

Mineralisation is widespread in the Katangan basin, with ore deposits broadly distributed along the Lufilian arc, and occurring at several stratigraphic levels, including the Lower Roan (e.g. Mufulira), Mwashia/Nguba (e.g. Frontier), and Nguba (e.g. Kamoa). Their stratigraphic distribution in the Zambian Copperbelt is shown in fig. 2.13. Mineralisation styles are equally varied, ranging from disseminated to pre- and post-folding vein-hosted, shearzone-hosted, and/or with a supergene component. (Binda and Mulgrew, 1974; Torrealday et al., 2000; Selley et al., 2005; Schmandt et al., 2013; Hendrickson et al., 2015).

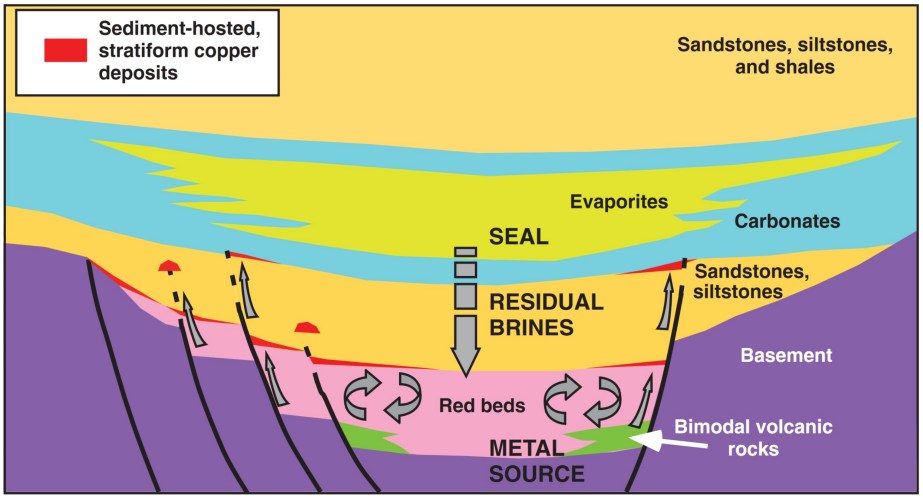

Figure 2.12: An idealised model of the sediment-hosted Cu-deposits, showing fluid circulation through red bed clastics as the Cu-source, evaporites providing a seal and source for saline brines, and faults that provide a fluid pathway towards reductants and Cu-pricipitation sites (Hitzman et al., 2010).

Ages of mineralisation vary considerably, from Lower Roan to Mwashia and post-Lufilian (Muchez et al., 2015). Disseminated sulphides from Kamoto show Re-Os ages of 821 $\pm$ 51 Ma, 820 $\pm$ 62 Ma, and 762 $\pm$ 33 Ma, indicative of diagenetic mineralisation occurring shortly after initial Lower Roan extension (Muchez et al., 2015). It is unclear, however, whether these ages represent individual mineralisation events or a prolonged period of sulphide precipitation.

Sillitoe et al. (2017) argued that both disseminated and vein-hosted mineralisation in the Zambian Copperbelt occurred during the late stages of the Lufilian orogeny, between $\sim$ 540 - 490 Ma, on the basis of Re-Os molybdenite ages. However, though molybdenite mineralisation appears to be late-Lufilian in age, Hitzman and Broughton (2017) clarified that this likely does not apply to all mineralisation in the Zambian Copperbelt, and that there is still ample evidence to suggest diagenetic mineralisation and sulphide precipitation over large timescales. The evidence includes sulphides occurring interstitially between detrital grains and authigenic cement, foliated and deformed sulphides which are cut by Lufilian-age mineralisation, and sulphides being associated with palaeo-redox boundaries (Hitzman and Broughton, 2017).

In the classical Zambian Copperbelt, mineralisation is restricted to the Lower Roan. A distinction is generally made between mud-rich, argillite- or siltstone-hosted and arenite-hosted ore deposits (Binda and Mulgrew, 1974; McGowan et al., 2003; Selley et al., 2005). The mud-rich, often

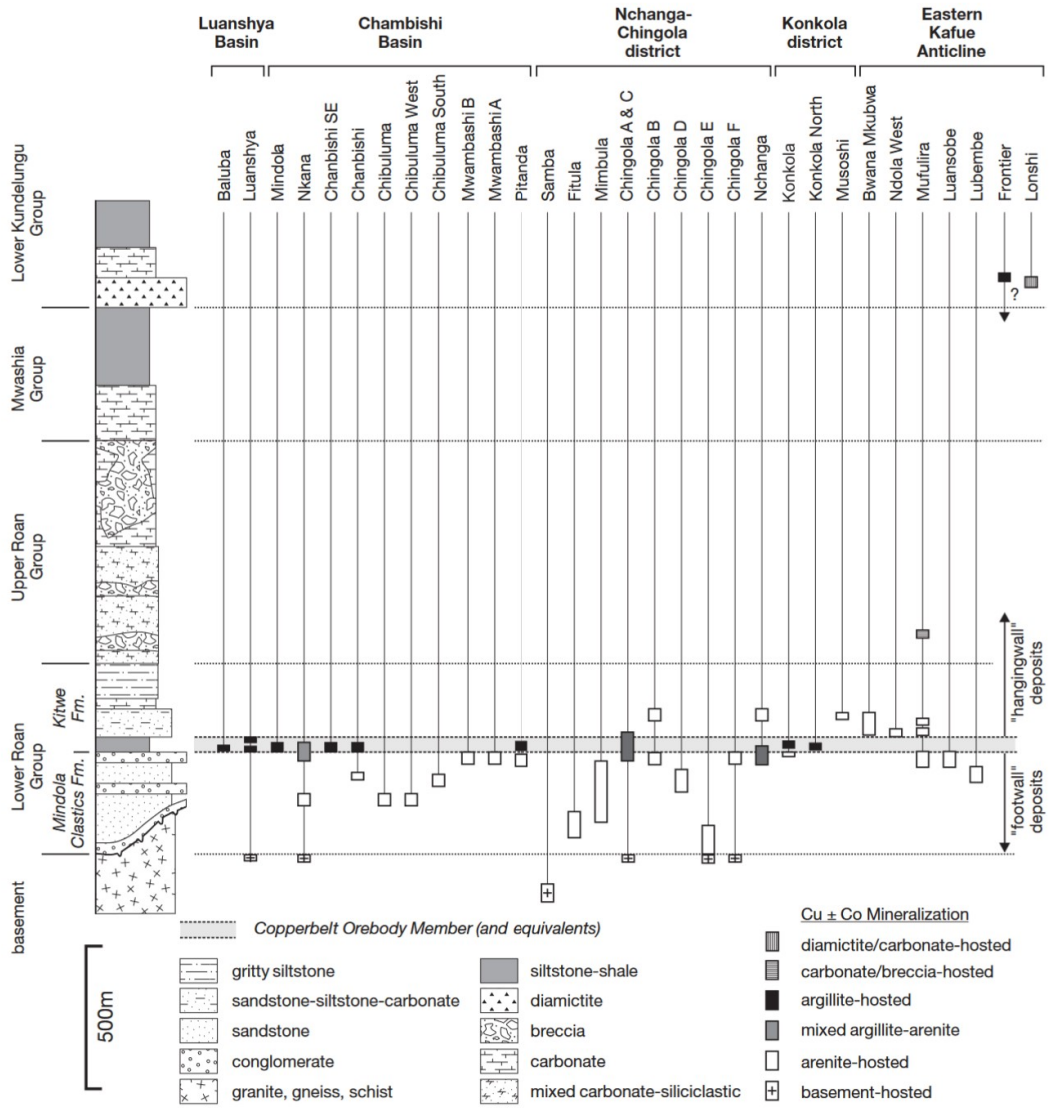

Figure 2.13: Stratigraphic distribution of mineralised horizons in the Zambian Copperbelt (vertical scale approximate), showing mineralisation existing predominantly in the Copperbelt Orebody Member, but also occurring much higher in the stratigraphy (Selley et al., 2005).

argillite, deposits are more laterally extensive along-strike, tend to be dolomitic, and may be carbonaceous. These account for more ore volume than their arenite-hosted counterparts (Binda, 1994; Selley et al., 2005).

Arenite-hosted deposits occur both above and below the ”ore shale” unit, or in both the ”Hanging Wall” and ”Footwall”, in local Copperbelt terminology. They are often lenticular in geometry, with shorter extents along-strike, occurring at sites that share similarities with structural hydrocarbon traps (Selley et al., 2005). That hydrocarbons played a role in the precipitation of sulphides has

been invoked for some arenite-hosted Cu-deposits (e.g. Mufulira, Mwambashi). Strongly depleted carbon-isotope values, and structurally favourable geometry hydrocarbon traps support this model, where hydrocarbons would represent a mobile, buoyant, reductant for ore fluids to precipitate their metal budget at (McGowan et al., 2003; Selley et al., 2005).

The Fishtie Cu-deposit in Zambia, and Kamoa Cu-deposit in the D.R.C. show that mineralisation is not restricted to the basal portions of the Katangan stratigraphy (Broughton and Rogers, 2010; Schmandt et al., 2013; Hendrickson et al., 2015). The Fishtie deposit is located on the south-eastern margin of the basin in a small sub-basin. It hosts $\sim$ 55 Mt Cu with a grade of 1.04 % at a 0.5 % Cu cut-off. It comprises Cu-oxides, sulphides and mixed oxide-sulphide ores, which occur adjacent to faults, possibly of synsedimentary origin, within the siltstones and diamictites of the Nguba Group (Hendrickson et al., 2015).

The Kamoa deposit in the north-western part of the basin, in the D.R.C., hosts 759 Mt of ore at 2.57 wt% Cu (Twite et al., 2019) and is the most recent discovery in the Katangan basin. It comprises laterally extensive stratiform mineralisation hosted in thick diamictites of the Nguba Group that overlie terrestrial Mwashia clastics (Broughton and Rogers, 2010; Schmandt et al., 2013; Twite et al., 2019). Mineralisation is restricted to the uppermost Mwashia and lowermost Nguba successions (Schmandt et al., 2013). Sulphide precipitation appears to have occurred in two stages, the second being mineralising. Mineralisation appears to have occurred in a single event, compared to the more common multiple mineralisation events, on account of sulphur isotope ranges being restricted (Schmandt et al., 2013).

The Kansanshi Cu-Au deposit in the Domes region of Zambia contains an estimated 267 Mt of ore at 1.28 wt% Cu with 0.16 g/t Au. It differs from its sediment-hosted counterparts by being hosted in intensely sheared Katangan metasediments, comprising biotite-garnet schists, phyllites and marbles (Torrealday et al., 2000; Broughton et al., 2002). Mineralisation is predominantly vein hosted, but also occurs as finely disseminated pyrrhotite, chalcopyrite and bornite (Kampunzu et al., 2009). Re-Os dating of molybdenite yielded mineralisation ages of 512 Ma and 502 $\pm$ 1.2 Ma, during basin inversion (Torrealday et al., 2000; Kampunzu et al., 2009).

Combined, these deposits make the Katangan basin one of the most significant copper-producing regions in the world (Hitzman et al., 2005). Deposits in the D.R.C. and Zambia together accounted for approximately 14% of global copper supply (USGS, 2023).

Chapter 3

Application of facies analysis in the Zambian Copperbelt and its stratigraphic implications for the Katangan basin

3.1 Introduction

Many detailed descriptions of Katangan stratigraphy and sediments in Zambia have been made – particularly at a mine scale (Mendelsohn, 1961; Clemmey, 1974, 1976; Eden, 1974; Binda, 1994); however, they have not been placed in a facies framework that can (a) be applied across the Zambian Copperbelt and (b) relates facies to each other. Consequently, interpretation of sediments has tended to be limited to individual cores or lithostratigraphic units. This has complicated the understanding of the basin's stratigraphy and depositional systems, leading to a multitude of lithostratigraphic correlations, and debate surrounding interpretation of certain units (Mendelsohn, 1961; Eden, 1974; Garlick, 1981; Binda, 1994; Cailteux and De Putter, 2019).

Facies descriptions have generally been more extensive in the Democratic Republic of the Congo (D.R.C.) than in Zambia. Facies in the Mwashya and Nguba Groups in the D.R.C have been described in detail by Schmandt et al. (2013); Kennedy et al. (2019); Twite et al. (2019); Delpomdor

et al. (2020); Mambwe et al. (2020), with facies in the Kundelungu Group described in Batumike et al. (2007). Facies of the Grand Conglomerat across the basin were described by Wendorff and Key (2009) and Master and Wendorff (2011).

Similar facies schemes are rare in the Zambian Copperbelt, with Bull et al. (2011) establishing a facies scheme for the Chambishi sub-basin. Binda (1994) proposed the idea of a ”unitarian treatment of the Copperbelt stratigraphy, thereby improving the understanding of regional depositional patterns”. This chapter expands on the above by applying a facies analysis approach to the entire Katangan stratigraphy in the Zambian Copperbelt.

The term facies was first used by Gressly (1838) to describe the lithological and palaeontological characteristics of a stratigraphic unit and relate them to their origin. Walther (1894) expanded on this by developing the idea that vertical successions of facies reflect lateral shifts in depositional environment. Since then, facies analysis and facies models have evolved to encapsulate and better understand the complexity of a wide range of depositional environments, e.g. Reading (1978); James and Dalrymple (2010); Miall (2013). This work follows the definition of Teichert (1958) as ”the sum of lithologic and paleontologic characteristics of a sedimentary rock from which its origin and the environment of its formation may be inferred.”

The purpose of this work was three-fold: 1. To create a comprehensive basin-scale facies scheme robust enough to cope with variability between mines, and natural sedimentological variation. 2. For the facies scheme to provide an intuitive framework that is expandable and flexible enough to be applied at, and adjusted to, different scales of observation. 3. Fit facies units into a framework of facies associations and successions to allow for a first-order interpretation of gross depositional environments from drill core.

Standardised facies schemes for a variety of depositional systems are well-established (Eyles et al., 1983; Pickering et al., 1986; Miall, 2013), but they tend to be focused on Phanerozoic systems, and often require outcrop and the observed relationships of architectural elements to one another for interpretation (Miall, 1985). The facies framework presented here is intended to fit both the inherent constraints and advantages of available data in the Katangan basin: limited outcrop and abundant continuous drill core.

3.2 Methodology

11503 m of diamond drill core were logged in ten cores across the Zambian portion of the Katangan basin (fig. 3.1). Physical core logging was supplemented by high-resolution imagery generously provided by First Quantum Minerals Ltd. and the Lubambe Copper Mine.

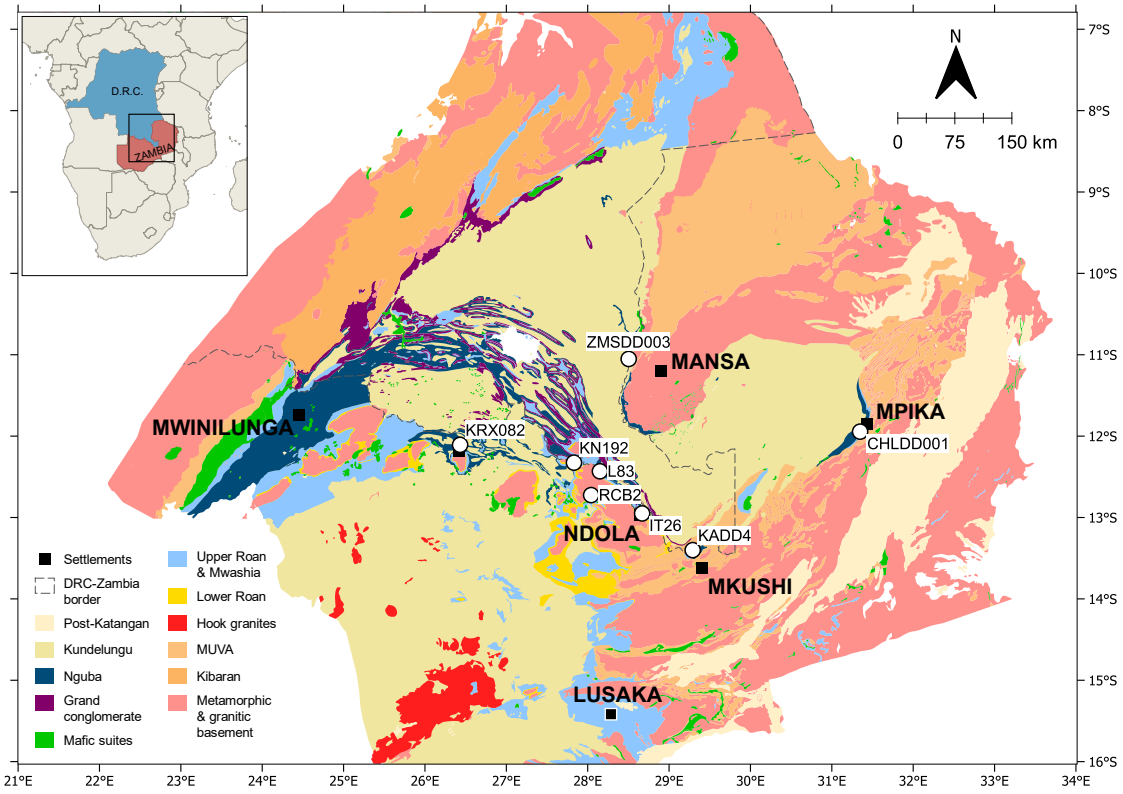

Figure 3.1: Geological map of the Zambian Copperbelt, showing core distribution. Collar codes and locations: KRX082 (Solwezi), KN192 (Lubambe, Konkola sub-basin), RCB2 (Chambishi sub-basin), L83 (Mufulira), IT26 (Ndola), KADD04 (Lusale), ZMSDD003 (Mansa), and CHLDD001 (Chilonga).

Cores were logged on a m-scale, and on a dm-scale or cm-scale where facies variation was high, sedimentary structures were well-preserved, or surfaces were deemed to be of stratigraphic significance (e.g. interpreted unconformities, flooding surfaces).

Facies were described in detail by eye using a hand lens and defined based on their composition, macroscopic texture (after Wentworth (1922)), sorting, grain shape, and sedimentary structures, bedding and bed contacts (Ingram, 1954). Lithological classification was based on Pettijohn et al. (1987) and Dunham (1962). Estimates of carbonate content were based on acid tests on core or

visually estimated abundance of discrete carbonate grains, where present. Colour was not used as a diagnostic measure, as it was not always a primary facies characteristic due to pervasive alteration. Clast counts of clasts exceeding 1 cm in diameter were performed at 0.5 m intervals on the two diamictite units in the ZMSDD003 core. Facies were only ascribed to units thicker than 30 cm.

Facies occurrences were counted, and thicknesses of facies units measured where feasible. Facies unit thicknesses (i.e. the aggregate thickness of beds in a succession comprising a single facies) could be accurately measured for 65% of total core length. In 35% by length of core, contacts between facies units were indistinct or gradational, which compromised comparable facies thickness measurement. Facies proportions expressed as percentages therefore represent the proportion of a given facies with respect to the total length of core in which facies thicknesses could be non-arbitrarily measured. Facies were placed into facies associations: groups of facies that were observed to recur and had genetic commonalities (Anderton, 1985). Type examples of facies successions were selected to illustrate the transitions between different facies associations. Facies successions allow definition of general depositional environmental trends which were quantified for different stages of basin evolution. Descriptive facies definitions are tabulated, and provided in full in Appendix I. This is to 1.) characterise in detail facies which have not been described previously, 2.) emphasise how facies in the scheme are distinguished, 3.) show how the proposed facies scheme complements or deviates from established facies and lithostratigraphic units in the literature.

Facies in this scheme were also compared to previously described facies for the Zambian Copperbelt (e.g. Binda and Van Eden (1972); Bull et al. (2011); Master and Wendorff (2011)). Due to the variety of lithostratigraphic schemes developed for the Zambian Copperbelt (e.g. Mendelsohn (1961); Binda (1994); Selley et al. (2005)), facies described herein have also been compared to units that are not formally facies, or have strict definitions, but are well-established informally in the Zambian Copperbelt (e.g. 'shales with grit' (Mendelsohn, 1961)). Two cores logged in this thesis, RCB2 and IT26 from the Chambishi sub-basin and Ndola, respectively, have been logged previously by Bull et al. (2011) and RCB2 also by Woodhead (2013).

As deposits are often named after nearby settlements, to avoid ambiguity, names such as 'Mufulira', 'Lubambe', etc. will throughout this thesis refer to localities or areas; where deposits or mines are meant, they will be described as such, e.g. 'Mufulira deposit', 'Kansanshi mine' etc. .

3.3 Facies scheme

The facies scheme consists of 9 facies classes, containing 36 including facies and sub-facies (table 3.1). It is arranged in order of increasing grain size and/or carbonate content. These facies make up 17 facies associations that are ascribed to 5 broad depositional environments (table 3.2). Not all listed facies or facies associations need to be present to define a given facies association or depositional environment, respectively. However, interpretations will generally become more robust the more are present.

The proposed framework is hierarchical and allows for new facies to be incorporated into the scheme, or existing facies to be further subdivided, depending on the scale of interpretation required.

Facies class	Code	Facies, *sub-facies*	Recognition criteria	Lithology	Structure	Depositional process interpretation
Fine-grained	dMs	Dark mudstone	- Dark laminated mudstone containing < 10% silt	- Mudstone - rare silty laminae (< 10%) - often carbonaceous	- Continuous planar lamination - Sets of thin laminites - Fissile in parts	- Low energy, settling out of suspension (Pickering et al., 1986) - Low energy, starvation of coarse sediment supply (Trabucho-Alexandre, 2015)
Fine-grained	SlMs	Silty mudstone	- Mudstone containing 10 – 50 % silt to fine sand	- Mudstone - Often carbonaceous - Silt, fine sand (10 – 50 %)	- Thick laminae, mostly planar, rarely wavy, forming laminites - Laminae often sharp-based, fining-up - Rare mudclasts, and intraclast conglomerates	- Low energy settling out of suspension, periodic agitation by wave action (Pickering et al., 1986) - Low energy starvation of coarse sediment supply (Trabucho-Alexandre, 2015)
Fine-grained	LSl	Laminated siltstone	- Siltstone - Abundant lamination, often striped appearance	- Siltstone - Minor fine sandy laminae (< 10%)	- Continuous planar or wavy lamination, often fining upwards from a sharp base - Frequent laminites - Scour marks, gutter casts - Ripple cross-lamination, often in dm-scale co-sets - Isolated soft-sediment deformation structures	- Low energy settling out of suspension, periodic agitation by wave action (Pickering et al., 1986) - Repeated thin fining-up units could represent deposition from very dilute turbulent flows (Stow and Shanmugam, 1980)
Muddy sand	SstMs	Sandy mudstone	- Very poorly sorted - Mixed mudstone, sand - ≥ 50% mudstone and siltstone punctuated by laminae and thin beds of sand or gravel	- Mudstone, siltstone (≥ 50%) - Sand and gravel, often arkosic - Rare anhydrite (< 10%) - Sand grains fine to gravel-sized, moderately to highly rounded, low to high sphericity	- Muddy units show abundant thin continuous and discontinuous wavy lamination - Sandy laminae, wavy or discontinuous - Coarser beds show basal scour - Granule to fine gravel intraclasts abundant - Upward-increase in mud:sand ratio common - Poor sorting - Bed thickness generally thin to medium	- Mud-rich cohesive flows deposited via cohesive freezing (Lowe, 1982; Dasgupta, 2003; Talling et al., 2012; Shanmugam, 2021). - Flows sufficiently competent to transport granule-sized clasts, but insufficiently turbulent to generate grading (Lowe, 1982; Lowe and Guy, 2000)
Muddy sand	Wck	Wacke	- Very poorly sorted mud-sand admixture - Varied and abundant structures - 15 – 50% mud, silt	- Sandstone, often arkosic (50 – 85%) - Sand grains medium to gravel-sized, angular to rounded with moderate to high sphericity - Mud, silt (15 – 50%)	- Sandy units may be chaotically structured, graded, or massive - Primitive planar and trough cross-lamination - Sand lenses, abundant discontinuous lamination - Bed thickness tends to be medium - Diffuse cm to dm-scale interbedding of muddy and sandy units common	- Deposited rapidly from sand-rich sediment gravity flows (Talling et al., 2012, Shanmugam, 2021) - Fluid turbulence was either dampened or restricted to certain parts of the flow (Lowe, 1982; Nemec and Steel, 1984; Shanmugam, 2000) - Cross-laminated units could represent re-working by currents, hyperpicnal input (Zavala, 2020)
Muddy sand	MsSst	Interbedded mudstone and sandstone	- Mudstones and sandstones interbedded in varying proportions	- Mudstone, siltstone - Sand, commonly arkosic or sub-arkosic - Rare carbonate grains (<10%) - grains fine to very coarse, variable roundness, sphericity	- Muddy units variably laminated Sandy units may show: - Graded sandy units, primitive Bouma sequences - Cross-stratification, variable lamination - Variable sorting - Thinly to thickly bedded	Varied, may include: - Turbulent, dilute sediment gravity flows (Pickering et al., 1986; Talling et al., 2012, Shanmugam, 2021) - High-density turbulent flows (Lowe, 1982) - Sandy debris flows (Shanmugam, 1996, 2000) - Currents in the lower flow regime (Allen, 1966; Miall, 2013) - Bottom currents (Stow and Smillie, 2020)
Muddy sand	*MsgSst*	*Interbedded mudstone and graded sandstone*	- Interbedded graded sandstone and laminated mudstones, siltstones - Mudstone, siltstone	- Mudstone, siltstone (≥ 50%) - Sandstone fine to coarse-grained - Sand grains are sub-rounded to rounded with moderate	- Primitive Bouma sequences Muddy units: - Abundant lamination - Thinly to medium-bedded Sandy units:	- Low-density, highly turbulent flows (Talling et al., 2012; Shanmugam, 2021) - Sandy units likely represent bedload, muddy beds the lofted portion of the flow which settles out of suspension (Lowe, 1982; Garcia, 1994; Haughton et al., 2009)

			≥ 50% of the sub-facies	to high sphericity	- Fining up to fine sand on a cm to dm-scale - Sharp, scoured or graded bases - Thinly to thickly bedded	- Where bases of sands are graded, bottom currents (Stow and Smillie, 2020)
Muddy sand	*tMsSst*	*Thinly interbedded mudstone and sandstone*	- Interbedded sandstones, thin intercalated mudstone or siltstones - < 10% mudstone, siltstone	- Sandstone, often arkosic - Sand grains are angular to sub-rounded with moderate to high sphericity - mudstone, siltstone (< 10%)	Sandy units: - Often structureless, sometimes fining upwards - Lamination, cross-stratification - Moderately poorly to moderately well-sorted - Thinly to thickly bedded Muddy units: - Abundant planar and wavy lamination - Thin to medium-bedded	- Sands likely transported as bedload, deposited from lower flow regime currents (Allen, 1966; Miall, 2013). - Muds and silts were deposited out of suspension, prior to renewed coarse clastic input (Jopling and Walker, 1968; Allen, 1970)
Muddy sand	*MscSst*	*Interbedded mudstone and clean sandstone*	- Disorderly interbedding of mature, light-coloured, sandstones and mudstones - Varied and abundant structures	- Sandstone, sub-arkosic - Sand grains medium to very coarse, sub-rounded to well-rounded, with moderate to high sphericity - Mudstone, siltstone (≤ 50%) - Rare carbonate grains (< 10%), medium to coarse, sub-rounded	Sandy units: - Generally well-sorted - Planar lamination and ripple cross-lamination - Very thin to thickly bedded Muddy units: - Abundant continuous and discontinuous planar lamination, soft-sediment deformation - Thinly bedded - Interbedding frequently chaotic	- High-density turbulent flows or sandy debris flows (Lowe, 1982, Shanmugam, 1996, 2000). Where the sub-facies is clearly stratified, better sorted, and current-generated structures are more prevalent: - Introduction of sand as bedload into a low-energy setting, deposition from currents in the lower flow regime (Allen, 1966) - Oscillatory flows possible (Allen, 1966; Miall, 2013)
Muddy sand	Het	Heterolithic	- Thin interbedded sandstones and silt or mudstones - Characteristic wavy, lenticular, or flaser lamination	- Sandstone, arkosic to sub-arkosic - Sand grains fine to coarse, round to sub-angular, low to high sphericity - Mudstone, siltstone (10 % – 50 %)	- Wavy, flaser, and lenticular lamination - Cm-scale ripple lamination may be present - Fining-up may occur on a cm-scale - Poorly sorted to moderately well-sorted - bedding thickness commonly thin	- Cyclically variable current strength or sediment supply, e.g. alternation of slack water and current or wave influence (Martin, 2000) - Conditions favourable for both sand and mud deposition and preservation (Reineck and Wunderlich, 1968; Reineck and Singh, 1980)
Sand	LSst	Laminated sandstone	- Variably sorted sandstones - Abundant lamination	- Sandstone, sub-arkose, arkose - Grains fine to granular, subrounded to subangular, moderate to high sphericity	- Abundant thin and thick continuous planar lamination - Variable bedding thickness, thin to thick - Rare scour marks	- Deposition from unidirectional currents likely in the upper flow regime (Allen, 1966; Ashley, 1990)
Sand	*wLSst*	*Well-sorted laminated sandstone*	- Sandstone, sub-arkosic or arkosic - Well-sorted - Abundant planar lamination	- Sandstone, sub-arkosic, or arkosic with < 50% feldspar, minor lithic component - Grains fine to coarse, , sub-angular to sub-rounded, high sphericity	- Gentle fining-up - Thin planar lamination is common, - Coarser portions of the facies more massive - Mostly well-sorted, becoming less sorted with increasing grain size - Bed thickness thin to medium	- Deposition from unidirectional currents in the upper flow regime (Allen, 1966; Ashley, 1990) - Substantial winnowing of lithics and muds
Sand	*pLSst*	*Poorly sorted laminated sandstone*	- Sandstone, sub arkosic or arkosic - Moderately to poorly sorted	- Sandstone, sub-arkosic or arkosic - In parts micaceous, ≤ 15% - Grain fine to very coarse, mostly coarse, sub-angular to	- Occasional fining-up within units - Thin and thick planar lamination is common, sometimes wavy - Coarser portions of the facies more massive - Scour marks rare	- More proximal deposition than the wLSst sub-facies from unidirectional currents in the upper flow regime (Allen, 1966; Ashley, 1990) - Periodic waning of flow strength to deposit finer material

			- Abundant planar lamination	sub-rounded, moderate to high sphericity	- Poorly sorted - Bed thickness thin to thick	
Sand	XSst	Cross-stratified sandstone facies	- Sandstone, showing ripple-lamination, cross-bedding	- Sandstone, commonly sub-arkosic or arkosic - Grains fine to coarse, sub-angular to sub-rounded, moderate to high sphericity	- Asymmetric ripple cross-lamination in dm-scale co-sets, with bed- parallel, sharp bounding surfaces - Climbing ripples may be present - Trough and planar cross-bedding, co-sets < 1 m thick, with planar, sub-parallel bounding surfaces - Bed thickness is commonly thin or medium	- Sub-aqueous ripple and dune migration in the lower flow regime (Ashley, 1990; Miall, 2013) - Presence of climbing ripples indicates periods of increased accumulation rate (Ashley et al., 1982) - Bi-directional or oscillatory flows possible (Reineck and Singh, 1980)
Conglomerate	CCgm	Clast-supported conglomerate	- Granular, gravel and cobble conglomerates - Clast-supported fabric	- Conglomerate, arkosic to litharenitic - Clast shape angular to rounded, variable sphericity - Sandy matrix, generally arkosic, coarse to granular - Matrix mud content < 25%	- Variably stratified - May be disorganised or abundantly structured, depending on sub-facies - May show fining-up within beds - Thin mud-rich beds may be present - Poor to very poor sorting - Bed thickness thin to thick	- Streamflow or current-generated where the sub-facies is stratified, texturally mature, with units repeatedly fining-up (Nemec and Steel, 1984; Todd, 1989) - Cohesive debris flows, deposited via frictional freezing, with sandy cross-stratified units representing streamflow between periods of coarser mass flow input (Lowe, 1982; Nemec and Steel, 1984; Todd, 1989)
Conglomerate	*fCCgm*	*Fine stratified clast-supported conglomerate*	- Clast-supported conglomerate, 15 mm maximum clast size (medium pebble) - Stratified, structured	- Typically oligomict, sub-arkosic to litharenitic - Clasts predominantly sub-rounded, moderate sphericity - Mud, silt < 10%	- Planar lamination common - Frequent fining upwards within units - Cm to dm-scale cross-beds - Poor sorting - Bed thickness thin to medium	- Deposited from bedload in unidirectional currents (Nemec and Steel, 1984; Todd, 1989). - Cross beds and coarse planar laminated units indicate lower and upper plane bed sedimentation, respectively (Allen, 1970)
Conglomerate	*sCCgm*	*Coarse stratified clast-supported conglomerate*	- Clast-supported conglomerate, 15 mm minimum clast size (medium pebble) - Stratified	- Oligomict to polymict - Clasts round to sub-angular, moderate to high sphericity - Matrix commonly coarse to granular arkosic sand	- Beds and bed sets can fine-upwards - Poorly developed internal erosion surfaces - Poorly developed imbrication - Diffuse stratification with increasing grain size - Bedding thickness is medium to thick	- Current-generated where stratified, texturally mature, with units repeatedly fining-up (Nemec and Steel, 1984; Todd, 1989) - Cohesive debris flows, deposited via frictional freezing, where texturally immature and stratification is less distinct (Lowe, 1982; Nemec and Steel, 1984)
Conglomerate	*dCCgm*	*Disorganised clast-supported conglomerate*	- Clast-supported conglomerates - Poorly stratified or unstratified - Extreme textural immaturity	- Typically oligomict, mostly arkosic - Clasts round to highly angular, very low to high sphericity - Matrix muddy to sandy	- Diffusely stratified, or unstratified - Stratification often shown by abrupt variation in clast:matrix ratios, rather than changes in grain size - Extreme textural immaturity, very poor sorting - Medium to very thickly bedded	- Limited turbulence, cohesive debris flows deposited via cohesive freezing (Lowe, 1982; Nemec and Steel, 1984; Shanmugam, 2021) - In parts limiting inter-granular dispersive pressure (Lowe, 1982; Todd, 1989) - Very proximal deposition, e.g. talus (Sanders, 2010)
Diamicite	Dia	Diamictite	- Matrix-supported conglomerates - Polymict, oligomict	- Clast compositions varied, e.g. quartzite, granite, schist - Clasts angular to rounded, low to high sphericity, granule to cobble-sized - Muddy matrix	- Dropstones, lonestones - Ice-rafted debris - Imbrication - Stratification often indistinct - Where discernible, thinly to thickly bedded	- Limited fluid turbulence, deposition from cohesive flows via cohesive freezing (Lowe, 1982; Dasgupta, 2003; Shanmugam, 2021) - Sub-aerial debris flow freezing at the terminus of a glacier (Lawson, 1982) - Glacial rain-out, ice rafting
Diamicite	*crDia*	*Clast-rich diamictite*	- Matrix-supported polymict - > 20 % clasts - poorly sorted	- Clast compositions varied (quartzite, gneiss, mica schist) - Clasts angular to rounded, low to high sphericity, granule to cobble-sized	- 'Wrap-around' fabrics - Imbrication in the most clast-rich portions - Ice-rafted debris - Continuous lamination, sometimes as laminites	- Limited fluid turbulence, deposition from cohesive flows via cohesive freezing (Lowe, 1982; Dasgupta, 2003; Shanmugam, 2021) - Sub-aerial debris flow freezing at the terminus of a glacier (Lawson, 1982)

				- Muddy matrix	- Where discernible, medium to very thickly bedded	- Ice rafted debris suggest glacial influence Bennett et al. (1996)
Diamicite	*cpDia*	*Clast-poor diamictite*	- Matrix-supported polymict - ≤ 20 % clasts	- Clast compositions as varied as *crDia* - Clasts sub-angular to rounded, moderate to high sphericity, < pebble-sized - Muddy matrix	- Predominantly unstructured - Rare planar lamination - Lonestones, dropstones - Thin sandy interbeds rare - Stratification unclear or absent - Thickly to very thickly bedded	- Where lonestones, striated clasts or dropstones are present: glacial rain-out, ice rafting (Bennett et al., 1996; Hoffmann et al., 2004). - Deposition from cohesive flows via cohesive freezing (Lowe, 1982; Dasgupta, 2003; Shanmugam, 2021)
Diamicite	*CaDia*	*Carbonate diamictite*	- Matrix-supported polymict, oligomict - > 20 % of clasts composed of carbonate	- Oligomict, polymict - Significant carbonate component, > 20% of clasts composed of carbonate - Clasts sub-rounded to rounded; low to high sphericity	- Isolated cm- to dm-scale clast-supported beds - Lamination rarely deformed around clasts - Clast-rich units sub-horizontally to horizontally imbricated - Poorly stratified or unstratified - Thickly bedded, clast-supported intervals thinly to medium-bedded	- Cohesive flows, with matrix strength supporting intraclasts, deposited via cohesive freezing (Lowe, 1982; Shanmugam, 2021) - Where clasts clearly deform underlying laminae a weak glacial influence is possible (Bennett et al., 1996)
Fine-grained clastic carbonate	CaMs	Interbedded carbonate-mudstone	- Silty mudstone interbedded with carbonates - < 50 % carbonate within a facies unit	- Mudstone - Carbonate, commonly dolomitic (< 50%) - Minor siltstone (< 10%)	- Continuous planar lamination - Rare asymmetrical shear structures, soft-sediment deformation mudstones - Isolated edgewise conglomerates, scour marks - Carbonate beds thin to medium-bedded - Mudstone beds medium to very thickly bedded	- Suspension settling in a low energy environment, rare oscillatory flow (Reineck and Singh, 1980) - Periodic agitation of sediment and proximal or in-situ re-deposition (Sepkoski, 1982) - Source of the carbonate is difficult to constrain, possibly precipitation, or dolomitisation of ooids (Hood et al., 2015; Hood and Wallace, 2018)
Fine-grained clastic carbonate	CaSl	Carbonate-bearing siltstone	- Siltstones containing > 10% carbonate	- Siltstone - Carbonate (> 10 %) - Carbonate frequently dolomitic	- Carbonate may be disseminated, finely laminated, or – rarely – thinly interbedded - Abundant planar and wavy lamination - Rare scour marks, edgewise conglomerates - Bed contacts mostly sharp, rarely erosional - Bed thickness tends to be thin or medium	- Suspension settling in a low energy, carbonate producing environment (James and Dalrymple, 2010) - Periodically elevated energy conditions to generate wavy lamination and scour the substrate - Where carbonate forms discrete beds, possibly direct precipitation, or dolomitised ooids (Hood et al., 2015)
Fine-grained clastic carbonate	lSlCa	Laminated silty carbonate	- Conspicuous striped appearance - Tightly interbedded carbonate and siltstone or mudstone	- Carbonate (50 – 75%) - Siltstone, mudstone (25 – 50%)	- Abundant, dense wavy lamination - Laminae and thin beds compositionally graded - Dm to m-scale packages of rhythmites and laminites, often resembling varves - Thinly or very thinly bedded	- Suspension settling in a low-energy setting that may be periodically agitated by oscillatory flows - Gradual variations in clastic sediment supply during deposition Zolitschka et al. (2015) - Cyclical processes controlling deposition (Reineck and Singh, 1980; Zolitschka et al., 2015)
Sandy carbonate	CaHet	Carbonate-bearing heterolithic	- Thin interbedded sandstones and silt or mudstones - > 10 % carbonate - Wavy, lenticular, or flaser lamination	- Sandstone - Sand grains fine to medium - Mudstone, siltstone - Carbonate, commonly dolomitic (> 10%) - Minor anhydrite (< 10%)	- Abundant planar and wavy lamination - Muddy, silty, or carbonate flasers - Symmetrical sand lenses - Carbonate tends to occur in the matrix and as micritic lamination, or thin beds - Thinly to medium-bedded	- Fluctuating, bi-directional, or oscillatory flow in a mixed clastic-carbonate system (Reineck and Wunderlich, 1968; Siahi et al., 2016) - Conditions favourable for both sand and (carbonate) mud deposition and preservation (Reineck and Wunderlich, 1968; Tucker, 1984)

Sandy carbonate	CaSst	Carbonate-bearing sandstone	- Predominantly clastic sandstone, < 50 % carbonate as grains or in matrix	- Sandstone, sub-arkosic to sub-litharenitic - Carbonate, principally dolomite (< 50%)	- Continuous planar lamination - Planar and trough cross-stratification, herringbone cross-stratification. - Cross-bed bounded by planar, horizontal bedding surfaces - Thinly to thickly bedded	- Deposited from oscillatory, bi-directional or uni-directional currents in a moderate to high-energy marine setting (Tucker, 1984; Ashley, 1990) - Subaqueous ripple and dune migration (Allen, 1966) - Proximal clastic source (Siahi et al., 2016)
Sandy carbonate	SstCa	Sandy carbonate	- Carbonate and interbedded carbonate-bearing sand, silt or mudstone - > 50 % carbonate	- Carbonate, commonly dolomitic (> 50%) - Carbonate grains varied, packstone to ruddstone - Sandstone, sub-arkosic to sub-litharenitic	- Planar lamination, lamination common - Cross-lamination rare - Dm-scale sets of clastic-carbonate laminites	- Possible depositional mechanisms varied - High-energy shallow marine setting (Siahi et al., 2016) - Bi-directional flows and rapid fluctuations in energy likely predominated (James and Dalrymple, 2010; Siahi et al., 2016).
Conglomeratic carbonate	CaCgm	Clast supported carbonate conglomerate	- Clast-supported conglomerate, > 20 % carbonate clasts - Similar to *dCCgm*, but with carbonate component	- Carbonate, often dolomitic - Carbonate clasts low sphericity, gravel to pebble-sized vary in roundness - Sandstone, litharenitic, lithic greywacke	- Carbonate clasts may be imbricated - Isolated soft-sediment deformation and pipe-like water-escape structures - The facies is diffusely stratified or unstratified, but appears thickly bedded	- Deposited from cohesive debris flows via cohesive freezing (Lowe, 1982; Shanmugam, 2021) - Limited turbulence during transport (Lowe, 1982; Miall, 2013) - Inter-granular dispersive pressure likely limited, with mud in the matrix possibly acting as a lubricant during movement (Lowe, 1982)
Carbonate	MCa	Massive carbonate	- Crystalline carbonate with little discernible primary structure	- Carbonate, predominantly dolomitic - Mud, silt (< 20%) - Anyhydrite (< 5%)	- Rare mud-rich laminae - Mm to cm-scale stylolites - Bed contacts often unclear - Where discernible, medium to thickly bedded	- Interpretation difficult due to limited diagnostic sedimentary structures - Clastic supply possibly restricted or distal - Possibly syn-sedimentary precipitates, or biotically mediated (Hood et al., 2015; Hood and Wallace, 2018)
Carbonate	LCa	Laminated carbonate	- Crystalline carbonate, commonly dolomitic -Abundant lamination	- Carbonate, predominantly dolomitic - Minor sand, silt, mud - Minor anhydrite	- Abundant lamination, planar or wavy - Grading in laminae may be present - Thin to medium-bedded	- Deposited in a mixed clastic-carbonate environment, with varying degrees of wave action and reworking of beds - Minor clastic component suggests a distal or restricted clastic sediment supply (Hood et al., 2015; Siahi et al., 2016)
Carbonate	*pLCa*	*Planar laminated carbonate*	- Carbonate, often dolomitic - Abundant planar lamination - < 10% silt, mud	- Carbonate, often dolomitic - Mud, silt (< 10%)	- Abundant thin planar lamination - Wavy thin laminae rare - Lamination is parallel, sometimes slightly graded - Bedding thickness may be difficult to discern, but appears thin to medium	- Deposited in a low-energy environment, with little to no oscillatory flow agitating the substrate - Minor clastic component suggests a distal or restricted clastic sediment supply (Hood et al., 2015; Siahi et al., 2016).
Carbonate	*vLCa*	*Variably laminated carbonate*	- Carbonate, often dolomitic - Planar and wavy lamination abundant - Higher clastic content (< 50 %)	- Carbonate, commonly dolomitic - Sand, silt, mud in varying proportions (total < 50 %) - Minor anhydrite (< 10 %)	- Lamination abundant, ranges from thick to thin, planar to wavy - Cross-lamination rare - Thinly to medium-bedded, bed contacts commonly sharp	- Depositional mechanisms difficult to constrain on account of recrystallisation - Low-energy carbonate-producing environment with fluctuating clastic sediment input likely (Siahi et al., 2016) - Continuous reworking of beds, deposition from currents or oscillatory flows (Allen, 1966)
Carbonate	Rk	Red karst	- Red colouration of clays in dissolution structures within carbonate	- Carbonate, often dolomitic - Minor clay seams - Calcite common in void spaces	- Cauliflower and nodular structures in carbonate - Dissolution structures, fenestral fabrics - Irregular clay seams - Remnant lamination in carbonate	- Dissolution of primary carbonates (Kenny and Knauth, 2001) - Seawater percolating through void spaces (James and Dalrymple, 2010).

					- Sharp bounding surfaces	
Carbonate	AnCa	Anhydrite-rich carbonate	- Carbonate with abundant anhydrite	- Carbonate, predominantly dolomitic - Anhydrite (> 10%) - Silt, mud (< 25%)	- Chickenwire and enterolithic textures - Cm-scale displacive anhydrite nodules - Secondary anhydrite in void spaces or as veins - Bed thickness thin to thick, contacts sharp	- Evaporitic conditions, displacive anhydrite textures the result of early diagenesis (Christeleit et al., 2015)
Carbonate	Mic	Microbialite	- Sandy and silty carbonates with microbially-induced sedimentary structures (MISS) - MISS criteria Noffke (2009)	- Carbonate - Sand - Silt (< 10%)	- Cm-dm scale stromatolitic structures, may be domal and rounded, or columnar - Variety of orientations, commonly upright or inclined - Thickness of units difficult to discern, in the order of m's - 10s m	- Growth of microbial structures in intertidal and sub-tidal zones (Beukes and Lowe, 1989; Noffke, 2009; Hood et al., 2015)

Table 3.1: Tabulated facies scheme for the Zambian Copperbelt.

Environment	*Facies association*	*Facies*										
Terrestrial	Proximal alluvial fan	pLSst	XSst	fCCgm	sCCgm	dCCgm						
	Distal alluvial fan	wLSst	pLSst	XSst	fCCgm	sCCgm						
	Fluvial	wLSst	pLSst	XSst	tMsSst	fCCgm	sCCgm					
	Glaciofluvial	pLSst	XSst	fCCgm	cpDia							
Deltaic	Fan-delta	SstMs	Wck	fCCgm	sCCgm	dCCgm						
	Delta plain	wLSst	pLSst	MscSst								
	Delta slope	SstMs	Wck	MscSst	fCCgm							
	Prodelta	SlMs	LSl	MsgSst	lSlCa							
Coastal	Intertidal	SlMs	LSl	wLSst	Het	CaHet	CaSst	SstCa	pLCa	vlCa	Rk	
	Sabkha	CaHet	CaSst	SstCa	MCa	pLCa	vLCa	AnCa				
	Microbial mat	CaHet	SstCa	MCa	pLCa	vLCa	Mic					
	Foreshore	wLSst	XSst	CaSst	SstCa							
Shelf	Carbonate ramp	CaSl	lSlCa	CaSst	SstCa	MCa	pLCa	vLCa				
	Glaciomarine	dMs	XSst	fCCgm	cpDia	crDia	CaMs	lSlCa	MCa			
	Transition zone	SlMs	LSl	CaMs	CaSl	lSlCa						
	Deep water	dMs	SlMs	CaMs								
Slope	Subaqueous slope	SstMs	Wck	MsgSst	tMsSst	cpDia	crDia	CaDia	CaMs	CaCgm		

Table 3.2: Depositional environment and facies association table, showing which facies combine to form particular facies associations, that combine to characterise certain depositional environments.

3.4 Facies associations

3.4.1 Proximal alluvial fan facies association

The proximal alluvial fan association contains the pLSst, XSst, fCCgm, sCCgm, and dCCgm facies, arranged in sharp-based upward-fining successions. It is well-expressed in the RCB2 core and continuous units of this facies can reach thicknesses of 100's m (fig. 3.2).

At its base, the facies association is composed predominantly of unstratified or poorly stratified conglomeratic facies (dCCgm, sCCgm) 10's - 100's m in thickness. These pass into finer conglomeratic facies (fCCgm) and texturally and compositionally immature sandstone facies (XSst, pLSst) 10's - 100's m in thickness. These may be punctuated by thinner ($<$ 10 m) units of sharp-based or erosional conglomeratic facies. Internal erosional surfaces are likely, but not easily discerned in core. The facies association as a whole fines upwards, the proportion of sand increasing up-section. Using grain size and angularity as simple measures of proximality, the facies are arranged in aggradational or retrogradational stacking patterns.

These characteristics are shared by modern and ancient alluvial fan systems (Bull, 1977; Nemec and Steel, 1984; Went, 2005; James and Dalrymple, 2010). The coarsest basal facies, reaching cobble and boulder size in the RCB2 core, suggest proximal deposition. Deposition via debris flows is interpreted to have predominated initially, on account of the abundance of poorly stratified conglomerates (e.g. dCCgm facies) in the basal 10's - 100's m of this association (Nemec and Steel, 1984). Subsequent deposits show increasing evidence of reworking by fluvial systems, resulting in cross-stratified and laminated sandstone facies becoming more prevalent. Periodic sheetfloods and high-energy fluvial input re-introduced thinner conglomeratic units (Bull, 1977).

The interpretation of alluvial fans forming a significant proportion of basal clastics in the Lower Roan Group of the Zambian Copperbelt is well-established, with 100's m of coarse terrigenous sediment in the Chambishi sub-basin and across the Copperbelt being interpreted as alluvial fan and streamflow deposits (Eden, 1974; Clemmey, 1976; Sweeney et al., 1986; Binda, 1994; Bull et al., 2011).

3.4.2 Distal alluvial fan facies association

The distal alluvial fan facies association also comprises fining-up successions of wLSst, pLSst, XSst, fCCgm, and sCCgm facies, but lacks the poorly stratified dCCgm facies. The facies association generally shows higher textural and compositional maturity, and reduced grain size (< cobble), than its proximal counterpart. The type cores for this facies association are RCB2 and IT26, where the facies association can reach thicknesses of 10's - 100's m (fig. 3.2).

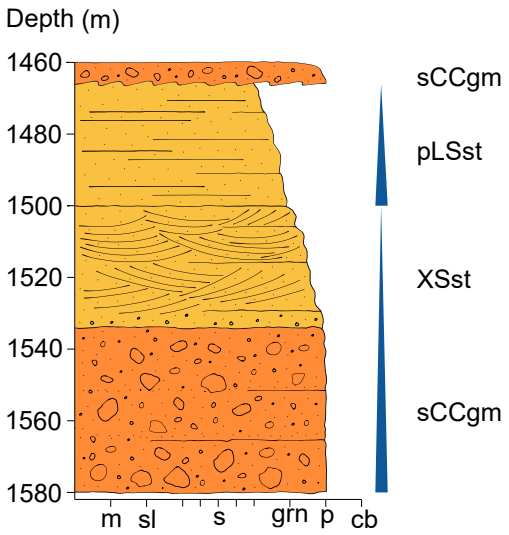

Figure 3.2: Type log for the alluvial fan facies associations, showing a 120 m logged section of the RCB2 core. Conglomerate and sand facies form a broad fining-up succession, transitioning from proximal to distal alluvial fan facies associations. Blue arrows indicate fining trends and sediment sources becoming more distal.

The basal portion of the facies association comprises well-stratified or fine pebbly conglomerate facies (sCCgm, fCCgm) 10's m in thickness. These facies are overlain by sandy facies of successively increasing textural and compositional maturity (XSst, LSst) in packages 10's - 100's m thick, which make up the most of the facies association. There is a weak trend of facies becoming more sub-arkosic up-section. The facies association occurs above the proximal alluvial fan facies association and tends to be aggradational or retrogradational.

The conglomeratic facies were deposited predominantly via sheetfloods and debris flows (Bull, 1977; Nemec and Steel, 1984; Went, 2005). The overlying sandy facies are interpreted as more mature fluvial systems. The most well-sorted and texturally mature sand facies may have aeolian

origin (Eden, 1974; Clemmey, 1976; Brookfield, 1977). The abundance of sandy facies with well-developed structures and co-occurrence with the proximal alluvial fan facies association suggests sedimentation was dominated by streamflow, rather than mass flows, on distal portions of alluvial fans.

3.4.3 Fluvial facies association

The fluvial facies association is predominantly sandy, with minor conglomeratic units, and composed of the wLSst, pLSst, XSst, tMsSst, fCCgm, and sCCgm facies. It is predominantly aggradational, but may show an overall fining-up trend over a scale of 10's - 100's m (fig. 3.3). It may show considerable similarity to the distal alluvial fan facies association, but is generally more compositionally and texturally mature. The RCB2 and KRX082 cores are type cores for this facies association, with fluvial successions 100's m in thickness.

It comprises coarse arkoses and sub-arkoses at its base, 10's - 100's m thick, often showing current-generated structures (XSst, pLSst, wLSst). These facies may be interbedded with thin, stratified, current-generated conglomerate facies (sCCgm, fCCgm). These interbedded sand-conglomerate couplets tend to be metres to 10's m's thick. Towards the top of the facies association, cleaner sandstones become more common and sandy facies may be sharply interbedded with thin mudstones (wLSst, tMsSst). These mixed sandstone-mudstone facies comprise much of the facies association in core KRX082. The facies association is predominantly aggradational, or retrogradational, where it occurs below tidal mudflat facies associations (e.g. core KRX082), or passes sharply into a delta slope facies association (e.g. core RCB2).

This facies association is interpreted as having a fluvial origin, sharing characteristics of ancient and modern fluvial successions, e.g. repeated fining-up successions, often with pebbles or gravels at their base, passing through cross-stratified and planar-laminated sandstones, capped by thin mud-rich units (Miall, 1985; Nichols and Fisher, 2007; Turner, 2010). Stratified conglomeratic facies likely represent lag deposits or channel bars, as they are thin compared to the host succession (commonly $<$ 5 m), and may have erosional bases (Miall, 2013). Much of the channel fill comprises coarser sandy facies (e.g. LSst, XSst) with low mud proportion. Thin mud units of the tMsSst facies that punctuate the successions every 1 - 5 m in the KRX082 core are interpreted as abandoned channels (Nichols and Fisher, 2007; Reineck and Singh, 1980; Miall, 1985). Though they may rep-

resent floodplain deposits, with compaction and tectonic fabrics obscuring grading, this is deemed to be less likely on account of a lack of vegetation during the Precambrian favouring braided fluvial systems (Davies and Gibling, 2010).

An abundance of fluvial deposits has been described in the basal clastics of the Katangan basin (e.g. Mufulira, Chambishi SE) (Eden, 1974; Binda, 1994; Selley et al., 2005; Bull et al., 2011). Eden (1974) described in detail cross-bedded sandstones at Mufulira that had previously been interpreted as aeolian in origin, but were reinterpreted as fluvial deposits and channels.

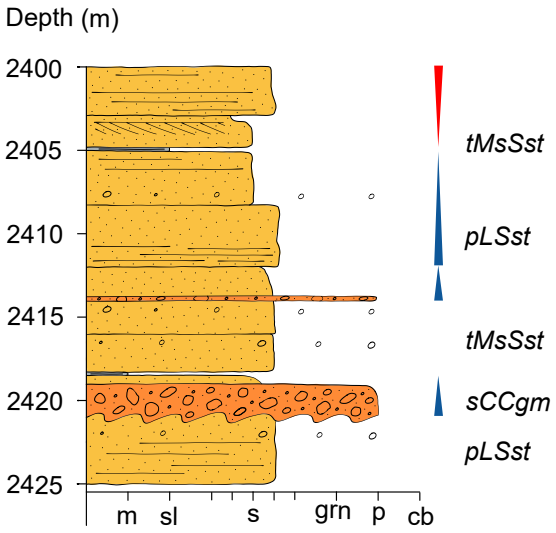

Figure 3.3: 25 m long type log for the fluvial facies association, showing a section of the KRX082 core in Solwezi. Stratified conglomerate facies punctuate sandy facies that fine upwards and are punctuated by thin mud units.

3.4.4 Glaciofluvial facies association

The glaciofluvial facies association comprises the pLSst, XSst, fCCgm, and cpDia facies. It occurs in packages metres thick; the type core for the facies association is ZMSDD003 (fig. 3.4).

Compositionally immature (often lithic-rich), poorly sorted, coarse facies (XSst, fCCgm) occur in packages metres thick and characterise the basal portion of this association; both the constituent facies and the succession as a whole may show an erosional base (e.g. core ZMSDD003). Coarser facies are sharply overlain by diamictite facies (Dia) metres thick. The facies association appears to be predominantly aggradational, rapidly retrograding towards its top and into the glaciomarine facies association.

The glaciofluvial facies association is regarded as distinct from its fluvial counterpart by virtue of its association with glacial diamictites. Only where diamictites can be identified with reasonable certainty as having a glacial origin (e.g. lonestones or deformed laminae around dropstones) has this facies association been ascribed.

The facies association is interpreted to represent fluvial systems operating in advance of a glacier, with conglomerates and cross-bedded sands representing lag deposits, dunes or channel bars (Eyles et al., 1983; Aitken, 1998).

The glaciofluvial facies association has been well-documented in the Katangan basin, and has been interpreted as periglacial outwash beds and glaciofluvial sandstones (Master and Wendorff, 2011). The interpretation of the facies association proposed here is in agreement with observations in the Luapula Beds around Mansa, where glacial diamictites occur with immature cross-bedded glaciofluvial sandstones (Wendorff and Key, 2009).

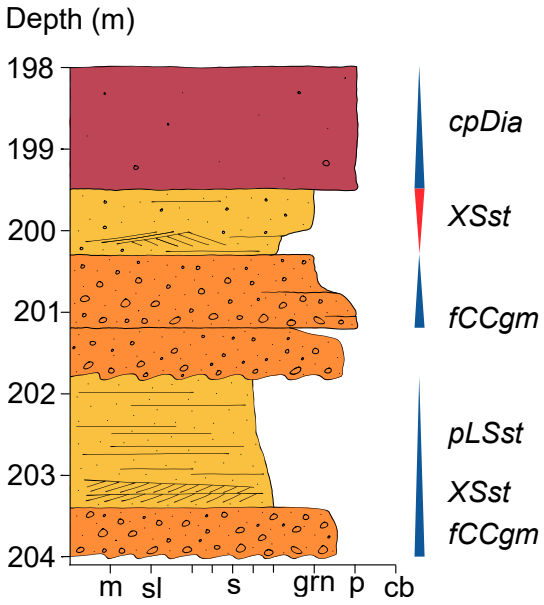

Figure 3.4: 6 m long log for the glaciofluvial facies association in the ZMSDD003 core. Fluvial conglomerate and sand facies with internal erosion surfaces are sharply overlain by a clast-poor diamictite, interpreted as glacial, forming a deepening succession. Blue arrows represent deepening-upwards, and red arrows shallowing-up trends.

3.4.5 Fan-delta facies association

The fan-delta facies association contains the SstMs, Wck, fCCgm, sCCgm, and dCCgm facies. It is characterised by extreme textural and compositional immaturity, rapid upwards fining and coarsening on a scale of metres - 10's m, and steep depositional slope angles from soft-sediment deformation. It occurs in packages 10's m thick. The type core for this facies association is KN192 (fig. 3.5).

The facies association is composed of disorganised (i.e. unstructured, extremely textural immature) and poorly stratified conglomerate facies (dCCgm, sCCgm) at its base. These are overlain by texturally and compositionally immature gravelly and sandy facies, frequently with high ($\leq$ 50%) mud proportion (fCCgm,pLSst, Wck, MscSst). Bed contacts and facies contacts are often diffuse on account of poor sorting. The facies association aggradational or progradational, based on repeated coarsening-up cycles over 10's m, that may show an overall shallowing-up trend, and is often closely associated with delta slope and prodelta facies associations. It is differentiated from the alluvial fan facies associations by evidence for steeper depositional slope angles, and rapid facies changes from subaerial to subaqueous settings interpreted from the juxtaposition of CCgm, SstMs, and Wck facies.

Slope angles may be moderately steep, tentatively approximated to be 10° in the basal parts of the KN192 core, suggesting deposition on a mature or intermediate-maturity fan-delta (Kiefer et al., 2021). The coarse grain size, pronounced textural immaturity and steep dip of beds is characteristic of fan-delta plains (Lønne and Nemec, 2004). Sedimentation is interpreted to have taken place predominantly via mass flows (Shultz, 1984), sandier facies likely being the result of sheetfloods and impersistent fluvial systems operating on the fan-delta plain (Patranabis-Deb and Chaudhuri, 2007). Where textural immaturity is extreme (e.g. euhedral feldspar clasts in the dCCgm sub-facies) sediment may have been introduced via rockfalls, resulting from talus slopes in the upper reaches of the fan (Sanders, 2010). Fan-deltas have previously been interpreted at Konkola by Sweeney et al. (1986) and in the wider Zambian Copperbelt by Selley et al. (2005).

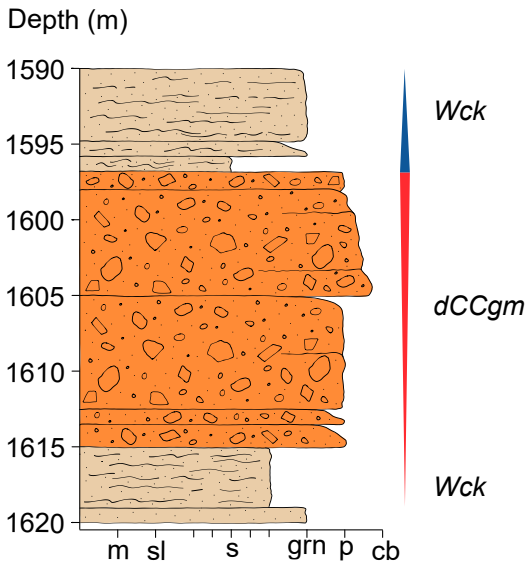

Figure 3.5: 30 m long type log for the fan-delta facies association in the KN192 core in which proximal fan or talus slope conglomerates shallow up from, and are bounded at their top by, wackes deposited by subaqueous sediment gravity flows.

3.4.6 Delta plain facies association

The delta plain facies association consists of the wLSst, pLSst, and MscSst facies, showing interbedding of clean sand, mudstone and siltstone facies over a range of 10's m, often with complex arrays of primary structures, including abundant lamination, cross-stratification and soft-sediment deformation. The facies association is 10's m thick and is well-expressed in the KN192 core (fig. 3.6).

It characterised primarily by interbedded dark mudstones and clean sands (MscSst) that occurs in units 10's m thick, sometimes separated by laminated sand facies (pLSst, wLSst). Contacts between facies packages are commonly sharp, possibly erosive . The facies association is aggradational, not showing clear shallowing-up or deepening-up over 10's m, or progradational forming coarsening-up cycles metres - 10's m thick. As it shares similarities with the fluvial facies association, it is only ascribed when co-occurring with delta slope and prodelta facies associations.

The compositional maturity and presence of ripple bedforms is evidence of agitation and persistent reworking by lower flow regime currents, either in a fluvial or shoreface setting (Allen, 1966; Miall, 2013). The interbedding of these units with mudstones likely result from channel avulsion or

river flood deposits (Pontén and Plink-Björklund, 2007), or may represent a series of sand flows or crevasse channels into an inter-distributary bay. The latter is considered less likely on account of a lack of vegetation exerting a limiting control on levee development during the Precambrian (Davies and Gibling, 2010). The abundance of soft-sediment deformation structures is evidence of very rapid deposition, supporting a deltaic interpretation for this facies association (Martinsen, 1989). Though deltaic deposits (other than fan-deltas) have not been documented in detail in the Zambian Copperbelt, and this facies association is only cautiously proposed, Fleischer (1984) also invoked the possibility of sedimentation in deltaic settings at Chibuluma.

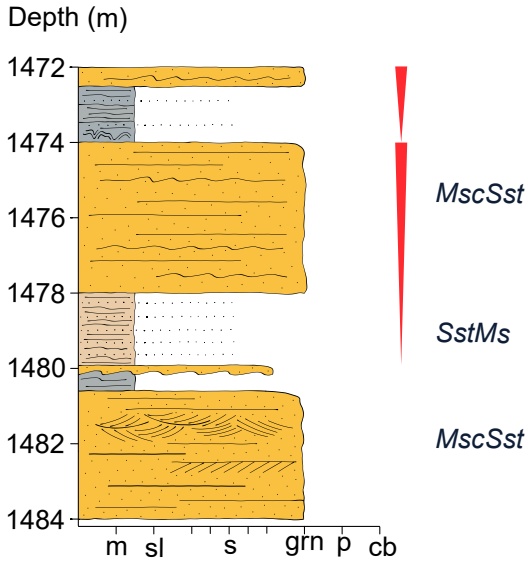

Figure 3.6: 8 m long log of the delta plain facies association in the KN192 core, showing clean structured sandstones interbedded with muddy siltstones. They are separated by sandy mudstones which are interpreted to form part of the delta slope facies association, supporting a broadly deltaic interpretation.

3.4.7 Delta slope facies association

The delta slope facies association comprises the SstMs, Wck, MscSst, and fCCgm facies, and is assigned when these facies occur in proximity to terrestrial facies associations. The facies association occurs in packages 10's m thick, approaching 100 m in the RCB2 core, which, with the KN192 core, are the type cores for this facies association (fig. 3.7).

Sandy mudstone facies (Wck, SstMs) predominate, forming units 10's m in thickness, with minor

quantities of interbedded muddy sandstone facies (MscSst) and intercalated thin beds of conglomerate (fCCgm). These facies transition into one another, forming coarsening-up or fining-up cycles on a scale of metres - 10's m, but on a scale of 10's - 100's m form part of shallowing-up successions, generally comprising prograding prodelta, fan-delta plain, or delta plain facies associations.

The abundance of poorly sorted sandy mudstone and wacke facies suggests sandy debris flows and high density turbidites were the predominant depositional mechanisms. Textural immaturity, evidence of rapid deposition from sediment gravity flows, and high sediment supply are seen as evidence of deposition in a delta slope setting (Mastalerz, 1995; Haines et al., 2010). Coarse grain size and paucity of fining-up at bed-scale within the facies preclude this facies association from being interpreted as a prodelta environment.

The delta slope facies association has not been characterised as such in Copperbelt literature thus far. It may clarify the uncertainty described by Eden (1974) regarding the depositional setting of the carbonaceous wacke at Mufulira (e.g. fluvial, deltaic, or slope-derived). The problematic facies (likely SstMs or Wck) are unlikely to represent channel deposits, nor low-density turbidites, on account of their lack of grading, and high mud contents. Instead, they likely represent mud-rich subaqueous debris flows, and the sandier portions possibly traction carpets of high-density turbidity currents, possibly in advance of a prograding delta.

The proposed facies scheme may also clarify the depositional mechanism for the 'shales with grit unit' (equivalent to the SstMs facies) (Mendelsohn, 1961; Walker, 1966; Binda, 1994). The sandy mudstone facies is characteristic of the delta slope and subaqueous slope associations. Its interpretation differs from that proposed by Bull et al. (2011), who argued it represented a low-energy intertidal setting, between a shoreface and subtidal carbonate-producing zone, and that of Woodhead (2013), who proposed it represented an evaporitic mudflat deposit. A sediment gravity flow interpretation is favoured on account of outsized clasts (up to fine pebbles) and very poor sorting, which characterise competent flows with limited turbulence (Lowe, 1982). Undulose bed contacts, poor sorting, apophyses indicative of high-energy emplacement, and a lack of evidence of wave-reworking support a sediment gravity flow interpretation (Lowe, 1982; Pickering et al., 1986). The shales with grit unit rarely shows the cyclicity common to facies of the intertidal facies association (e.g. Het, LSl, CaHet, LCa). It also lacks the primary evaporitic structures (e.g. anhydrite nodules, enterolithic bedding) which characterise the sabkha facies association, and does not contain

significant quantities of carbonate. Instead, any anhydrite present in this association could be secondary, or represent a deep water evaporite succession periodically disturbed by sediment gravity flows (Fortuin and Krijgsman, 2003; Roveri et al., 2020). Intertidal conditions may have prevailed between periods of delta slope sedimentation, but the shales with grit unit itself is interpreted here as being sub-tidal and deposited on, or adjacent to, a slope.

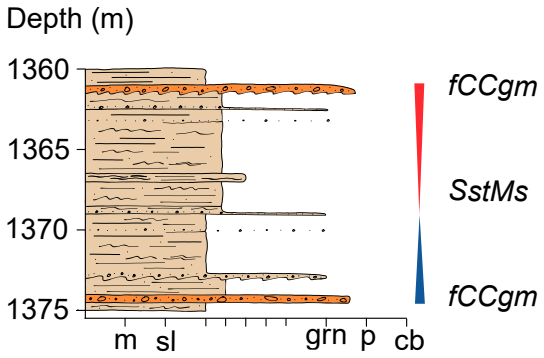

Figure 3.7: 15 m long type log for the delta slope facies association, showing a section of the KN192 core. Sandy mudstones with an abundance of primary structures predominate, punctuated by conglomerate and lenses of coarse sand units that stack aggradationally.

3.4.8 Prodelta facies association

The prodelta facies association is composed of the SlMs, LSl, MsgSst, and lSlCa facies. It is only assigned when co-occurring with delta slope or delta plain facies associations. The facies association is metres to 10's m thick, and well-expressed in cores RCB2 and KN192 (fig. 3.8).

In the KN192 core, graded sandstones and mudstones predominate, with interstitial laminated siltstones (MsgSst) and minor laminated silty carbonates (lSlCa), coarsening upwards. In the RCB2 core, silty mudstones and laminated siltstones predominate (SlMs, LSl facies). The facies association commonly underlies or overlies the delta slope facies association, forming part of broader progradational successions 10's - 100's m thick.

The facies association is dominated by sediments deposited by suspension settling. The absence of agitation by currents suggests deposition took place below the storm wave base (Pickering et al., 1986). Hyperpycnal flows or turbidity currents periodically introduced coarser sediment into a low-energy setting proximal to a slope (Melvin, 1986; Zavala, 2020), sometimes forming partial Bouma sequences (e.g. core KN192). The co-occurrence of this facies association with the delta

slope facies association supports its interpretation as a prodelta, rather than a more distal deep water succession.

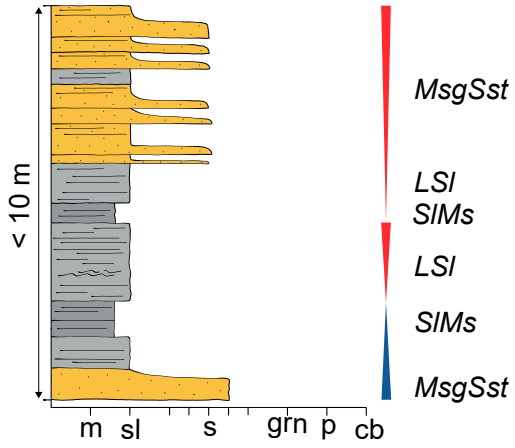

Figure 3.8: Type log for the prodelta facies association in the KN192 core, comprising repeated fining-up sandstone beds interspersed with laminated silts and mudstones. Facies show an overall progradational trend over the whole section.

3.4.9 Intertidal facies association

The intertidal facies association comprises fine laminated facies, often of mixed clastic-carbonate composition: SlMs, LSl, wLSst, Het, CaHet, CaSst, SstCa, pLCa, vlCa, and Rk. The facies association forms packages 10's m thick, approaching 100 m thick in core L83. Type cores for this facies are L83 and KN192 (fig. 3.9).

Abundant wavy lamination and heterolithic units characterise this association. Fine clastic facies (Het, LSst, LSl, SlMs) may be interbedded with mixed clastic-carbonate facies (CaHet, SstCa, CaSst, CaSl). Where clastic and carbonate facies co-occur, the proportion of carbonate facies (CaHet, pLCa, vLCa) tends to increase upwards through the facies association. Interbedding of facies occurs on a scale of decimetres - 10's m, with facies contacts frequently being diffuse. Individual carbonate facies and successions may be broken up by emergent surfaces (Rk). These occur every 10 - 30 m for 10's - 100's m in core KN192. The facies association is predominantly aggradational, often amplified, and tends to become retrogradational towards its top. In core KN192 the facies association shows significant amplification, with an amplification factor of ~ 30. It occurs in close proximity to, and frequently alternates with, the sabkha, microbial mat, foreshore and carbonate

ramp facies associations.

This facies association is interpreted as having been deposited in a mostly low energy, tidally-dominated depositional system. The variability of facies and carbonate content suggests both clastic sediment supply and influence of wave action varied significantly, with a tendency for carbonate content to decrease over time. Abundant heterolithic units are clear indicators of intertidal sedimentation, sometimes in a carbonate-producing setting (Reineck and Wunderlich, 1968; Siahi et al., 2016). Agitation by wave action was limited where only planar lamination, fining-up laminae and bedding are abundant. Where wave action was greater, sandy (LSst) and sandy carbonate (SstCa, CaSst) facies were introduced, often showing ripple cross-stratification. Clastic sediment supply was likely restricted where carbonate facies predominate. Thin interbedding and alternation of facies may show cyclicity in this facies association, on a scale of metres - 10's m, persisting in successions up to 100's m thick, with the proportion of clastics generally reducing upwards. These characteristics bear similarities to modern intertidal and lagoonal systems (James and Dalrymple, 2010). Periodic emergence is supported by cycles of closely spaced, thin oxidised emergent surfaces (Rk). The proximity of this facies association with sabkha and microbial mat facies associations further supports an intertidal interpretation.

Intertidal sediments have been noted by several authors, e.g. Eden (1974); Annels (1984); Sweeney et al. (1986), and are widespread across the Zambian Copperbelt. The intertidal facies association proposed here is in agreement with previous descriptions of tidal sediments, which note cyclicity and close association to evaporitic, foreshore, and possibly lagoonal sediments (Bull et al., 2011). Fleischer (1984) argued that the ore shale unit in the Chambishi Southeast prospect were deposited in an intertidal, possibly sabkha, environment.

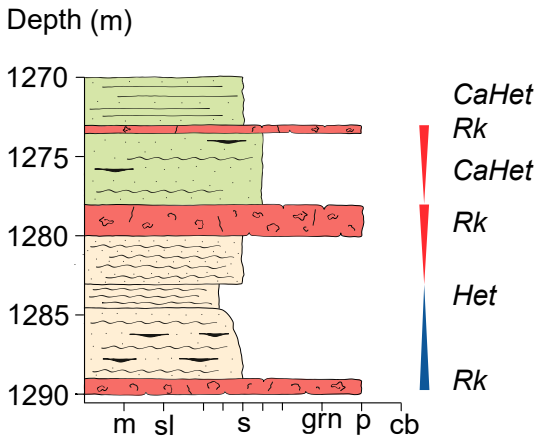

Figure 3.9: 20 m long type log of the intertidal facies association in the KN192 core. Heterolithic and carbonate-bearing heterolithic facies predominate, generally aggrading or prograding, separated by emergent surfaces showing dissolution textures (Rk facies).

3.4.10 Sabkha facies association

The sabkha facies association is characterised by evaporitic minerals, as well as casts and pseudomorphs thereof, in successions comprising the following clastic and carbonate facies: CaHet, SstCa, MCa, pLCa, vLCa, and AnCa. It occurs in packages 10's - 100's m thick. The type core for this facies association is L83 (figs. 3.10, 3.12). Carbonates in this facies comprise almost exclusively dolomite, though to what extent this dolomite is primary or secondary is not clear.

The facies association comprises sandy carbonate (CaHet, CaSst, SstCa), laminated carbonate (LCa) and massive carbonate facies (MCa) with abundant primary anhydrite (AnCa), as well as gypsum casts, and pseudomorphs after both gypsum and anhydrite (Bull et al., 2011). These facies alternate, and are sharply or gradationally interbedded. Mixed clastic-carbonate facies units tend to become thinner (metres - 10's m) and less abundant up-section, being replaced by thicker carbonate-rich or carbonate-only facies (10's - 100's m in thickness). Primary anhydrite textures are better-developed in sandier and siltier facies, where nodular and enterolithic textures are abundant. Secondary anhydrite may fill small veins and vugs, as well as occurring in cm-scale bedding-parallel layers. The facies association tends to be aggradational, often not showing significant shallowing or deepening on a scale of 10's - 100's m, and co-occurs with the intertidal facies association.

The prevalence of carbonate facies with evaporitic facies attests to periodic submergence. Abundant anhydrite units and gypsum casts indicate that brines supersaturated in $CaSO_4$ were present at or

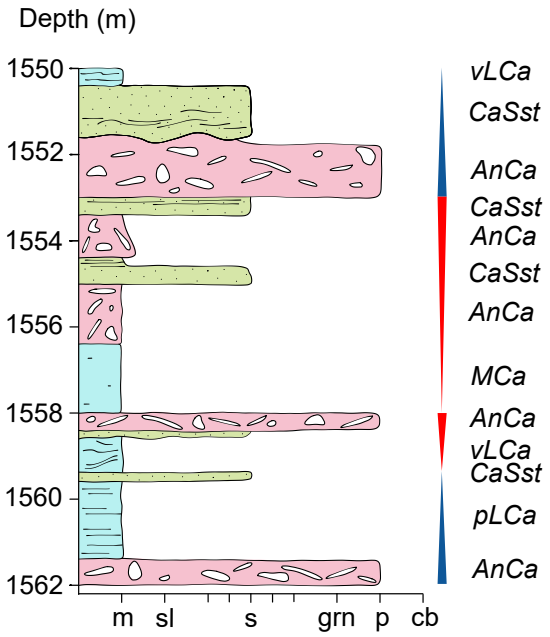

Figure 3.10: 12 m long type log of the sabkha facies association, showing a section of the L83 core. Facies variation is high, comprising predominantly dolomitic carbonate units, often containing abundant primary and secondary anhydrite, punctuated by carbonate-bearing sandstone units with sharp or erosive bases. The succession aggrades on a scale of 10's m.

near the surface (Handford, 1981; Roveri et al., 2020). The frequent co-occurrence and alternation with the intertidal facies association suggests a coastal sabkha environment is the most plausible depositional setting (Handford, 1981).

This description and interpretation is in agreement with previous work on evaporitic sediments that are widespread across the Zambian Copperbelt (Annels, 1974; Selley et al., 2005; Bull et al., 2011). Anhydrite-bearing supratidal mudflats were described by Annels (1974) and "sabkha-like" conditions invoked by Clemmey (1974).

3.4.11 Microbial facies association

The microbial facies association comprises the CaHet, SstCa, MCa, pLCa, vLCa, and Mic facies. It tends to be 10's m thick, but may be 100's m thick (e.g. KN192). Cores IT26 and KN192 are type cores for the facies association (figs. 3.11, 3.13).

Stromatolitic microbialites (StMic) characterise this facies association, occurring in packages mostly 10's m, but sometimes up to 100's m, thick. Microbialite packages are separated by intervals of carbonate facies with varying clastic component (CaHet, SstCa, MCa, LCa) up to 10's m in

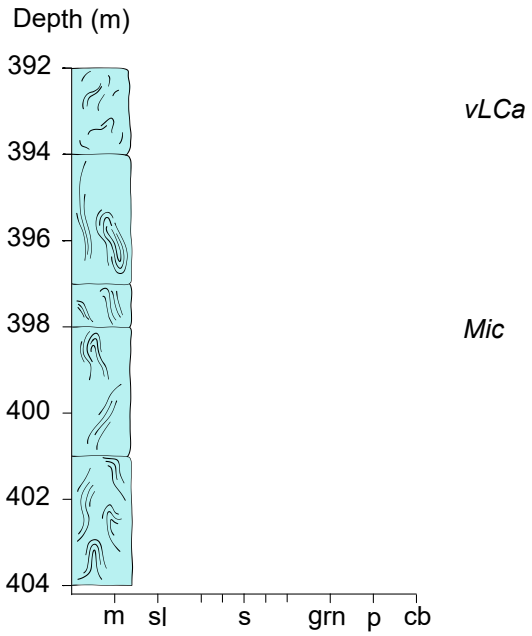

Figure 3.11: 12 m long type log of the microbial facies association, showing a section of the KN192 core in which domal and curved vertical and sub-vertical laminated structures are observable.

thickness. Transitions between microbialite facies and non-microbialite facies tend to be gradational over metres - 10's m. The facies association co-occurs with the sabkha, intertidal, foreshore and carbonate ramp facies associations. It tends to form part of retrogradational successions that are commonly 10's m thick, but may reach 100's m in thickness.

The microbial facies association is interpreted to represent intertidal microbial mats or sub-tidal stromatolite fields and biostromes. Where microbial facies occur with intertidal and sabkha facies associations, there is a greater clastic component, and intraclastic rudstones are present, an intertidal setting is deemed most likely for stromatolites (Hood et al., 2015). Microbialites interbedded with sandier facies may also represent tidal channels (Beukes and Lowe, 1989). Where microbialites co-occur with the carbonate ramp facies association and the proportion of clastic material is lower, they could represent sub-tidal stromatolite fields and reefs (Clemmey, 1974; Hood et al., 2015; Turner et al., 2000).

Clemmey (1974) described algal dolomites and stromatolitic structures up to 6 m thick in Nkana, with Binda (1994) noting stromatolites on both sides of the Kafue anticline. Biotically mediated carbonates have been interpreted to represent both intertidal algal mats and reefs (Clemmey, 1974; Binda, 1994; Bull et al., 2011).

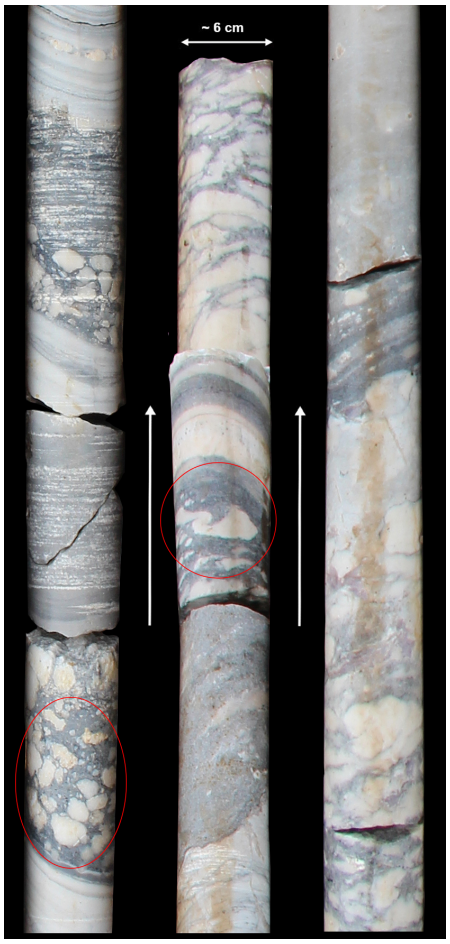

Figure 3.12: The AnCa facies in the L83 core, characteristic of the sabkha facies association. Nodular anhydrite and enterolithic structures (circled red) embedded in grey silty dolomite are abundant. Arrows indicate way-up for the three cores, the bottom of the core is lower left.

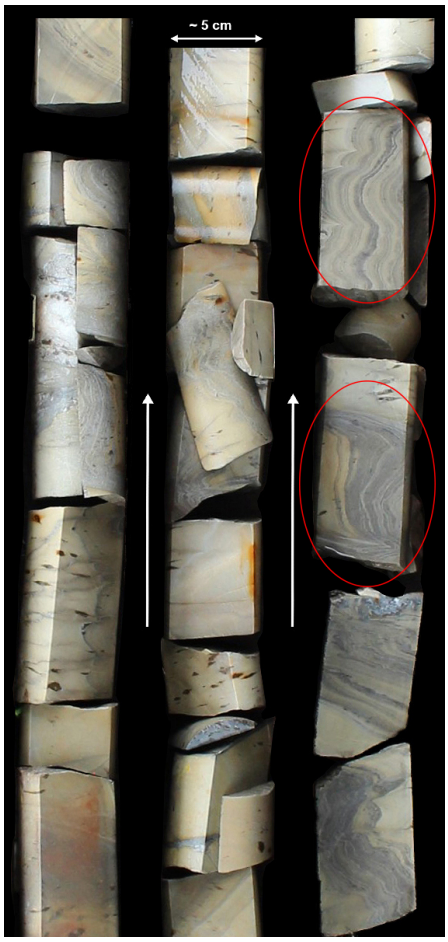

Figure 3.13: The StMic facies in the IT26 core, showing microbially induced sedimentary structures that characterise the facies (circled red), which are interpreted as domal and columnar stromatolites. Arrows indicate way-up for the three cores, the bottom of the core is lower left.

3.4.12 Foreshore - shoreface facies association

The foreshore to shoreface facies association is characterised by plane-laminated and cross-stratified sandy carbonate and sandstone facies: wLSst, XSst, CaSst, and SstCa. The facies association is 10's m thick, and well-expressed in core IT26 (fig. 3.14).

Constituent facies form packages metres to 10's m thick; facies contacts are rarely erosional, and more commonly sharp, though they become more diffuse with increasing carbonate content. There is a weak trend of increasing carbonate-content (both detrital and cement) up-section within the

facies association, particularly when transitioning into the carbonate ramp facies association. The facies association occurs with the microbial mat, intertidal, sabkha, and carbonate ramp facies associations, and commonly shows gentle retrogradational facies stacking on a scale of 10's m where it transitions into the carbonate ramp facies association. Where interbedded with intertidal and sabkha facies associations, the foreshore - shoreface facies association tends to be thinner, metres in thickness, increasing in thickness to 10's m where it is interbedded with the carbonate ramp facies association.

The compositional maturity, abundant evidence of wave-reworking in the form of trough cross-stratification, and traction sedimentation are characteristic of modern foreshore and shoreface settings (Tucker, 1985; Frey and Howard, 1988; Antia et al., 1994). Abundant planar lamination may be attributed to bi-directional sheet flows (e.g. swash and backwash) in the foreshore domain, whereas trough-cross stratified portions may represent a significant influence of oscillatory flows, possibly representing sand bars (Frey and Howard, 1988; Ashley, 1990; Antia et al., 1994). The strong coupling of these facies with other coastal facies associations supports this interpretation.

Quartzites in Nchanga have been interpreted by Binda (1994) as littoral sand sheets, with a possible marine origin also invoked for arenites south of Chibuluma. A marine origin has also been inferred for the 'glassy quartzite' unit in the Lower Roan (Binda and Mulgrew, 1974).

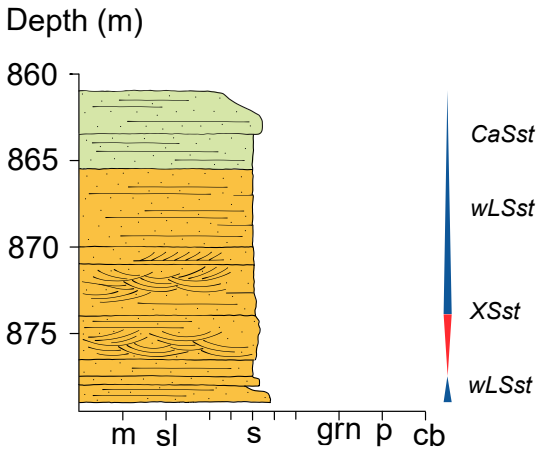

Figure 3.14: 18 m long type log for the shoreface facies association, showing a section of the IT26 core. Well-sorted and cross-stratified sandstones gently deepen into carbonate-bearing sandstone units. Planar and ripple lamination is abundant, with the lower parts of the facies association showing well-developed trough cross-beds.

3.4.13 Carbonate ramp facies association

The carbonate ramp facies association predominantly comprises carbonate facies with only a minor clastic component: CaSl, lSlCa, CaSst, SstCa, MCa, pLCa, and vLCa. It makes up a significant proportion ($\sim$ 1/3 by thickness) of the stratigraphy in the ten cores logged and occurs in packages 10's to often 100's m thick. L83 is the type core for this facies association (fig. 3.15).

Carbonate facies, which are now mostly dolomitic in composition (MCa, LCa), rarely show diagnostic primary features due to pervasive recrystallisation. They form successions 10's to 100's m thick. Mixed clastic-carbonate facies (CaSst, SstCa, CaSl, lSlCa) show more developed primary structures (e.g. cross-stratification, graded laminae, rhythmites). Carbonate-bearing siltstones (CaSl) are the most volumetrically abundant facies in this association, forming continuous units 100's m thick. Coarser mixed clastic-carbonate facies occur in successions 10's m thick. Contacts between coarser, more clastic, facies are generally sharp. Finer clastic-carbonate and carbonate facies show more diffuse or gradational transitions. Isolated emergent surfaces (Rk) may punctuate this facies association (e.g core L83). The facies association is aggradational to retrogradational. It is found in association with intertidal, foreshore, microbial and transition zone facies associations.

Detailed interpretation of this facies association is limited by pervasive dolomitisation and recrystallisation of carbonates, obscuring diagnostic primary structures in hand specimen. Only in clastic-carbonate facies can primary structure be discerned sufficiently for a first-order approximation of depositional processes (e.g. wave influence) to be inferred. The lack of evidence for sediment-gravity flows (i.e. CaDia, CaCgm facies) and limited clastic facies therefore leads to the facies association being broadly interpreted as a carbonate ramp. Where there is sufficient clastic material to identify primary structure, or ooids are identifiable, planar and cross-laminated sandy carbonates may represent barrier bars or sand shoals on the inner ramp (Tucker, 1985; Siahi et al., 2016). Clean, crystalline carbonate units may speculatively represent recrystallised ooid shoals, or carbonate crystals precipitating and falling out of suspension (Hood et al., 2015; Hood and Wallace, 2018).

The abundance of silty and massive carbonates possibly represent carbonate mud with minor clastic influence, and is interpreted to have formed on the distal portions of the ramp, either below the storm wave base or in a restricted marine setting. Sharply bounded oxidised surfaces showing dissolution structures and red clays (i.e. Rk facies) could be attributed to periodic emergence of the ramp and

possible vadose alteration (Kenny and Knauth, 2001; James and Dalrymple, 2010), though this is difficult to distinguish from basin-wide hydrothermal alteration (Selley et al., 2005). Where there is evidence of rhythmites (e.g. core ZMSDD003), a restricted carbonate-producing setting is inferred, on account of limited wave reworking and cyclical, possibly seasonal, clastic input and carbonate precipitation (Zolitschka et al., 2015; Siahi et al., 2016).

The difficulty of assigning precise depositional environments to many recrystallised carbonate units was emphasised by Bull et al. (2011). This makes interpreting large parts of the stratigraphy problematic, as carbonate units are common and laterally extensive, with Binda (1994) suggesting a shallow carbonate platform possibly existing across the whole of the Copperbelt. Some workers have referred to reefs, e.g. (Mendelsohn, 1961; Clemmey, 1976), suggesting a rimmed shelf; however, uncertainties lie in proving long-range continuity between microbial build-ups in space and time across the Copperbelt.

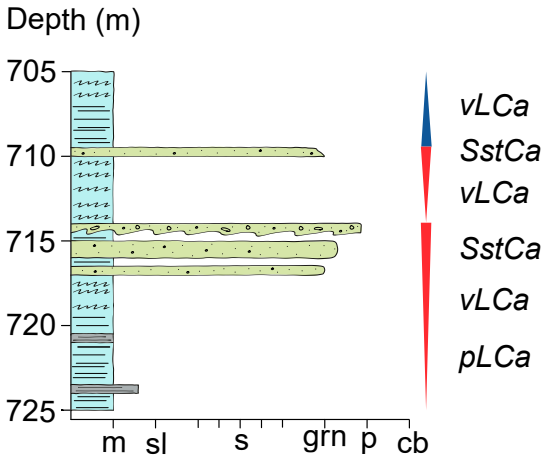

Figure 3.15: 20 m long type log for the carbonate ramp facies association in the IT26 core, showing laminated carbonates, sometimes with enigmatic serrated textures and thin interstitial mudstones and siltstones, shallow upwards into coarse sandy carbonate facies.

3.4.14 Glaciomarine facies association

The glaciomarine facies association is characterised by diamictite facies where a glacial origin can be reasonably assumed on account of lonestones, dropstones or ice-rafted debris (Bennett et al., 1996). It includes the dMs, XSst, fCCgm, cpDia, crDia, CaMs, lSlCa, and MCa facies. The two diamictite facies are juxtaposed in figures 9.13 and 9.14. The facies association is metres to 10's m thick and is well-expressed in cores L83 and ZMSDD003 (fig. 3.18).

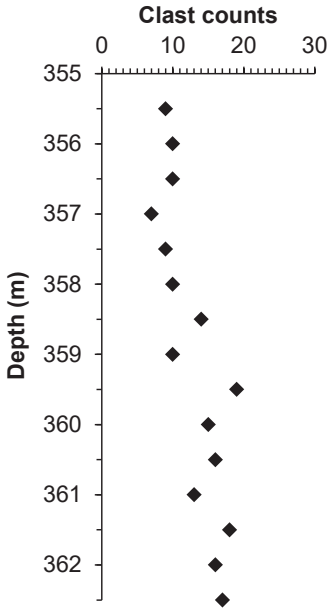

Figure 3.16: Clast counts for the crDia subfacies in the ZMSDD003 core, measured at 0.5 m intervals, showing higher clast proportion and tendency for upwards clast quantity reduction.

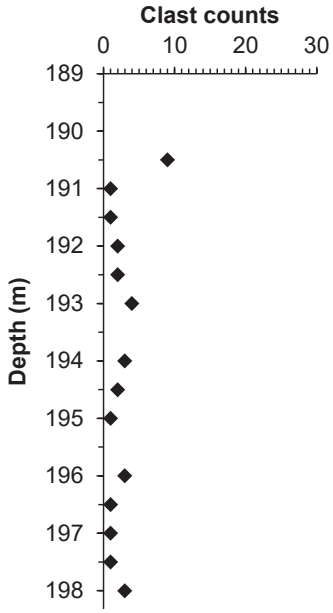

Figure 3.17: Clast counts for the cpDia subfacies in the ZMSDD003 core, measured at 0.5 m intervals, showing significantly lower clast counts ($<$ 10 clasts / 0.5 m).

Clast-poor diamictite facies (cpDia) are the most diagnostic of this facies association, containing lonestones and dropstones (though these are rare) forming units metres to 10's m thick. These may be sharply underlain by mudstone facies (dMs) and interbedded mudstones and carbonates (CaMs), 10's m thick. In the ZMSDD003 core, clast-poor diamictites sharply overlie texturally and compositionally immature coarse clastic facies (XSst, fCCgm). Diamictite facies are often sharply overlain by carbonate facies (MCa, lSlCa), 10's m in thickness. The clast-rich diamictite facies (crDia) is less diagnostic of a glacial origin, as it frequently represents debris flow deposits (Kennedy

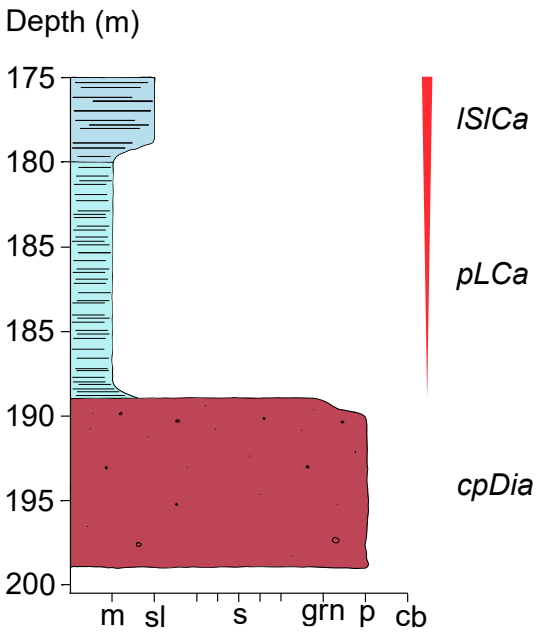

Figure 3.18: 24 m long type log for the glaciomarine facies association, showing a section of the ZMSDD003 core. Clast-poor diamictite facies, interpreted to be of glacial origin, are sharply overlain by planar laminated carbonates, followed by laminated silty carbonates.

et al., 2019). However, it may contain ice-rafted debris in mud-rich intervals suggesting a possible weak glacial component (e.g. core IT26). The facies association is often coupled with the transition zone and deep water facies associations. In the ZMSDD003 core it overlies the glaciofluvial facies association.

The facies association is interpreted to represent deposition of material in advance of an ice front. Proximal or distal deposition may cautiously be inferred from clast quantity, dropstones and underlying facies associations. Clast-rich diamictite facies that show glacial influence, or clast-poor diamictite facies underlain by terrestrial facies associations (e.g. the glaciofluvial facies association) are interpreted as more proximal (Eisbacher, 1985). Clast-poor diamictite facies may be interpreted as more distal glaciomarine sedimentation when occurring with transition zone and deep water facies associations (Hoffmann et al., 2004).

The interpretation of this facies association is in agreement with Master and Wendorff (2011)'s interpretation of much of the Grand and Petit Conglomerat, also describing dropstones, as well as faceted and striated clasts. Binda and Van Eden (1972) and Wendorff and Key (2009) invoked ice-rafting as the mechanism introducing clasts into distal portions of the basin.

3.4.15 Transition zone facies association

The following fine-grained, structured, clastic and mixed clastic-carbonate facies comprise the transition zone facies association: SlMs, LSl, CaMs, CaSl, and lSlCa. It forms successions 10's to 100's m thick and is well-expressed in cores CHLDD001 and L83. (fig. 3.19)

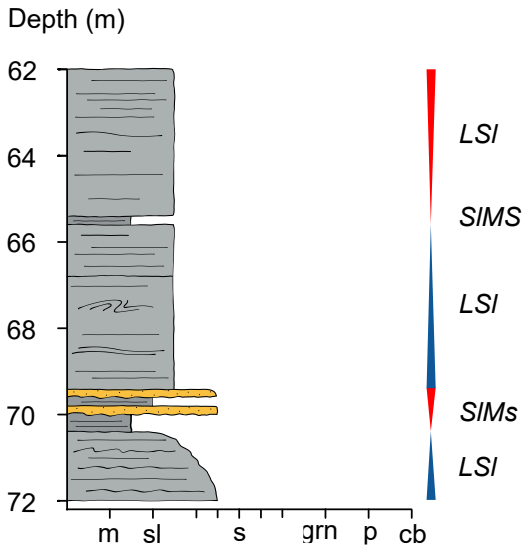

Figure 3.19: 10 m long type log for the transition zone facies association in the CHLDD001 core. Laminated mudstones and siltstones with thin intercalated sandy beds show abundant lamination, and soft-sediment deformation, forming part of an overall aggradational facies package.

Fine clastic facies (SlMs, LSl), and carbonate-bearing siltstone facies (CaSl, lSlCa) predominate. These form packages 100's m thick and may pass transitionally into interbedded carbonate and mudstone packages (CaMs) 10's m in thickness. Evidence of the substrate being reworked by storms or wave action occurs in the form of planar and wavy lamination, hummocky and ripple cross-lamination. The facies association is generally aggradational or retrogradational and occurs with the carbonate ramp and deep water facies associations.

The transition zone facies association is dominated by facies deposited from suspension, occasionally showing evidence of current re-working (Reineck and Singh, 1980; Tucker, 1985). It is differentiated from the deep water facies association by the abundance of silty facies, and variety of lamination. Abundant graded laminae in laminite packages suggest periodic sediment flux into a low-energy environment. Wavy and ripple lamination, and minor scour are attributed to wave or storm influence (Pickering et al., 1986). Deposition near the storm wave base is further supported

where edgewise conglomerates are present (Sepkoski, 1982).

3.4.16 Deep water facies association

The deep water facies association comprises fine-grained facies, dMs, SlMs, and CaMs, that do not show evidence of wave-reworking (fig. 3.20). It forms packages 10's to 100's m thick. The type core for the facies association is KN192.

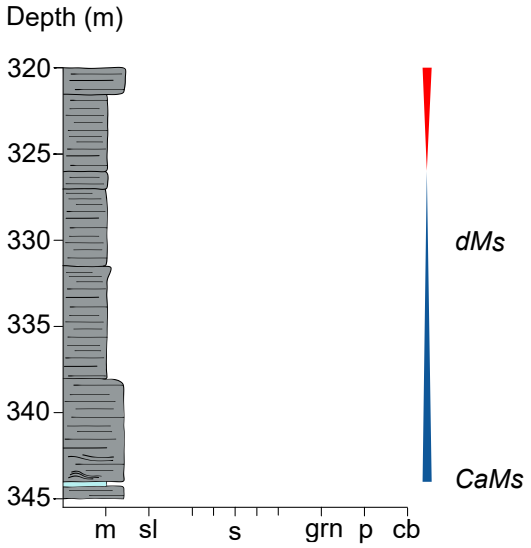

Figure 3.20: 25 m long type log for the deep water facies association, showing a section of the ZMSDD003 core. Laminated carbonate-bearing mudstone facies are overlain by planar-laminated dark mudstones. A possible cm-scale slump structure occurs at the base of the dark mudstone succession.

Mudstone facies (dMs) are ubiquitous, forming packages 10's m thick, sometimes showing a minor silty component (SlMs). These may be interbedded with carbonate beds (CaMs) forming interbedded mudstone-carbonate units 10's m to 100's m thick. Planar lamination characterises this facies; wavy laminae or thin silty beds are rare or absent. Contacts between facies are gradational or indistinct. The facies association occurs with the transition zone and distal glaciomarine associations.

Facies in the deep water association are interpreted to have been deposited by suspension settling below the storm wave base due to an absence of bed working or storm-related deposits (Pickering et al., 1986). The carbonaceous composition of many mudstones that could be ascribed to this facies association have been interpreted to have been deposited in dysoxic or anoxic conditions by Selley

et al. (2005). A distinction between a deep lacustrine or marine setting is only suggested where a significant lateral extent can be proven, or there is evidence of evaporite minerals, both of which would favour a deep marine setting.

Though not explicitly stated, Binda (1994) implied that what was termed the 'basinal ore shale' in the Lower Roan was deposited in deeper water than its more marginal equivalents.

3.4.17 Subaqueous slope facies association

The submarine slope facies association comprises the SstMs, Wck, MsgSst, tMsSst, cpDia, crDia, CaDia, CaMs, and CaCgm facies, interpreted to have formed as a result of sediment gravity flows or movement along a slope. The facies association occurs in packages 10's m thick; its type cores are KN192 and L83 (fig. 3.21).

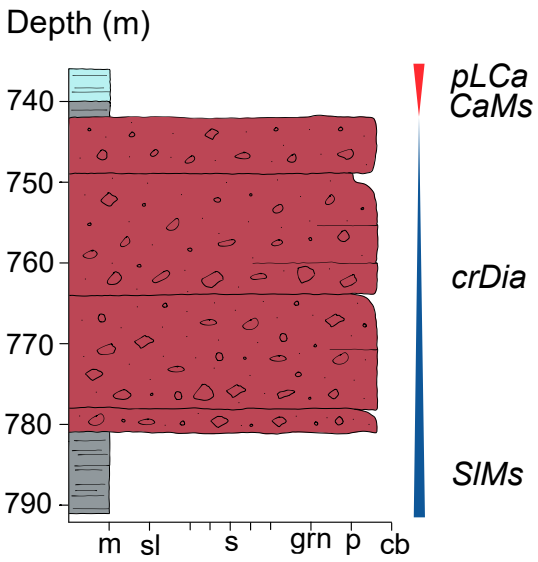

Figure 3.21: 55 m long type log for the subaqueous slope facies association in the L83 core. Clast-rich diamictite facies sharply overlie silty mudstones, forming a deepening succession, which shallows up into carbonate-bearing mudstone and laminated carbonate facies.

Some facies in this association also occur in the delta slope and prodelta facies associations, such as sandy mudstones (SstMs), muddy sandstones (Wck) and graded sandstones and mudstones (MsgSst). These facies may be sharply interbedded with one another on a scale of decimetres - 10's m, and commonly occur in packages metres to 10's m thick in the subaqueous slope facies association. It is differentiated from deltaic facies associations by not occurring in proximity to, or

with, terrestrial facies associations.

Coarse carbonate-bearing facies (CaCgm, CaDia) are found closely associated with each other in the KN192 core and are 10's m thick. Clast-rich diamictite facies (crDia) 10's m thick, and some carbonate-bearing mudstone facies (CaMs) with slump structures may be interpreted as derived from slope-driven processes. Coarser facies in the facies association (CaCgm, CaDia, crDia) tend to share sharp contacts with adjacent facies. Facies transitions tend to become more diffuse with increasing mud content (SstMs, MsgSst, CaMs). The facies association often does not show clear fining or coarsening-upwards successions, possibly being aggradational. It tends to be bounded above or below by transition zone and deep water facies associations.

The facies association is interpreted as representing deposition on, or at the foot of, subaqueous slopes on account of its constituent facies being interpreted as sediment gravity flow deposits (Lowe, 1982; Talling et al., 2012). Interbedded mudstones and graded sands likely represent turbidites (Bouma et al., 1962). Wacke, carbonate conglomerate, clast-rich diamictite and carbonate diamictite facies are broadly interpreted as subaqueous debris flows (Lowe, 1982; Shanmugam, 2000). Carbonate conglomerate and diamictite facies could represent carbonate platform shedding (Pickering et al., 1986). The facies association's carbonate facies, proximity to the transition zone and deep water facies associations preclude a subaerial slope interpretation.

Bull et al. (2011) suggested carbonate reef shedding and sediment gravity flows could be a depositional mechanism for some carbonate beds in the Chambishi sub-basin. Wendorff and Key (2009) described conglomerate successions likely deposited by both from debris flows and turbidites at the Mushishima River and Itawa.

3.5 Type examples of facies successions

Facies associations often stack in facies successions that are characteristic of, or particularly prevalent in, particular periods in the Katangan basin's history. Given the limitations of using only 1D drill core for determining depositional environments, not all successions can be interpreted with equal confidence. The following are three examples of readily interpretable facies successions, that illustrate key parts of the basin's stratigraphic architecture.

Lower Roan to Upper Roan Group, core KN192: fan-delta → intertidal facies succession

Core KN192 represents the type core for a fan-delta facies association overlain by a delta slope facies association, which transitions up into the intertidal facies association (fig. 3.22). A $\sim$ 10 m thick unit of crudely fining-up coarse conglomeratic facies (fCCgm) at the base of the succession is sharply overlain by a 10's m thick unit of sandy mudstone facies (SstMs). Upwards-thinning conglomerate facies ($<$ 2 m thick) punctuate the succession of sandy mudstone facies at intervals of 10's m. Conglomeratic units are replaced up-section by initially thin ($<$ 1 m thick) units of carbonate-bearing facies and emergent surfaces (lSlCa, CaHet, Rk), which generally coarsen-upwards, and increase in frequency and thickness (to 10's m) towards the top of the succession.

The basal portion of the succession is interpreted to represent a retrograding fan-delta, with thin conglomeratic units and sandy mudstones episodically being washed off the delta plain onto the delta slope as debris flows and high-density turbidites. The deposition of thin carbonate units is interpreted to record the onset of shallowing-up, recording cyclical emergence and fan-delta expansion as intertidal zones become more extensive. The switch from retrogradational clastic facies to generally aggradational mixed clastic-carbonate facies could be explained by the clastic source becoming more distal and/or low-relief, with a reduced tectonic control on subsidence, or a more arid climate with reduced run-off and increased carbonate productivity.

This style of facies succession (clastic successions being replaced by paralic carbonate-rich facies) is also preserved in other parts of the basin (e.g. core RCB2 in the Chambishi sub-basin, core IT26 in Ndola) and appears common in the Lower Roan (Mendelsohn, 1961; Clemmey, 1976; Binda, 1994). This suggests alluvial fans, and fan-deltas prograding into lacustrine or marine environments, were

widespread. The lateral extent and continuity of intertidal and lagoonal deposits, compared to the alluvial and fluvial successions that they overlie, suggests a significant change in basin configuration. The transition from predominantly (fan-)deltaic, deeper water sedimentation, characterised by an abundance of sediment gravity flow deposits, to cyclical intertidal and marine deposition dominated by carbonate units is interpreted to represent a stratigraphically significant interval. It is interpreted to record a regional shallowing, and attenuation of fault-control on subsidence.

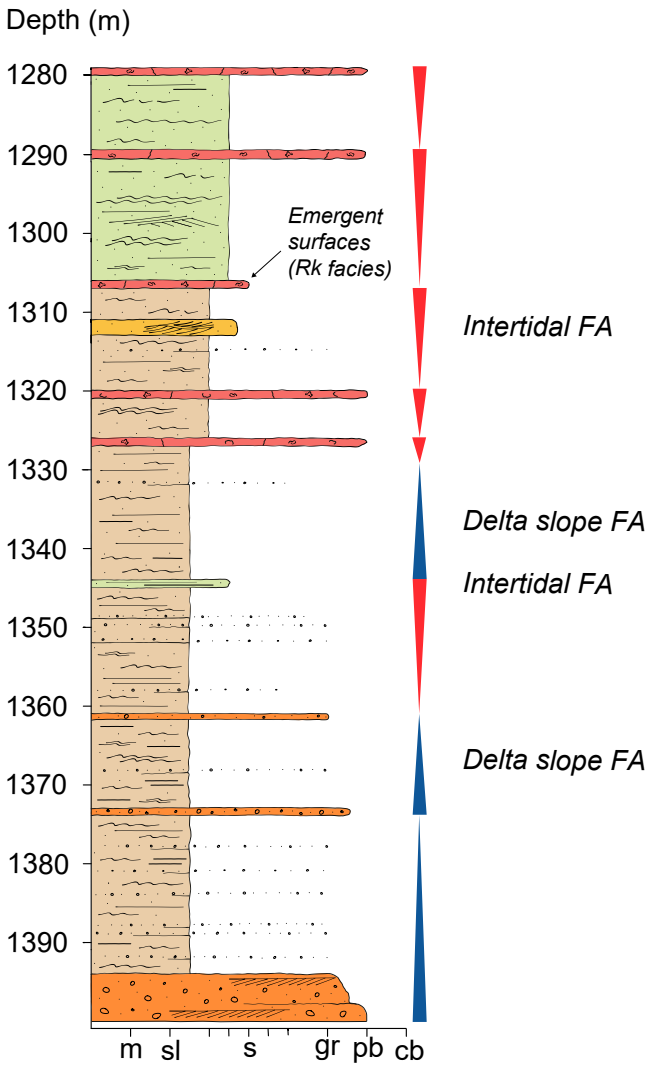

Figure 3.22: 120 m long succession of fan-delta and delta slope to intertidal facies associations in core KN192. Note upwards thinning and fining of conglomerate units, and subsequent thickening of carbonate units, as the succession switches from overall retrogradational to overall progradational.

Mwashia to Nguba Group, core KN192: deep carbonate ramp → submarine slope succession

KN192 and L83 are type cores for a deep carbonate ramp facies association deepening-upwards into a submarine slope facies association (fig. 3.23). In core KN192, carbonate-bearing siltstones facies (CaSl) form the base of the succession, which is interrupted by a thin set of carbonate-diamictite (CaDia) beds. The diamictite units share diffuse contacts with the underlying siltstones, though dolomitisation has possibly obscured originally erosive bases. The diamictite beds pass sharply into carbonate-bearing siltstone facies which gradationally transition into stromatolitic carbonates (StMic). These share a diffuse contact with a $\sim$ 40 m thick package of carbonate-bearing diamictite (CaDia) and interstitial carbonate conglomerate facies (CaCgm). Isolated clasts within the diamictites might represent dropstones, though the evidence for this is not conclusive. A sharp transition to carbonate-bearing mudstones (CaMs) marks the top of the succession.

The lower portions of the succession are interpreted to represent a transition zone setting, likely on a deep carbonate ramp, with possible stromatolite fields. The diamictite and conglomerate facies are interpreted to predominantly represent debris flows and shedding of the Upper Roan carbonate shelf. The presence of stromatolites just below diamictites generated via debris flows suggests rapid deepening and generation of submarine topography during the upper Mwashia or lower Nguba times. A glacial influence cannot be discounted, with carbonate clasts possibly plucked from stromatolitic reefs. A general lithostratigraphic correlation of this succession with the Grand Conglomerat is supported by thick carbonate units (not shown in figure 3.23) above the carbonate-bearing mudstone facies at the top of the succession, and debris flow deposits indicating submarine topography that was not present in underlying Upper Roan successions. Debris flows deposited in the Zambian Copperbelt during the Mwashia and early Nguba times could therefore be interpreted as significant downlapping surfaces, analogous with diamictite units in Kamoa (Schmandt et al., 2013; Kennedy et al., 2019) with glaciomarine units representing very approximate chronostratigraphic markers where they can be firmly identified (Master and Wendorff, 2011; Halverson et al., 2020).

Nguba to Kundelungu Group, core ZMSDD003: Deep water → glaciofluvial → glaciomarine succession

The ZMSDD003 core is the type core for a likely sequence boundary separating a succession of deep water sediments from glaciofluvial and glaciomarine facies associations (fig. 3.24).

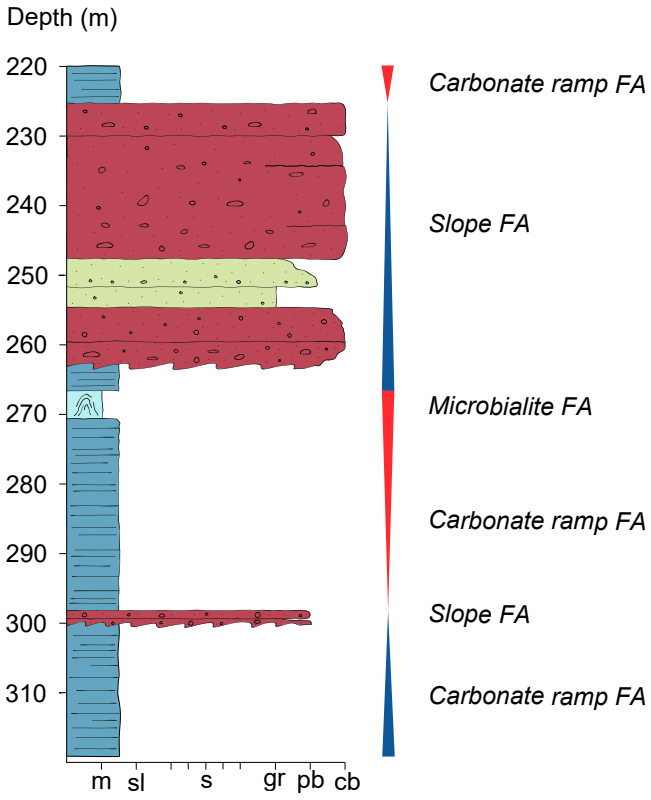

Figure 3.23: 100 m long deep carbonate ramp to slope facies association succession in core KN192. Note possible stromatolitic textures just underneath the carbonate diamictite, possibly representing a source for the carbonate clasts in the overlying diamictite.

The base of the succession comprises silty mudstones (SlMs). These are unconformably overlain by a 5 m thick unit of texturally and compositionally immature fine conglomeratic (fCCgm) and sandstone facies (XSst) eroding into the underlying mudstones. Some sandstone beds crudely fine upwards and show unidirectional cross-bedding and planar lamination. Coarser clastic facies sharply transition upwards into a 10 m thick mud-rich, clast-poor diamictite (cpDia) unit. This is overlain by thinly laminated carbonate units and silty carbonate rhythmites (lSlCa).

The base of this succession comprises deep water sediments, likely deposited at or below the storm wave base. What are interpreted to be glacial outwash beds erode into these facies, forming a stratigraphically significant unconformity. These facies are overlain by glaciomarine facies representing the Petit Conglomerat. The position of this unconformity near Mansa, on the Bangweulu block, likely marks the basin margin and indicates that depositional systems shifted basinwards during early Kundelungu times, forming a possibly 2nd or 3rd order sequence boundary (Catuneanu et al.,

2009; Master and Wendorff, 2011).

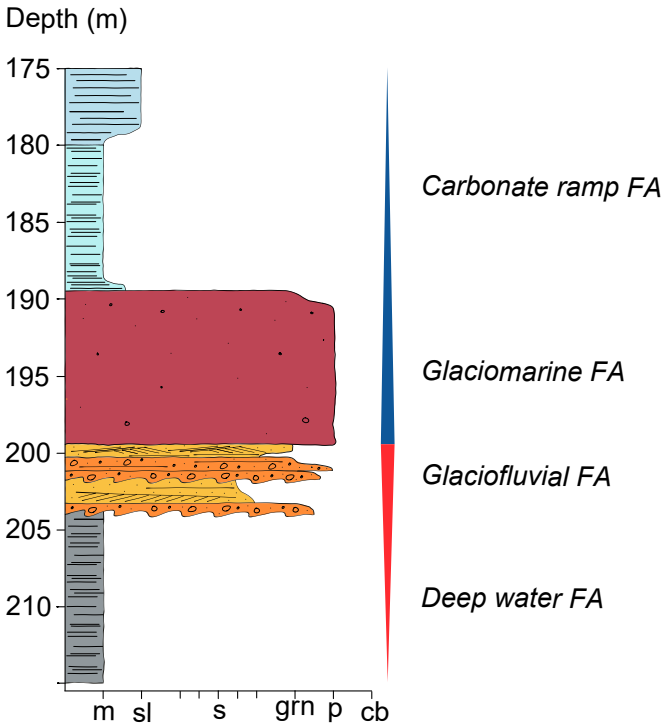

Figure 3.24: 40 m long succession of deep water to glaciofluvial and glaciomarine facies associations in core ZMSDD003, initially shallowing up, then deepening. Note the erosional contact at the base of the glaciofluvial facies association.

3.6 Stratigraphic evolution

The proposed facies scheme allows for plausible generalised depositional environments to be determined for each major stage in the stratigraphic evolution of the Katangan basin. At the large scale of the following discussion, at the stratigraphic Group level, stratigraphic units are considered to represent, and refer to, broad time intervals in the basin's history. For clarity, names of stratigraphic Groups used here broadly overlap with the lithostratigraphic schemes established in the Zambian Copperbelt by Selley et al. (2005) and Batumike et al. (2007). Quantitative facies distributions, based on 8 cores across the basin, are provided for each stratigraphic Group, with Groups defined using the sequence stratigraphic correlation 1 presented in Chapter 4. These are supplemented by simplified block diagrams based on classical rift stratigraphy models, intended to show general facies trends throughout the basin's evolution (Nottvedt et al., 1995; Gawthorpe and Leeder, 2000; Holz et al., 2017).

Lower Roan

Deposition in the Lower Roan was predominantly terrestrial, comprising alluvial fan, fluvial and fan-delta systems. Topographic relief was high, evidenced by abundant coarse, immature facies (fig. 3.25). The thickness of continuous stacked fluvial successions ($>$ 1 km in core KRX082) suggests significant accommodation space generation, outpaced by sediment supply, resulting in protracted terrestrial sedimentation in many parts of the basin. Rapid facies transitions and amplified aggradational successions suggest accommodation space generation was predominantly fault-controlled in much of the Copperbelt. Periodic fault movement and flooding of sub-basins lead to subaqueous deposition, generating turbidite and slope successions, when the rate of local accommodation space generation exceeded the rate of sediment supply (e.g. core KN192). Notable is the paucity of carbonate facies (fig. 3.25).

The variability in stratal geometry, ranging from progradational to retrogradational, is characteristic of early continental rift basin stratigraphy with particularly rapid fault-driven subsidence (Gawthorpe and Leeder, 2000; Holz et al., 2017). The general interpretation of the Lower Roan recording syn-rift basin fill is in agreement with well-established interpretations for the Lower Roan (Binda, 1994; Selley et al., 2005; Bull et al., 2011). The abundance of alluvial fan, fluvial and fan-

delta deposits, and significant lateral facies variation has been noted by several authors (Clemmey, 1976; Eden, 1974; Bull et al., 2011), and is illustrated in figure 3.26. These facies are interpreted to have been initially deposited in disconnected half-graben during the early phases of extension, and subsequently more connected graben in the late Lower Roan, derived directly from surrounding basement (Binda, 1994; Selley et al., 2005; Bull et al., 2011).

Lower-Upper Roan transition

The transition from Lower Roan to Upper Roan is characterised by a more pronounced fining-up trend, transitioning from predominantly aggradational to retrogradational successions. These retrogradational successions represent a shift in the balance of accommodation space generation rate and siliciclastic sediment supply (A/S) that has been related to the rift climax (Selley et al., 2005; Holz et al., 2017). To what extent they do is difficult to determine in the absence of independent chronological constraints, as A/S ratios can vary significantly along depositional strike (Schlager, 1993), especially in deltaic settings, which appear common in the Lower Roan.

The suggestion of lateral equivalence of retrogradational successions at a roughly similar stratigraphic level has been used by previous authors to argue in favour of a significant transgression. The surface separating the Upper and Lower Roan is traditionally the first clear, laterally extensive carbonate unit (Selley et al., 2005; Bull et al., 2011). The transition between Lower and Upper Roan tends to show a successive upwards thickness reduction in conglomeratic units, with the first carbonates appearing. Alluvial fans and fan-deltas likely became more laterally extensive, their outer portions transitioning into shallow, tidally influenced carbonate mud and sandflats, or lagoons (e.g. core IT26). Marine influence, recorded by carbonate units, intertidal, and foreshore successions became more frequent, suggesting sub-basins rapidly began to connect. Sabkha environments began to develop, with episodic emergence of sub-tidal deposits (fig. 3.25). Such a broad re-organisation associated with siliciclastic sediment supply shifting towards the basin margins as the basin broadens is a typical feature of their transition from fault-dominated syn-rift to thermally dominated post-rift subsidence (White and McKenzie, 1988; Holz et al., 2017).

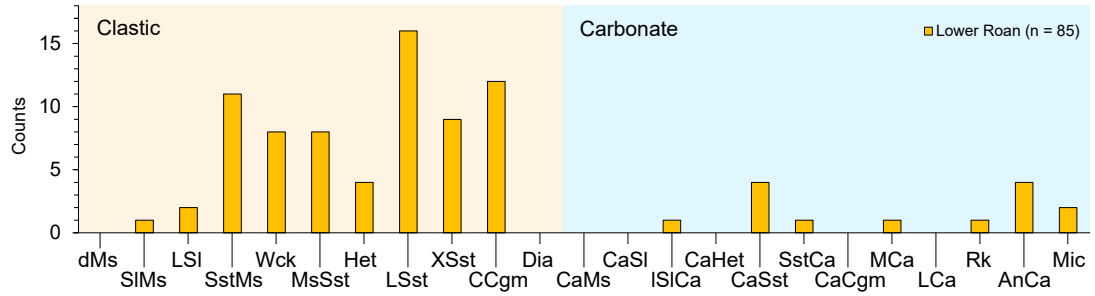

Figure 3.25: Facies occurrence counts (i.e. number of separate countable facies units) in the Lower Roan Group showing clear preponderance of clastic facies. Carbonate-bearing facies represent the transition towards the Upper Roan Group.

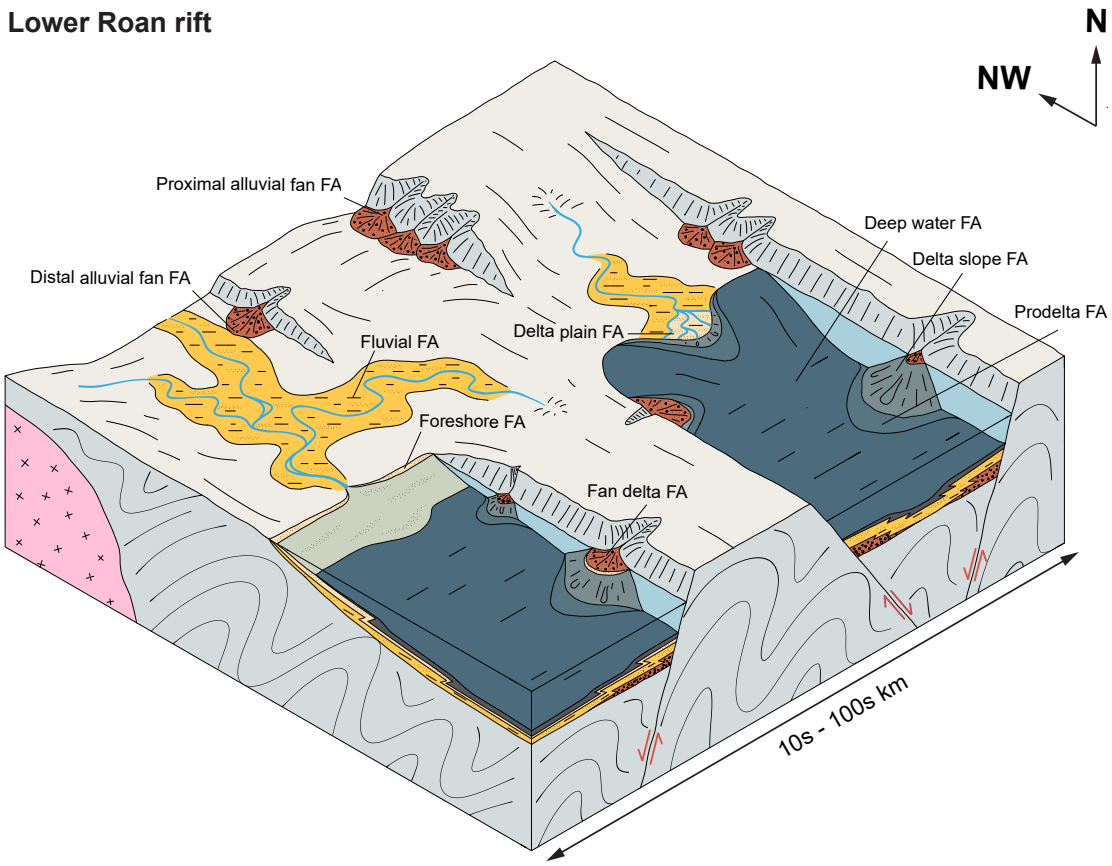

Figure 3.26: A schematic block diagram showing conceptual succession and distribution of gross depositional environments the Zambian Copperbelt during the syn-rift stage of basin evolution. Terrestrial deposition predominates, with prevalent facies associations marked. The block diagram does not represent a specific location, but is an amalgamation of depositional system trends observed throughout the Zambian Copperbelt stratigraphy.

Upper Roan

The Upper Roan is dominated by carbonate and mixed clastic carbonate facies. Terrestrial sediment supply was significantly attenuated during this time, with the abundance of fine sands and silts, and absence of siliciclastic conglomerate facies indicating denudation of the hinterland and fault-control on subsidence diminishing. The reduction in occurrence of abrupt facies transitions, abundance of facies alternation and gradational facies contacts suggests deposition on a shallow-dipping basin, with eustasy possibly playing a greater role in driving accommodation space generation.

Periodic emergence of sub-tidal deposits generated cycles of emergent, possibly karstified, surfaces. Biotically mediated carbonates predominated in the intertidal and sub-tidal realm; intertidal mudflats, lagoons, and sabkhas comprised extensive coastal regions. These features are indicative of thermal subsidence being the main tectonic subsidence mechanism (Holz et al., 2017). Abundant evaporite minerals indicate an arid climate predominated for much of the Upper Roan. This is supported by clastic sediment supply being almost completely shut off (fig. 3.27), as drainage systems dried up and coarse clastic supply was restricted. The Upper Roan therefore likely represents an extensive epicontinental sea in an arid shallow-dipping basin with denuded fault-topography and mixed clastic-evaporitic margins (fig. 3.28). Restricted parts of the basin are inferred to be plausible sites for salt precipitation.

The base of the Upper Roan in the classical Copperbelt likely marks a sediment-restricted post-rift unconformity, or its correlative conformity (Bosence et al., 2009). This is on account of emergent surfaces (e.g. core KN192), the abrupt switch from predominantly clastic to predominantly carbonate facies, abundance and lateral continuity of sabkhas and intertidal zones (e.g. cores RCB2, L83), and attenuated fault-control on stratigraphy (Holz et al., 2017).

The prevalence of intertidal mudflats, sabkha environments, hypersalinity, and an extensive carbonate shelf in the Upper Roan is well-established (Annels, 1974; Clemmey, 1976; Binda, 1994; Selley et al., 2005; Bull et al., 2011). This work is in agreement with previous interpretations of a widespread and long-lived carbonate shelf existing across much of the Zambian Copperbelt during the Upper Roan.

The 'Kitwe Barren Gap reef' was interpreted by Clemmey (1974) as being a palaeo-island, suggesting that reefs on horst blocks could have formed palaeo-islands along much of the Zambian Copperbelt. Binda (1994) argued for a carbonate platform covering much of the basin during the

Upper Roan. This is supported by Bull et al. (2011)'s interpretation of a low-relief 'attached carbonate platform' developing in the Chambishi sub-basin after fault-control on stratigraphy had waned.

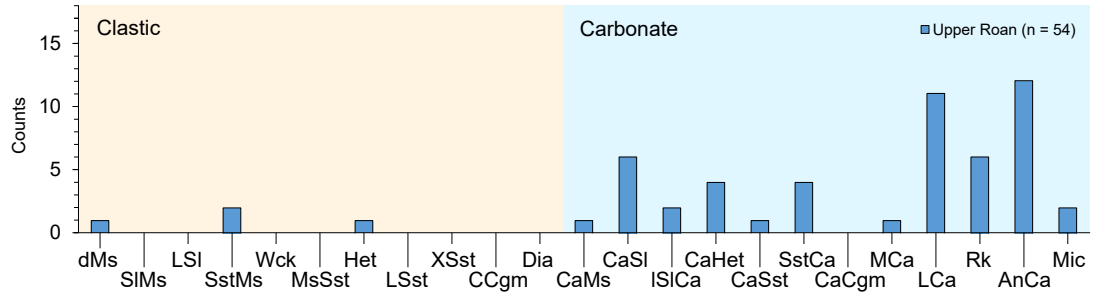

Figure 3.27: Facies counts in the Upper Roan Group showing a clear reversal of facies trends compared to the Lower Roan, with clastic facies being almost absent and carbonate facies predominating.

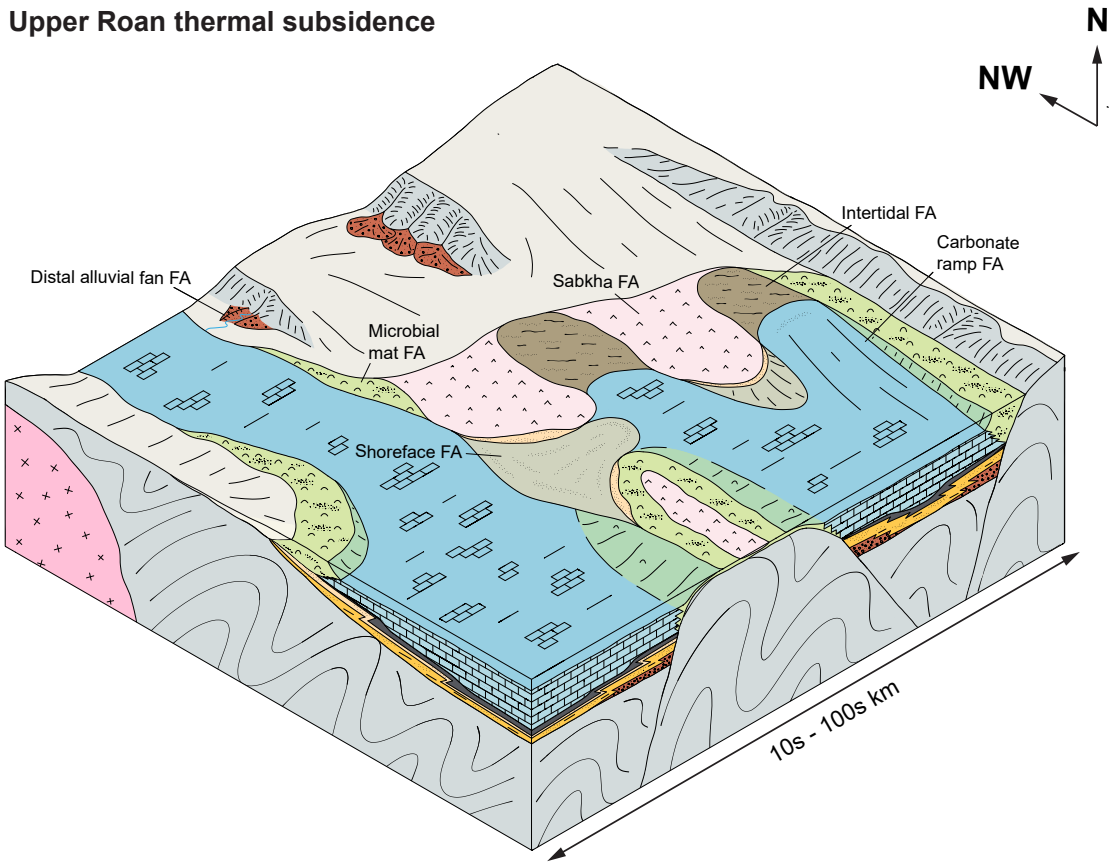

Figure 3.28: A schematic block diagram of the Zambian Copperbelt during Upper Roan Group times, showing a more connected basin with abundant carbonate facies as part of an epicontinental sea.

Mwashia

The Mwashia Group marks a significant deepening of the basin, and a rapid drowning of shallow marine facies in the Zambian Copperbelt. Transition zone and deep water facies predominate (fig. 3.29), periodically shallowing into stromatolitic carbonates on the basin margins (e.g. IT26). Mwashia shallow marine facies (e.g. CaSst) appear absent in the classical Zambian Copperbelt around the Kafue anticline. Silty carbonates and interbedded carbonates and carbonaceous shales are widespread, likely representing sediment-starved distal portions of carbonate ramps (fig. 3.30). Wacke and sandy mudstone facies are common (e.g. core CHLDD001). A reduction in total facies count is in-part due to increased facies thicknesses and reduced facies transitions.

Facies successions are aggradational or gently retrogradational. The presence of subaqueous debris flows and slope-derived facies suggests that renewed fault-controlled subsidence could have generated significant submarine topography. Carbonate clast-rich conglomerates (e.g. core KN192) likely represent downlapping surfaces generated by shedding of portions of the Upper Roan carbonate shelf. Though whether they are derived from fault-bounded platforms or distally steepened ramps is unclear (Cook et al., 1972; Schlager et al., 1994). Extensive, low volume, tholeiitic mafic suites occur across the Katangan basin during this time (Kampunzu et al., 2000; Key et al., 2001). The Mwashia Group is therefore interpreted to represent the basin widening and re-rifting, drowning the Upper Roan carbonate shelf, and marks a stratigraphically significant unit marking the onset of a second phase of extension in the basin.

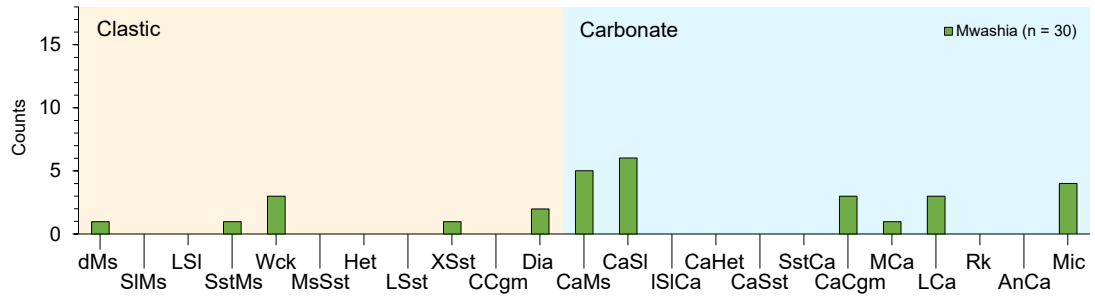

Figure 3.29: Facies counts in the Mwashia Group. Fine-grained facies with some carbonate content predominate, as do microbial facies. Diamictites are also introduced (towards the top of the Mwashia in core KN192).

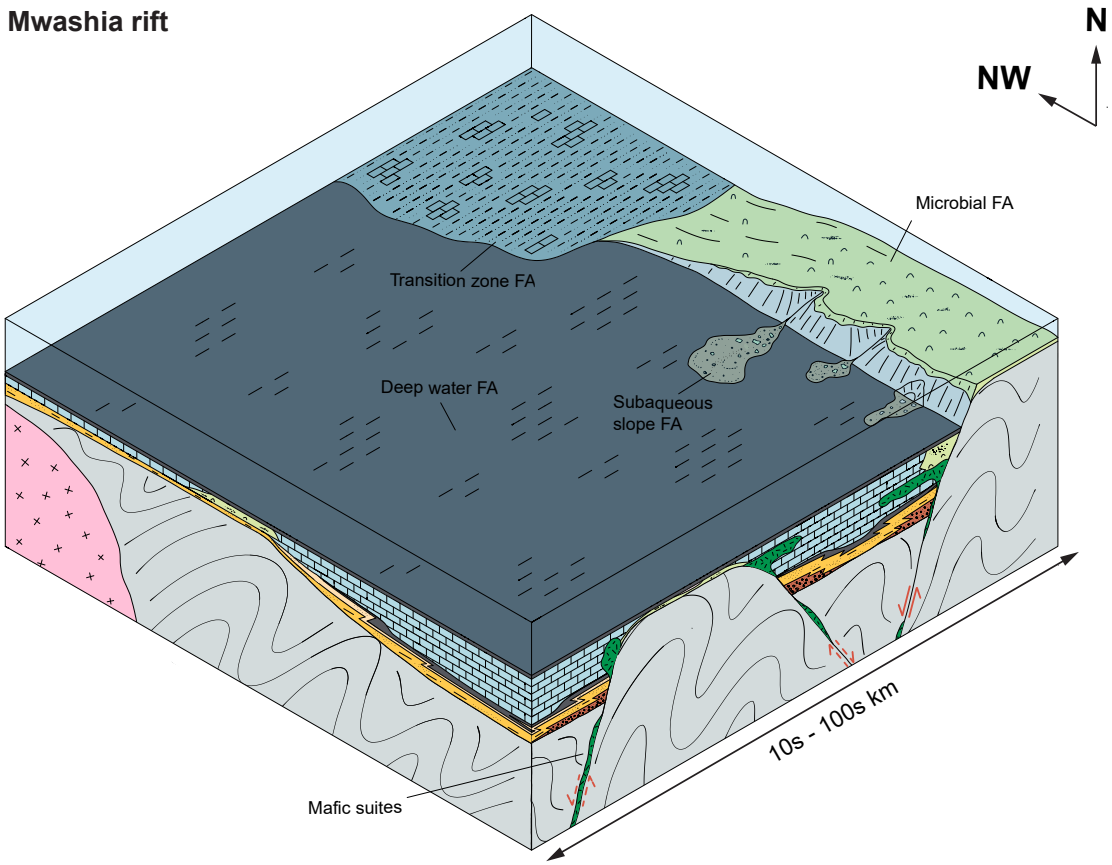

Figure 3.30: A schematic block diagram of the Zambian Copperbelt during renewed rifting in Mwashia times. Deep carbonate ramps predominated, with biotically mediated carbonates at the basin's margins. The basin began to widen and deepen, with renewed extension resulting in emplacement of mafic suites.

This interpretation matches that of Selley et al. (2005) and Bull et al. (2011), who interpreted Mwashia sediments to have been deposited sub-tidally, with carbonaceous shales covering the interpreted carbonate platforms. Resumption of tectonically controlled subsidence was invoked as the mechanism driving basin deepening. This coincided with widespread, low-volume, tholeiitic magmatism (Kampunzu et al., 1991, 2000; Key et al., 2001). Intrusive mafic bodies predominate in the Zambian Copperbelt, commonly intruded into the upper portions of the Upper Roan, and Mwashia Groups (Selley et al., 2005). The basin widening and deepening during a second phase of extension is evidenced more clearly in the D.R.C., where Poudingue and Mwashia sediments lie unconformably on Kibaran basement (Kennedy et al., 2019).

Nguba

The Nguba Group is defined lithostratigraphically by laterally extensive diamictites at its base, frequently overlain by carbonate units, correlatable across the Katangan basin (Wendorff and Key, 2009; Master and Wendorff, 2011). In most of the Zambian Copperbelt, Nguba diamictites lie conformably on Mwashia strata, though on the basin margins they rest unconformably on basement (e.g. core ZMSDD003 in Mansa). Diamictites tend to be clast-rich, often representing debris flows. The abundance of diamictites that have been interpreted here (e.g. cores L83 in Mufulira, KN192 in Lubambe, IT26 in Ndola) as being derived from debris flows supports Kennedy et al. (2019)'s conclusions, and could cast doubt on the chronostratigraphic significance of individual diamictite units assigned to the Grand Conglomerat. Glacial influence may be inferred in several locations across the Katangan basin, particularly on the Bangweulu block (Wendorff and Key, 2009; Master and Wendorff, 2011), suggesting widespread, though possibly diachronous, glaciation that broadly coincided with the resumption of extension in the basin. The basin likely remained deep throughout Nguba times, dominated by transition zone or deep water facies (fig. 3.31, 3.32), and distal sedimentation at or below the storm wave base. Intermittent periods of shallowing appear to have been brief. Following diamictite deposition (glacial or slope-derived), fault-control on subsidence likely diminished again throughout Nguba times, and post-extension thermal subsidence took over as the main subsidence mechanism.

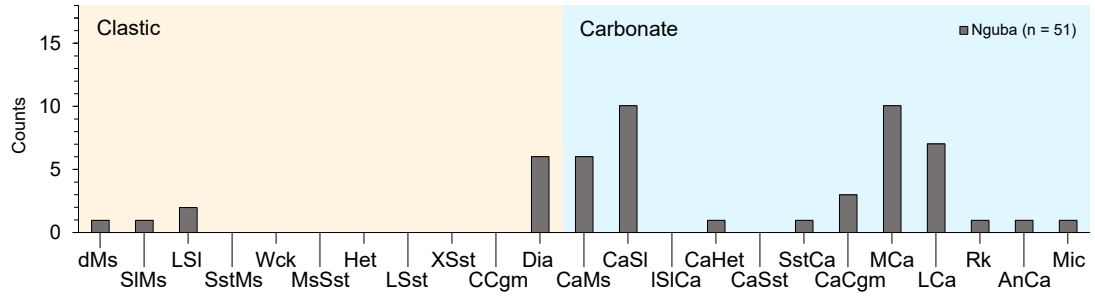

Figure 3.31: Facies counts in the Nguba Group showing an abundance of diamictites representing the Grand Conglomerat, and a preponderance of finer facies with carbonates. Note the paucity of microbial facies.

This interpretation agrees with previous work (Wendorff and Key, 2009; Master and Wendorff, 2011; Cailteux and De Putter, 2019). The basin broadening and deepening during Mwashia and Nguba times was also proposed by Wendorff and Key (2009), who noted diamictites resting un-

conformably on the Bangweulu block (as is the case in core ZMSDD003 in Mansa). Glaciofluvial sediments are more common in the North of the basin, with increasing marine influence southwards (Wendorff and Key, 2009).

A more detailed treatment of Grand Conglomerat stratigraphy is provided by Wendorff and Key (2009), Master and Wendorff (2011), and (Kennedy et al., 2019).

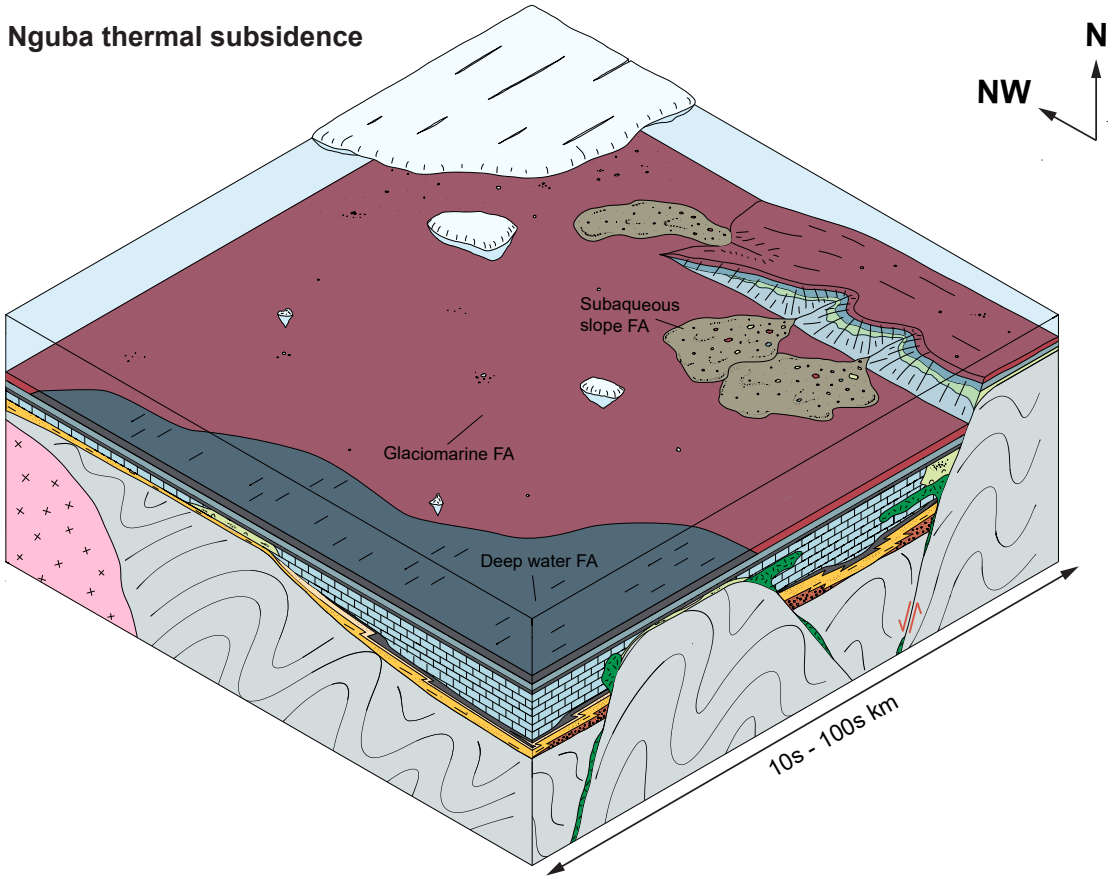

Figure 3.32: A schematic block diagram of the basin during Nguba times showing laterally extensive diamictites, both debris flow and glacially derived, representing the Grand Conglomerat, and a preponderance of finer facies as the basin remained deep following Mwashia rifting.

Kundelungu

The Kundelungu Group is not well-exposed in the Zambian Copperbelt. It is demarcated by diamictites of the Petit Conglomerat at its base, overlain by carbonates (Batumike et al., 2007). Like the Grand Conglomerat, the diamictite units attributed to the Petit Conglomerat are lithostratigraphically correlatable across the Zambian Copperbelt (Master and Wendorff, 2011). The diamictites are clast-poor, showing clearer evidence of glacial influence, and are interpreted as more distal.

The Petit Conglomerat conformably overlies Nguba sediments in most of the Zambian Copperbelt. However, in Mansa (core ZMSDD003) glaciofluvial units erode into Nguba strata, before being overlain by glacial diamictites. Whether the erosional unconformity at the base of the Kundelungu is associated with the basin beginning to invert (John et al., 2004), or due to glaciation-induced sea level fall is unclear. However, the surface is interpreted as a stratigraphically significant unconformity, marking a switch to progradational facies architecture on both the western and eastern margins of the basin near Mwinilunga and Mansa (Master and Wendorff, 2011).

Kundelungu facies above the Petit Conglomerat attest to a mixed clastic-carbonate system (fig. 3.33), and a gentle deepening of the basin. Facies counts are reduced on account of limited Kundelungu stratigraphy in the Zambian Copperbelt, and increased facies thicknesses in the deeper parts of the basin. What is exposed of Kundelungu stratigraphy above the Petit Conglomerat unconformity suggests mostly monotonous sedimentation on the shelf, periodically shallowing into supratidal successions. Terrestrial sediment sources likely remained distal throughout much of the Kundelungu. These conclusions support those of Wendorff and Key (2009) and Master and Wendorff (2011) who also identified a possible erosional unconformity at the base of the Petit Conglomerat in the Luapula beds, and invoked a glaciofluvial origin.

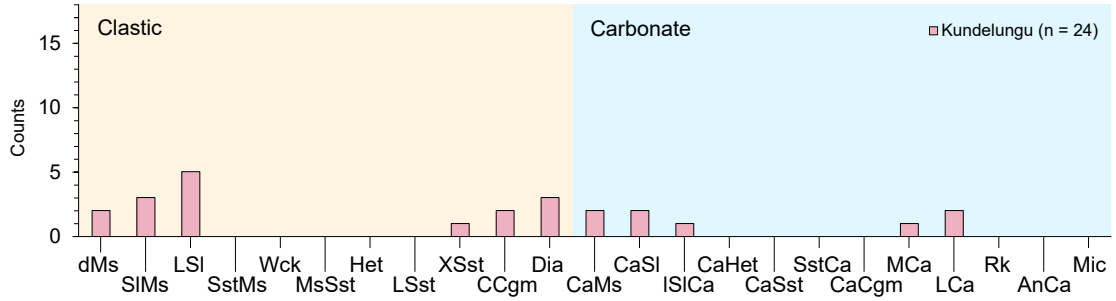

Figure 3.33: Facies counts in the Kundelungu. Note that the facies distribution changes as a result of the ZMSDD003 core being situated on the basin edge, introducing coarser clastic facies (XSst, CCgm). In the deeper portions of the basin, finer clastic and mixed clastic-carbonate facies predominate.

3.7 Discussion

The proposed general stratigraphic evolution of the Zambian Copperbelt has several implications for stratigraphy and mineralisation. The ore shale unit has been interpreted as a transgressive sur-

face marking the first time separate sub-basins became connected and open marine deposition predominated (Selley et al., 2005). The ”shale belt” described by Fleischer (1984) shows widespread mud-rich deposits along strike of the Kafue anticline. However, to what extent the ore shale represents a single regional transgressive deposit connecting different sub-basins, is unclear.

Fleischer (1984) and Selley et al. (2005) showed in cross sections that the ore shale occurred above, or appeared continuous above elevated palaeotopography in the Chambishi sub-basin. However, the cross sections were made along-strike, and not perpendicular to the basin axis across structural domains. The ore shale is frequently interpreted as an inter-tidal deposit (Eden, 1974; Fleischer, 1984), and Binda (1994) interpreted the ore shale as having been deposited in topographic lows between patch reefs growing on former basement highs. However, in Lubambe and Chambishi it is likely turbiditic, and deposited below the storm wave base. As the 'ore shale' can represent several facies (e.g. MsgSst, Wck, Het) and is not in itself an indicator of any particular depositional environment, it is very possible that the ore shale is regionally diachronous. The lack of an independent correlation marker to demonstrate possible chronostratigraphic significance, and little evidence of all ore shale units on structural highs being deposited in deep water, leaves open the possibility that 'ore shales' are locally or sub-regionally simply the oldest major set in any given succession of chemically reduced units, with a variety of depositional settings.

There is an increasing understanding that salt played a major role in the Katangan basin's evolution and played a significant role in the mineralization potential of the basin (De Magnée and Francois, 1988; Jackson and Warin, 2003; Selley et al., 2018). Though so far no halite has been observed in the basin, large breccia bodies attest to significant accumulations of now-dissolved evaporites. The effects of halokinesis on Katangan stratigraphy fall outside the scope of this work; however, the proposed facies scheme may provide a framework with which the sources of thick evaporite successions and their adjoining facies may be better understood. Jackson and Warin (2003) suggested that a sufficiently mechanically weak layer must have been present to form the salt structures interpreted in the Katangan basin. Sabkhas successions are unlikely to be sufficiently incompetent to represent this layer, as they are intercalated with siliciclastic and carbonate beds (Jackson and Warin, 2003). Minor remnant anhydrite occurring with sandy mudstone facies could indicate that sediment gravity flows were introduced into a deep water evaporitic basin. If the volumes of breccia broadly correspond to salt volume, sabkhas are unlikely to represent a sufficiently large source, and

would be an insufficiently buoyant medium required to generate the interpreted salt structures. A deep water origin for the now missing salt therefore appears more likely (Christeleit et al., 2015).

3.8 Conclusions

The proposed facies scheme provides the first unified facies framework for Katangan stratigraphy in the Zambian Copperbelt. It allows for general sedimentological and environmental interpretations to be made across the basin using a structured and repeatable workflow – applicable particularly to drill core. Placing facies into facies associations and successions has allowed for the stratigraphic evolution of the basin to be more clearly and quantitatively resolved.

The overall stratigraphy, and the assemblage and stacking patterns of the interpreted depositional environments, are consistent with those of an archetypal rift basin. Clear sedimentological and stratigraphic evidence has been provided for two phases of extension and thermal subsidence, punctuated by two widespread glaciation events. The Lower Roan Group is dominated by coarse clastic syn-rift fill and fault-controlled subsidence. The Upper Roan likely represents an epicontinental sea with extensive marginal coastal regions and sabkhas as the basin underwent thermal subsidence. The Mwashia Group shows a resumption of extension as the basin deepened and stepped out. The Nguba Group is lithostratigraphically demarkated by the Grand Conglomerat at its base, though the diamictites that comprise this unit are likely diachronous. The basin mostly remained deep during Nguba times. The Kundelungu Group overlies the regionally correlateable Petit Conglomerat and likely represents a distal quiescent basin prior to inversion.

The facies scheme is intended to provide comprehensive coverage of much of the stratigraphy, but will invariably not cover all facies present in the basin. There will be more facies to describe, and sub-divisions of facies to make (e.g. matrix-supported conglomerates, structured sandy carbonates, oolitic carbonates). A greater resolution in the carbonate facies is needed for more detailed interpretations of the carbonate lithologies that make up much of Katangan stratigraphy.

The proposed facies scheme is intended to provide a foundation for a unified approach to interpreting the Zambian Copperbelt's stratigraphy. It can be used to interpret the depositional systems of under-explored parts of the basin, leaving room for expansion and modification in future.

Chapter 4

Sequence stratigraphic correlations for the Katangan basin of Zambia, and their uncertainties and implications

4.1 Introduction

Udden (1912) was one of the first to characterise in detail cyclicity in coastal successions. Wanless and Weller (1932) expanded on this, coining the term 'cyclothems' for repetition of facies successions in coal-bearing formations. Wheeler (1958) and Sloss (1962) identified the significance of time-equivalent stratigraphic surfaces, and packages of sediment bounded by unconformities. The advent of seismic stratigraphy (Payton, 1977) allowed the concepts of cyclicity and time-equivalent surfaces to be combined. Sequence stratigraphy deals with the stratal relationships of repeated, genetically related successions of sediments within a chronostratigraphic framework bounded by key stratigraphic surfaces, traditionally unconformities or their correlative conformities (Posamentier et al., 1988; Wagoner et al., 1988; Wilgus et al., 1988).

There are a variety of sequence stratigraphic models, which are differentiated by how key stratigraphic surfaces are defined and assigned with respect to parameters such as the start and end of baselevel fall, end of regression, and end of transgression. These include depositional sequence models I - IV, genetic sequences and transgressive-regressive sequences (Posamentier and Vail,

1988; Wagoner et al., 1988; Hunt and Tucker, 1992; Catuneanu et al., 2009). One of the most commonly accepted definitions of a sequence is: "a relatively conformable sets of strata that are bounded by unconformities and correlative conformities at their top and base" Payton (1977); Catuneanu et al. (2009). However, more recently the definition has been generalised to a package of sediments bounded by the same key stratigraphic surface showing cyclical change in stratal stacking patterns (Catuneanu, 2017). Sequences are divided into systems tracts which reflect changes in stratal stacking in response to sediment supply and accommodation space generation, resulting in characteristic stacking patterns of aggradational, progradational, or retrogradational successions or parasequences (Payton, 1977; Wilgus et al., 1988; Catuneanu et al., 2009). Parasequences are defined as "a genetically related succession of beds or bed sets separated by flooding surfaces" (Catuneanu et al., 2009). Depositional sequence model III, which is followed in this work, defines sequences as bounded at their tops and bases by unconformities or their correlative conformities (SB – sequence boundaries), which are measured at the end of baselevel fall (Posamentier and Vail, 1988). In this model, each sequence comprises four systems tracts: 1. A progradational to aggradational lowstand systems tract (LST) with an unconformity at its base, marking the end of baselevel fall; 2. A retrogradational transgressive systems tract (TST) beginning at the end of the regression; 3. An aggradational or progradational early highstand systems tract (HST) beginning at the end of the transgression at the maximum flooding surface (MFS); 4. An aggradational to progradational late highstand systems systems tract, beginning at the onset of baselevel fall (Posamentier and Vail, 1988; Catuneanu et al., 2009). A comparison between different depositional sequence models is shown in figure 4.1.

Where several key stratigraphic surfaces are present in a succession, they are assigned an order within a hierarchy to avoid mixing up sequences of different magnitudes (e.g. time scales, (Vail, 1991)). Following Vail (1991), 1st-6th order sequences occur in cycles $>$ 50 Myr, 3-50 Myr, 0.5-3 Myr, 0.08-0.5 Myr, 0.03-0.08 Myr, 0.01-0.03 Myr, respectively. Alternatively, hierarchies can be assigned by interpreted magnitude of change represented by a sequence boundary (Embry, 1993). The benefits of a sequence stratigraphic approach over a lithostratigraphic one include a predictive capability for facies distribution, stratal geometry and stratigraphic architecture. This has allowed sequence stratigraphy to become an effective exploration tool for hydrocarbons (Payton, 1977; Posamentier and Allen, 1999) and mineral deposits (Ruffell et al., 1998). The method

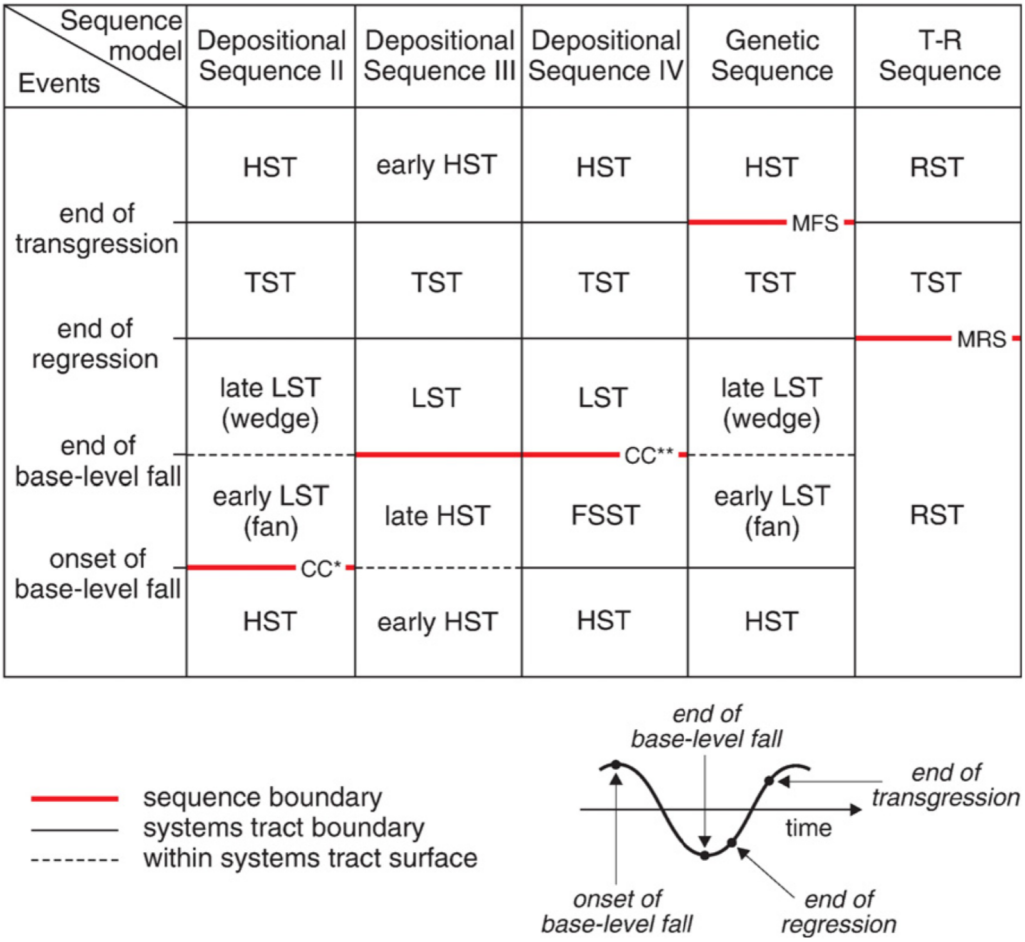

Figure 4.1: A comparison of different nomenclature, timings, and definitions used for different depositional sequence models from Catuneanu et al. (2009). LST: lowstand systems tract; TST: transgressive systems tract; HST: highstand systems tract; FSST: falling-stage systems tract; RST: regressive systems tract; TR: transgressive–regressive; CC: correlative conformity; MFS: maximum flooding surface; MRS: maximum regressive surface. A detailed exposition of the various models can be found in Catuneanu et al. (2009).

allows for the identification, through facies shifts, of key stratigraphic surfaces, that will be approximately synchronous if defined by changes in accommodations space driven by fluctuations in base level. This allows a logically consistent, testable stratigraphic framework to be constructed. Such a model has chronostratigraphic implications and can partially compensate for the paucity of actual geochronological constraints within the Katangan basin, at least in longer-duration, higher-order, sequences.

Previous work on sequence stratigraphy in the Katangan basin has been limited, both in spatial and stratigraphic extent (Bull et al., 2011; Woodhead, 2013). The aim in this work was to expand a

sequence stratigraphic approach across the entire Katangan Supergroup where possible, based on the proposed facies scheme and a repeatable, uncertainty-sensitive, framework for key stratigraphic surfaces.

4.2 Methodology

Seven cores, shown in figure 4.2, were used to develop sequence stratigraphic correlations. The KADD04 core from Lusale was omitted on account of facies successions being ambiguous and no clear sequence stratigraphic surfaces being able to be picked. Cores were mostly logged on a m-scale. Sections of core were logged on a dm-scale where sedimentary structures were exceptionally well-preserved or indicative of a particular depositional process, facies variation was high, or where a surface was deemed to be of possible stratigraphic significance. Facies were assigned using the scheme described in Chapter 3. Upwards fining and coarsening successions were then identified, and interpreted as upwards deepening or shallowing successions based on the depositional process interpretations for each facies comprising the succession. Repeated facies successions separated by flooding surfaces were interpreted as parasequences; however, clear flooding surfaces separating bed sets and facies successions could rarely be confidently determined based on facies analysis alone. This is on account of pervasive dolomitisation of the abundant carbonate facies, ambiguities concerning depositional environments and water depths of facies, and lack of supplementary data to confirm repetitive successions (e.g. gamma ray logs).

Key stratigraphic surfaces that separated facies successions – or parasequences, where they could be determined – were then identified. Sequence boundaries (SB) were interpreted using the following criteria: 1. Erosive bases showing clear scour beneath a unit; 2. Rapid reduction in sediment maturity and introduction of coarse or angular material; 3. Sharp juxtaposition of facies interpreted to be shallower above facies interpreted to be deeper; 4. Aggradational or progradational facies stacking above a candidate surface; 5. Oxidisation along a candidate surface; 6. Dissolution features. Criteria 5 and 6 characterise the red karst facies and may be interpreted as emergent surfaces, but were deemed the least reliable on account of ubiquitous hydrothermal alteration and dissolution.

Maximum flooding surfaces (MFS) were interpreted when the following were present: 1. Signifi-

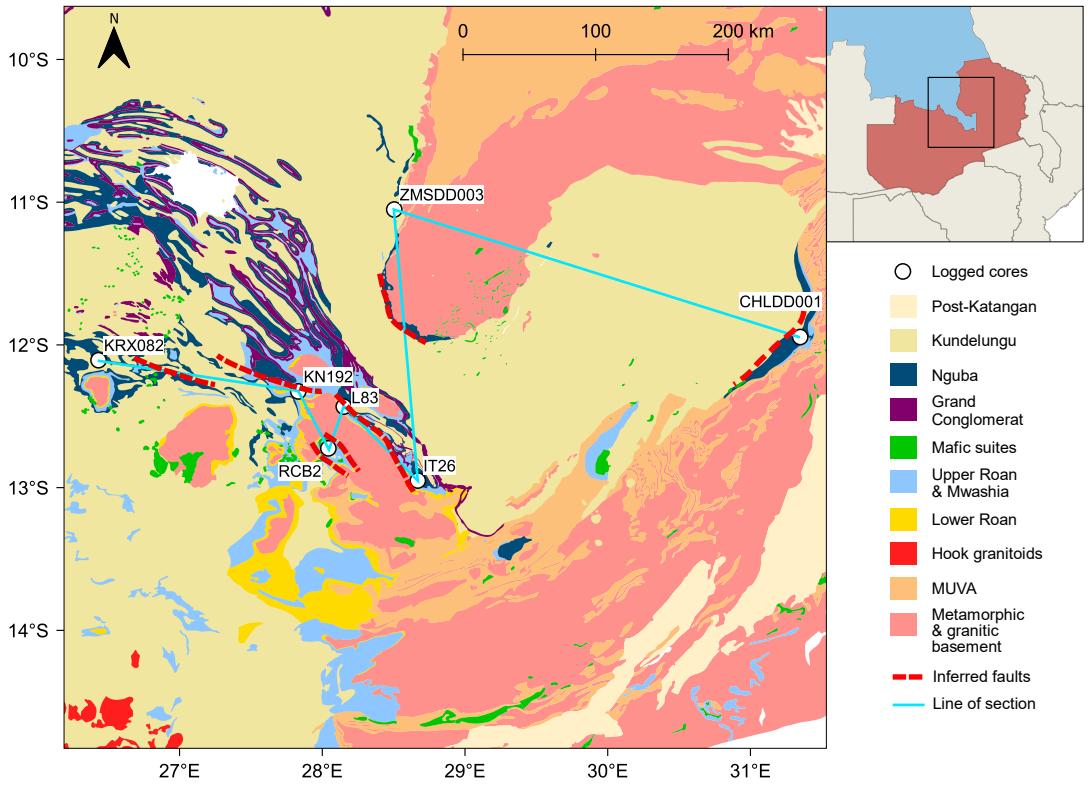

Figure 4.2: Map showing the line of section across cores logged across the Domes region, classical Copperbelt, and eastern part of the Katangan basin: KRX082 (Solwezi), KN192 (Lubambe), RCB2 (Chambishi), L83 (Mufulira), IT26 (Ndola), ZMSDD003 (Mansa), CHLDD001 (Chilonga). Dashed red lines represent inferred normal faults.

cant grain size reduction compared to underlying units; 2. Facies juxtaposition of facies interpreted to be deeper than their underlying facies; 3. Retrogradational facies successions below the surface, aggradational or progradational successions above it; 4. Sharp bases to units that show a clear grain size reduction compared to underlying units; 5. More chemically reduced units overlying more oxidised units. Criteria 5 was deemed the least reliable on account of pervasive hydrothermal influence on redox state, though it appeared to become more reliable towards the basin margins (particularly near Mansa).

To account for uncertainties and ambiguities regarding interpretation from core (e.g. due to pervasive dolomitisation, hydrothermal alteration), a composite measure was used to indicate uncertainty envelopes for each candidate key surface. On the core logs, asterisks denoted the number of criteria fulfilled to crudely quantify confidence in a surface being of stratigraphic significance (e.g. MFS***** were weighted more heavily than MFS*** during correlation).

Surfaces were correlated in accordance with the depositional sequence III model (Wagoner et al., 1990; Catuneanu et al., 2009). In this model, the base of the LST represents the end of base level fall, with maximum flooding surfaces forming at the end of a transgression, forming the base of the HST (Wagoner et al., 1990). A slight modification was made to account for the fact that early and late HSTs could not be clearly differentiated in core, and were therefore simply grouped into a single-phase HST. This model also has the advantage of making the sequence boundary a more easily correlatable and laterally extensive surface associated with the end of base level fall, as opposed to its onset (Posamentier and Vail, 1988; Posamentier and Allen, 1999).

From the Upper Roan Group upwards, carbonates, now mostly dolomitised, and shelf facies are more abundant, making identification of falling-stage systems tracts (FSST) difficult (Hunt and Tucker, 1992; Plint and Nummedal, 2000). This precluded the use of the depositional sequence IV model (Hunt and Tucker, 1992), as a FSST could rarely, if ever, be confidently distinguished in core from a late HST. Depositional sequence model II would require the identification of the surface associated with the onset of base level fall, which could not be performed confidently based on facies analysis alone, and avoided as a result (Posamentier et al., 1988).

Sequence boundaries were correlated first, followed by intervening maximum flooding surfaces, then transgressive systems tracts. In guiding the correlation, and in an attempt to avoid correlating surfaces of different hierarchical level, systems tract thicknesses were kept broadly uniform where possible, which implies broadly comparable accommodation space generation rates. System tract thicknesses were allowed to change in logical relation to the coastal-shelf-slope geometries implied by the facies associations and associated with the depositional sequence model III.

Breccias, interpreted to be remnants of evaporites, were assumed to be allochtonous and were not correlated. This was due to it not being possible to discern in drill core whether breccia units represented the basal source unit of evaporites, or were part of a larger discordant salt structure.

Facies associations were then correlated between cores using the observed progradational, retrogradational or aggradational stacking patterns to characterise each systems tract. It was assumed that the onset of deposition of the Lower Roan Group represented basement onlap in a terrestrial rift as part of a transgressive systems tract (Martins-Neto and Catuneanu, 2010).

Paucity of chronological constraints in the basin made establishing precise sequence stratigraphic orders difficult. Though Vail's (1991) sequence hierarchy was predominantly used in this work,

the uncertainties relating to the tectonostratigraphic evolution of the basin, facies analysis in core, wide drill hole spacing, and chronostratigraphic constraints, leads to overlap with Embry (1993)'s model of sequence orders. Possible cycle orders are suggested for each core. 'High order' cycles refer to lower frequency, $<$ 3rd order cyclicity, and 'low order' cycles refer to higher frequency, $\geq$ 3rd order, cyclicity (Vail, 1991; Embry, 1993). An attempt was made to keep the hierarchy broadly consistent across correlations, but some aliasing of hierarchical stratal surfaces is inevitable.

Inferred structural controls are shown in figure 4.2. Regional structural constraints for the basin are poor, and are based on regional geophysical interpretations in Daly et al. (2024), and Selley et al. (2005, 2018); Kennedy et al. (2019). As most cores do not reach basement, missing stratigraphy between the total depth and the basement was augmented with data from literature. To account for different justifiable sequence stratigraphic interpretations of the core datasets, two sequence stratigraphic correlations are presented, and examples of alternative interpretations provided.

Importantly, both stratigraphic frameworks assume that the units of the lower diamictite unit, the Grand Conglomerat, are tectonically triggered, rather than representing synchronously deposited basin fan deposits as part of a Sturtian lowstand systems tract. This choice is based on several observations: 1. the Grand Conglomerat diamictites in the Zambian Copperbelt rarely show features that can be interpreted as unambiguously glacial in origin, 2. tholeiitic magmatism prior to the Sturtian glaciation indicates renewed extension in the basin (Tembo et al., 1999; Key et al., 2001), 3. the Grand Conglomerat comprises very thick ($>$ 1km) mass flow diamictes in Kamoa which contain or overlie Mwashia mafic bodies and is interpreted to be tectonically triggered (Schmandt et al., 2013; Kennedy et al., 2019), 4. facies evidence for deepening during the Mwashia across much of the Kafue anticline and eastern part of the basin is interpreted as evidence of renewed extension and basin deepening. Glacial influence on the Grand Conglomerat is however not excluded, it merely raises the question of to what degree the Grand Conglomerat can be used as a time line. The stratigraphic impact of glaciation as part of Sturtian and Marinoan 'Snowball Earth' events are addressed in more detail in the discussion.

4.3 Results

4.3.1 Solwezi

The KRX082 core in Solwezi is 2511 m long, and intersects an intensely folded and sheared section overlying a thick ($>$ 1.3 km) traditionally Lower Roan Group clastic succession (fig. 4.3). The core does not reach basement.

Medium to thickly bedded, texturally immature laminated and cross-stratified sandy facies (pLSst, XSst) predominate in the lower portions of the core, punctuated by thin stratified conglomerate units (sCCgm). These facies form a continuous aggradational fluvial succession $\sim$ 500 m thick, overlain by a 150 m thick intertidal or floodplain succession, comprising more mud-rich facies (Het). This is sharply overlain by immature sandy facies which aggrade for $\sim$ 600 m and increase upwards in interstitial dolomite content, the upper 200 m of which show a more pronounced tectonic fabric that obscures primary sedimentary structures. Amplification factors (total facies association thickness divided by estimated water depth) in the basal clastic succession are high, estimated to be $>$ 100.

The upper half of the core comprises intensely sheared and isoclinally folded section of garnet-bearing metasediments, marbles, and schists, as well as two units interpreted to be metadiamictites. The degree of metamorphism and folding precludes this upper section from being precisely correlated with the traditional Katangan stratigraphy at this stage. However, the abundance of metacarbonates and the presence of metadiamictites suggest that the folded sediments predominantly comprise post-Lower-Roan stratigraphy.

Sequence stratigraphic correlations 1, 2

Both sequence stratigraphic correlations place the lowermost aggradational fluvial succession into the syn-rift TST (Bosence, 1998), with the low to moderate-confidence MFS1 being placed at the top of the sandy succession at a depth of $\sim$1330 m, where breccias and carbonates appear, 10's m below the intensely deformed section of the core. This interpretation relies on carbonate-bearing sandstones likely being deposited in water depths that exceed intertidal water depths. However, on account of the increasing metamorphic grade towards the top of the Lower Roan succession, this interpretation is uncertain.

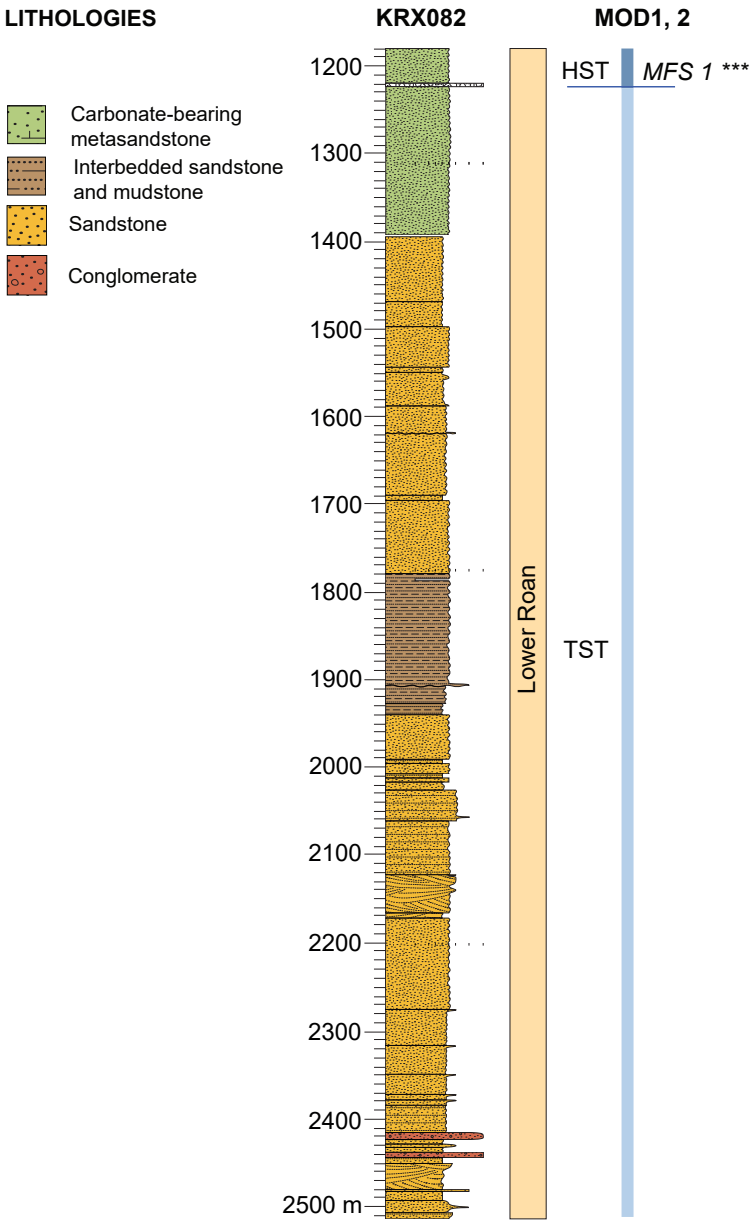

Figure 4.3: A stratigraphic log of the lower half of the KRX082 core in Solwezi underneath the metamorphic thrust sheet, showing a thick transgressive systems tract (TST), with a MFS1 interpreted at the top of the succession. MOD1, 2 refers to interpretations for sequence stratigraphic correlations 1 and 2; which in this core are identical. Asterisks denote confidence in the stratigraphic surface.

Alternative sequence stratigraphic interpretations

An alternative interpretation involves placing the low-confidence MFS1 at the base of the intertidal succession, on the basis of facies juxtaposition (deeper on shallower), reduced grain size, and weak retrogradational trend leading into the surface. This surface could represent a minor deepening, before aggrading sandstone successions as part of a HST again predominate. No interpretation of the basal clastic succession in the KRX082 core shows a marked or significant deepening, but the possibility of the more mud-rich succession representing floodplain deposits, results in sequence stratigraphic correlations 1, 2 being preferred for now.

4.3.2 Lubambe/Konkola North

The KN192 core in Lubambe (formerly Konkola North) is 1648 m deep, intersecting the Kundelungu, Nguba, Mwashia, Upper Roan and Lower Roan Groups in the Konkola sub-basin (fig. 4.4). The core does not reach basement.

Clast-supported conglomerate (CCgm), wacke (Wck) and sandy mudstone (SstMs) facies make up most of the lowermost 320 m of the core, forming predominantly aggradational fan-delta successions. These are punctuated by minor deepenings represented by muddier turbiditic facies (MsgSst, SstMs).

The fan-delta succession transitions upwards into a 150 m thick section of aggradational intertidal facies (Het, CaHet), which show abundant emergent surfaces (Rk). Intertidal facies retrograde upwards into a 450 m thick, gently deepening succession of carbonate ramp facies (CaSl, MCa). Two 40-60 m thick brecciated units, composed of highly altered carbonates, siltstones and mafic clasts occur in the lower part of this section occur in the lower part of this section, comprising highly altered carbonates, siltstones and mafic clasts.

The carbonate ramp facies retrograde into what are interpreted as deep shelf facies (dMs). This sharp retrogradation is succeeded by carbonate ramp facies (CaMs, CaSl, MCa, Mic) that gently shallow upwards. The carbonates were likely biotically mediated, showing haematite-stained stromatolitic structures. At the top of the 150 m thick stromatolitic section, a deepening is interpreted on the basis of stromatolitic structures being replaced by silty carbonate (CaSl) facies. These are sharply punctuated, and eroded into, by a prograding stack of carbonate diamictite and conglomerate facies (CaDia, CaCgm).

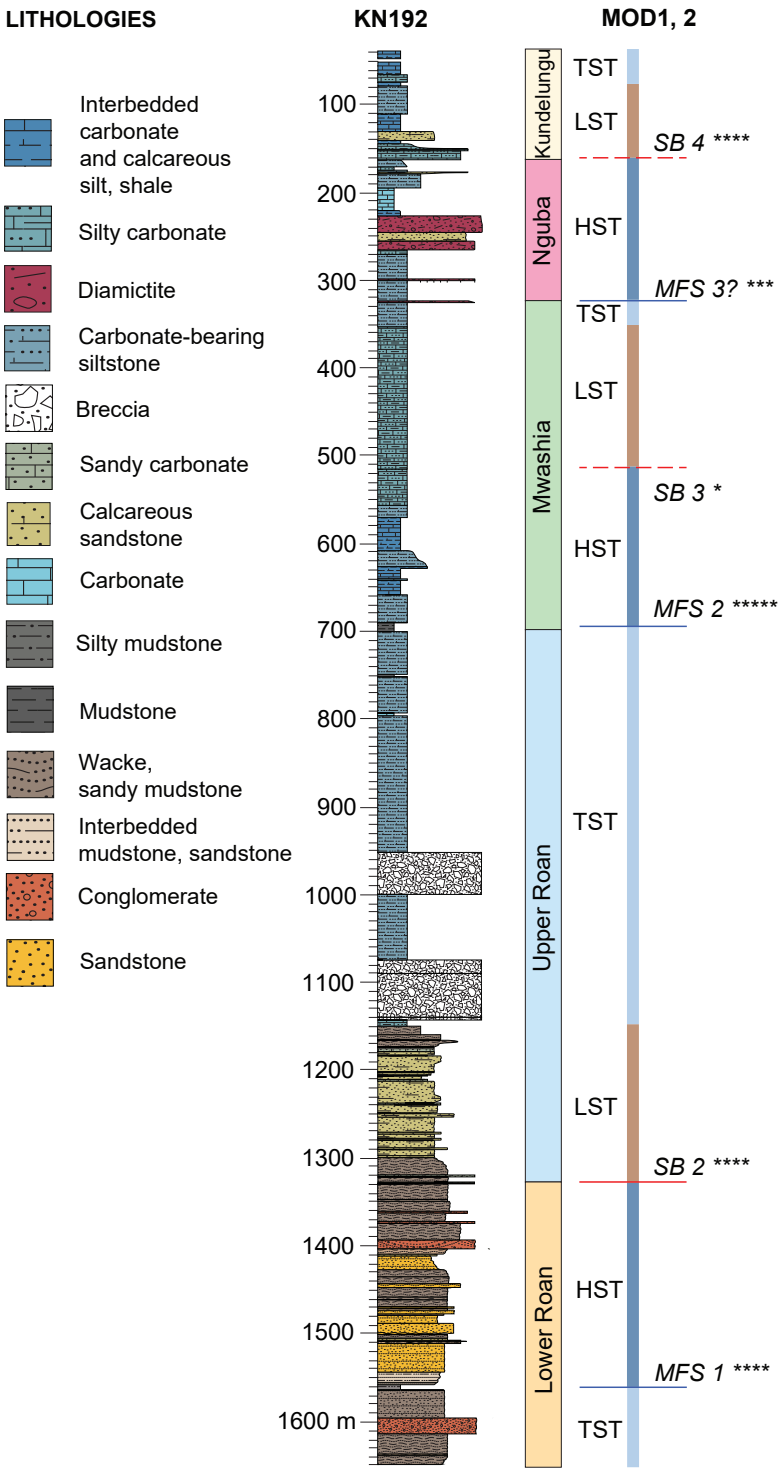

Figure 4.4: A stratigraphic log of the KN192 core in Lubambe showing a section through the siliciclastic Lower Roan, and more carbonate-dominated Upper Roan, Mwashia, and Nguba Groups. MOD1, 2 refers to interpretations for sequence stratigraphic correlations 1 and 2; which in this core are identical.

The carbonate diamictite facies pass upwards into a deep shelf succession that shallows into an enigmatic 30 m thick section of variably oxidised (Rk) carbonate conglomerate (CaCgm) and carbonate-bearing siltstone facies (CaSl), possibly representing storm deposits. They are less likely to be slope-derived on account of the highly tabular geometry of the carbonate clasts, suggesting limited transport distance. These are overlain by a retrogradational succession of deep carbonate ramp facies.

Sequence stratigraphic correlations 1, 2

Both sequence stratigraphic correlations place the lowermost portion of the fan-delta succession into a syn-rift TST, showing high, $<$ 3rd order (Vail, 1991; Embry, 1993), cyclicity. The lowermost turbiditic facies form the high-confidence MFS1 (based on facies juxtaposition, retrogradation below the surface, reduced grain size, chemically reduced) that leads into an aggradational HST. A thin surface comprising the red karst (Rk) facies overlying the fan-delta slope succession is seen as the first of a set of stratigraphically significant emergent surface, forming the SB2, which separates the Lower Roan from the Upper Roan (fig. 4.5). The surface forms a moderate confidence unconformity or correlative conformity on the basis of facies juxtaposition (shallow on deep), facies stacking, oxidisation and dissolution structures.

The interpreted unconformity does not stand out as a major forced regression surface in isolation, as it forms part of a repeated succession of low ($>$ 3rd) order (Vail, 1991; Embry, 1993)) emergent surfaces. However, it is still deemed to be of significant stratigraphic importance, as using Embry (1993)'s hierarchy, it can be interpreted as higher order regression surface separating Lower Roan fan-delta from Upper Roan intertidal successions representing a fundamental change in basin configuration.

The Upper Roan Group forms part of a more prolonged TST with low-order cycles predominating initially. From the Upper Roan into the Kundelungu Group, lower order cyclicity is not clearly distinguishable and key surfaces are generally interpreted as being higher (possible 2nd or 3rd) order, with upwards-reducing facies variation and increasing carbonate content obscuring higher frequency low-order sequences (Vail, 1991). It is capped by a 10 m thick black mudstone unit, which is interpreted as the high-confidence, higher order, (Vail, 1991; Embry, 1993) MFS2 on account of facies juxtaposition (deeper on shallower), retrogradational facies below the surface, reduced grain

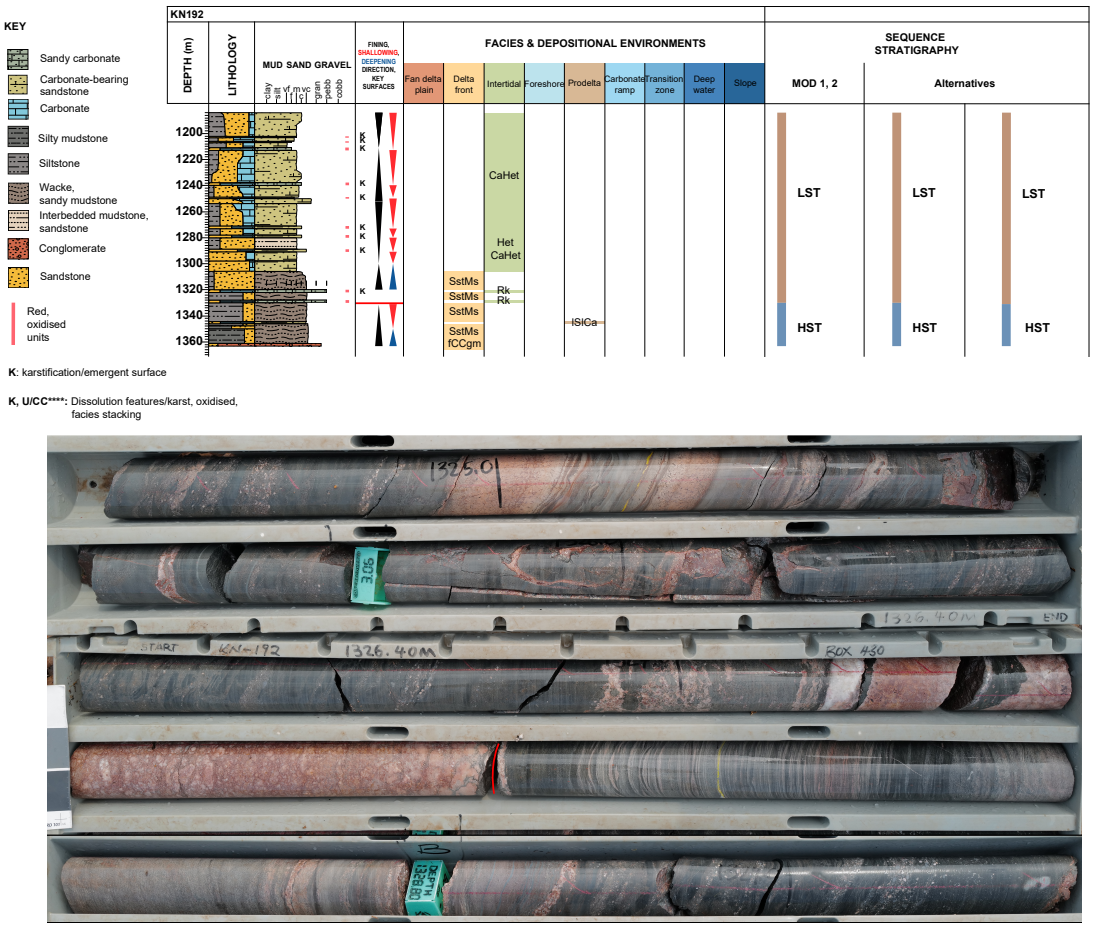

Figure 4.5: Log and core photographs of the Lower to Upper Roan transition section of core KN192 in Lubambe. The interpreted unconformity or correlative conformity (SB2) separates the delta slope facies below with the predominantly intertidal facies above. The core photograph shows this section with red emergent surface sharply juxtaposed with deeper water facies below (red line shows the SB2 surface). Cores young from bottom right to top left, with depths marked on the core.

size, being chemically reduced, and with a sharp basal surface. The MFS2 is interpreted to mark the base of the Mwashia Group. The rest of the Mwashia Group forms part of a microbialite-dominated LST, demarkated by a low-confidence SB3 (interpreted as a correlative conformity) at its base, that rapidly passes through a TST into the moderate-confidence, high-order MFS3 delineated by the first thin diamictite unit. This is on account of the first diamictite unit being interpreted as a sharp-based transgressive surface, with subsequent diamictite units aggrading or prograding above it.

This MFS marks the base of the Nguba Group, which comprises what are interpreted to be down-lapping, slope-derived, diamictite units that prograde into the basin, and that transition upwards into a storm-influenced carbonate ramp. The oxidised edgewise conglomerates of this shelf succession

are interpreted to represent a moderate-confidence correlative conformity (SB4) that marks the base of the base-Kundelungu LST, on account of dissolution features, oxidisation, coarse clast size (up to pebble) and it capping a shallowing-up succession. The deepening succession that overlies it is interpreted to represent the beginning of a TST.

Alternative sequence stratigraphic interpretations

Alternative interpretations of the core include a more prolonged Mwashia HST that terminates above the diamictites in the oxidised storm-influenced shelf succession. In this model, the carbonate diamictites would be generated from local highstand shedding carbonate reefs that aggraded as part of a HST (Schlager et al., 1994), rather than being transported down the basinal shelf slope. This model would bring what is traditionally the Upper Roan, Mwashia and lower Nguba Groups into one sequence. This is deemed less likely on account of the clasts in the carbonate diamictites and conglomerates often being rounded and high-sphericity, suggesting significant transport distances.
A different interpretation would similarly bring the Upper Roan, Mwashia and lower Nguba Groups into one sequence. However, the MFS2 would be located at the base of the first diamictite.

4.3.3 Chambishi

The RCB2 core in the Chambishi sub-basin is 1840 m long and is a type core for classical Copperbelt stratigraphy, intersecting the Lower and Upper Roan Groups (fig. 4.6). It does not reach basement.

The basal section of the core comprises 300 m of poorly stratified cobble conglomerates (CCgm). These transition upwards into a 200 m thick succession of immature laminated and cross-stratified sandy facies (LSst, XSst), which crudely fine upwards and are punctuated by thin conglomeratic units. The basal section of the core is interpreted to represent an alluvial to fluvial succession.
Two missing core sections (30 and 20 m thick, respectively) result in a data gap in the following succession. However, the succession appears to retrograde towards the top, as sand and conglomerate facies are replaced by wacke (Wck), sandy mudstone (SstMs) and muddy sandstone (MsSst) facies. These further deepen into plane-laminated siltstones (LSl) and thin dolomitised carbonate (MCa) units. Despite the missing core, this $\sim$ 80 m thick section, which includes the 'ore shale' unit, is interpreted as a significant deepening in a fluvial $\rightarrow$ delta slope $\rightarrow$ prodelta succession.
This succession is succeeded by a 200 m thick aggradational to progradational succession of delta

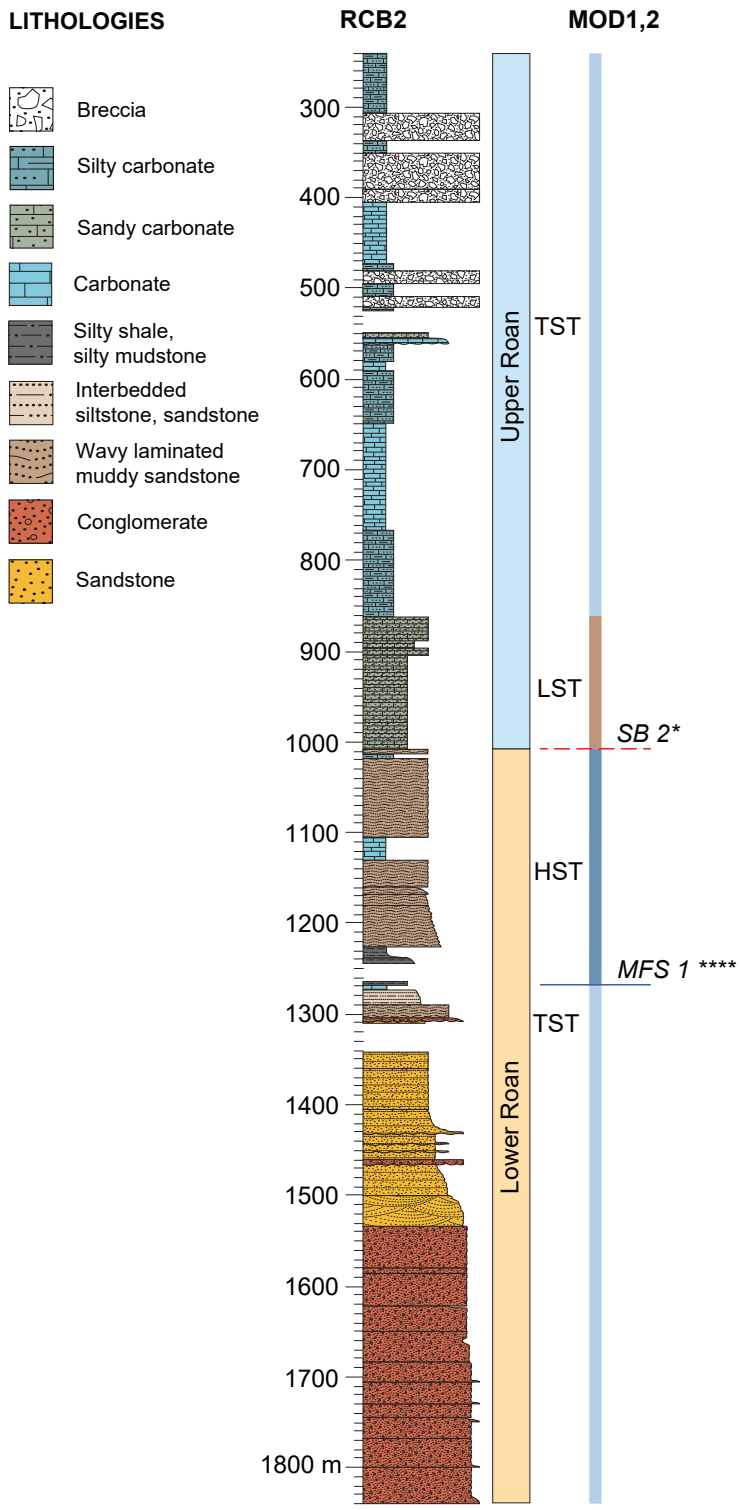

Figure 4.6: A stratigraphic log of the RCB2 core in Chambishi, showing Lower and Upper Roan sections forming a type example of Zambian Copperbelt stratigraphy. MOD1, 2 refers to interpretations for sequence stratigraphic correlations 1 and 2; which in this core are identical.

slope and possibly delta plain facies, separated by a 20 m thick anhydrite-bearing carbonate (AnCa) unit. Delta slope facies shallow upwards into a 140 m thick section of intertidal (CaHet) and sabkha (AnCa) facies. These are overlain by a 300 m thick succession of laminated (LCa) and anhydrite-bearing carbonate (AnCa) facies, possibly showing microbial structures (Mic). This succession becomes gently retrogradational towards its top with sandy carbonate (SstCa) and carbonate-bearing siltstone facies (CaSl) being interpreted to form part of a carbonate ramp or lagoon.

The subsequent 300 m of core comprise an enigmatic section of various carbonate facies (LCa, AnCa, CaSl, Mic) broken up by four breccia units 10's m thick. These breccias comprise predominantly dolomite and siltstone (or silty dolomite) clasts, with some containing altered mafic clasts.

Sequence stratigraphic correlations 1, 2

Both models place the lower order alluvial fan, fluvial and delta successions into a syn-rift TST, culminating in the high-confidence MFS1, marking the base of a HST. Similarly to core KN192, the MFS1 coincides with prodelta 'ore shale' facies, and is given a high confidence on account of facies juxtaposition (deeper on shallower), overlying a retrogradation facies succession, having a reduced grain size, and being more chemically reduced (containing sulphides including pyrite).

The overlying HST comprises aggrading to prograding delta and delta slope successions, showing lower order cyclicity. These pass transitionally into intertidal and sabkha facies which are interpreted to form part of an aggradational LST. The exact depth of the SB2 could not be clearly defined. The end of the LST and beginning of the TST is equally uncertain, but is interpreted to be at the base of a $\sim$100 m thick laminated carbonate unit interpreted to represent a lagoonal or carbonate ramp environment. Above this surface, a series of possibly deepening successions (sabkha $\rightarrow$ intertidal $\rightarrow$ carbonate ramp), showing low-order cycles occurring with upwards-increasing frequency, are interpreted as the TST that persists for much of the Upper Roan.

Alternative sequence stratigraphic interpretations

There are significant uncertainties relating to pervasive dolomitisation and insufficient primary sedimentary structures to provide approximate interpretations of depositional water depths in the Upper Roan of the RCB2 core. These uncertainties allow the base of the TST to be moved by as much as 200 m, past a thick anhydrite-bearing carbonate unit, interpreted as the sabkha facies association, to

the base of a likely microbial carbonate, significantly extending the period of the base-Upper-Roan LST.

4.3.4 Mufulira

The L83 core in Mufulira is 1569 m long, and traditionally intersects the Kundelungu, Nguba, Mwashia and Upper Roan Groups. Unusually, the core contains the both the Grand and Petit Conglomerat (fig. 4.7). It does not reach basement.

The basal section of the core comprises a 170 m broadly aggradational succession of interbedded carbonate (AnCa, LCa and sandy carbonate (SstCa, CaSst) facies, interpreted as a sabkha to intertidal succession. This is overlain by a 140 m thick breccia section, composed predominantly of highly altered mafic clasts and dolomitised carbonate.

Breccia units are sharply succeeded by a 60 m thick carbonate succession, which show 3 pronounced red oxidised sections with dissolution features (Rk facies), each several metres thick. Notably, the lowermost Rk facies unit directly overlies the brecciated section, which does not show any red oxidation. These retrograde towards their top into more silty carbonate facies (CaSl, LCa), which become sharply interbedded carbonate-bearing mudstone facies (CaMs). Pervasive dolomitisation and enigmatic structures preclude precise palaeoenvironmental interpretation of these. As a result, they are broadly interpreted as intertidal to shelf carbonates, with plane-laminated carbonate-bearing mudstone facies interpreted as being deposited below the storm wave base on the mid-outer shelf.

A thin mudstone unit leads into a 40 m thick poorly bedded diamictite unit (crDia), interpreted to be a debris flow deposit. This is succeeded by a thin carbonate-bearing mudstone unit (CaMs) and what is interpreted to be a shallowing into a 100 m thick massive carbonate (MCa) succession, followed by enigmatic variably laminated carbonate facies (vLCa).

Mud and silt proportion increases up-section, into a cryptic succession of laminated carbonates (vLCa), possibly showing microbial structures (Mic), carbonate-bearing mud and siltstones (CaMs, CaSl), interpreted to be gently retrogradational. These pass transitionally into laminated siltstones (LSl) that are overlain by a second 40 m thick diamictite unit (cpDia). These are interpreted as a deepening succession, though whether they represent distal shelf or slope deposits is unclear.

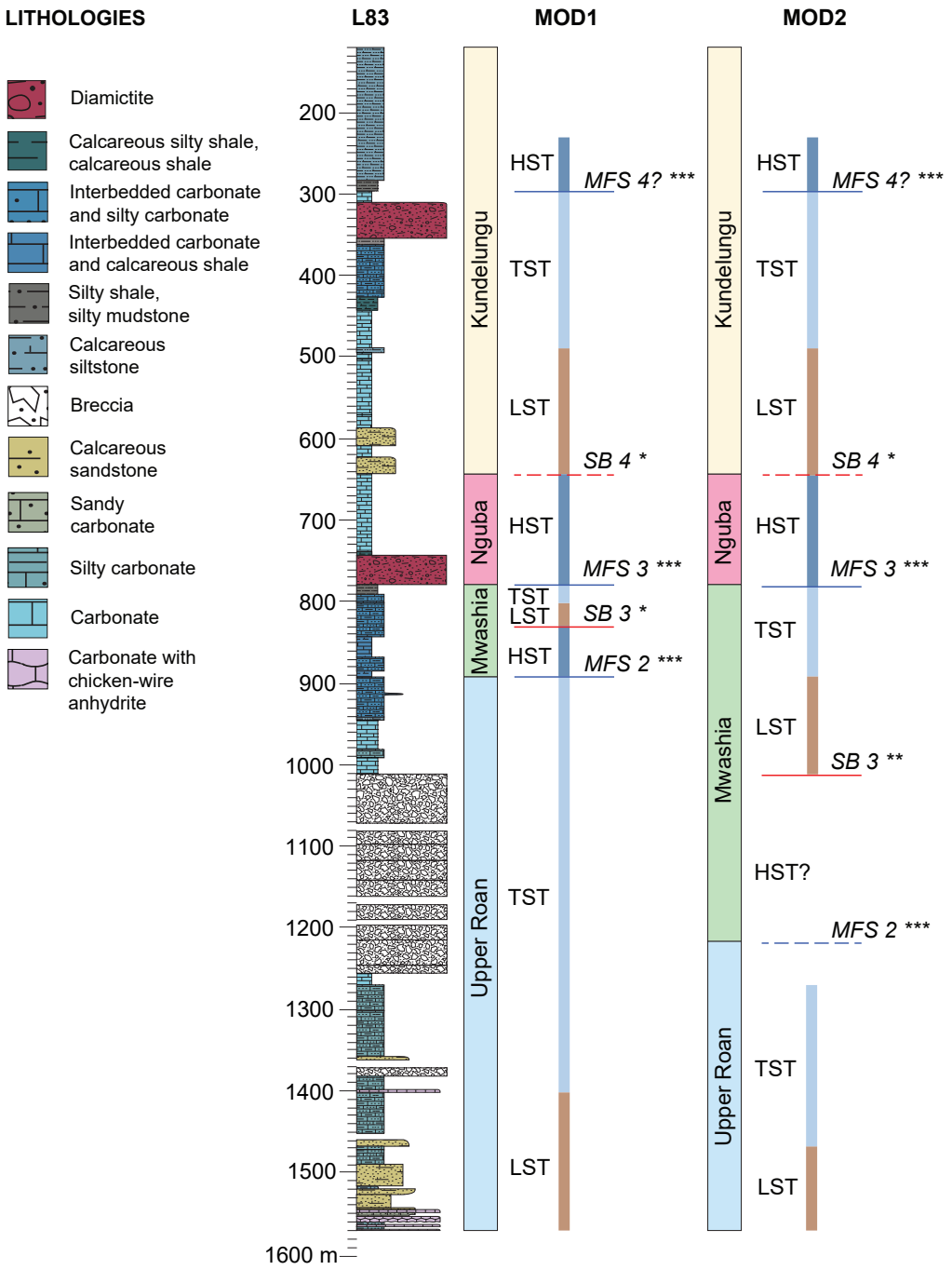

Figure 4.7: A stratigraphic log of the L83 core in Mufulira, showing Upper Roan, Mwashia, Nguba, and Kundelungu Groups. MOD1, 2 refers to sequence stratigraphic correlations 1 and 2. Note that the brecciated interval and overlying karst facies shown in figure 4.8 allow for two viable sequence stratigraphic arrangements.

The diamictite unit is sharply overlain by a massive carbonate unit (MCa), which passes into silty mudstone (SlMs) and carbonate-bearing silstone facies (CaSl). The latter show wavy lamination and are interpreted to have been deposited at or above the storm wave base, forming part of a gentle shallowing succession.

Sequence stratigraphic correlation 1

The aggradational intertidal and sabkha successions at the base of the core are interpreted to form part of the Upper Roan LST. These pass transitionally into a TST as sabkha deposits become thinner. The brecciated section is enigmatic, but interpreted in this model as forming part of a now-brecciated TST. Both the Upper Roan LST and TST show initially lower order cyclicity, becoming higher order towards MFS2.

The breccias are interpreted to be salt-related (Jackson and Warin, 2003; Selley et al., 2005, 2018). It is postulated they originate from more basinal halite successions. Their emplacement is interpreted to post-date the TST succession they are found in, on account of the containing mafic clasts assumed to be of Mwashia-age.

From the Upper Roan Group onwards, low order cyclicity is less evident, on account of deeper water and carbonate facies predominating.

Notably, in sequence stratigraphic correlation 1, the oxidised carbonates (Rk facies) are interpreted to be of hydrothermal origin, and of no sequence stratigraphic significance. The deep shelf carbonate-bearing mudstone units are interpreted as the moderate-confidence MFS2, on account of facies juxtaposition (deeper on shallower), retrogradational facies stacking below, and being more chemically reduced. The MFS2 is interpreted as the base of the Mwashia Group. This leads into the inferred SB3, and a section of lower order condensed LST and TST whose lower bounds are poorly defined and obscured by dolomitisation and alteration.

The first diamictite succession is interpreted as the Grand Conglomerat, and a deepening event, aggrading or prograding as part of a HST. Its base forms the moderate-confidence, likely high-order MFS3 (facies juxtaposition, retrogradational facies stacking below, chemically reduced), that is interpreted to represent the base of the Nguba Group, again assuming that diamictites are derived from extensionally driven subaqueous topography and hence represent a deepening.

The HST shallows into what is interpreted as an aggradational to progradational above-storm-wave-

base carbonate ramp succession forming the poorly defined SB3. The overlying LST diffusely transitions into a TST.

The end of the TST and onset of the HST is unclear and depends on assumption made regarding Marinoan glaciation (Master and Wendorff, 2011; Hoffman et al., 2017). The MFS at the base of the overlying HST was placed above the diamictite unit interpreted to be the Petit Conglomerat, on account of the evidence for its glacial origin being somewhat stronger (cpDia facies, (Master and Wendorff, 2011)), and maximum transgression being presumed to occur during deglaciation. A shallowing succession of aggrading or prograding shelf facies above the diamictite suggest they could form part of an HST during Kundelungu times.

Sequence stratigraphic correlation 2

Sequence stratigraphic correlation 2 differs from the model 1 in that the red oxidised carbonate is interpreted to be of stratigraphic significance, possibly representing a karst or terra rossa, resulting from dissolution in the vadose or phreatic zone.

The low-order cyclicity sabkha and intertidal successions are still interpreted as a LST, though the TST begins earlier, above the last thick sabkha succession.

The MFS2 and subsequent HST is now obscured by what is assumed to be halokinetic brecciation. The Rk facies above the brecciated section form the low-confidence, higher order unconformity or correlative conformity, SB3, (fig. 4.8), on account of dissolution features or karstification, and being conspicuously oxidised compared to breccias below. The rest of the sequences are as in model 1, with the MFS3 at the base of the Grand Conglomerat, and cryptic middle-upper Nguba carbonate succession, and a post-Marinoan MFS.

This model relies heavily on one stratigraphic interval and the set of surfaces it encompasses, which could be hydrothermal in origin, rather than a karst forming the SB3. However, it does alleviate the systems tract compression prior to the Grand Conglomerat that is invoked in model 1, and without additional evidence cannot be excluded as a viable sequence stratigraphic arrangement.

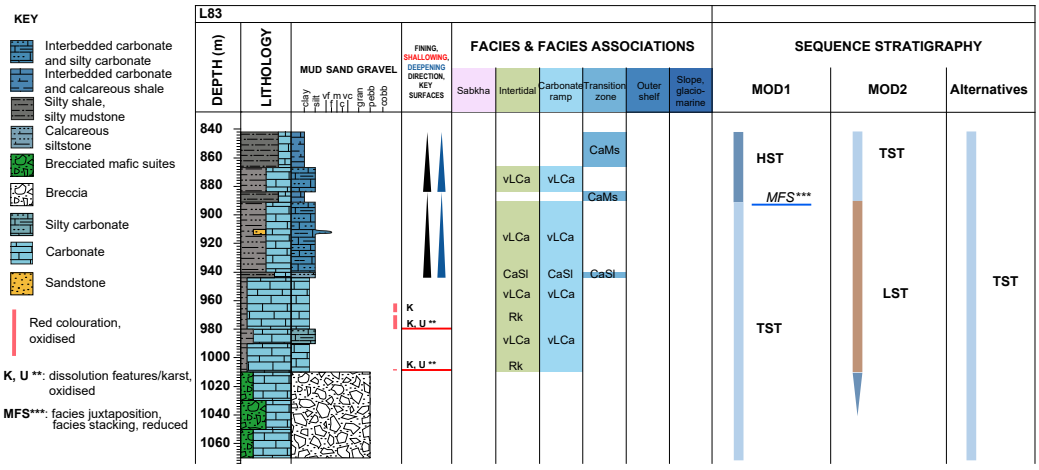

L83 3185 - 3210 ft (970 m - 978 m)



L83 3210 - 3234 ft (978 m - 986 m)



L83 3308 - 3333 ft (1008 m - 1016 m)



Figure 4.8: Log and core photographs of the surfaces assumed in correlation 2 to be unconformities or correlative conformities in core L83. They show the brecciated section, comprising highly altered carbonates and mafic suites, sharply leading into a thin oxidised Rk facies unit, an unoxidised dolomite unit, and a thicker oxidised Rk facies unit. Cores young from bottom right to top left.

Alternative sequence stratigraphic interpretations

The abundance of carbonates, their frequent lack of diagnostic primary structures, and abundant alteration generates significant uncertainty in terms of sequence stratigraphic interpretation. This uncertainty allows for several other possible interpretations. These include placing the entire Upper Roan into a LST and TST, and interpreting the Mwashia mudstones as part of the upper TST, culminating in a MFS at the base of the Nguba (Grand Conglomerat).

4.3.5 Ndola

The IT26 core is 1039 m long, traditionally intersecting the Nguba, Mwashia, Upper and Lower Roan Groups, and basement; depending on the stratigraphic interpretation, it may be considered to only intersect the Nguba and Mwashia Groups, and basement (fig. 4.9).

A 50 m thick coarse clastic succession lies unconformably on basement, forming an aggradational stack of alluvial fan facies (CCgm, LSst). These retrograde through a 20 m thick succession of distal alluvial fan or fluvial facies into a mixed section of alternating intertidal (Het) to delta slope (Wck) facies, which form minor deepening-shallowing cycles (possibly parasequences). The overlying 270 m thick generally aggradational succession of sabkha (AnCa) and intertidal (Het) facies episodically retrogrades into carbonate ramp/shoreface (CaSst, XSst) facies. This is succeeded by a 140 m thick section of cryptic carbonate facies (vLCa) that are capped by a sharp-based 10 m thick regressive section of carbonate-bearing mudstone facies (CaMs), interpreted as being deposited below the storm wave base. A 110 m thick aggradational stromatolitic succession (Mic) overlies this, retrograding at its top into mud-rich facies and a 40 m thick diamictite succession (crDia).

The diamictite units are overlain by deep shelf facies (CaMs) that shallow upwards into a carbonate ramp. This carbonate ramp succession contains a thin oxidised section showing dissolution structures. This is overlain by a 240 m thick succession of deeper carbonate ramp facies (CaSl, MCa, LCa) with what is interpreted to be a gentle retrogradational trend.

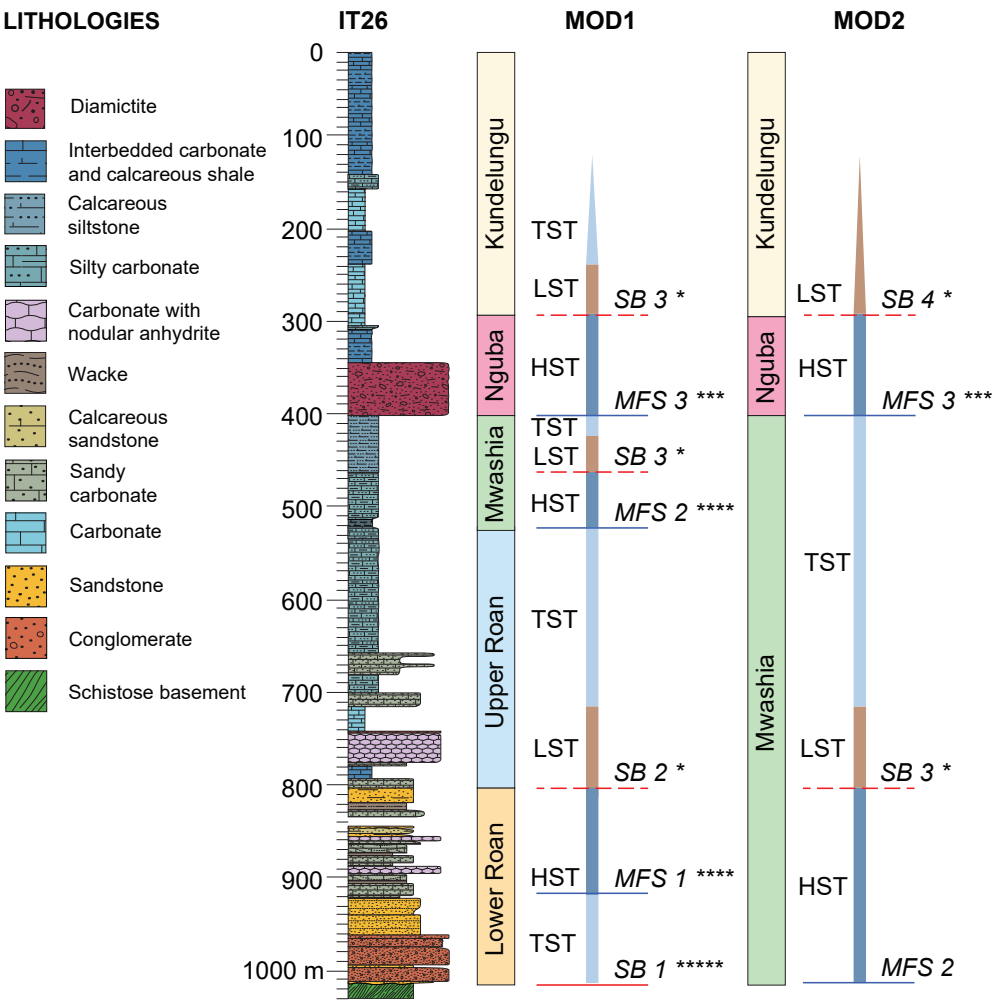

Figure 4.9: A stratigraphic log of the IT26 core in Ndola. MOD1, 2 refers to sequence stratigraphic correlations 1 and 2. Depending on the interpretation of key surfaces, the core shows the complete Katangan stratigraphy (Lower Roan to Kundelungu Groups), or only half of it (Mwashia, Nguba, Kundelungu Groups).

Sequence stratigraphic correlation 1

The basal unconformity is interpreted as a high-order (1st or 2nd) sequence boundary, SB1. The retrogradational alluvial fan → fluvial → delta slope succession that erodes into basement and shows pronounced low-order cyclicity is interpreted to form part of a Lower Roan syn-rift TST, that leads into the moderate to high confidence MFS1. This is on account of facies juxtaposition (deeper on shallower), retrograding facies below and aggrading to prograding facies above MFS1, sharp surfaces and being more chemically reduced.

The aggradational succession of low-order cyclicity sabkha, intertidal and upper shoreface facies is

interpreted to form a HST which passes transitionally into a sabkha-dominated LST, with SB2 being poorly defined, fomring a diffuse boundary characterised by low-order cyclical paralic successions between the Lower and Upper Roan Groups. This LST leads into a TST marked at its base by a deepening into a clastic-carbonate shoreface, making up the rest of the Upper Roan. Low-order cycles are replaced by higher order cycles from the Upper Roan upwards on account of facies aliasing. The base of the overlying HST is marked by the high-confidence MFS2 (facies juxtaposition, retrograding facies below and aggrading to prograding facies above, sharp surfaces, and chemically reduced), that is interpreted to form the base of the Mwashia Group. It leads into condensed LST and TSTs above, both of which have unclear lower bounding surfaces (e.g. SB3) and fall into the stromatolitic facies succession. The base of the diamictite unit, interpreted to be the Grand Conglomerat, is interpreted to represent the moderate-confidence MFS3, on account of facies stacking, facies juxtaposition, and sharp basal surfaces.

The Nguba HST shallows up into a LST marked at its base by a low-confidence unconformity or correlative conformity, SB4, on account of oxidisation and dissolution features in a thin carbonate interval. The enigmatic carbonate ramp succession is then interpreted to retrograde, forming part of a TST.

Sequence stratigraphic correlation 2

Sequence stratigraphic correlation 2 avoids model 1's possibly problematic condensing of systems tracts in the microbial carbonate succession by: 1. interpreting the high-order basal unconformity as an erosive MFS2, associated with basin expansion during Mwashia times (Key et al., 2001; Selley et al., 2005; Kennedy et al., 2019), and 2. interpreting what is the base-Mwashia MFS3 in model 1 as a high-confidence, low-order, FS as part of a more prolonged TST.

Alternative sequence stratigraphic interpretations

The basal unconformity could be interpreted to be a proximal expression of the correlative conformity marking the SB2, making the basal clastic succession of Upper Roan age, rather than Lower Roan. The overlying sabkha and intertidal facies would still be Upper Roan in age (unlike model 2), but their flooding would form part of an early TST. However, the presence of proximally derived immature facies and likely deltaic or fan-delta sedimentation makes this model less plausible.

4.3.6 Mansa

The ZMSDD003 core adjacent to the Luapula River, near Mansa, is 387 m long and intersects the Kundelungu and Nguba Groups (fig. 4.10). The core reaches basement.

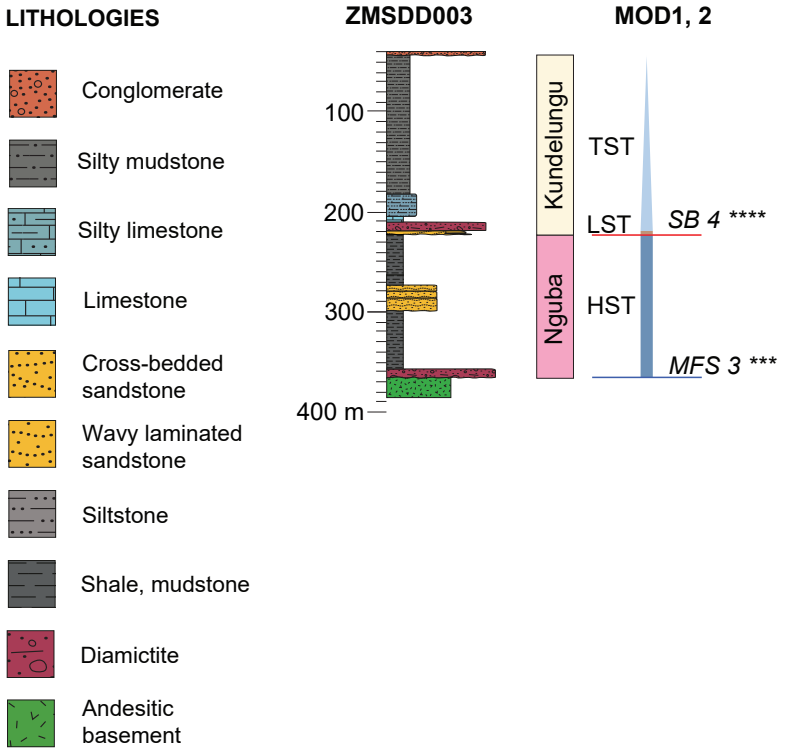

Figure 4.10: A stratigraphic log of the ZMSDD003 core near Mansa, showing the Kundelungu Group overlying the Nguba Group which unconformably lies on basement. Note the high-confidence erosional SB4 truncating mudstones of the underlying Nguba HST. MOD1, 2 refers to interpretations for sequence stratigraphic correlations 1 and 2; which in this core are identical.

The basal section of the core comprises a 10 m thick diamictite (crDia) unit sitting unconformably on basement. This is overlain by an aggradational or possibly progradational deep shelf or upper slope succession (CaMs, dMs, SlMs). At its top, this is eroded into by a thin set of coarse clastic beds (CCgm, XSst), interpreted to be of fluvial origin, which are sharply overlain by second 10 m thick diamictite unit. The diamictite unit passes sharply into a 190 m thick shelf succession comprising laminated carbonate facies (LCa) at its base, which pass into silty carbonates (lSlCa) and laminated siltstones (LSl). The siltstone facies are interpreted to have been deposited around the storm wave based and are eroded into at their top by a thin conglomerate unit.

Sequence stratigraphic correlation 1, 2

The basal diamictite that sits on basement is interpreted as the Grand Conglomerat and forms the moderate-confidence, higher order, MFS3 (based on lithological juxtaposition, deep water facies stacking above the surface) marked at its base by a moderate to high-confidence, high-order erosional surface The potential slope and deep shelf succession above it is interpreted to gently aggrade or prograde as part of a HST during Nguba times. The base of the thin overlying LST is marked by the high-confidence, high-order, erosional unconformity SB4 (fig. 4.11), on account of facies juxtaposition (shallow on deeper), an erosive base, oxidised material, and coarser grain size. The SB4 unconformity marks the regionally correlatable base of the Kundelungu Group.

The thin fluvial or glaciofluvial succession is overlain by a second diamictite, interpreted to be the Petit Conglomerat, which forms the base of a TST that leads into an initially carbonate, then clastic-dominated shelf succession. Poor facies resolution on account of predominantly deep water sedimentation precludes identification or lower order cycles.

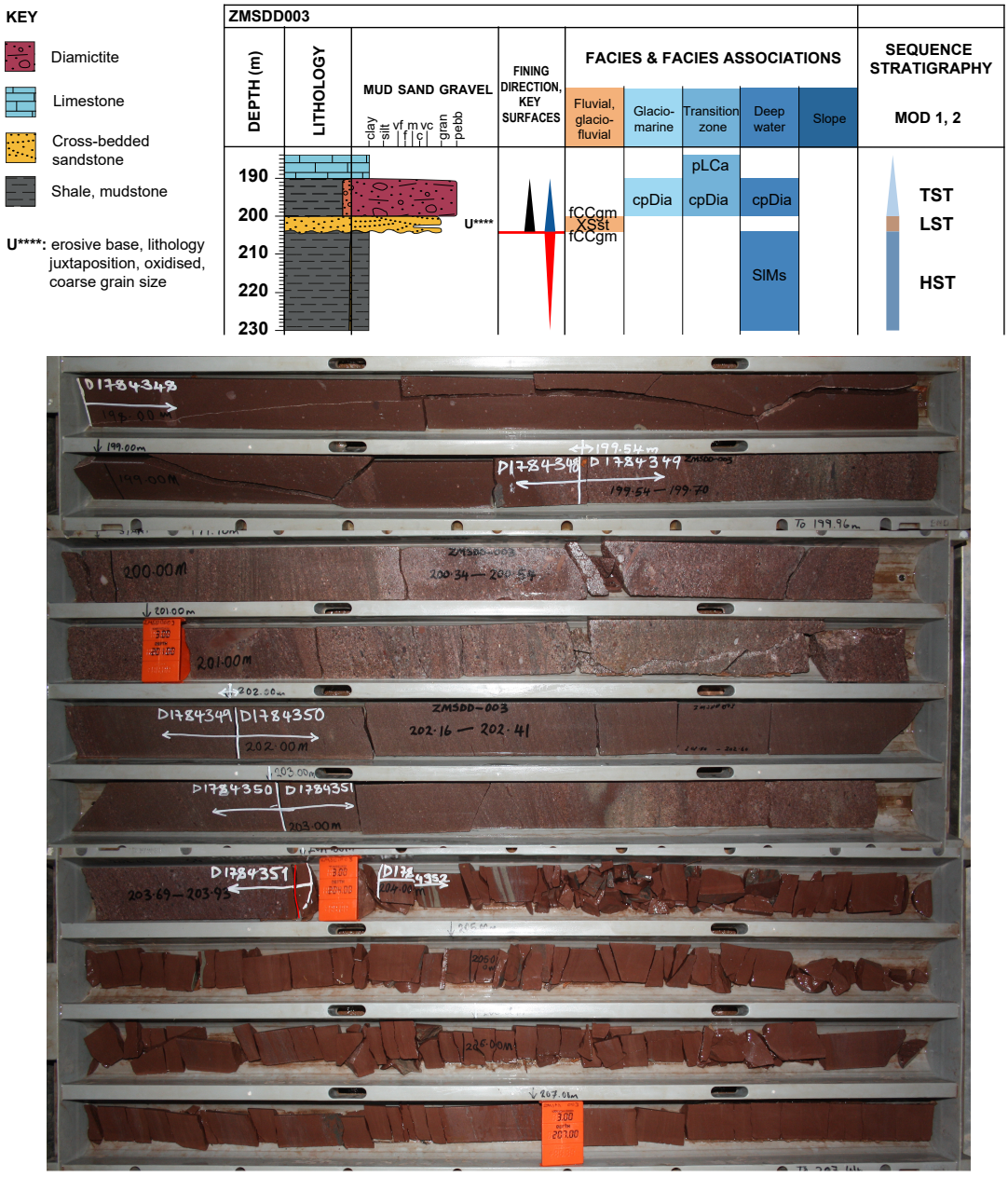

Figure 4.11: Log and core photographs of the base-Kundelungu unconformity in the ZMSDD003 core. The interpreted unconformity surface is marked by a red line. Coarse fluvial or glaciofluvial facies erode into shelf mudstones and are overlain by diamictite facies (cpDia). Cores young from bottom right to top left.

4.3.7 Chilonga

The CHLDD001 core near Chilonga is 700 m deep, intersecting what are interpreted here as Mwashia and Nguba Groups (fig. 4.12). Whether the mafic bodies at the base of the core sit on basement is unclear.

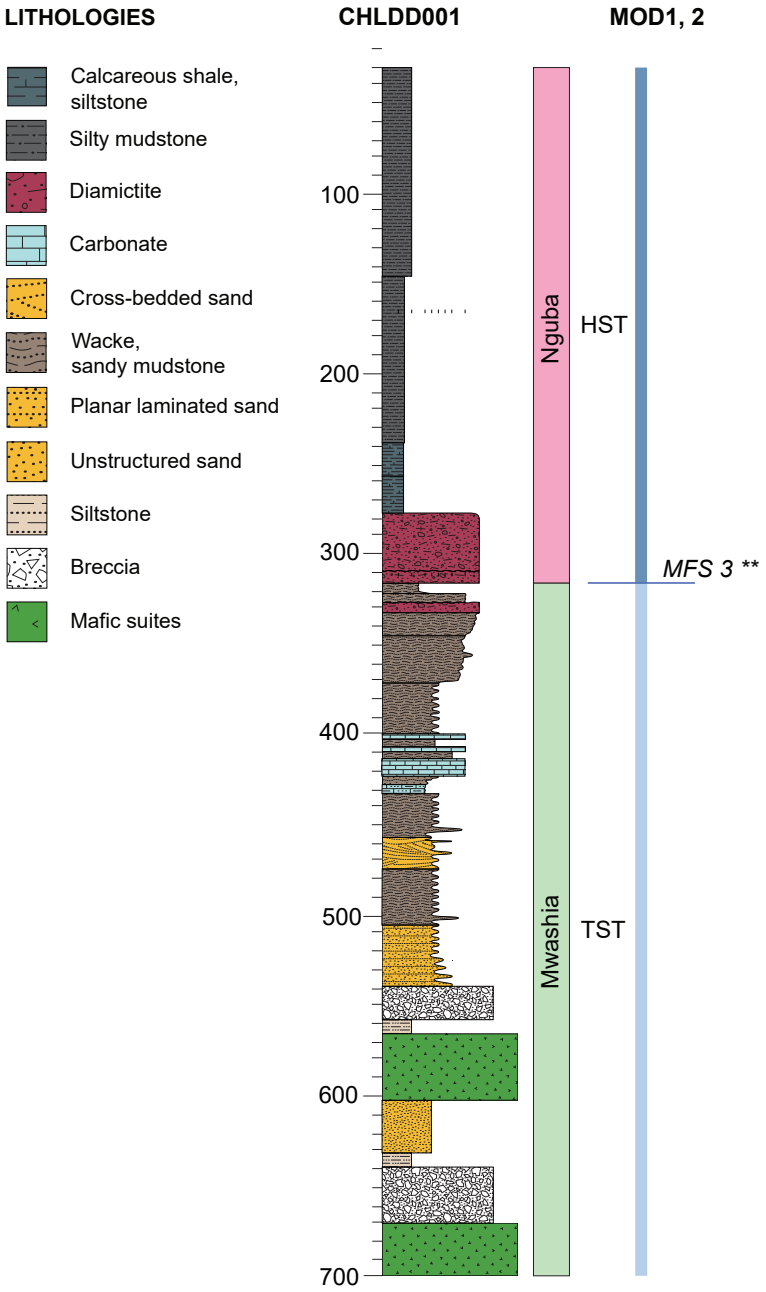

Figure 4.12: A stratigraphic log of the interpreted Mwashia and Nguba Groups in the CHLDD001 core near Chilonga. MOD1, 2 refers to interpretations for sequence stratigraphic correlations 1 and 2; which in this core are identical.

The basal portion of the core comprises a 160 m thick mixed section of mafic units, breccias, and fine siliciclastics (silts and sands). This section is overlain by a $\sim$ 130 m thick retrogradational succession of sand (XSst) and wacke facies (Wck), interpreted as delta slope or slope deposits. This passes upwards into an interbedded succession of wacke (Wck), sandy mudstone (SstMs) and carbonate conglomerate (CaCgm) facies, interpreted as slope deposits. A coarsening-up section comprising wackes and sandy mudstones is then interbedded with a 5m thick diamictite (cpDia) unit, and then overlain by a second 40 m thick diamictite unit capping the succession.

The diamictites pass transitionally into a gentle shallowing-up shelf succession comprising first carbonate-bearing mudstone (CaMs), then silty mudstones (SlMs) facies. These are overlain by laminated siltstone (LSl) facies, which were deposited at or above the storm wave base.

Sequence stratigraphic correlation 1

The mafic and brecciated section is enigmatic and precludes detailed interpretation at this stage, but is interpreted to lead into a TST on the basis of possible intertidal (Het) facies in the brecciated section being overlain by deeper water delta slope or slope facies. These form what is interpreted as a Mwashia-age, based on the presence of mafic suites (Key et al., 2001), retrogradational succession that leads into the moderate-confidence higher order MFS3 (on account of facies juxtaposition and facies stacking) at the base of the second diamictite unit. The diamictite units are interpreted to be the Grand Conglomerat. The shallowing-up shelf succession above the diamictites forms part of a HST during Nguba times.

Alternative sequence stratigraphic interpretations

An alternative interpretation would place the low to moderate confidence MFS3 (facies juxtaposition and facies stacking) in the carbonate conglomerates below the diamictites, which could represent shedding of a steepened carbonate ramp or platform, placing the overlying succession in a prolonged HST.

4.3.8 Sequence stratigraphic correlation 1: synchronous terrestrial rifting across the Kafue anticline

Sequence stratigraphic correlation 1 implies synchronous terrestrial rifting across what is classically considered to be the Lower Roan (Mendelsohn, 1961; Binda, 1994; Selley et al., 2005). Key stratigraphic surfaces and the sequence stratigraphic classification of Groups is shown in figure 4.13.

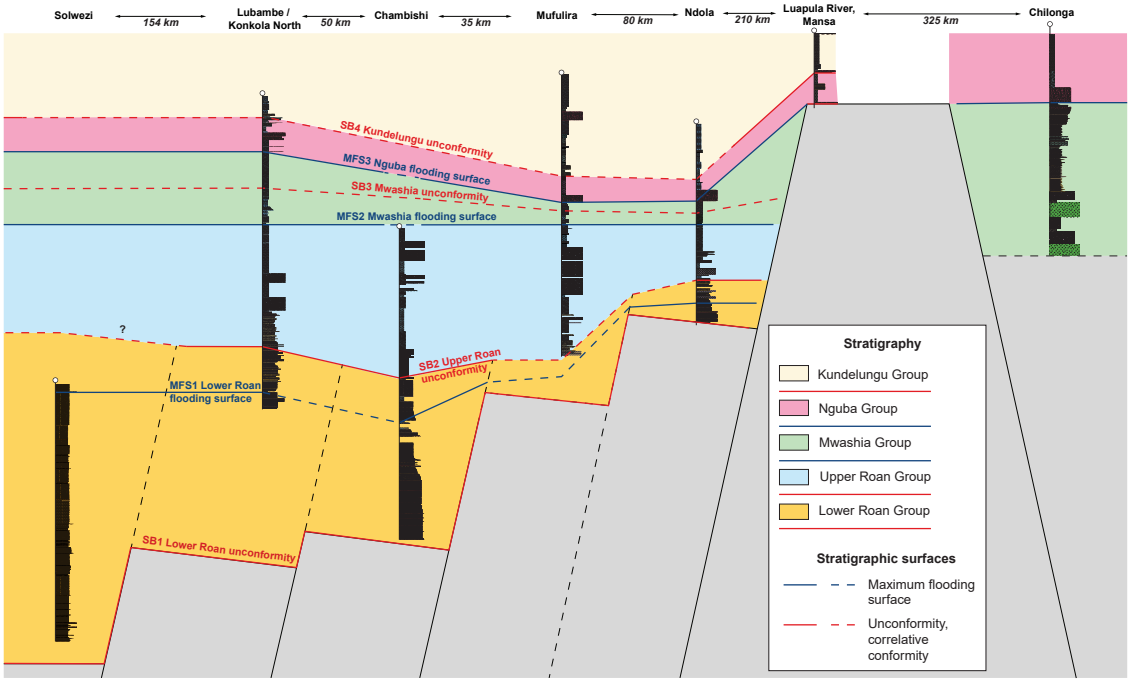

Figure 4.13: Sequence stratigraphic correlation 1 framework along the line of section shownin figure 4.2, showing logged cores and key stratigraphic surfaces that bound the Lower Roan, Upper Roan, Mwashia, Nguba and Kundelungu Groups.

Lower Roan TST

The Lower Roan stratigraphy thickens WNW towards the Domes region, being deepest in Solwezi and shallowest in Ndola on the SE margin of the Kafue anticline. The Bangweulu Block and eastern arm of the basin do not appear to record Lower Roan rift stratigraphy (based on core ZMSDD003). Deposition initially took place in disconnected sub-basins and half-graben, seemingly with little to no sediment transfer between them (Selley et al., 2005). Solwezi and Chambishi represent significant depocentres, and are represented as half-graben on the sequence stratigraphic sections due to the geometry of the line of section (see fig. 4.2).

The syn-rift clastic succession comprises lower order cycles of predominantly alluvial fan (e.g.

Chambishi sub-basin, Ndola), fan-delta (e.g. Konkola sub-basin) and fluvial (e.g. Solwezi) successions, generally aggrading, sometimes becoming retrogradational towards their top (fig. 4.14).

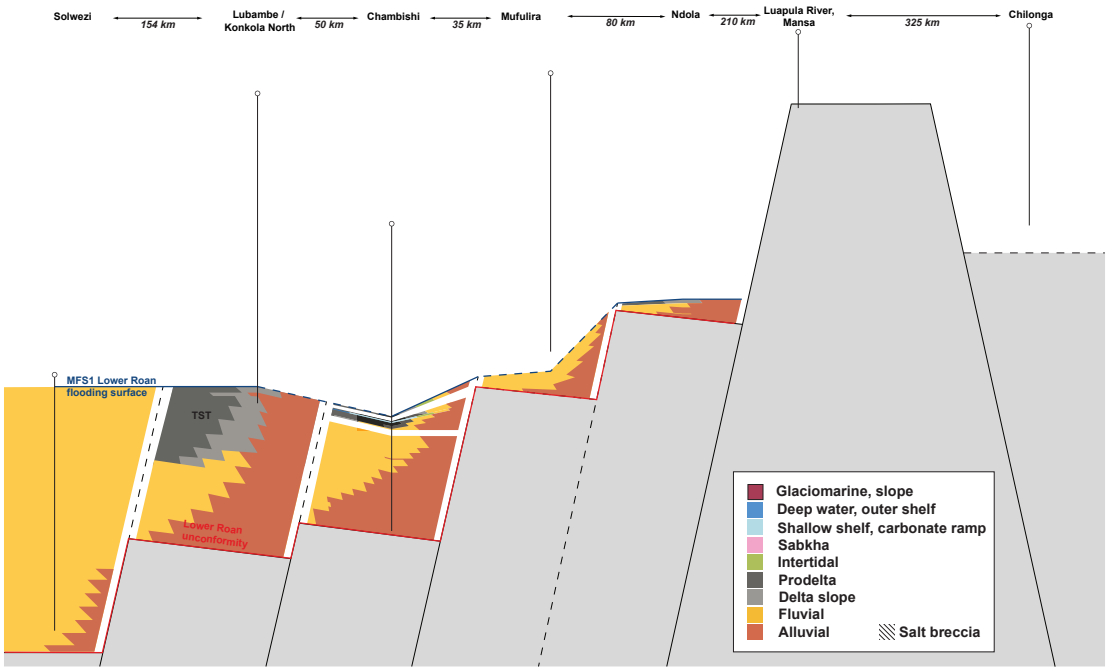

Figure 4.14: Sequence stratigraphic section across the Kafue anticline, Bangweulu block and eastern part of the basin during the Lower Roan TST, with low-order cyclicity, proximal terrestrial sedimentation predominating in disconnected sub-basins. Vertical lines represent core constraints

Rifting and fault-control on topography is evidenced by the abundance and spatial extent of disconnected depocentres across the Katangan basin, and thicknesses of facies successions far exceeding depositional water depths in both subaerial and subaqueous settings.

At Solwezi, the very thick aggradational facies stacking attests to sediment supply being very high: it is dominated by fluvial sedimentation throughout the entire basal succession, with little to no significant deepening.

The first widespread transgressive surface in the traditional Copperbelt is marked by the lowermost flooding surface, MFS1, characterised by prodelta and deep water deposits along the NE Kafue anticline, and delta slope deposits across the SE Kafue anticline. This surface is interpreted to represent a simultaneous deepening across much of the Lower Roan rift basin. To what extent this deepening resulted in connection between sub-basin is unclear, as sediment gravity flow and deeper water facies could have been deposited diachronously within respective isolated sub-basins. A degree of persistent fault control is inferred on account of rapidly alternating facies assemblages in the HST

overlying the interpreted MFS1.

Lower Roan HST, Upper Roan LST

The Lower Roan HST comprises predominantly aggrading successions across much of the Kafue anticline, with a greater proportion of subaqueous facies persisting following the initial transgression and onlap. Early sabkhas and intertidal zones developed in the southern part of the Kafue anticline, potentially resulting in partial connection of sub-basins. The Solwezi core, KRX082, is enigmatic on account of uncertainties regarding the delineation of the MFS1, but appears to become more marine during the HST with terrestrial sands becoming marine (on account of carbonate being present) but without a clear FS separating the two.

The higher-order (Embry, 1993) base Upper Roan unconformity and correlative conformity is marked by a significant shallowing, and widespread aggradational paralic successions, extensive low-cyclicity sabkha and intertidal zones prograding basinwards (fig. 4.15). Erosion is not expressed at this surface, possibly due to basinwards restricted supply of coarse siliciclastic material and increasing aridity, evidenced by sabkhas.

This LST succession overlies and appears to correlate across Lower Roan structural highs along and on the Kafue anticline (Mendelsohn, 1961; Selley et al., 2005). The transition from Lower to Upper Roan Groups is interpreted to represent a fundamental change in stratigraphic architecture, following a cessation of fault activity and a widening of the basin as it entered its flexurally driven thermal-sag phase (White and McKenzie, 1988). Concomitant retreat of clastic sources to the basin margins may also account for the switch to predominantly carbonate deposition.

Upper Roan TST, Mwashia HST

The Upper Roan TST marks a significant transgression, culminating in widespread and thick carbonate accumulations. These indicate the basin gradually widened during the late Upper Roan, with terrestrial clastic input becoming more marginal and onlapping onto basement. Intertidal zones rapidly deepened into carbonate ramps and deeper shelf facies showing higher order cyclicity. Deeper water, possibly outer shelf, deposition predominated in the Konkola sub-basin, with a carbonate shelf extending across much of the Kafue anticline (fig. 4.16).

The Chambishi sub-basin forms an outlier on account of sabkhas and intertidal zones persisting into the late Upper Roan. This could be the result of misinterpretation of ambiguous local facies assem-

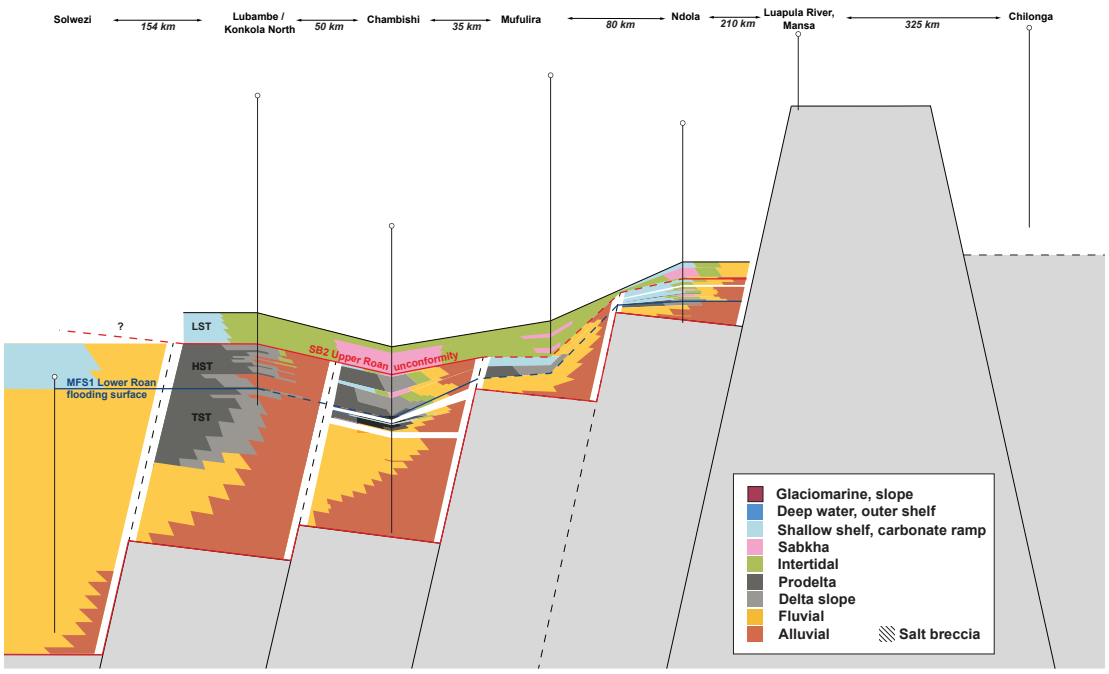

Figure 4.15: Sequence stratigraphic cross-section showing widespread intertidal and sabkha successions forming the Upper Roan LST.

blages with insufficient diagnostic criteria for accurate depositional interpretations. Alternatively, local sediment supply and accumulation rates could have been sufficiently high for less pronounced retrogradation.

Mwashia extension is interpreted to be expressed in the base-Mwashia MFS2, representing a significant deepening and extension of the basin. Deep water facies are present across the Kafue anticline, being thickest in the North, and thinning towards the southeast. This high-order MFS is interpreted here to be broadly coeval with Mwashia magmatism (Key et al., 2001) and inititation of Poudinge deposition (Schmandt et al., 2013; Kennedy et al., 2019).

Mwashia LST, Mwashia TST, Nguba HST

Throughout the Mwashia, the basin remained relatively deep, with a minor shallowing event marking a possible correlative conformity (SB3) and onset of a LST, resulting in progradation of carbonate ramps onto deeper shelf facies (fig. 4.17). These deepen into a thin TST, onlapping onto Bangweulu block. The basin extended eastwards during this time, with deposition at Chilonga characterised by downlapping slope facies.

The base of the Nguba HST is delineated by slope-derived diamictites downlapping onto underlying carbonate ramp and deep shelf facies across the Kafue anticline, forming the high-order (possibly 1st or 2nd order (Vail, 1991; Embry, 1993)) MFS3. The basin remained deep across the Kafue anticline and eastwards towards Chilonga during the Nguba HST.

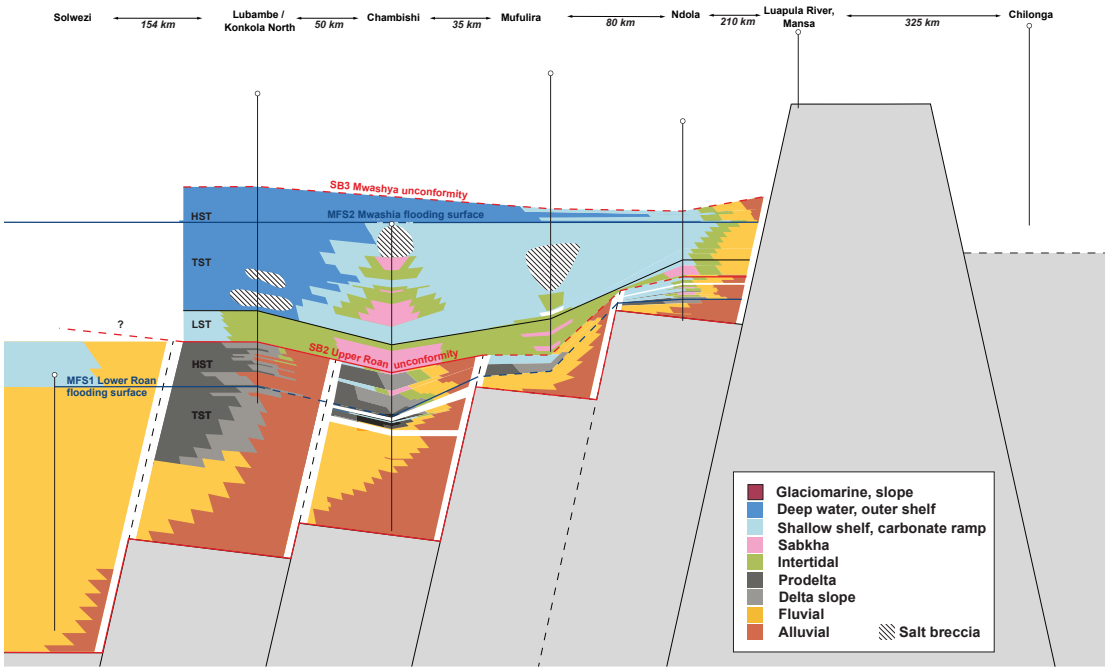

Figure 4.16: Sequence stratigraphic cross section showing the Upper Roan TST and Mwashia HST marking a pronounced deepening and expansion of the basin.

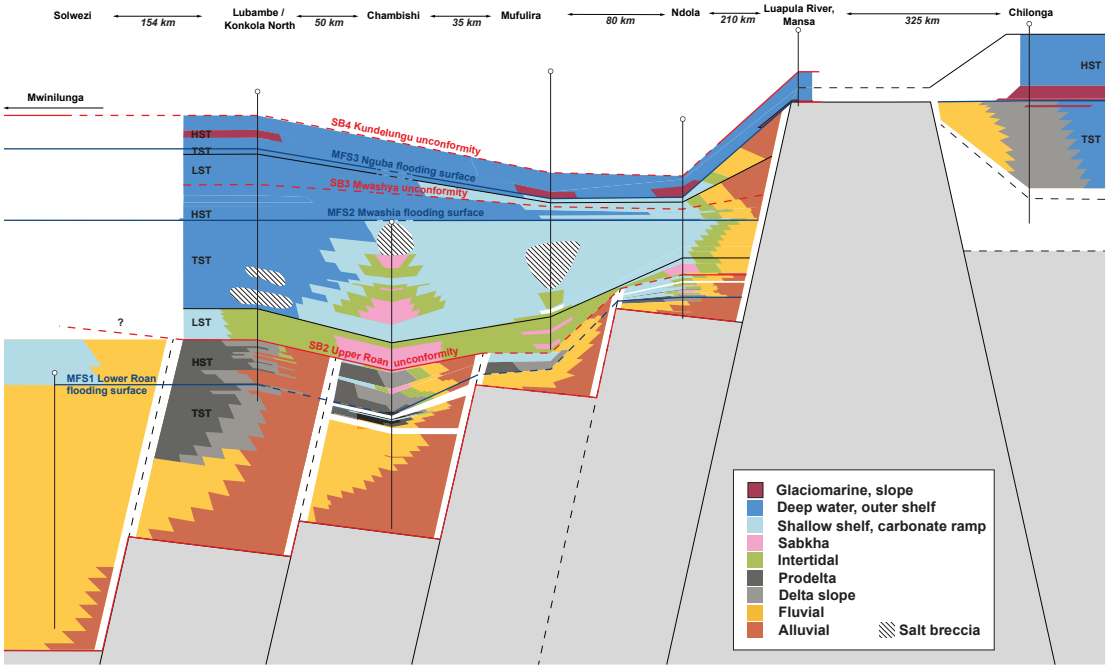

Figure 4.17: Sequence stratigraphic cross section showing deposition being initiated in Chilonga during the Mwashia TST, and the basin remaining deep during the long-lived Nguba HST, comprising the Grand Conglomerat diamictites.

Kundelungu LST

The base-Kundelungu SB4 marks a significant change in basin stratigraphy, with fluvial facies eroding into deeper water Nguba successions. The well-expressed high-order erosional unconformity is interpreted as a forced regression surface and marks the onset of a basinward facies shift and progradation of terrestrial facies over underlying deep shelf facies (fig. 4.18). This trend is mirrored on the western margin of the basin with a pronounced (though not clearly unconformable) shallowing of shelf facies into fluvial successions, marking what is interpreted to be a time-equivalent sequence boundary on both eastern and western margins of the basin.

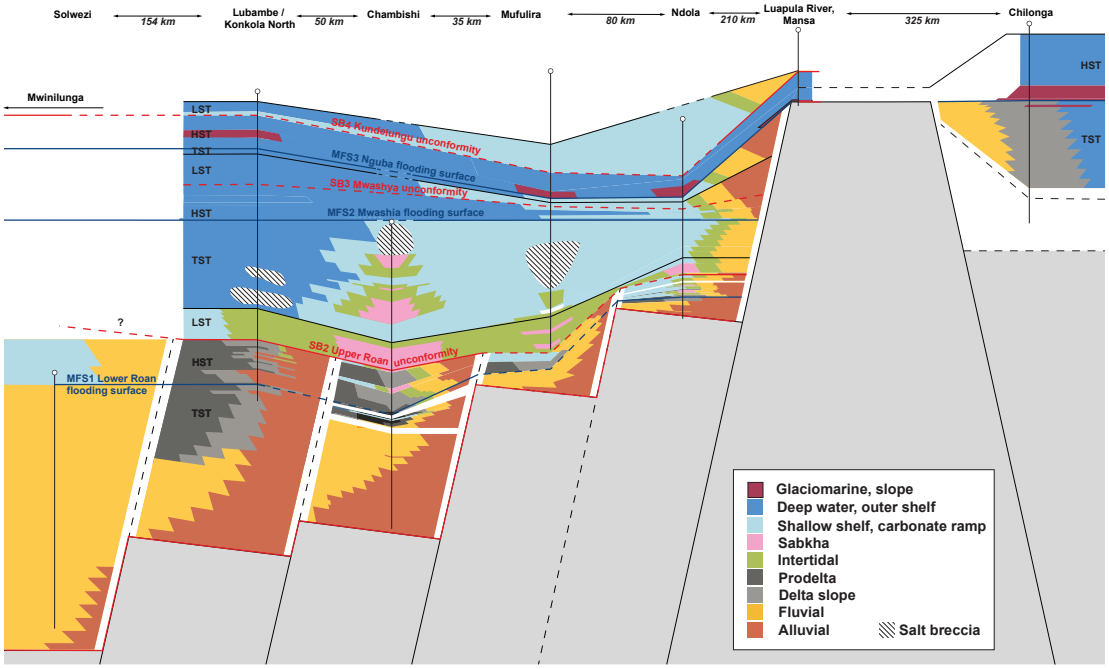

Figure 4.18: Sequence stratigraphic section showing the high-order base-Kundelungu erosional unconformity, SB4, that marks a significant basinward facies shift.

Kundelungu TST

The overlying Kundelungu TST is marked at its base by a deepening into subaqueous diamictites, often with greater evidence for glacial influence (e.g. lone stones, dropstones). These diamictites are commonly overlain by carbonate successions that become increasingly clastic (fig. 4.19). Shoreface to deep shelf conditions prevail throughout the Kundelungu TST successions that are preserved on both eastern and western margins.

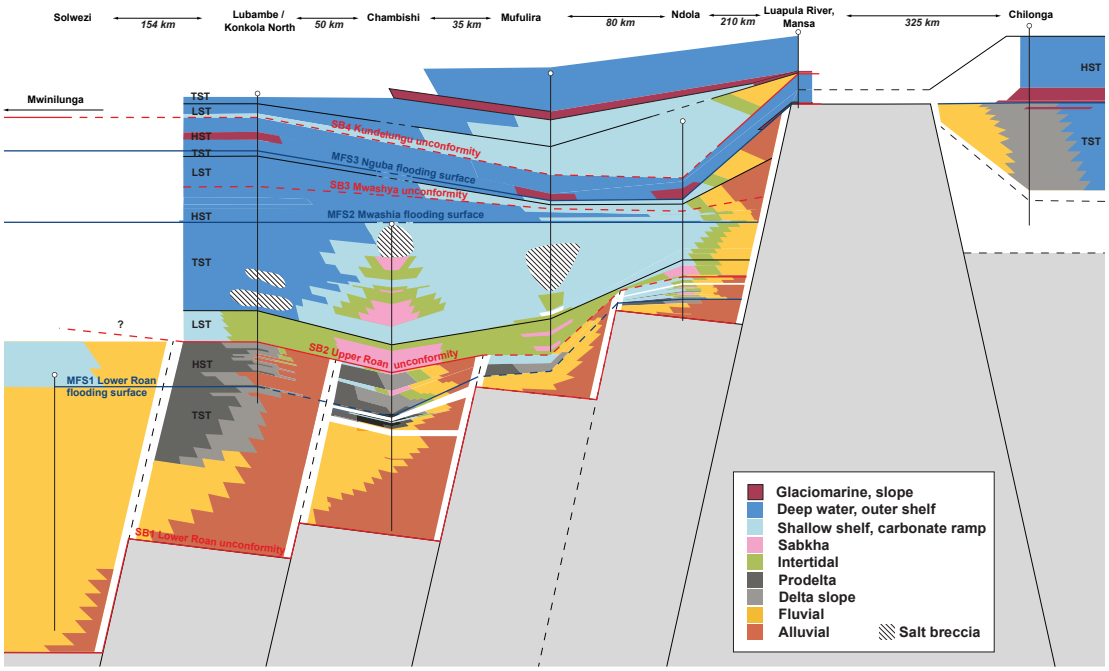

Figure 4.19: Sequence stratigraphic section showing Petit Conglomerat diamictites forming part of the Kundelungu TST.

4.3.9 Sequence stratigraphic correlation 2: diachronous terrestrial rifting across the Kafue anticline

Sequence stratigraphic correlation 2 is an alternative framework derived from different significance being attached to key stratal surfaces in cores L83 and IT26. It implies that some units which have traditionally been attributed to the Lower Roan in Ndola, on account of their lithology, are of Mwashia age. Key stratigraphic surfaces and the sequence stratigraphic classification of Groups is shown in figure 4.20.

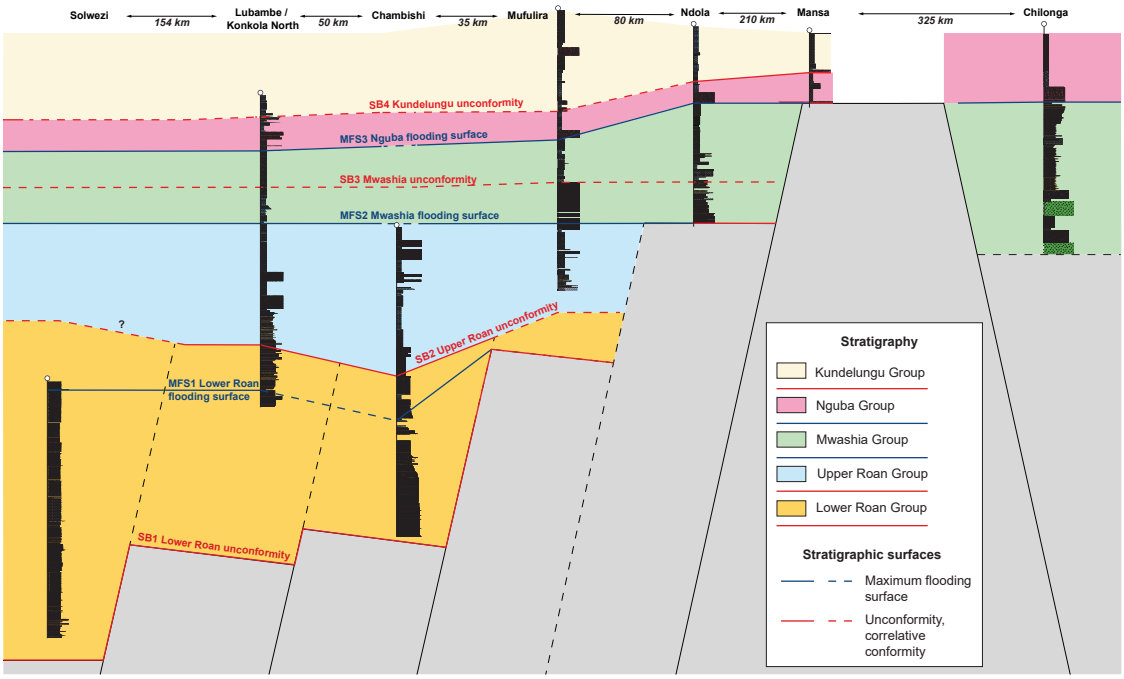

Figure 4.20: Sequence stratigraphic correlation 2 framework, showing key stratigraphic surfaces that bound each stratigraphic Group. In contrast to sequence stratigraphic correlation 1, basal clastics in Ndola are assigned to the Mwashia Group.

Lower Roan TST

As in the synchronous rifting model, the initial Lower Roan rift forms part of a TST, with alluvial fan and fluvial sedimentation predominating across the Domes and NW Kafue anticline. The facies architecture is typically aggradational, low-cyclicity, showing high ($>$ 100) amplification factors, with facies successions significantly exceeding depositional water depths. Similarly, the syn-rift clastic succession thickens towards the NW, with little sediment transfer being interpreted across structural domains (fig. 4.21). In contrast to the sequence stratigraphic correlation 1, the southeast-

ern Kafue anticline (around Ndola) is not involved in initial Lower Roan rift TST deposition.

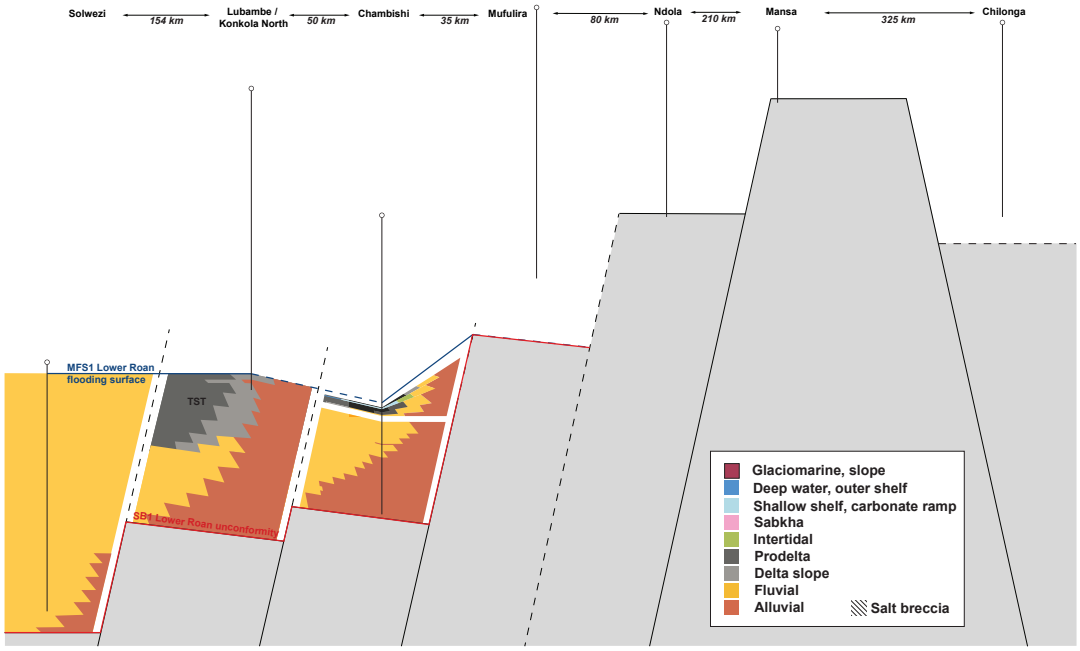

Figure 4.21: Sequence stratigraphic section showing a narrower Lower Roan rift, filled with low-order cycles of proximally derived clastic facies.

Lower Roan HST, Upper Roan LST

The Lower Roan HST is assumed to be expressed across the Domes and NW Kafue anticline (e.g. Konkola and Chambishi sub-basins) as in the synchronous Kafue rift model, with aggrading successions predominating and the deepest water facies in the succession being interpreted as the higher-order MFS1, due to the assumption of this surface developing synchronously across several sub-basins (Embry, 1993). Solwezi remains enigmatic, but represents the thickest Lower Roan clastic succession. Initiation of sedimentation in Mufulira is cautiously inferred to coincide with MFS1 (fig. 4.22). The L83 core does not reach basement, and a detailed facies analysis of the Lower Roan in Mufulira was not possible. Therefore, ambiguities exist with regards to local palaeobathymetry and transgressive episodes in the traditionally lithostratigraphically defined Lower Roan around Mufulira. Delta slope or subaqueous slope settings that could represent deepening events are possible if the 'carbonaceous wacke' and 'argillitic sandstone' (Eden, 1974) broadly correspond to the wacke and sandy mudstone facies proposed in this work.

The post-rift thermal sag phase is interpreted to start at the SB2. High-frequency and low-cyclicity intertidal and sabkha systems shifted basinward across structural highs in the NW Kafue anticline,

with Mufulira representing a more marginal depositional system. As in the synchronous Kafue rift model, the causes of waning clastic supply – sources being too distal or climatic change, or both (Bosence, 1998) – are uncertain; however, deposition in Ndola is implied not have started at this stage.

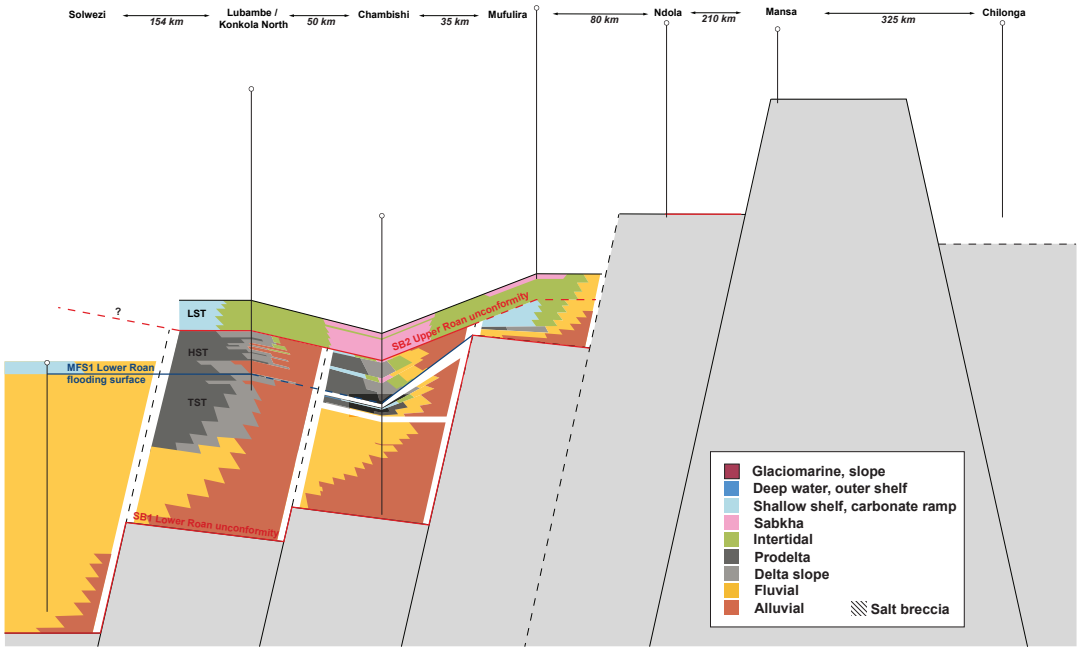

Figure 4.22: Sequence stratigraphic section showing the Upper Roan LST prograding and aggrading above disconnected or partially connected Lower Roan sub-basins.

Upper Roan TST

The Upper Roan TST is similar to that of the synchronous Kafue rift model, with low-order cyclicity paralic successions retrograding and transgressing westwards. The seemingly long-lived nature of sabkhas in Chambishi during this deepening remains difficult to account for.

What is interpreted to form part of an extensive epicontinental sea extended across the central Domes region and NW Kafue anticline, with Mufulira representing more clastic margins. The shoreline is interpreted to have stopped short of Ndola (fig. 4.23).

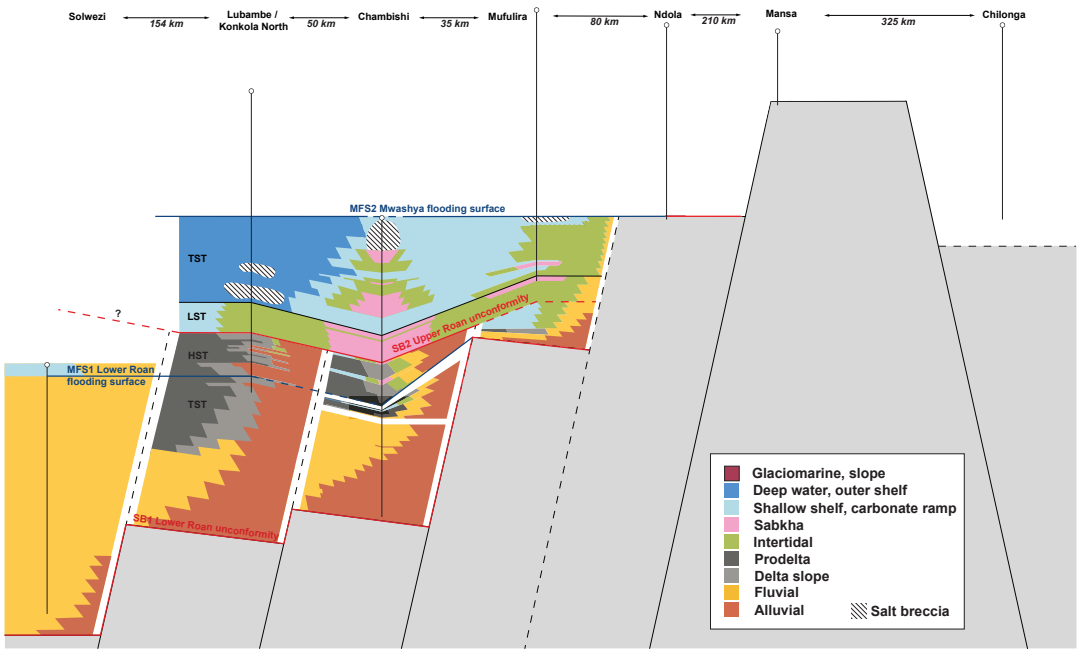

Figure 4.23: Sequence stratigraphic section showing the Upper Roan TST and westwards retrograding paralic facies culminating in the high-order Mwashia flooding surface.

Mwashia HST, LST, TST

The Mwashia HST begins with the pronounced high-order MFS2 resulting from the basin expanding towards the SE at Ndola, E towards Chilonga, and NW at Kamoa (Schmandt et al., 2013; Kennedy et al., 2019).

Relatively thin, initially aggradational, then retrogradational coarse clastic successions that show low-order cyclicity sit unconformably on basement at Ndola mark the onset of sedimentation during Mwashia times. The basal erosional surface in the IT26 core is inferred to be a proximal expression of a basinal MFS2 (fig. 4.24). Delta slope or slope facies are overlain by aggradational intertidal and sabkha successions, which could indicate a resumption of fault-control on topography in the Ndola area, which could be broadly coeval with Poudinge deposition in Kamoa (Kennedy et al., 2019).

The Mwashia LST, and SB3, is expressed more clearly in the diachronous Kafue rift model than the synchronous model, with a shallowing-up to sabkha facies in Ndola and a possible karstification of carbonate facies in core L83 (Mufulira). A subsequent transgression resulted in an interpreted drowning of the Mwashia carbonate shelves, and coincided with sedimentation beginning in the eastern part of the basin at Chilonga.

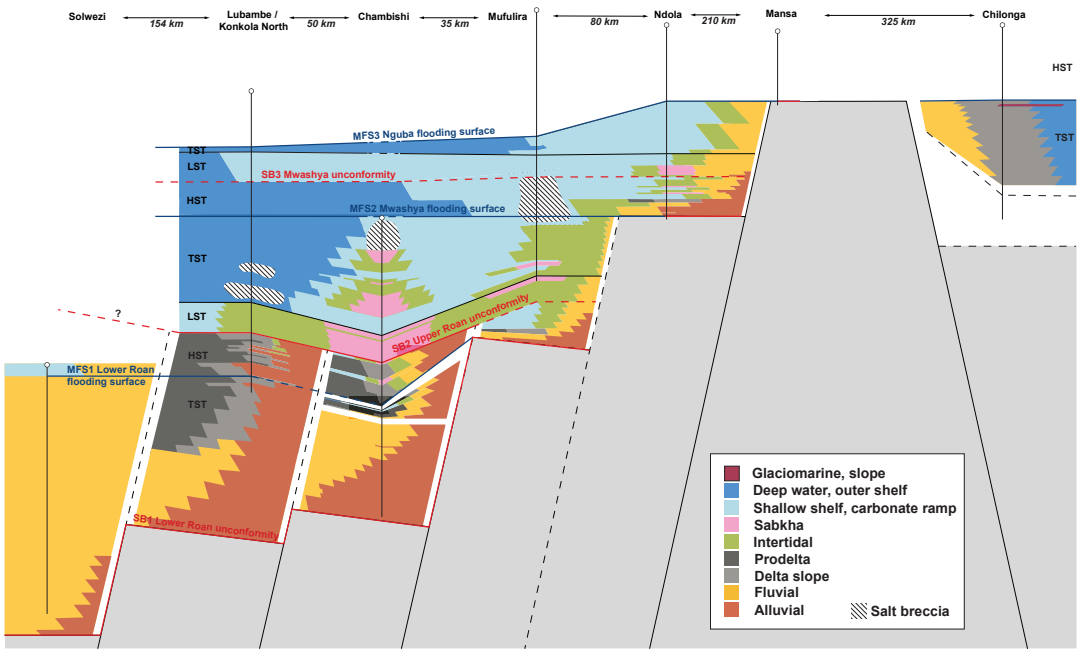

Figure 4.24: Sequence stratigraphic section showing the Mwashia Group overstepping the Roan basin margins and Mwashia-age clastics being deposited in Ndola. Deposition is initiated in Chilonga during this time.

Nguba HST

As in the synchronous Kafue rift model, the downlapping diamictite units of the Grand Conglomerat are interpreted as the high-order MFS3, forming the base of a HST. The basin remained deep across the Kafue anticline and the east of the basin in Chilonga during the Nguba HST. High-order cycles of deep water facies also overstepped, and rested unconformably on, the Bangweulu block (fig. 4.25).

Kundelungu LST, TST

The Kundelungu LST is demarcated by the same high-order sharp erosional surface as in the synchronous Kafue rift model, SB4, interpreted as a forced regression with fluvial facies eroding into the deep water successions of the underlying Nguba HST (fig. 4.26). This shallowing is expressed in more basinward sections in carbonate shelves, with water depths possibly reaching the storm wave base, on account of edgewise conglomerates being interpreted in the KN192 core (Lubambe). The subsequence transgressive systems tract is characterised by a deepening to mid-outer shelf depths and deposition of diamictites, likely of glacial origin, belonging to the Marinoan Petit Con-

glomerat.

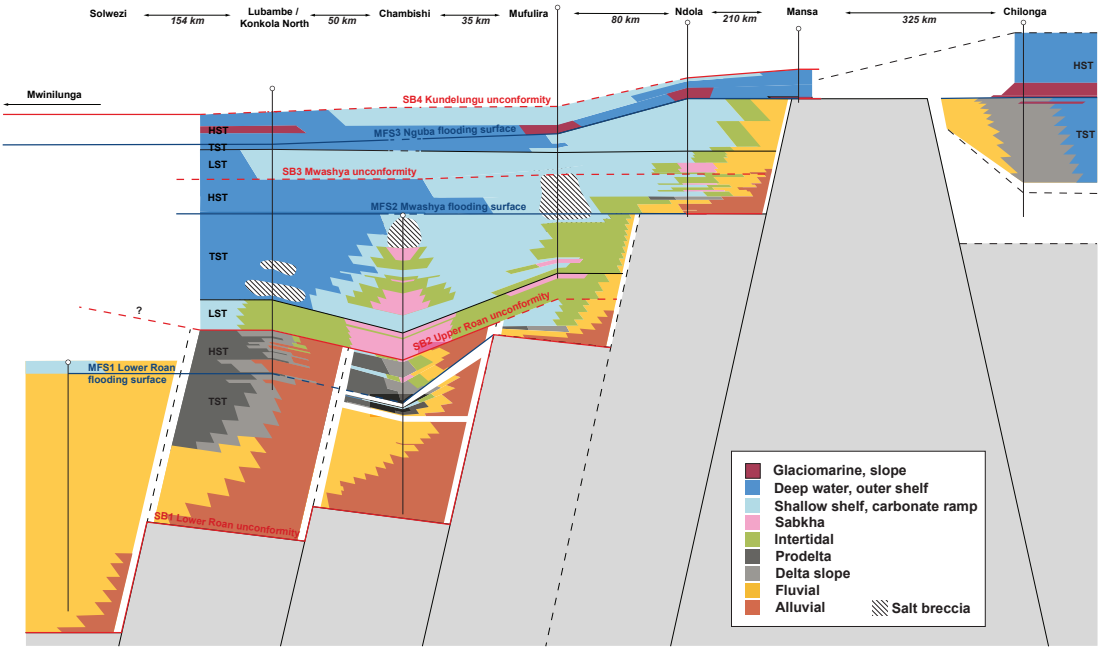

Figure 4.25: Sequence stratigraphic section showing the high-order Nguba MFS3 and long-lived HST stepping over the margins of the Bangweulu block in Mansa.

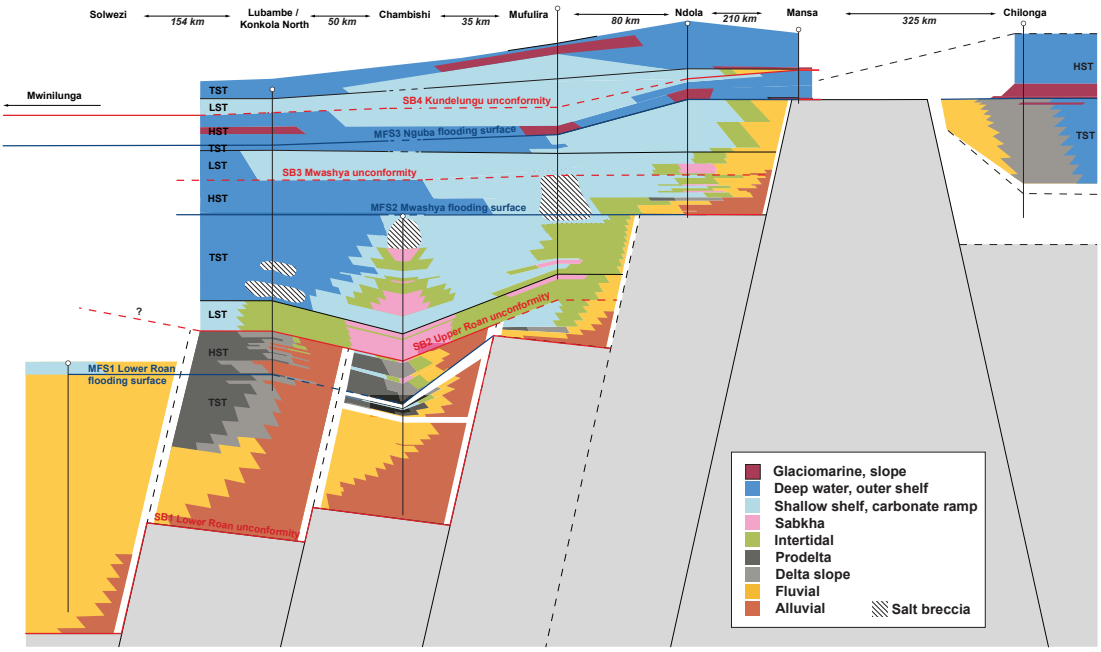

Figure 4.26: Sequence stratigraphic section showing the high-order base-Kundelungu unconformity SB4 and associated basinward facies shift, and Petit Conglomerat diamictite deposition initiating the subsequent TST.

4.4 Discussion

4.4.1 Sequence hierarchies

The main sources of uncertainty in the sequence stratigraphic analysis were the limitations inherent in environmental interpretation based on facies analysis from core alone, including alteration, the paucity of structural data, and the large spacing between cores. In addition, there is the inherent possibility of erroneously correlating key stratal surfaces of different hierarchical level (e.g. a parasequence boundary with a sequence boundary). This is a particular problem for nearshore facies which record interpretable relative base level changes with greater frequency than alluvial or deeper water settings.

Though precise ordering of sequences is not feasible on account of constraints mentioned previously, most of the post-Roan Katangan stratigraphy can be resolved to 2nd or 3rd order cycles (Vail, 1991; Embry, 1993). Terrestrial and paralic successions tend to show lower order (possibly 4th or 5th order) cycles and are best developed during the Lower and Upper Roan, and/or on the basin margins (e.g. Ndola in the diachronous Kafue rift model). On account of data limitations and poor chronological constraints, both Vail (1991) and Embry (1993)'s sequence hierarchies are deemed applicable, though (Embry, 1993)'s provides greater flexibility provided spatial resolution of data are sufficiently high.

4.4.2 Comparison to previous sequence stratigraphic interpretations

Both sequence stratigraphic correlations provided herein are an alternative to the sequence stratigraphic correlations proposed for Katangan stratigraphy by Bull et al. (2011), shown in figures 4.27, 4.28, which were restricted to the Chambishi basin. Their interpretation of the RCB2 core in Chambishi placed six sequences into what has herein been interpreted to represent a TST-HST-LST-TST package that comprises the Lower and Upper Roan Groups. For the IT26 core in Ndola, Bull et al. (2011) proposed seven low-order sequences covering the Lower Roan to Nguba Groups, which in this work make up only two higher order sequences. The upwards-thickening of sequences proposed by Bull et al. (2011) also contradicts a rift model for the Zambian Copperbelt's stratigraphy,

with three sequences covering ∼200 m of Lower Roan syn-rift fill, and only one sequence covering ∼300 m of overlying Upper Roan carbonates. This would imply initially slow subsidence and/or sedimentation during the Lower Roan, which then accelerated during the Upper Roan, which is not typical of rift basin subsidence (Xie and Heller, 2009; Allen and Allen, 2013).

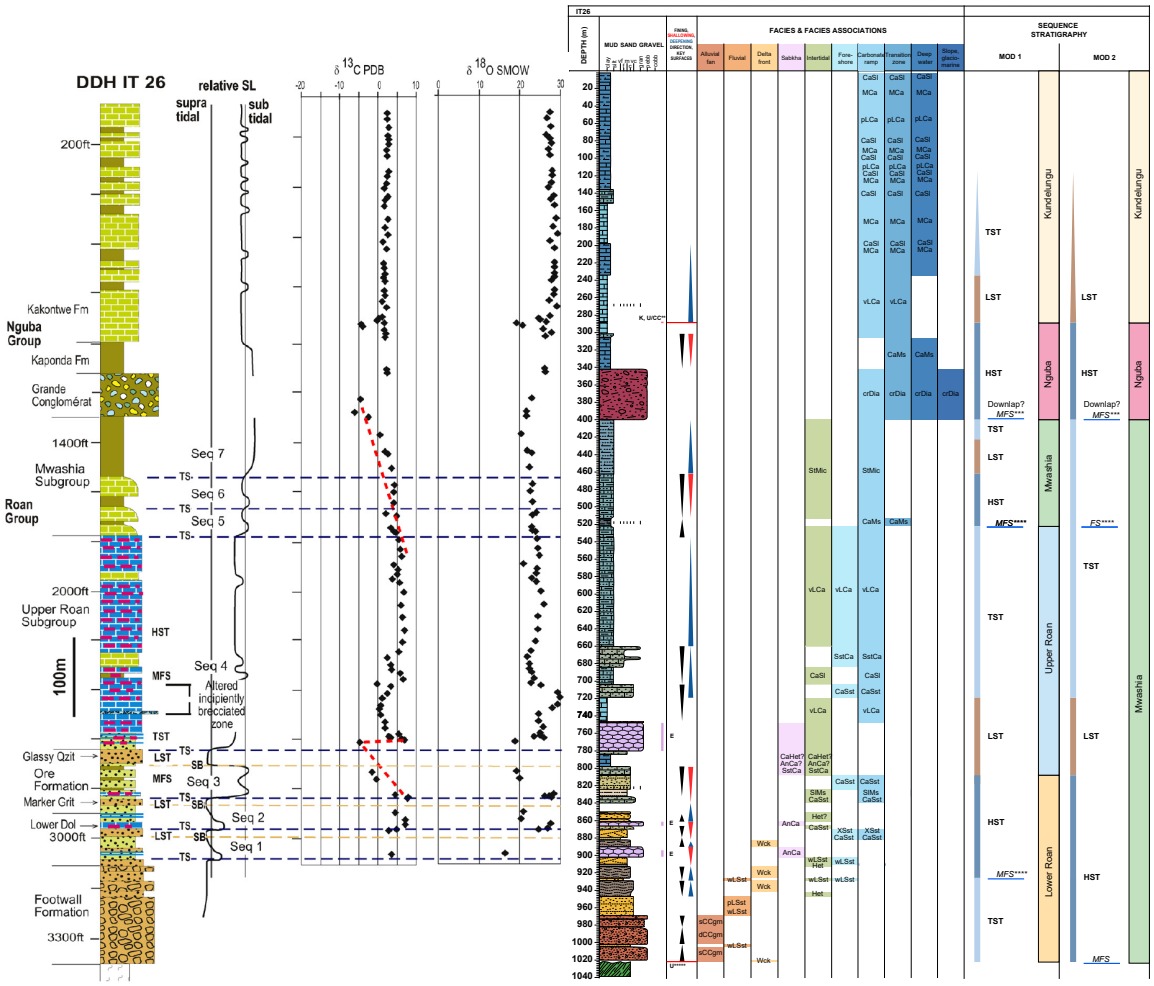

Figure 4.27: A comparison of sequence stratigraphic interpretations of the IT26 core from Bull et al. (2011) (left) and this work (right). Note the dilation of sequence thickness as facies resolution attenuates, and parasequences being mistaken for sequences in Bull et al.'s (2011) interpretation. The complete stratigraphic log for IT26, including key, is provided in Appendix 2.

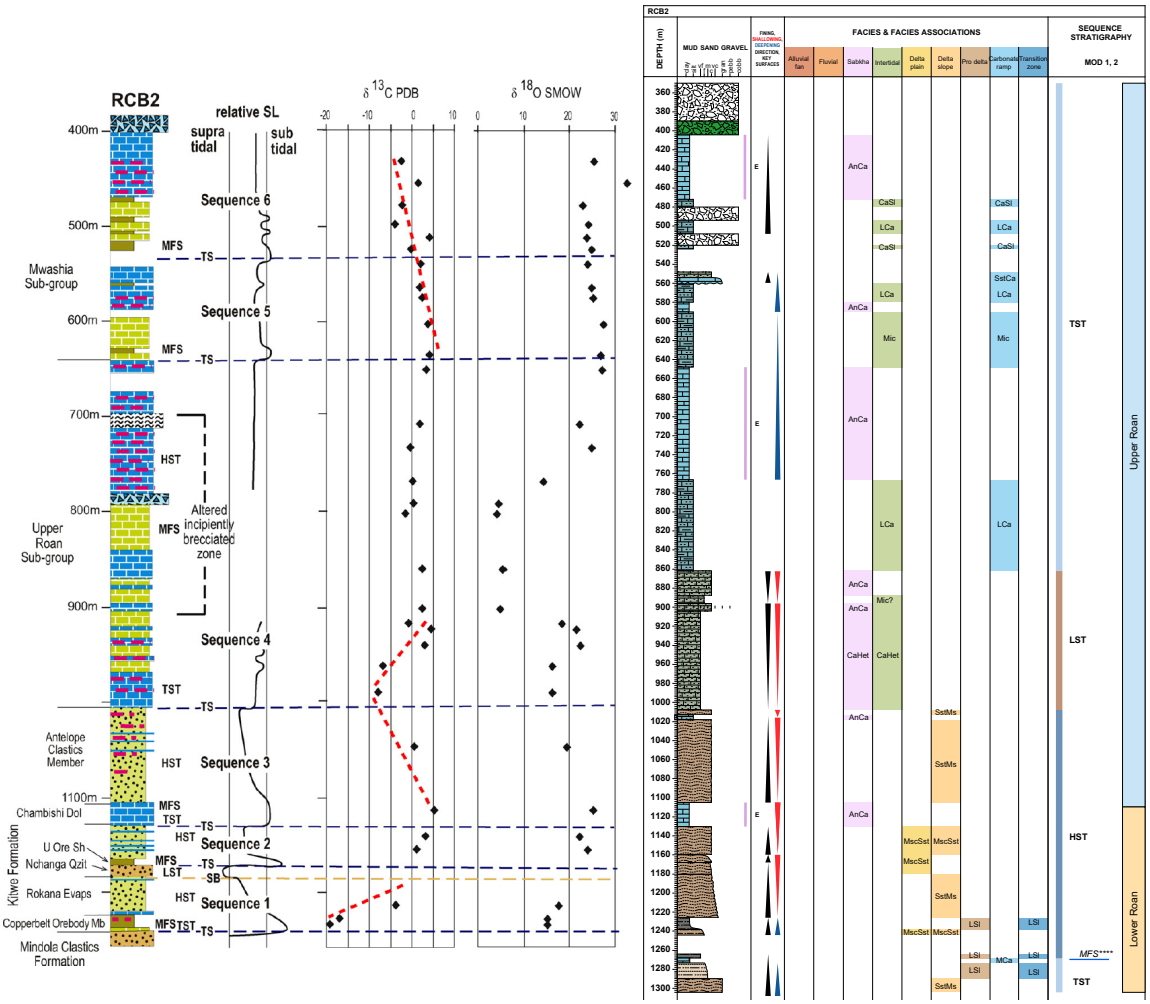

Figure 4.28: A comparison of sequence stratigraphic interpretations of the RCB2 core from Bull et al. (2011) (left) and this work (right). Note the three sequences in Bull et al.'s (2011) interpretation fitting into the Lower Roan HST proposed in this work. The complete stratigraphic log for RCB2, including key, is provided in Appendix 2.

4.4.3 Diachronous rifting

Both sequence stratigraphic correlations support a two-phase rift evolution for the Katangan basin. A terrestrial rift was expressed as initially aggradational facies deposited in disconnected half-graben structures. A second rift is interpreted to be expressed in the Zambian portion of the Katangan basin by the MFS2 and a marked deepening of facies below the storm wave base (e.g. deep shelf facies in cores KN192 and L83, slope facies in core CHLDD001). Mwashia rifting is further supported by widespread tholeiitic mafic bodies across the traditional Copperbelt and Domes region (Mendelsohn, 1961; Kampunzu et al., 1991; Tembo et al., 1999), and more extensive mafic suites

in the western and eastern part of the basin (Unrug, 1983; Key et al., 2001). Though both models invoke two stages of rifting, they show that uncertainties relating to key surfaces and palaeoenvironmental interpretation allow for diachroneity in sediments that are lithostratigraphically ascribed to the Lower Roan (Mendelsohn, 1961; Clemmey, 1976). The more diachronous Kafue rift model implies that the basal clastics at Ndola are broadly coeval with the Poudinge at Kamoa (Kennedy et al., 2019), and crucially that the initial Lower Roan rift was narrower, with the subsequent Mwashia extension resulting in more extensive basin widening than implied by the more synchronous Kafue rift model.

The predominance of half-graben structures, rapid lateral changes and fluctuations in sediment supply and localised subsidence can convolute stratigraphic architecture in the early stages of rift basin evolution and can make reliably assigning systems tracts difficult (Bosence, 1998; Martins-Neto and Catuneanu, 2010; Holz et al., 2017). This is not helped by the limitations of Neoproterozoic basins, which include a lack of biostratigraphic data, complex alteration history, tectonic fabrics, and ambiguities regarding differences between Precambrian and modern sedimentary settings and processes (Eriksson et al., 1998; Kunzmann et al., 2020).

4.4.4 The 'ore shale'

The northern northern part of the Kafue anticline shows a well-developed deepening from terrestrial successions towards a maximum flooding surface, which may coincide with the 'ore shale' unit. The extent to which this MFS is correlatable across sub-basins, and not merely a result of localised fault-control is unclear, however. In the proposed models it is assumed the MFS1 is synchronous across sub-basins, and the basal clastics forming part of a TST is deemed reasonable.

Significant variation in sediment supply and accommodation space along-strike and down dip during the syn-rift phase could explain the thickness of aggradational fluvial successions in Solwezi (A=S), with no well-defined ore shale, compared to the Konkola and Chambishi sub-basins where it is inferred A>S during the time of ore shale deposition.

During the Upper Roan, evidence for widespread aridity and evaporation likely exerted a limiting control on sediment supply and possibly obscures what might in more temperate climates become a more clearly defined post-rift unconformity. Alternatively, if a classical steers-head basin geometry

(White and McKenzie, 1988) is assumed, it is plausible that sediment sources were too distal, and intertidal zones too broad, for coarse siliciclastics to reach what were previously syn-rift depocentres.

The ore shale unit has historically been described lithologically, but rarely using a facies analysis approach (Mendelsohn, 1961; Binda and Mulgrew, 1974; Binda, 1994; Bull et al., 2011). It can comprise several facies (e.g. MsgSst, LSl, Wck, Het), some of which do not necessitate a synchronous deepening across the Kafue anticline (e.g. intertidal, sabkha environments). Where the ore shale was deposited in intertidal or sabkha settings (Binda, 1994), and subsequently overlain by carbonates, it is the latter that may indicate a significant flooding event, not the ore shale. Diachroneity within the ore shale is therefore highly plausible, as ore shale units that do not form a clear MFS do not have any independent chronological constraints and mineralisation occurs along strike of the Kafue anticline for 100's km (Selley et al., 2005). The 'ore shale' being deposited on structural highs(Fleischer, 1984; Selley et al., 2005) may simply represent a heterolithic facies, that is not indicative of a significant synchronous deepening across the basin. This is illustrated in the two rift models proposed. The synchronous Lower Roan Copperbelt rift model is more similar to traditional interpretations of Zambian Copperbelt stratigraphy, with mineralisation restricted to the Lower Roan. However, the diachronous Copperbelt rift model places the Ndola ore shale into the Mwashia, making it equivalent in time to the deposition of the basal clastics and early diamictites in Kamoa (Kennedy et al., 2019).

4.4.5 Neoproterozoic glaciations as time lines

A major assumption made in both sequence stratigraphic correlations shown here is that the Grand Conglomerat, interpreted to be of Sturtian age (Key et al., 2001; Master and Wendorff, 2011; Kennedy et al., 2019), represents a deepening of the basin, and the moderate-confidence MFS3 as a result of Mwashia extension. Though tectonics are deemed to represent the primary control on the Grand Conglomerat, there is sufficient evidence of widespread glaciation in the basin (Stutzer, 1911; Robert, 1940; Binda and Van Eden, 1972; Master and Wendorff, 2011) to consider its potential impact on Katangan stratigraphy.

The Grand Conglomerat could represent a glaciation-induced basin fan, as part of a LST (Hoffman

et al., 2017). Carbonate diamictite facies in Lubambe (core KN192) could have also been generated via over-steepened reefs collapsing (Cook et al., 1972). However, the facies that comprise the underlying Mwashia Group are interpreted as shallow to deep shelf successions. They do not show evidence of forced regression and subaerial exposure, which the postulated $\leq$1000 m falls in sea level during Sturtian glaciation would lead to. Smaller (e.g. $<$ 200 m) fluctuations could be masked by uncertainties in palaeobathymetric estimates for carbonate and shelf successions; however the ice volumes invoked for 'Snowball Earth' events would undoubtedly generate eustatic fluctuations in excess of 200 m (Liu and Richard Peltier, 2013; Creveling and Mitrovica, 2014; Hoffman et al., 2017).

Conversely, there is little evidence for a deglaciation-induced water depth increase above the Sturtian diamictite units in the basin. Though the facies support a deep basin interpretation during Nguba times, overstepping the margins of the Bangweulu block in Mansa, the paucity of well-developed turbidite or slope successions above the diamictite units along the Kafue anticline, and presence of above-storm wave-base siltstone successions in the eastern parts of the basin in Chilonga, do not lend strong support a major ($\leq$1000 m) sea level rise following Sturtian deglaciation.

There is stronger evidence for glaciation during the Marinoan on account of diamictites being more clast-poor, deposited above a correlatable LST, carbonate units appearing more regularly above them (Master and Wendorff, 2011), and the Petit Conglomerat being correlatable to Ghaub diamictites in Namibia (Hoffmann et al., 2004). The SB4 in Mansa is interpreted as a forced regression on account of underlying deep water facies. To what extent this is glacially controlled or tectonically (basin inversion) controlled, is unclear. However, the Petit Conglomerat shares similarities with other Marinoan diamictites globally (Hoffman et al., 2017), including in the Northern and Central Adelaide Geosyncline, where the base of Marinoan successions are also expressed as erosional surfaces marking the base of LST (Fromhold and Wallace, 2012). However, like the Grand Conglomerat, facies successions above and below Petit do support the magnitude of sea level changes that have been suggested for either the Sturtian or the Marinoan glacial episodes (Liu and Richard Peltier, 2013; Creveling and Mitrovica, 2014; Hoffman et al., 2017).

4.5 Conclusions

The >10 km core dataset available in the Zambian Copperbelt illustrated that the uncertainties are sufficiently large to generate two distinct, but justifiable and uncertainty-sensitive, sequence stratigraphic correlations. Both models shown provide a sequence stratigraphic framework that can underpin stratigraphic division in the Zambian Copperbelt into the four traditional Groups, with lower order cycles more discernable in the Roan Groups, and only higher order cycles identifiable in the Mwashia, Nguba and Kundelungu Groups. Sequence stratigraphic correlation 1 is most similar to archetypal interpretations of the Copperbelt, with what is traditionally considered the Lower Roan being deposited broadly synchronously and capped by a flooding surface, which may be interpreted as the rift climax.

Sequence stratigraphic correlation 2 deviates from this, indicating there is sufficient uncertainty in the facies successions and interpretations of key surfaces to invoke diachroneity in what has lithostratigraphically been interpreted to be the Lower Roan. This allows the basal clastics in the SE Copperbelt to be interpreted as Mwashia in age, and broadly synchronous with the Poudinge in Kamoa.

Both models show the limitations of using lithostratigraphy to understand mineralised 'ore shale' units, as different facies, deposited under different conditions and environments, can be mineralised, and may not correspond to one time-equivalent surface.

Reliance on facies analysis, uncertainties related to Neoproterozoic depositional systems, alteration and tectonic fabrics allows for many justifiable sequence stratigraphic correlations to be generated, only two of which are shown here, on account of them being deemed the most reliable based on highest-confidence surfaces. The two major glacial events that punctuate the Katangan stratigraphy likely exerted a significant control on the basin's stratigraphic architecture, though to what extent remains unclear.

The proposed sequence stratigraphic correlations expand on previous work by providing greater stratigraphic and spatial scope, and correlating individual facies successions between cores to correspond with the stratal geometry expected for each systems tract.

A sequence stratigraphic approach, underpinned by detailed facies analysis, allows our understanding of Katangan stratigraphy to move away from 'layercake' models, and towards a more dynamic

perspective on Katangan stratigraphy, which places the stratigraphic architecture in the context of subsidence, sediment supply and transport pathways. The proposed models, and the workflows and caveats that underpin them can begin to lay the foundation for testable stratigraphic hypotheses with predictive capability for facies distribution. Specifically, the models are of value with regards to the spatial and temporal extent of coarse clastic units, reducing horizons, degree of aquifer connectivity, as well as lateral and vertical permeability contrasts.

Chapter 5

Quantifying the subsidence history of the Katangan basin and its Tonian rift episodes

5.1 Introduction

The Katangan basin's stratigraphy records a prolonged period of sedimentation of ∼300 Myr. The basin has been extensively studied for over a century (Studt, 1913; Mendelsohn, 1961), yet the underlying mechanisms for generating its accommodation space remain poorly understood. Several ideas have been proposed, from infilling of pre-Katangan topography (Mendelsohn, 1961; Binda, 1994), to a rift basin (Kampunzu and Cailteux, 1999; Key et al., 2001), or several rift basins (Selley et al., 2018), followed by an enigmatic period prior to basin inversion, involving a flexural basin.

Estimates of sediment thicknesses across the Katangan basin are varied. Maximum thicknesses of ∼ 11 km have been invoked in the Katangan Supergroup in the D.R.C. just north of the Zambian border (Selley et al., 2018), with up to 7 km in the Zambian Copperbelt (Selley et al., 2005). However, these thicknesses are aggregate thicknesses across broad basin domains, and are not fully preserved in any particular location.

Stratigraphic thicknesses preserved at the present day in a basin do not accurately represent depositional thicknesses, nor are they indicative of any particular subsidence mechanism, on account of

compaction and erosion. Both can only be determined with subsidence analysis, which has thus far not been attempted in the Katangan basin.

Subsidence analysis is based on four parameters that need quantifying: decompacted sediment thicknesses, palaeobathymetry, eustatic fluctuations, and their isostatic compensation (Watts and Ryan, 1976; Steckler and Watts, 1978; Sclater and Christie, 1980). Decompaction involves the restoring of stratigraphic thicknesses to remove the effects of compaction due to progressive burial. Quantification of water depth at the time of deposition is needed to constrain the water-filled accommodation space and hence the depth of the basement below the sea level datum and the load exerted on the crust. Eustatic corrections need to be applied, if possible, as a change in sea level relative to a datum represents a change accommodation space unrelated to subsidence or uplift, and an additional loading (or unloading) of the Earth's crust that must be isostatically compensated (Steckler and Watts, 1978).

The total subsidence experienced by a basin can be partitioned into two components: a tectonic driving force and subsidence due to sediment loading. Quantifying both allows basin formation mechanisms and sediment accumulation rates to be constrained. The process of reconstructing over time the partitioning tectonic driving force and sediment loading is known as 'backstripping' (Watts and Ryan, 1976). Comparing tectonic subsidence profiles of different basins allows a first-order discrimination of basin forming mechanisms to be made. Rift basins have characteristic concave-up subsidence profiles, whereas foreland basin tend to be convex-up, and cratonic basin showing more gentle and prolonged subsidence (Xie and Heller, 2009).

McKenzie (1978) developed the uniform extension model to predict and quantify aspects of lithospheric extension. In this model, rifting is split into two phases: instantaneous initial fault-controlled subsidence, followed by exponentially decreasing thermal subsidence. In combination, they generate a concave-up tectonic subsidence profile that is characteristic of rift basins (Steckler and Watts, 1978; Xie and Heller, 2009).

Quantified subsidence analysis can therefore shed light on uncertainties surrounding formation mechanisms of the Katangan basin and provide a clearer understanding of its evolution in a broader geodynamic context.

5.2 Methodology

5.2.1 Type logs

Though there is an abundance of drill core in the Katangan basin, few cores have been drilled to basement. This, combined with variably exposed and incomplete stratigraphy as a result of folding and erosion, necessitates the creation of synthetic type logs. Type logs are a best-estimate of the full extent of the stratigraphy in a particular location, prior to any uplift or erosion. Synthetic type logs represent composite data based on drilled stratigraphy, correlation of cores, and estimates of uplift and stratigraphic record removed through erosion. Type logs were created for 8 cores across the basin in Solwezi (based on core KRX082), Konkola sub-basin (based on core KN192), Chambishi sub-basin (based on core RCB2), Mufulira (based on core L83), Ndola (based on core IT26), Lusale (based on core KADD04), Mansa (based on core ZMSDD003), and Chilonga (based on core CHLDD001), shown in figure 3.1).

Type logs included a best-estimate thickness range for each stratigraphic Group, and water depth ranges estimated from detailed facies analysis following guidance set out in Immenhauser (2009). Synthetic portions of types logs were based on correlation and comparison with nearby logged cores and on data from literature for each core; this is outlined in Appendix III. The stratigraphic division in the type logs is based on sequence stratigraphic correlation 1. In this model, the end of Lower Roan fault-controlled subsidence is synchronous across the basin, providing a correlatable chronostratigraphic surface across the basin.

5.2.2 Decompaction

Decompaction involves the restoring of stratigraphic thicknesses to remove the effects of compaction due to progressive burial. The process of decompaction requires understanding of porosity, burial processes, and porosity-depth relationships. These are described, and the decompaction computations derived, in Appendix IV.

Traditionally, porosity-depth curves are established empirically for each lithology or facies of interest, based on measurements of porosity of the same facies preserved at different burial depths.

However,such data are not available in the Katangan basin. Moreover, tectonic fabrics can obscure these porosity-depth relationships, and empirical porosity-depth curves were not able to be determined for the facies in the Katangan stratigraphy. Porosity-depth curves from the literature were therefore used to provide a first-order estimate. The 8 cores for which type logs were established were decompacted using the parameters in table 5.1. These parameter values were chosen on account of them representing a standard and accepted set of values (Allen and Allen, 2013; Müller et al., 2018). Where sediments were admixtures, parameters were used in the ratio of principal components (i.e. mud, sand, limestone).

Lithology	c	ϕ_0	Source
Shale/mudstone	0.51	0.63	Sclater and Christie (1980)
Sandstone	0.27	0.49	Sclater and Christie (1980)
Limestone	0.22	0.38	Turer and Maynard (2003)

Table 5.1: Parameters used in the decompaction procedure, where c is the compaction coefficient and ϕ_0 is the initial porosity.

5.2.3 Backstripping

Decompacting stratigraphic units allows for the depositional thicknesses of sediments and their rates of accumulation to be determined. However, the rate of sediment accumulation is not directly proportional to the rate of subsidence relative to a datum. Nor does decompaction allow for the partitioning of total basin subsidence into its principal components: subsidence due to sediment loading and subsidence due to tectonic forces. Backstripping is a technique that allows these two components to be quantified as a function of time, and is therefore a cornerstone of subsidence analysis (Watts and Ryan, 1976; Steckler and Watts, 1978).

Backstripping involves the 'stripping back' of successive sediment layers, correcting for changes in water depth, sea level, and isostasy, to isolate the tectonic component driving basin subsidence (Steckler and Watts, 1978). This is illustrated in figure 5.1.

Starting with an empty basin, sediment and water loads are added sequentially for each subsequent time step to effectively reconstruct the process of sedimentation by 're-filling' the basin over time. The process can also be performed in reverse, by "stripping back" each successive sediment

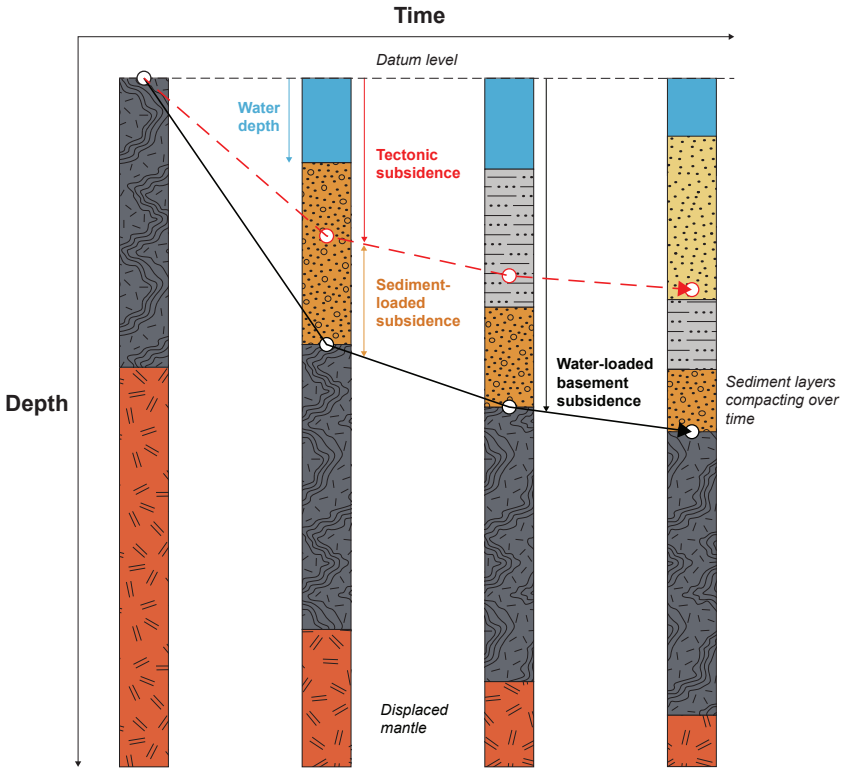

Figure 5.1: Schematic showing the process of backstripping, partioning the total (water-loaded) basement subsidence into its principal components of sediment loading and tectonic subsidence. With increasing sediment load, the mantle is displaced, and previously deposited sediment layers are compacted.

layer for which there is a time constraint and deconstructing the process of sedimentation over time. The technique was first employed by Watts and Ryan (1976) to partition tectonic and sedimentary subsidence using borehole data from the East Coast of the United States and the Gulf of Lion. A derivation of the backstripping equation is shown in Appendix IV.

Quantifying the isostatic response during backstripping has classically assumed Airy isostasy (Watts and Ryan, 1976; Steckler and Watts, 1978; Roberts et al., 1998). Airy isostasy is one-dimensional and assumes that the crust and mantle are mechanically weak. Shear stresses would therefore not be transmitted between individually loaded vertical sections of lithosphere. This may be the case in strongly-faulted crust, where fault planes can accommodate vertical shear (Watts and Ryan, 1976). However, as the lithosphere has a finite strength, its response to long-wavelength (i.e. laterally extensive) sediment loads will involve lithospheric flexure. Sediment loads are therefore distributed regionally, as opposed to locally beneath the load (Roberts et al., 1998). 1D Airy isostasy has been

assumed throughout the backstrip procedure on account of unknown flexural rigidity of the Katangan lithosphere during the Proterozoic.

Watts and Ryan (1976) found that tectonic subsidence in passive margin settings tends to be exponential, and that younger Atlantic-type margins subsided initially rapidly, compared to older Atlantic-type margins. This showed that backstripping could be used not only to understand processes within a basin, but also place a basin in a broader tectonic context.

Tectonic subsidence curves allow for the subsidence histories of different basins to be compared on a like-for-like basis without the convoluting effects of variable sediment loading. Backstripping can be used to generate a first-order estimate of basin forming mechanisms, as the general shapes of tectonic subsidence curves tend to be characteristic of particular tectonic settings (Xie and Heller, 2009). Distinctive subsidence profiles therefore allow for past tectonic regimes to be estimated for ancient basins (Xie and Heller, 2009).

Tectonic subsidence curves in rift basins and passive margins tend to show a broadly concave, asymptotic shape, with initially rapid subsidence rates that decay over time and become progressively linear (fig. 5.2). This is predominantly due to initial syn-rift faulting, followed by prolonged thermal relaxation and subsidence (McKenzie, 1978; Xie and Heller, 2009).

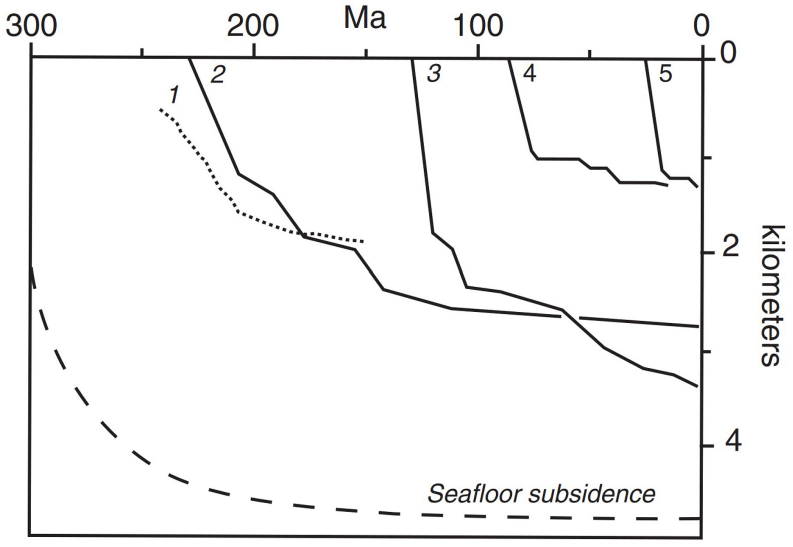

Figure 5.2: A selection of passive margin tectonic subsidence curves. The dashed line represents the seafloor thermal decay curve (shallowed by 500m). Curves 1-5 represent the Paleozoic Miogeocline, Moroccan Basin, Campos Basin, Gippsland Basin, and Gulf of Lion, respectively (Xie and Heller, 2009).

5.2.4 Palaeobathymetry

The majority of the Katangan basin's fill is Neoproterozoic, with the exception of the Biano Group, preserved in the D.R.C. (Cailteux and De Putter, 2019). The absence of fossils, results in any quantitative estimates of palaeobathymetry being reliant on facies analysis. Detailed facies analysis was combined with the framework set out by Immenhauser (2009) to generate an initial estimate of plausible water depth ranges for each major depositional environment (table 5.2).

Bathymetry	**Criteria**	**Maximum water depth (m)**
Terrestrial	Alluvial FA, fluvial FA	0
Intertidal	Intertidal FA	10
Shoreface	Shoreface FA, carbonate ramp FA evidence of persistent wave agitation	30
Transition zone	Transition zone FA, carbonate ramp FA, deep water FA, evidence of storm deposits	50
Shelf break	Deep water FA, absence of subaqueous slope FA (e.g. turbidites)	250
Slope	Slope FA	500

Table 5.2: Bathymmetry criteria and water depths used in the backstripping procedure.

5.2.5 Eustasy

Eustasy can have a significant impact on a basin's subsidence history. However, accurate eustatic corrections remain difficult to make. Several eustatic curves have been developed for the Phanerozoic, based on long- and short-term cycles of global sea level change, but these can vary by 50-100 m (Steckler and Watts, 1978; Haq and Schutter, 2008). For this reason, the eustatic term is often omitted. As no complete eustatic curves exist for the Proterozoic, the eustatic term is omitted by necessity.

However; the stratigraphy encompasses two periods of interpreted widespread glaciation, postulated

to be 'Snowball Earth' events, during the Sturtian and Marinoan, respectively (Master and Wendorff, 2011; Liu and Richard Peltier, 2013; Creveling and Mitrovica, 2014; Rooney et al., 2015; Hoffman et al., 2017). These events could have exerted a major control on Neoproterozoic sea levels globally, with localised sea level changes of up to 1000 m having been postulated (Liu and Richard Peltier, 2013; Hoffman et al., 2017). These have not been incorporated into the backstripping procedure for several reasons, outlined below.

Extensive tholeiitic magmatism and very thick aggradational successions of debris flows in Kamoa suggest rifting and extension during Mwashia and early Nguba times. Diamictites are therefore interpreted to be tectonically controlled (Kennedy et al., 2019), representing the resumption of subaqueous topography generation. Diamictite deposition as part of a tectonically controlled transgressive or highstand systems tract is inferred to be more likely, as a result.

As discussed in the sequence stratigraphic correlations, the Sturtian diamictite units could represent glacially derived debris flows as part of glaciation-induced lowstand systems tract. Liu and Richard Peltier (2013); Hoffman et al. (2017) argue for the ocean surface being lowered by $\sim$500 m during the Sturtian glaciation. However, such a significant fall in sea level, would result in major facies shifts and erosion, which is not observed in the basin's facies architecture in Zambia or the D.R.C (Kennedy et al., 2019). A eustatic fall of such magnitude would result in a significant basinward shift in facies and an unconformity, for which there is little evidence in the cores logged.

In addition to there being insufficient evidence to suggest a major eustatic fall during the Mwashia and Nguba, there is little evidence in the Katangan stratigraphy of a commensurate sea level rise that would accompany subsequent de-glaciation. Though the basin likely remained mostly during Nguba times (mostly below storm wave base), the paucity of turbidites successions or slope-derived facies indicates shelf environments, rather than abyssal settings predominating.

The possible effects of the Marinoan glaciation, for which there may be some stratigraphic evidence on the basis of a correlatable lowstand systems tract at the base of the Kundelungu, are covered in the discussion. However, there is again limited stratigraphic and facies evidence to support the major eustatic fluctuations that have been proposed by some (e.g. Liu and Richard Peltier (2013)).

5.2.6 Ages

The timing of sedimentation initiation in the basin is contentious. The maximum U/Pb age date for onset of deposition of 883 $\pm$ 10 Ma provided by Armstrong et al. (2005) represents the crystallisation age of the Nchanga granite. Initial sedimentation likely significantly post-dates this age, due to the time taken for exhumation. Though how long this time period was, is unknown. The microcline veins at Roan Antelope and Musoshi mines dated with Rb/Sr by Cahen et al. (1970) are significantly younger, but carry a large error, the upper limit of which overlaps the Nchanga granite dates. Detrital zircons from the Lower Roan Group indicate crystallisation at $\sim$840 Ma, providing a significantly younger maximum age for onset of deposition. Their populations are small, however. For this work, the Lower Roan is assumed to have been deposited from 840 Ma onwards, which allows $\sim$ 40 Myr for exhumation of the Nchanga granite. Mwashia magmatism is broadly constrained by U-Pb dates in the western part of the basin. Mafic units within the Grand Conglomerat and in contact below, also provides a maximum age for the deposition of $\sim$735 Ma (Key et al., 2001; Kennedy et al., 2019). Re-Os dates of shales underlying the Grand Conglomerat in Kipushi (D.R.C.) provide a slightly younger constraint of $\sim$727 Ma. Neither ages for the Grand Conglomarat provide a precise chronological constraint, but provide a sufficiently tight estimate. Neither of these overlap with globally accepted age ranges for the Sturtian glaciation; however local chronological constraints within the basin are deemed more suitable for the backstripping procedure. Additionally, Grand Conglomerat deposition is interpreted to be predominantly tectonically controlled, marginally post-dating magmatism, and may therefore be independent of any global age constraints for the Sturtian glaciation.

The age of the Petit Conglomerat is not constrained within the Katangan basin. Its deposition is assumed to be broadly coeval with the Ghaub diamictites in Namibia, which are regarded to be Marinoan in age (Hoffmann et al., 2004).

Deposition of the Kundelungu Group is interpreted to have ceased by 540 Ma, prior to basin inversion (Goscombe et al., 2000). The ages for individual stratigraphic units used in the backstripping computations is shown in table 5.3. The fixed parameters used in the backstripping procedure are shown in table 5.4.

Event	**Age (Ma)**	**Method**	**Source**
Onset of Lufilian orogeny	560-540	Compiled data	John (2004) , Goscombe et al. (2000)
	573 ± 5	Ar-Ar detrital muscovite	Master et al. (2005)
	592 ± 22	U-Pb monazite	Rainaud et al. (2005)
Petit Conglomerat	>639 – 635.5	Compiled data	Halverson et al. (2020)
	635.5 ± 1.2	U-Pb zircon	Hoffman et al. (2004)
Sturtian glaciation globally	∼717 – ∼660	Compiled data	Halverson et al. (2020)
Grand Conglomerat	727.3 ± 4.9	Re-Os shale	Rooney et al. (2015)
	760 ± 5 – 735 ± 5	U-Pb zircon	Key et al. (2001)
Mwashia magmatism	760 ± 5 – 735 ± 5	U-Pb zircon	Key et al. (2001)
Lower Roan depositional age	∼840	U-Pb detrital zircon	Halpin and Selley (2010)
	840 ± 13	U-Pb detrital zircon	Turlin et al. (2016)
	840 ± 42	Rb/Sr microcline	Cahen et al. (1970)
	877 ± 11	U-Pb zircon	Armstrong et al. (1999)
	883 ± 10	U-Pb zircon	Armstrong et al. (2005)

Table 5.3: Age dates used in the backstripping computations (bold) and ranges of chronological constrains for the Katangan basin's evolution.

Lithology	Density (kg/m^3)	Source
Shale	2700	Sclater and Christie (1980)
Sandstone	2650	Sclater and Christie (1980)
Limestone	2850	Turer and Maynard (2003)
Seawater density	1030	Allen and Allen (2013)
Mantle	3300	Allen and Allen (2013)

Table 5.4: Density parameters used in the backstripping calculations. Bulk sediment densities are not shown as they vary as a function of time, and are unique for each type log.

5.2.7 Uniform extension model

McKenzie (1978) was the first to model lithospheric stretching quantitatively and apply it to the formation of sedimentary basins. The model is now known as the *uniform extension model*, as vertical thinning and lateral stretching is uniform (Allen and Allen, 2013).

The uniform extension model invokes a two-stage process for lithospheric extension: (i) initial rapid fault-controlled subsidence (ii) subsequent thermal subsidence as the lithosphere cools and relaxes. Both stages combined yield the characteristic concave-up tectonic subsidence profiles observed in many rift systems (McKenzie, 1978; Steckler and Watts, 1978; Xie and Heller, 2009).

The premise of the model is illustrated in figure 5.3. It comprises crust, lithospheric mantle, as-

thenosphere, and a zone of extension, that are stretched uniformly by a factor of β, resulting in a thinning of the lithosphere and formation of a sedimentary basin.

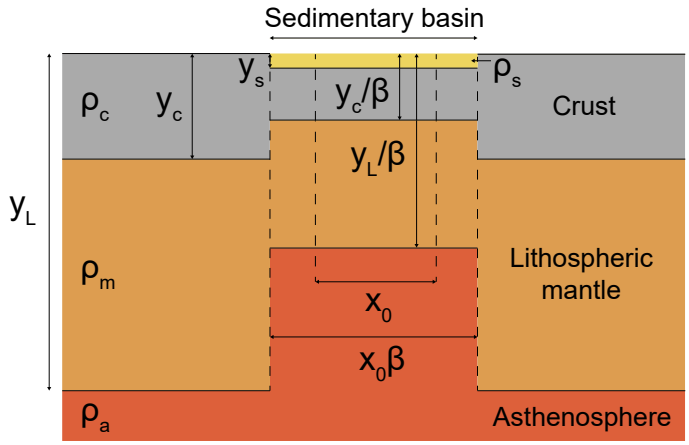

Figure 5.3: The uniform extension model as a schematic diagram, showing crust, lithospheric mantle and asthenosphere, with densities ρ_c, ρ_m, ρ_a. The crust has a thickness of y_c and the lithosphere a thickness of y_L. The crust is thinned by a stretch factor, β to y_c/β, the lithosphere to y_L/β, with the initial width of extension zone x_0 being stretched to $x_0\beta$, forming a sedimentary basin of thickness y_s with a fill density of ρ_s. Figure adapted from Allen and Allen (2013).

The uniform extension model can be used to as a simple forward model to generate tectonic subsidence curves for a given stretch (β) factor in a basin. Its derivation is provided in Appendix IV.

McKenzie (1978)'s model makes several assumptions, including: extension by pure shear (symmetrical extension, no fault block rotation), instantaneous rifting, Airy isostasy and uniform asthenospheric temperature throughout the rifting process. Despite these significant assumptions and simplifications, the uniform extension model remains a valuable reference model, providing a baseline capable of generating sufficiently clear first-order estimates for lithospheric extension (Sclater and Christie, 1980; Barton and Wood, 1984), and has successfully been applied to many rift basins (Barton and Wood, 1984; Huismans et al., 2001).

The uniform stretching model was applied to estimate β factors that best fit the tectonic subsidence profiles generated from backstripping. It is constrained by the error in depth and age provided by the backstripped subsidence plots.

Its use is predicated on the available evidence for rifting in the Katangan basin. Lower Roan evidence for rifting includes half-graben structures and rhombic fault networks (Selley et al., 2005),

rapid lateral facies transitions, and significant accommodation space generation with thick, amplified, aggradational successions of terrigenous material (e.g. in Solwezi, Konkola Chambishi sub-basins). Evidence for Mwashia age rifting is more clearly evident on the western and eastern margins of the basin, where tholeiitic mafic suites are extensive. In Kamoa, lavas and diamictite successions kilometres thick attest to large amounts of local accommodation space generation being coeval with magmatism (Schmandt et al., 2013; Kennedy et al., 2019).

It was assumed in the calculations that the fault-controlled subsidence phase lasted 10 Myr (Veevers, 1981), and that the Lower Roan to Upper Roan transition (Chapters 2, 3) represents the onset of thermal subsidence becoming the predominant mechanism driving tectonic subsidence across the basin. This is based on the sequence stratigraphic correlations proposed previously. Evidence for the Lower-Upper Roan transition representing the transition to the post-rift phase include: laterally extensive carbonate-rich facies belts above Lower Roan structural highs (Binda, 1994; Selley et al., 2005), clastic sediment supply being significantly attenuated, and units becoming correlatable between sub-basins, suggesting a more connected basin. This is associated with a fundamental change in sediment supply whether due to backstripping of the basin and clastic input becoming more distal, or climatic change, or both.

Tentative Mwashia age stretching factors were calculated using the stretched crust at the end of Roan rifting as the initial conditions for Mwashia extension. Mwashia extension was presumed to have started by 765 Ma at the latest (Key et al., 2001).

The basin fill was assumed to be water to enable comparison to tectonic subsidence signatures. Pre-rift lithospheric thickness was assumed to be 140 km based on best fit of β factors to tectonic subsidence profiles, and on estimates of Irumide lithospheric thickness (Sarafian et al., 2018). An asthenospheric temperature of 1400 °C was used to account for elevated mantle temperatures during the Neoproterozoic, and global mantle cooling over time (Ganne and Feng, 2017). Parameters used are shown in table 5.5, based on McKenzie (1978); Allen and Allen (2013); Ganne and Feng (2017); Sarafian et al. (2018).

Input	*Symbol*	*Value*	*Unit*
Initial lithospheric thickness	y_L	140000	m
Initial crustal thickness	y_c	35000	m
Mantle density	ρ_m^*	3330	kgm^{-3}
Crustal density	ρ_c^*	2800	kgm^{-3}
Basin fill density	ρ_s	1030	kgm^{-3}
Asthenospheric temperature	T_m	1400	°C
Volumetric coefficient of thermal expansion	α_v	3.28E-05	$°C^{-1}$
Thermal diffusivity	κ	0.000001	ms^{-2}

Table 5.5: Parameters used in uniform extension model computations, from McKenzie (1978); Allen and Allen (2013); Ganne and Feng (2017); Sarafian et al. (2018).

5.3 Results

5.3.1 1D burial history

The decompaction procedure yields 1D burial history profiles for the 8 cores used in the subsidence analysis (3.1). Thickness estimates in type logs were given ranges to partially account for stratigraphic uncertainties, possible erosional unconformities and removed stratigraphy. Upper burial depths estimates from type logs, not taking into account water depth, are shown in figures 5.4, 5.5. The Katangan stratigraphy generally thickens northwestwards. The greatest burial depths are reached in Solwezi, with the classical Copperbelt experiencing moderate burial, Mansa and Lusale being buried least and last. The Lower Roan is present in the Domes region and the classical Copperbelt. At time of deposition, the Lower Roan reached maximum thicknesses of ∼2.6 km in Solwezi and ∼1.8 km in the Konkola sub-basin, being thinnest at ∼0.35 km in Ndola. The depositional thickness of the Lower Roan was moderate in the Chambishi sub-basin and Mufulira, at ∼1.4 km and ∼0.8 km, respectively.

Initially rapid Lower Roan burial is observed in Solwezi, Konkola, Chambishi, tending towards more gradual burial in Mufulira and Ndola. Thickness trends of the Lower Roan across the Domes and Copperbelt regions are mirrored in the Upper Roan, though the latter experienced reduced burial rates. A change in burial rate between Upper and Lower Roan is most pronounced in Konkola.

Mwashia Group depositional thicknesses are less variable across the Zambian part of the Katangan basin, ranging from ∼0.7 km in Solwezi and Konkola to ∼0.17 km in Ndola. The Mwashia is also exposed in Chilonga, where its depositional thickness reached ∼0.55 km. Mwashia deposition

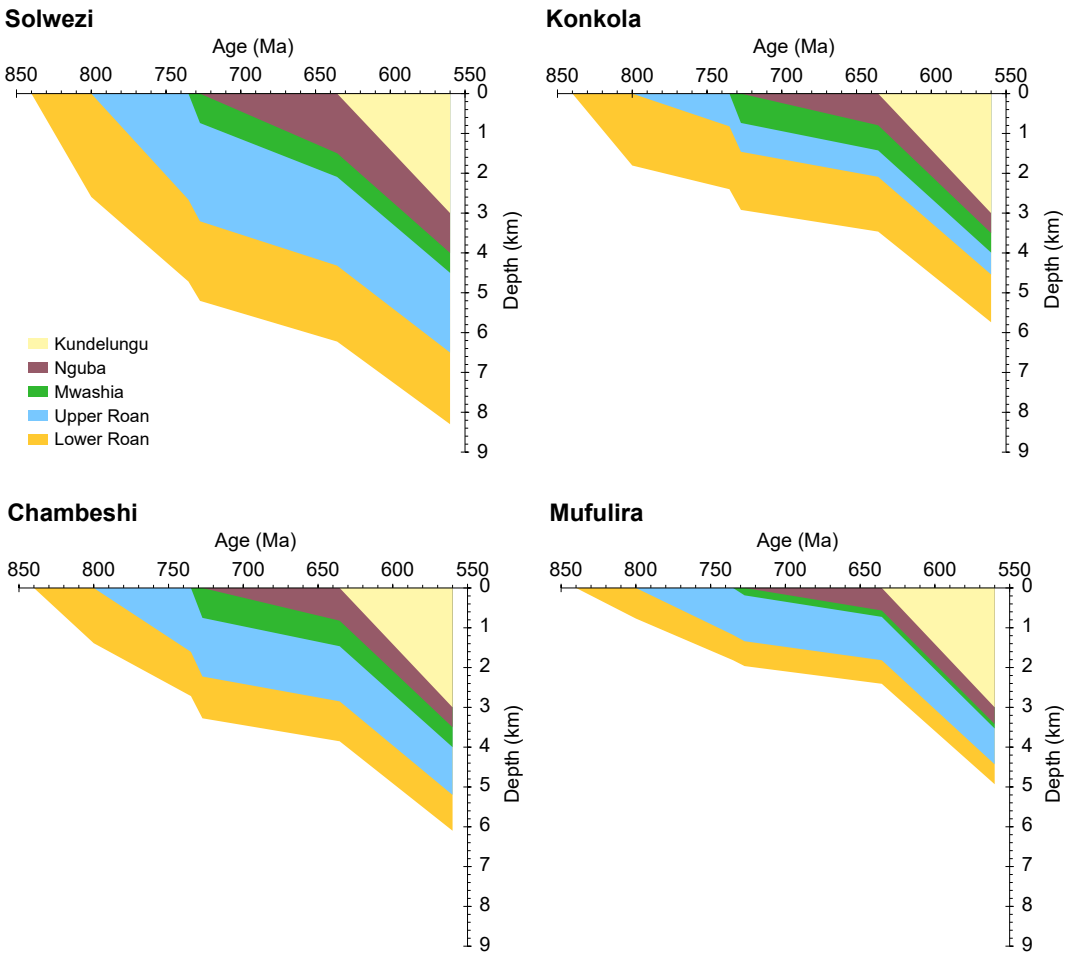

Figure 5.4: 1D burial histories for Solwezi, Konkola, Chambishi, and Mufulira.

induced a kink in the burial curve in Solwezi, Konkola, Chambishi and Chilonga.

Depositional thicknesses of the Nguba was likely highest in the Domes region, possibly reaching 1.5 km, and in Chilonga at ∼0.8 km, respectively. The Nguba was thinnest in Mansa and Lusale, with depositional thicknesses of < 0.5 km. Subsidence of the Nguba Group appears to have been more gradual than the Mwashia Group.

Kundelungu Group thicknesses are enigmatic. They likely exceed 100's m based on logged cores, but are based predominantly on > 2 km of material having been removed since the Miocene (Daly et al., 2020). It appears likely that subsidence rate increased significantly to accommodate ∼2-3 km of Kundelungu sediments. These basin-scale burial trends are shown in figure 5.6.

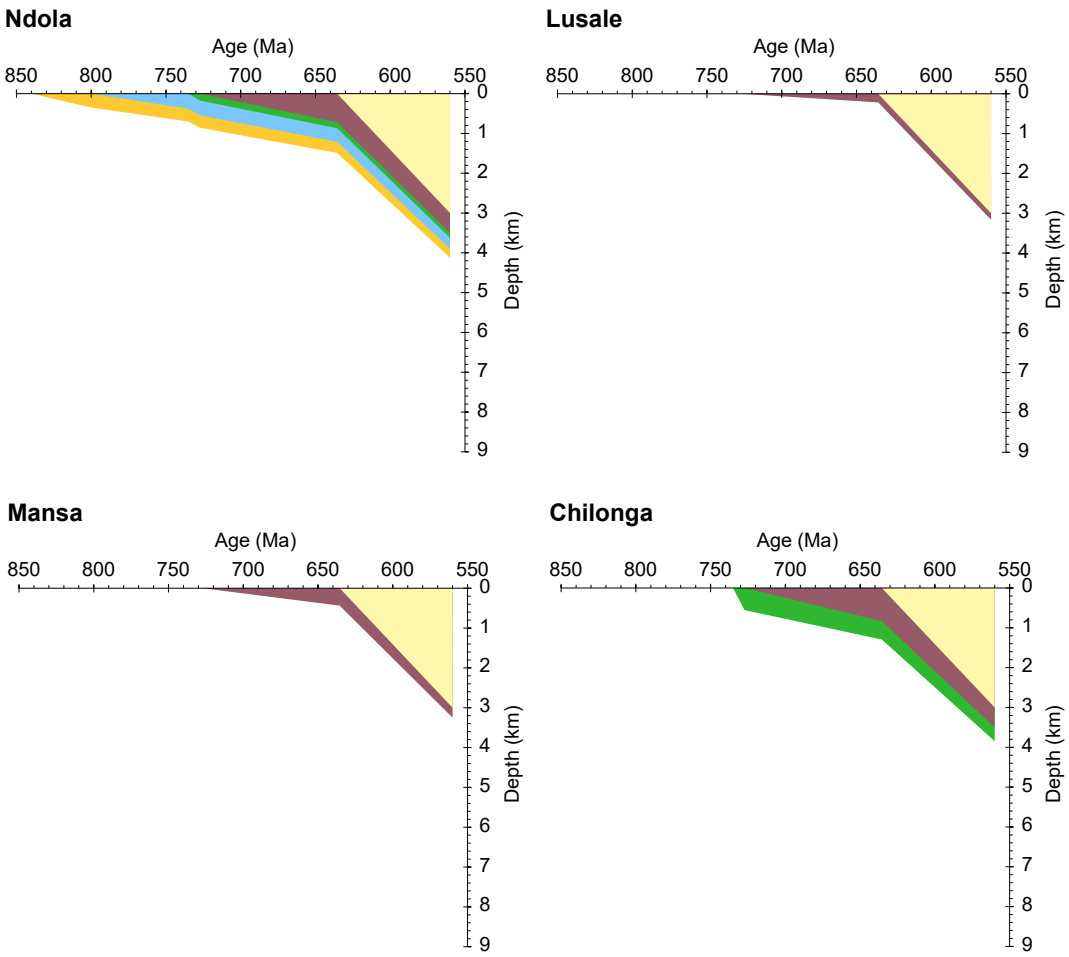

Figure 5.5: 1D burial histories for Ndola, Lusale, Mansa, and Chilonga.

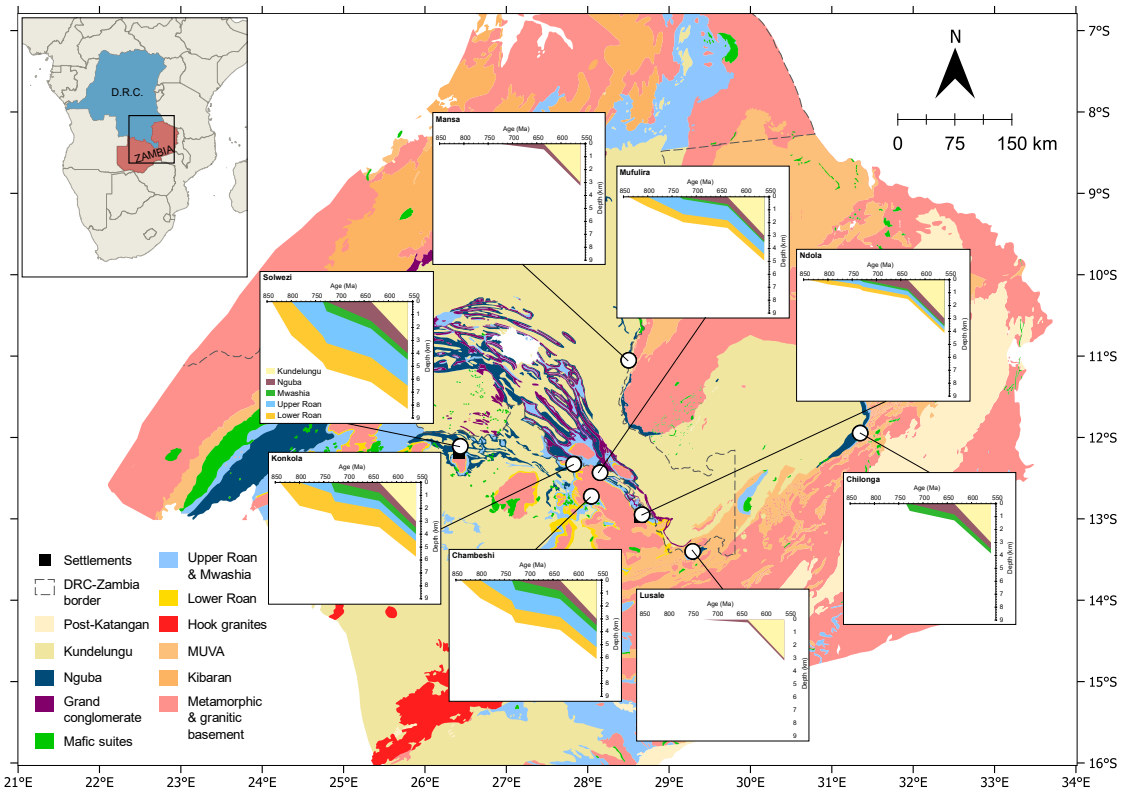

Figure 5.6: 1D burial histories across the Katangan basin, showing the basin deepening to the northwest, and in the eastern arm of the basin.

5.3.2 Backstripping and rift signatures

Backstripping results, supported by facies analysis, and within the restrictions of inadequate chronostratigraphic constraints, are consistent with rift tectonic subsidence profiles and provide the first quantification of subsidence in the Katangan basin (figs. 5.7, 5.8).

The Domes region and much of the Copperbelt show characteristic concave-up tectonic subsidence profiles during Roan subsidence. These are best-developed where the Lower Roan section is thickest: Solwezi, Konkola and Chambishi sub-basins, but are also present in Mufulira. Solwezi, Konkola and Chambishi show rapid Lower Roan subsidence. Slower Upper Roan subsidence is particularly evident in the Konkola and Chambishi. The tectonic subsidence profile in Ndola did not show clear evidence of Roan rifting, and resembled more prolonged and gradual cratonic subsidence. Solwezi shows significant depth uncertainty from the Mwashia onwards on account of uncertainties and assumptions in its type log.

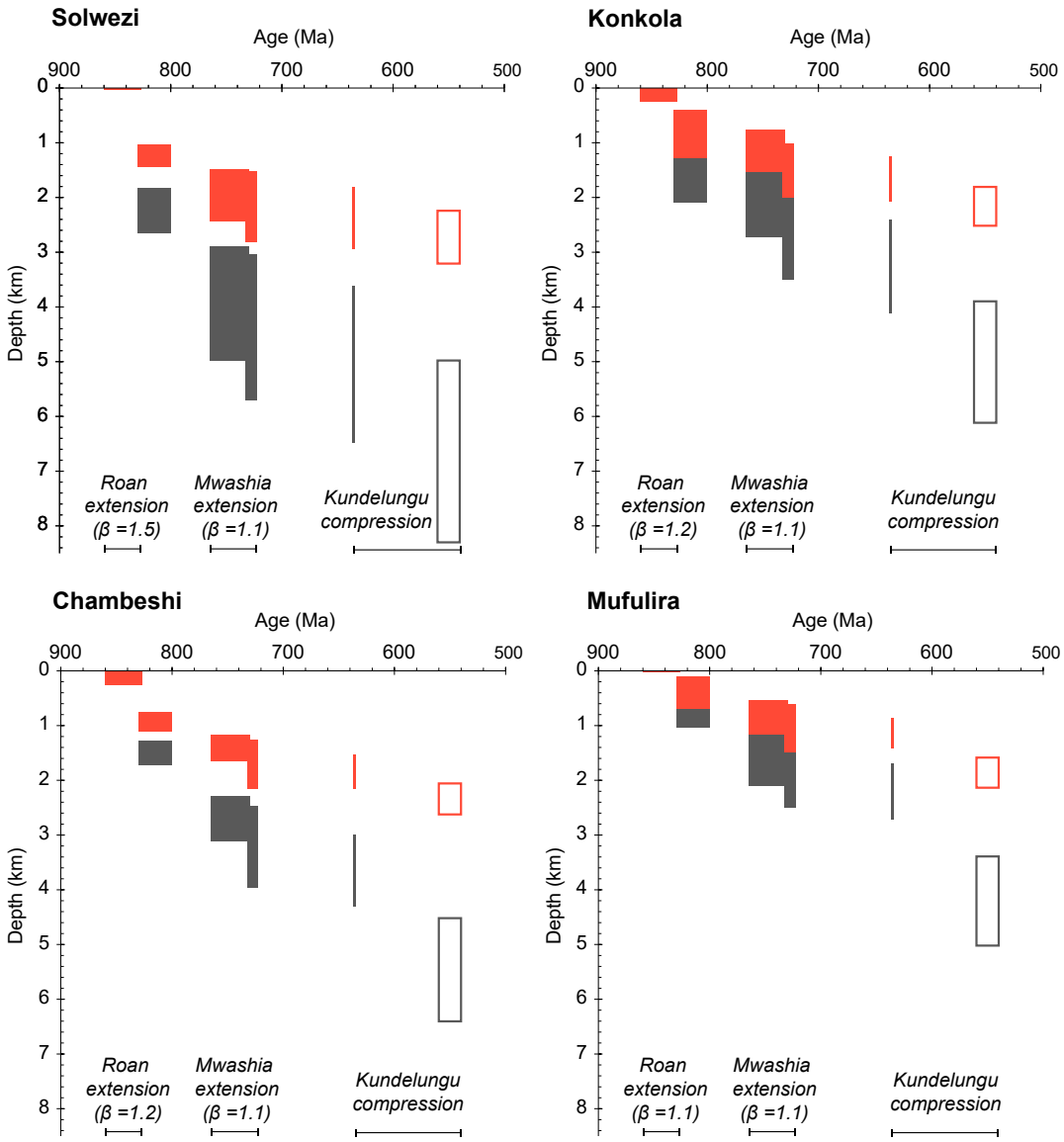

Figure 5.7: Tectonic subsidence profiles for Solwezi, Konkola, Chambishi, and Mufulira, showing clear Lower Roan, and less pronounced Mwashia, rift signatures. Red bars represent tectonic subsidence (area represents age and depth error), grey bars the water-loaded basement subsidence. Kundelungu subsidence bars are unfilled to indicate their uncertainty.

Mwashia tectonic subsidence was initially rapid in Solwezi, Konkola and Chambishi. Chilonga also shows a weak Mwashia rift signature, showing rapid Mwashia subsidence, which slows during Nguba times. Lusale and Mansa did not show clear rift signatures. Though not very pronounced, a sharp increase in Mwashia tectonic subsidence is evident across much of the basin, on account of facies showing pronounced deepening during this time. The Mwashia tectonic subsidence signature is therefore more sensitive to, and driven by, estimates of palaeobathymmetry.

Kundelungu subsidence has significant depth errors associated with uncertainties in depositional thickness across the basin.

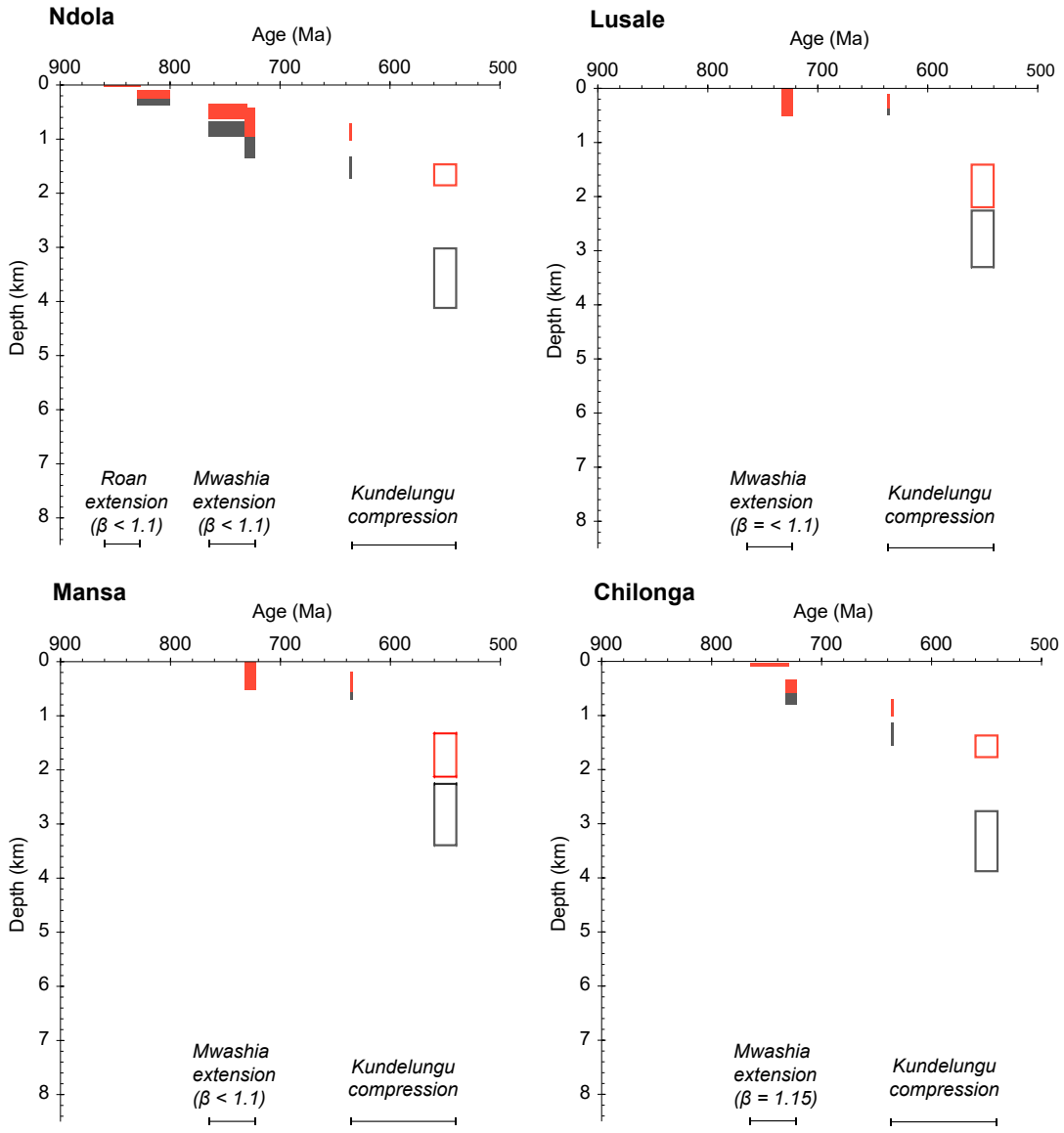

Figure 5.8: Tectonic subsidence profiles and for Ndola, Lusale, Mansa, and Chilonga. Chilonga shows a subtle rift subsidence profile. Red bars represent tectonic subsidence (area represents age and depth error), grey bars the water-loaded basement subsidence. Kundelungu subsidence bars are unfilled to indicate their uncertainty.

The uniform extension model is compatible with the backstripped subsidence profiles (figs. 5.9,5.10). The β-factor curves provide a satisfactory fit to tectonic subsidence curves in areas of the basin with a rift subsidence signature. β-factors for Lower Roan extension being highest in Solwezi (β = 1.4-1.5), moderate in Konkola and Chambishi (β = 1.2), and low in Mufulira (β = 1.1).

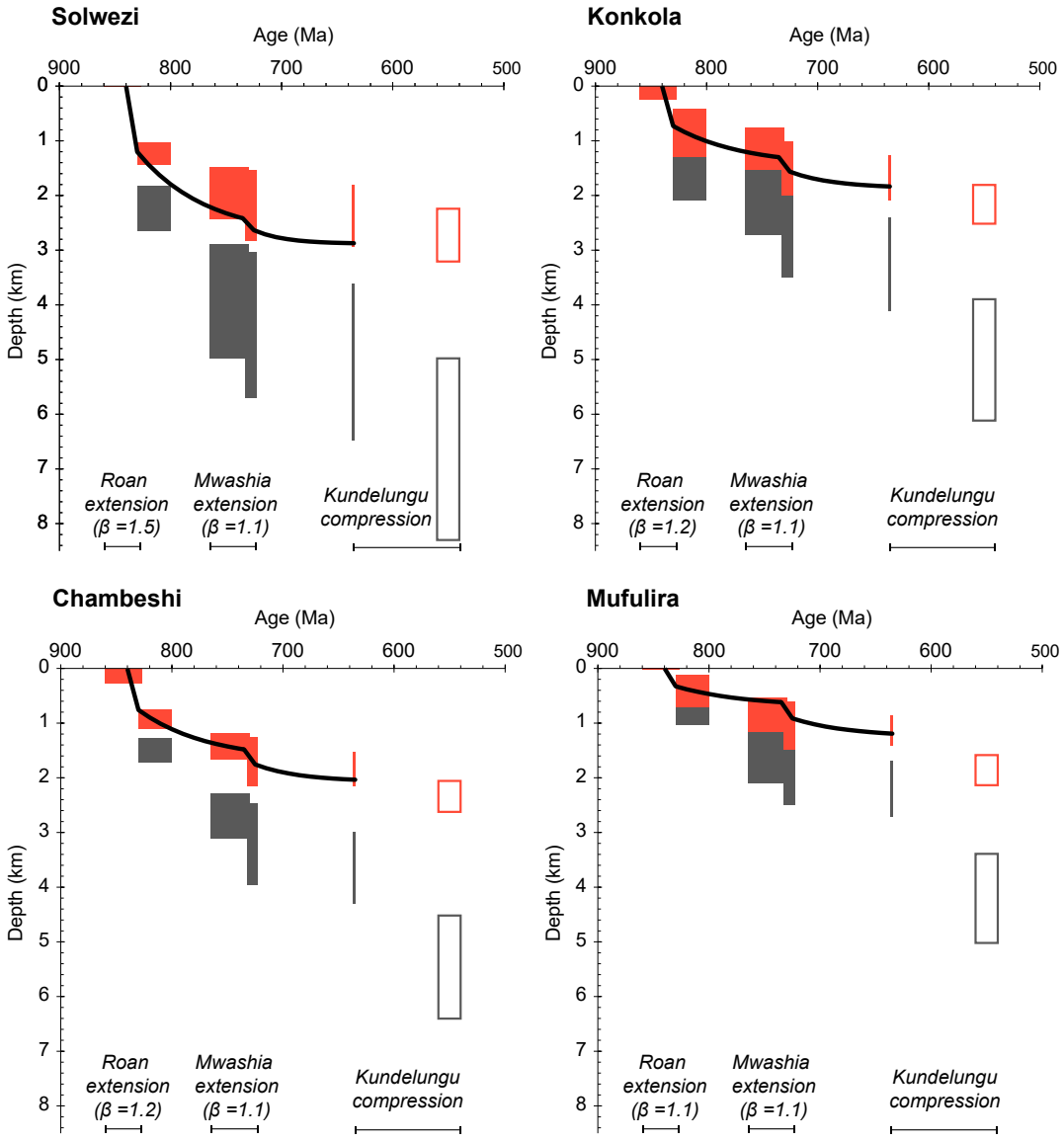

Figure 5.9: Tectonic subsidence profiles and β values for Solwezi, Konkola, Chambishi, and Mufulira. The black line represents the uniform extension model calibrated by tectonic subsidence constraints and stratigraphy, showing two phases of extension. Red bars show tectonic subsidence (area represents age and depth error), grey bars are water-loaded basement subsidence.

In Ndola, the uniform extension model over-estimated tectonic subsidence at a β-factor of 1.1, and did not match the backstripped tectonic subsidence, on account of the syn-rift (Lower Roan) thickness being too low. This further suggests that Ndola was not significantly affected by rifting, unlike the northern parts of the Copperbelt, and the Domes region.

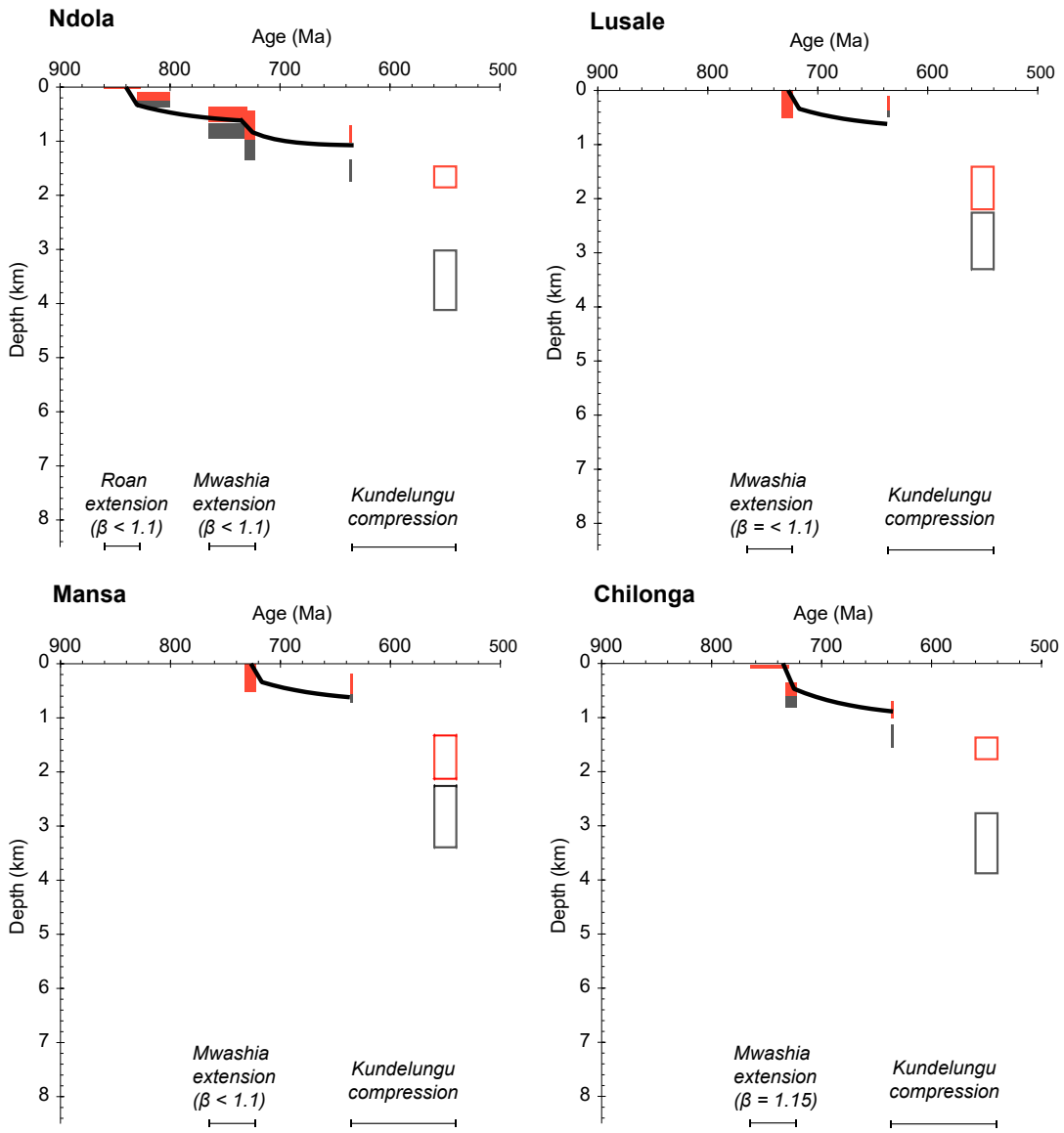

Figure 5.10: Tectonic subsidence profiles and β values for Ndola, Lusale, Mansa, and Chilonga. The black line represents the uniform extension model calibrated by tectonic subsidence constraints and stratigraphy. Only Chilonga shows a clear fit of the forward model with the backstripped tectonic subsidence. Red bars show tectonic subsidence (area represents age and depth error), grey bars are water-loaded basement subsidence.

The uniform extension model can also be applied to Mwashia subsidence, though the β-factors are significantly smaller. In Chilonga β-factors of 1.15 provide a good fit to the tectonic subsidence profile. The differences between Lower Roan and Mwashia rifting phases are shown in figure 5.11.

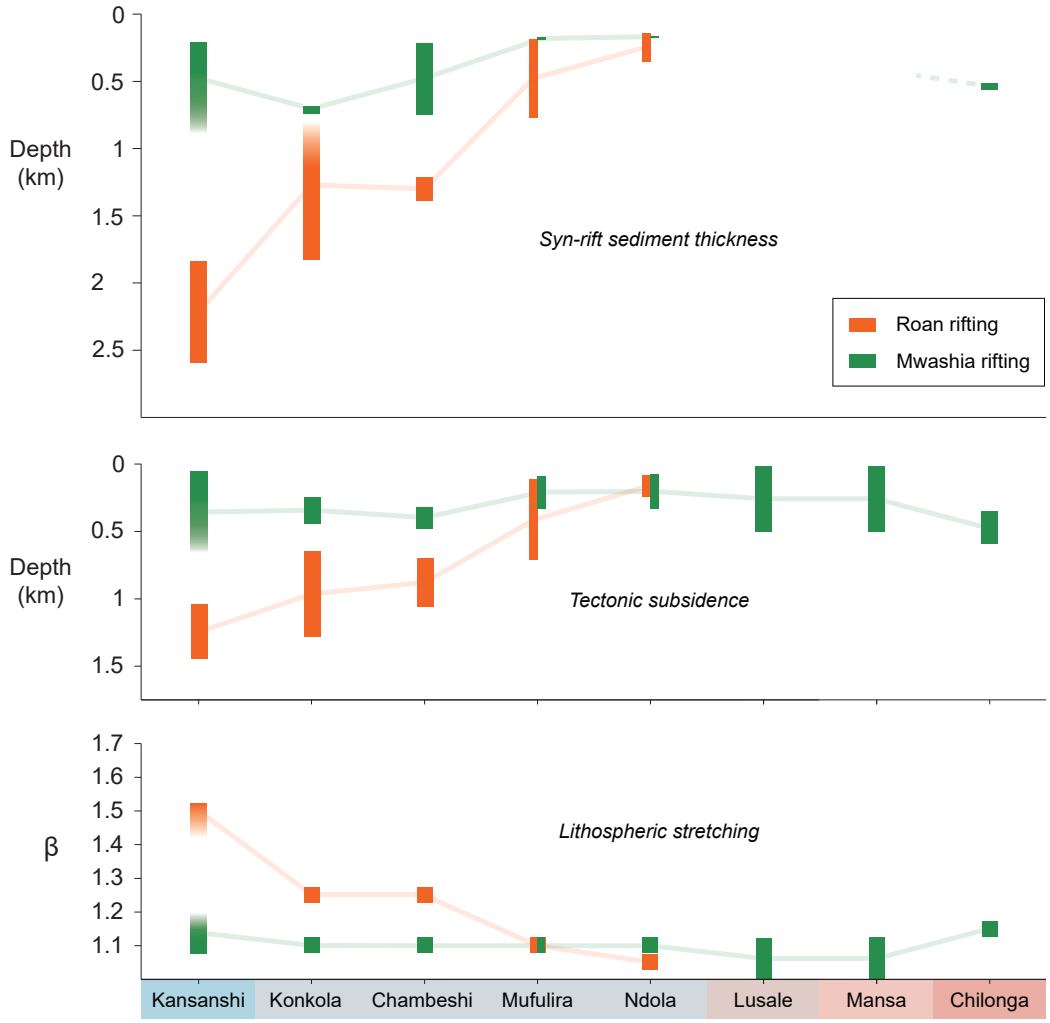

Figure 5.11: Partitioning of β-factors, tectonic subsidence and syn-rift sediment thickness into the two extensional phases in the Katangan basin. Mwashia rift signatures for syn-rift sediment thickness, tectonic subsidence, and lithospheric stretching are generally subdued.

Water-loaded basement subsidence shows similar trends, with the basin reaching maximum depths $>$ 2.5 km during the Lower Roan in Solwezi. Basin depth during the Lower Roan reduced towards the south-east, reaching $\sim$ 2 km in Konkola, 1 km in Mufulira, and $<$ 0.5 km in Ndola. The Mwashia represents a second, less pronounced, but laterally extensive phase of extension. A pronounced deepening of the basin is observed throughout the Domes region, Copperbelt, and to-

wards the easternmost part of the basin in Chilonga, with β factors of $\sim$1.1. This is with the exception of the SE margin of the Kafue anticline, where during Mwashia times tectonic subsidence again did not deviate significantly from a cratonic subsidence signature.

5.4 Discussion

Despite the limitations of 1D Airy backstripping and the assumptions underpinning the uniform extension model, quantitative subsidence analysis has significant implications for the formation and tectonic evolution of the Katangan basin.

The tectonic subsidence profiles, in conjunction with the basin's facies and structural architecture, are strong evidence of a rift origin for the Katangan basin. Forward modelling of lithospheric extension, informed by facies analysis and constrained by backstripping, provides β-factors of up to 1.5. These stretching factor match those of other rift systems (e.g. North Sea, Baikal rift, Oslo Graben) (Sclater and Christie, 1980; Barton and Wood, 1984; Huismans et al., 2001; Xie and Heller, 2009). Subsidence profiles, structural and stratigraphic evidence, as well as fit of the β-factor curves make rifting the most likely mechanism underpinning the formation of the Katangan basin.

Subsidence analysis generally supports the available stratigraphic evidence of the basin expanding during Mwashia rifting and stepping out over the initial Lower Roan Rift. Whereas the Lower Roan rift basin appears to have been extended throughout the Domes region and Zambian Copperbelt, Mwashia extension allowed the basin to expand westwards, resulting in significant magmatism along the Kibaran margin (Kampunzu et al., 2000; Key et al., 2001) and deep depocentres at Kamoa (Schmandt et al., 2013; Kennedy et al., 2019). The basin also extended towards the south and east, with Mwashia and Nguba deposition taking place in the Lusale sub-basin (Hendrickson et al., 2015), and near Chilonga. Between the two rift episodes, the Upper Roan and much of the Nguba are interpreted to have been accommodated via thermal relaxation of the lithosphere and represent periods of relative tectonic quiescence.

Crustal stretching in the Zambian part of the Katangan basin can be broadly subdivided into five domains (fig. 5.12. The Domes region experienced $\sim$65% lithospheric extension throughout the basin's extensional history (Lower Roan and Mwashia rifts). It forms the deepest known part of the basin, accommodating a pre-inversion stratigraphy likely in excess of 8 km thick. The Zam-

bian Copperbelt experienced moderate lithospheric extension (∼20 - 40%), reducing towards the south-east, with Ndola showing minimal lithospheric stretching. Lusale and Mansa similarly show negligible evidence for lithospheric extension. Chilonga forms part of the eastern arm of the basin, showing evidence for moderate (∼15%) lithospheric stretching.

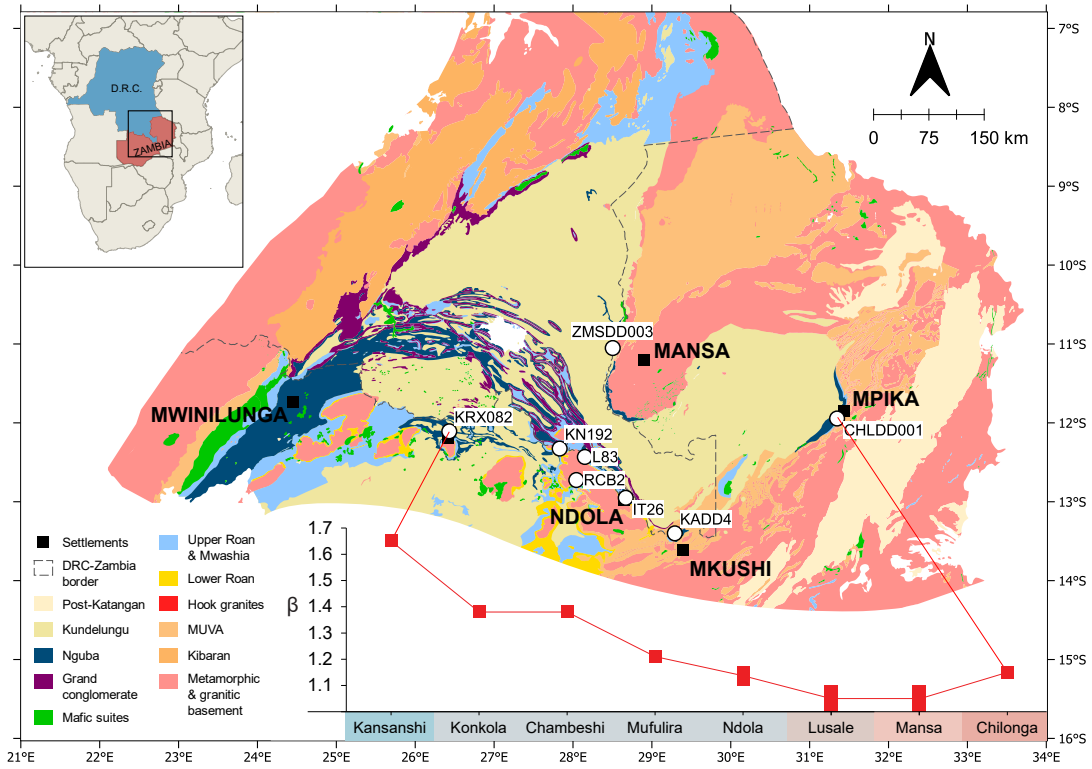

Figure 5.12: Cumulative stretching factor cross-section across the Katangan basin, showing highest stretching in the Domes region. The Zambian Copperbelt shows moderately stretched lithosphere, reducing towards the basin margins near Lusale and Mansa. Towards the eastern margin of the basin, the lithosphere was stretched again.

Lower Roan basin margins are interpreted to exist east of the Kafue anticline, on account of Ndola subsidence profiles not showing clear evidence for rift-related subsidence. Lusale and Mansa are interpreted to form basin margins to the North and South, with Chilonga likely forming a margin to the enigmatic eastern arm of the basin.

The great thicknesses of diamictites achieved in Kamoa suggest significant accommodation space generation during Mwashia and Nguba times, possibly indicating a shift in the locus of extension away from the initial Lower Roan rift. Part of the difference in thickness of Mwashia and Nguba sediments between Kamoa and the Zambian Copperbelt may be explained by sediment starvation.

However, the debris flow units (e.g. carbonate conglomerates) are thinner in the Zambian part of the basin, and suggest less submarine topography and less prolonged subsidence than was present around Nzilo.

The Mwashia rift signature may be subdued on account of palaeobathymetric error. Mwashia subsidence may be have been greater if the maximum water depth (500 m) is an underestimate. There is no reliable way at this stage to quantify the depth of slope deposits in the Katangan basin; if some were deposited at a maximum depth of 1000 m, then the Mwashia subsidence signature would be much more pronounced and β-factors higher.

An alternative explanation for the sharp increase in tectonic subsidence during the Mwashia would be a glaciation-induced eustatic fall. However, there is no clear evidence of a pre-Sturtian eustatic drawdown due to glaciation. The proposed magnitude of sea level rise induced by post-Sturtian de-glaciation of $\sim$500 m (Liu and Richard Peltier, 2013; Hoffman et al., 2017) are not clearly expressed in the Katangan stratigraphy either. Evidence for a eustatic fall is stronger for the Marinoan glaciation than the Sturtian on account of the SB4 erosional unconformity marking a lowstand underneath the Petit Conglomerat. However, the sea level rises invoked for post-Marinoan de-glaciation are even greater, with changes in freeboard of $\sim$1000 m (Liu and Richard Peltier, 2013). This is not evident in Katangan facies successions, even taking into account the low resolution of palaeobathymetric estimates from deep water facies. The SB4 is also not well-expressed across the basin, as would be expected of a $\sim$ 1000 m sea level fall caused by glaciation.

A paucity of chronological constraints hinder a more rigorous quantification of subsidence that takes into account eustatic fluctuation induced by widespread glaciation, as it is not clear where in the stratigraphic record glaciation-induced sea level fall started and stopped, nor where melt-induced sea level rise started and stopped, and to what extent they were diachronous. Despite the facies successions not supporting sea level changes of the magnitude invoked for 'Snowball Earth' events, widespread glacial deposits do exist in the Katangan, which would have likely affected sea level to some unknown degree. That being the case, it is deemed plausible that the Mwashia tectonic subsidence signature could be significantly underestimated by not taking into account sea level fall associated with Sturtian glaciation. Likewise, it is plausible that sea level fall during the Marinoan glaciation resulted in falling-stage or lowstand systems tracts.

Though the initial Lower Roan rift was mostly amagmatic – with the potential exception of the

Kafue rhyolites (Johnson et al., 2007) – it is possible that Mwashia extension triggered magmatism by overstretching the lithosphere that was pre-stretched by Lower Roan rifting. Assuming a moderately thick initial lithosphere ($<$ 140 km), stretching the lithosphere by 50% would likely have been insufficient in elevating the geotherm above the peridotite solidus to trigger melting. However, this does not explain why the most voluminous mafic suites occur in the western and eastern margins of the basin (Luawu (Kampunzu et al., 2000; Key et al., 2001), Mwinilunga and Chilonga, respectively) that were not affected by Roan extension. It can be postulated that Mwashia mafic suites occurring beyond the extent of the Lower Roan rift may have been controlled by pre-existing basement structure (Daly et al., 1989).

5.5 Conclusion

Quantitative subsidence analysis, informed by facies analysis, has shown beyond reasonable doubt that the Katangan basin is a rift basin. This is based on 1. tectonic subsidence profiles 2. facies and stratigraphic architecture 3. structure (Selley et al., 2005; Kennedy et al., 2019) 4. Mwashia magmatism (Kampunzu et al., 2000) and 5. fit of forward models using facies, stratigraphic and magmatic evidence as a priori constraints. Both inverse modelling and forward modelling show two distinct phases of extension during the Tonian, represented by the Lower Roan and Mwashia Groups. This lends significant weight to previous interpretations of the tectonostratigraphic evolution of the basin.

Tectonic subsidence signatures and β factors of $1.1 - 1.5$ match those of other known rift systems (Barton and Wood, 1984; Huismans et al., 2001; Xie and Heller, 2009).

The deepest part of the basin in the Domes region likely accommodated in excess of 8 km of Katangan stratigraphy prior to basin inversion, likely thinning to 2-3 km on the basin margins.

The Lower Roan represents a terrestrial rift, with significant extension of up to 50% in the more central parts of the basin. Mwashia rifting was mostly marine and less pronounced in Zambia, but still provided a measurable subsidence signature and resulting in renewed stretching of $\sim$10%. Mwashia extension is expressed better on the western and eastern margins of the basin in Zambia, and particularly well in Kamoa.

Upper Roan and Nguba Groups mostly represent periods of thermally driven subsidence between

the two rift episodes. Kundelungu subsidence remains enigmatic, mostly on account of missing sections and needs further study.

Eustatic fluctuations resulting from two widespread glaciations are very likely to have affected the basin's subsidence history, but quantifying the degree to which they did remains difficult.

The two-phase rift model presented here has implications for the tectonostratigraphic evolution of the basin, with extension exerting a primary control on structure, stratigraphic architecture, early basin heat flow, and development of hydrothermal systems in the basin.

Chapter 6

The mineralisation factor: remarks on quantifying mineralisation potential in sediment-hosted Cu systems

6.1 Introduction

The sediment-hosted Cu-system and its components has been described in detail by Hitzman et al. (2005, 2010). It relies on several key prerequisites for mineralisation, including: oxidised clastic sediments, a source of sulphur, sufficient fluid temperature, and a reductant.

From detailed facies analysis in the Katangan basin, it appears that thickness of oxidised siliciclastic successions, permeability, as well as reduction potential of horizons, play a clear role in mineralisation. Turbiditic siltstones (e.g. Lubambe) and diamictites (e.g. Fishtie (Hendrickson et al., 2015)) can have variable TOC (Ramli et al., 2021), and are not traditionally considered ideal reductants compared to, for example, shales (Raji et al., 2015). Nonetheless, argillites, siltstones, and diamictites across the Katangan basin are mineralised (Mendelsohn, 1961; Schmandt et al., 2013; Hendrickson et al., 2015). Likewise, mineralisation occurs above thin and thick basal clastic sections (e.g. Mufulira v.s. Kansanshi deposits), in units that vary in permeability (e.g. arenite, siltstone, argillite-hosted) (Mendelsohn, 1961; Tshiauka et al., 1995; McGowan et al., 2006)). Mineralisation does not appear to be restricted in time, occurring throughout the basin's history (Hitzman et al.,

2005; Selley et al., 2005; Schmandt et al., 2013; Muchez et al., 2015).

Of the sediment-hosted Cu-system components described by Hitzman et al. (2005), there does not appear to be one that exerts a primary control to the extent that it cannot be replaced by a favourable combination of all other components. The mineralising system in the Katangan therefore appears to have been able to compensate for individual components being sub-optimal (e.g. thin clastic source, low-quality reductant). A quantified measure of mineralisation potential needs to be able to cope with this variability by taking into account several components of the mineralising system and their ability to compensate for one another. As a crude first-order approximation of how to quantify the mineralising potential of a sediment interval, a mineralisation factor is tentatively proposed. This quantification is not a model per-se, merely an illustration of how problems concerning mineralisation potential in the basin may be approached using data from drill core.

6.2 Methodology

The mineralisation factor (m) is a dimensionless number describing the likelihood of mineralisation between a source layer and a reductant layer. The source and reductant form a simple one-dimensional two-layer system (fig. 6.1), where a less permeable reductant overlies a more permeable and oxidised Cu-source. It has the following components: source thickness (S), permeability of source (k_S), reduction potential of source (E_S), permeability of reductant (k_R), reduction potential of reductant (E_R) and heat flux (Q). This simplified framework assumes a closed hydrological cycle. On account of significant uncertainty regarding input parameters, a $\pm$ 10% error is applied to the final mineralisation factor. This particular framework clearly does not apply to more structurally-controlled deposits (e.g. Kansanshi (MacIntyre, 2019)), though the approach may be modified to take this into account.

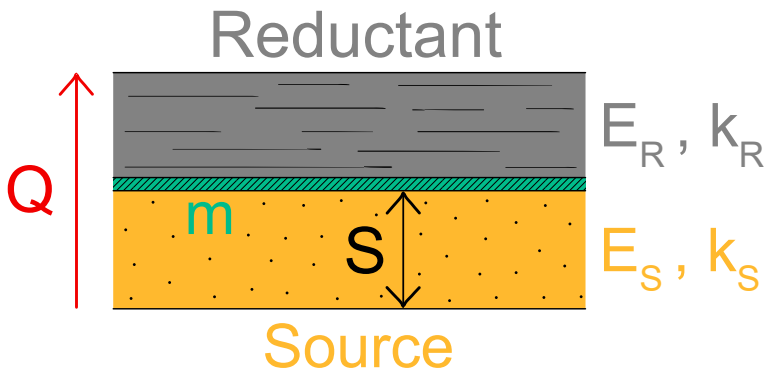

Figure 6.1: A schematic illustration of the components comprising the mineralisation factor (m) in green: a clastic source of thickness S, reduction potential (E_S), and permeability (k_S), underlying a reductant of reduction potential (E_R) and permeability (k_R). Both experience a heat flux (Q), which drives fluid convection.

Source

The copper source will comprise coarser, oxidised clastic successions. The thicker they are, the greater the source of copper is assumed to be. The source can be measured from core as the thickness of the siliciclastic succession (S) underlying a reductant, and in this framework must contain $<$15% mud.

Minimum threshold thicknesses are uncertain; for this work, 100 m is assumed to be a minimum thickness for mineralisation to take place, based on Lower Roan thicknesses across the traditional Zambian Copperbelt (Binda and Mulgrew, 1974; Binda, 1994).

Permeability values, though large in error, are based on empirical data from Freeze and Cherry (1979), and Allen and Allen (2013). Permeability ranges for sediments used herein are shown in table 6.1, rounded to the nearest power of ten. Glacial till is assumed to be lithologically indistinguishable from the diamictites (glacial or debris flow) in the Katangan, and for both to have comparable permeability ranges.

Reductant

The reductant layer is the site of mineralisation, where oxidised saline fluids precipitate their metal budget (Hitzman et al., 2005). Proportion of mudstone is suggested as a crude proxy for TOC, and hence reduction potential, in mudstones. This assumption is made on account of TOC tending to scale inversely with sand proportion in mixed sand-shale successions (Raji et al., 2015).

Lithology	Permeability (ms^{-2})
Gravel	10^{-7} – 10^{-10}
Clean sand	10^{-9} – 10^{-13}
Silty sand	10^{-10} – 10^{-14}
Silt, loess	10^{-12} – 10^{-16}
Limestone, dolomite	10^{-12} – 10^{-16}
Glacial till	10^{-13} – 10^{-19}
Shale, marine clay	10^{-16} – 10^{-20}

Table 6.1: Permeability of various lithologies, based on Freeze and Cherry (1979).

Mud is given as a percentage proportion in a given stratigraphic interval, and as a first-order approximation of reducing potential that is less cumbersome and more quickly applied than Eh/pH conditions based on mineral assemblages. Permeability values follow those in table 6.1.
The thickness of the reductant layer is not considered at this stage, nor are carbonate reductants. The latter is on account of it being less feasible to approximate TOC in carbonates in-core.

Redox and permeability gradients

The redox gradient between the source and mud-rich reductant is crudely quantified as the ratio of reducing potential of reductant to reducing potential of source (e.g. ratio of mud proportion in each unit). A sharp redox gradient is likely preferable for economic mineralisation. Reduced permeability of the reductant layer is likely conducive to mineralisation as it increases the residence time of mineralising fluid (Davey et al., 2020). The permeability contrast is given by the ratio of permeabilities in the reductant and source layer respectively. Both are expressed in log_{10} to reduce the range of permeability values, which often differ by several orders of magnitude.

Heat flow

Heat flow and thermal gradients exert a significant control on fluid flow in a basin (Yang et al., 2006). The McKenzie uniform extension model (McKenzie, 1978) provides a satisfactory first-order approximation of basin heat flux during rift evolution. It can be modified significantly to accommodate a more realistic set of parameters, but even in its original form serves as an adequate initial quantification for extension and heat flux. The magnitude of initial heat flux as a result of stretching by a factor of β is therefore interpreted to represent a key control on the mineralising system, driving fluid flow, as well as metal solubility (Hitzman et al., 2005).

Combining the above elements, for a given stratigraphic interval, between the top of the reductant and base of the source layer, the mineralisation factor is given as:

$$m = \frac{Q}{Q_\infty} + \frac{S}{S_{min}} + \frac{E_R}{E_S} + \frac{log_{10}k_R}{log_{10}k_S} \tag{6.1}$$

where

m: mineralisation factor (dimensionless)

Q: maximum syn-rift heat flux in Wm^{-2}

Q_∞: minimum post-rift heat flux in Wm^{-2}

S: present-day source thickness in m

E_R: reduction potential of reductant in % mud

E_S: reduction potential of source in % mud

k_R: permeability of reductant in m^{-2}

k_S: permeability of source in m^{-2}

The mineralisation factor calculated for type logs of five areas in the Katangan basin: Kamoa, Lubambe (based on core KN192), Chambishi (based on core RCB2), Ndola (based on core IT26), and Chilonga (based on core CHLDD001). In the case of Kamoa, a beta factor of 1.5 was assumed on account of syn-rift clastic thicknesses and parameters based on supplementary data from Kennedy et al. (2019) and Schmandt et al. (2013). The input parameters are shown in table 6.2, and results are shown in figure 6.2.

	Q_{max}	Q_∞	S	S_{min}	E_S	E_R	kS_{Smin}	kS_{max}	kR_{min}	kR_{max}
Kamoa*	0.045	0.03	1000	100	0.05	0.5	1.00E-10	1.00E-07	1.00E-19	1.00E-13
Lubambe	0.036	0.03	1000	100	0.05	0.6	1.00E-10	1.00E-07	1.00E-16	1.00E-12
Chambishi	0.036	0.03	600	100	0.05	0.6	1.00E-10	1.00E-07	1.00E-20	1.00E-16
Ndola	0.033	0.03	70	100	0.1	0.25	1.00E-10	1.00E-07	1.00E-20	1.00E-16
Chilonga	0.036	0.03	100	100	0.05	0.25	1.00E-13	1.00E-09	1.00E-14	1.00E-10

Table 6.2: Input parameters for the mineralisation factor, with maximum and minimum estimates given for permeabilities.

6.3 Results

The mineralisation factor allows for a gross ranking of mineralisation potential to be established, based on the assumptions outlined in the methodology.

Both the synthetic Kamoa section and Lubambe show the highest potential for mineralisation (m=23, 25, respectively) on account of a favourable combination of all model components: thick clastic source, high to moderate heat flow, moderate to high reductant quality, and sufficiently impermeable overlying reductants. Chambishi, shows similarly favourable, though not quite as elevated, potential (m=23) on account of the redox and permeability contrast between oxidised siliciclastics and reductants being sufficiently strong to partially overcome a signficicantly thinner Cu-source than is present in Kamoa or Lubambe.

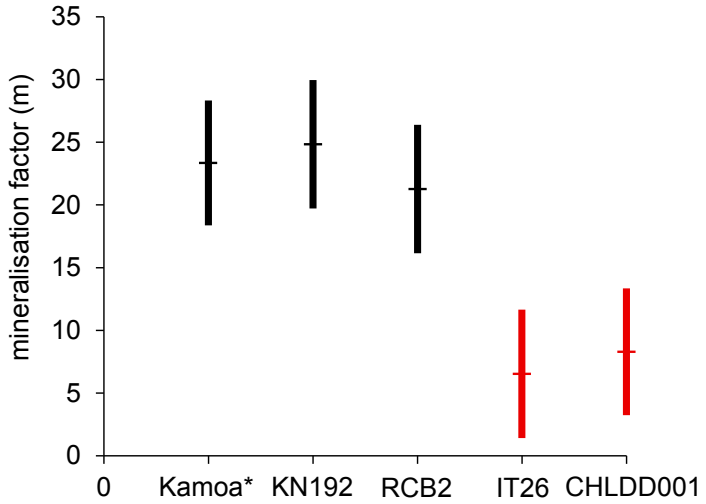

Figure 6.2: The mineralisation factor ranges for Kamoa, Lubambe (core KN192), Chambishi (core RCB2), Ndola (core IT26), and Chilonga (core CHLDD001). An arbitrary ± 5 uncertainty envelope is added to partially account for uncertainties in inputs. In this model, mineralisation appears most likely where $m > 15$.

In Ndola and Chilonga, smaller clastic source thickness appear to be major limitations to mineralisation potential. Chilonga has a marginally elevated mineralisation factor (m=8) on account of slightly higher redox and permeability contrasts between source and reductant.

Economic mineralisation appears more likely occur in areas where the mineralisation factor is greater than 15. Sub-economically mineralised cores in Ndola (IT26) and Chilonga (CHLDD001) both have mineralisation factors of less than 15.

6.4 Discussion

The model underpinning the mineralisation factor provides a simple framework that can provide a useful structure to begin to break down the mineral system into its key elements.

However, it clearly not represent the full complexity of any Cu-mineralising system. It is not indicative of volume or grade, and it being restricted to 1-D at this stage merely allows for first-order comparisons to be made between different parts of a basin.

Despite the simplicity of this approach, the method is effective at discriminating between areas of greater and lesser propensity for mudstone or shale-hosted mineralisation. Though there is insufficient data at this stage to constrain precise minimum thresholds for mineralisation, it is postulated that using this model a mineralisation factor of $\sim$15 is a possible minimum lower bound for mineralisation.

The framework would benefit from, and be of greater utility by, expanding it into 2- or 3-D, as well as incorporating aspects not considered herein.

Salinity likely exerts a significant control on copper mobilisation (Hitzman et al., 2010). Salinity will have varied depending on hydrological controls on the basin, availability of salt to dissolve, and time available to dissolve it. However, salinity estimates derived from fluid inclusions are deemed a sensible proxy that could easily be incorporated into the mineralisation factor framework. Salinity was likely significantly higher than the modern seawater average of $\sim$3,5 wt%, with some fluid inclusion studies suggesting salinities up to 39 wt% NaCl equivalent (Richards et al., 1988). A trend of fluid salinity increasing as a function of time was suggested by Selley et al. (2005). However, until a greater spatial and temporal resolution on fluid salinities in the Katangan basin is achieved, comparing past fluid salinities will remain a challenge..

The extent of fluid flow is equally difficult to constrain, but abundance of alteration across the basin, and widespread breccias suggest extensive fluid flow (Hitzman et al., 2005; Selley et al., 2005). Though the model currently assumes a closed hydrological system, the basin's hydrological architecture was likely very complex, varying as a function of time. The basement's contribution to available Cu-volume has likewise not been quantified, on account of limited data on basement Cu-

concentrations across the basin, but would represent another valuable term in the equation. Redox potential and and redox gradient between reductant and underlying source can be constrained using Eh/pH, based on observed mineralogy (Krumbein and Garrels, 1952; Hatch and Leventhal, 1992). However, Eh/pH diagrams assume equilibrium conditions for phase stability, and would require specific phase assemblages to constrain accurately. Quantification of redox potential and gradient using Eh/pH would be more accurate and rigorous, though potentially more cumbersome to quantify.

The assumption made in the model for the mineralisation factor is that organic-rich mudstones form the primary reductant, and hence mineralisation sites. However, carbonates can equally have elevated TOC (Al-Siyabi, 2005), and may explain why dolomitic units are frequently mineralised across the Zambian and Congolese Copperbelts (Mendelsohn, 1961; Eden, 1974; Selley et al., 2005).

The mineralisation factor is complemented by the proposed facies scheme which aids in understanding which facies and depositional environments are most amenable to high mud proportion and redox contrasts. When expanded into 2-D and 3-D, sequence stratigraphic correlations could help illuminate how the mineralisation factor changes spatially.

6.5 Conclusions

The proposed mineralisation factor provides satisfactory initial results to quantitatively rank the propensity for mineralisation in mud- or shale-hosted units, based on five locations in the Katangan basin. Mineralisation factors in excess of 15 appear in highly mineralised parts of the basin, whereas parts of the basin where mineralisation is sub-economic or absent have mineralisation factors less than 15. Further work is needed to quantify minimum thresholds for each variable, and a minimum threshold for m, which for now is postulated to lie at $\sim$15.

The approach does not intend to me an accurate model of the sediment-hosted Cu system, rather an approach that can be used and modified to help guide exploration efforts. It does so by encouraging an approach that breaks down a complex mineralising system into key elements that can be quantified, and targeted individually. By reducing the emphasis on individual components of mineral

system, and instead considering it as a sum of its parts, it takes a more holistic view of the mineral system.

Though 1-D at this stage, the spatial distribution of heat flow, redox contrasts, Cu source, salinity, etc. can be illuminated using the basin analysis techniques applied in the previous chapters. Combined with the proposed facies scheme, sequence stratigraphic frameworks, and subsidence history of the basin, the mineralisation factor could form part of an exploration toolkit that takes advantage of a mineral systems approach to complement existing detection-based exploration methods.

Chapter 7

Discussion

7.1 A dynamic stratigraphic perspective of the Katangan basin

A dynamic stratigraphic approach emphasises the role that genetic processes play at a range of spatio-temporal scales, to generate an understanding of basin fill. It synthesises sedimentology, sequence stratigraphy, chronostratigraphy, sediment routing systems, and places them in the context of basin subsidence, tectonic and climatic setting throughout a basin's history (Allen and Allen, 2013; Miall, 2022).

In contrast to 'layer cake' models of Katangan stratigraphy, which rely heavily on lithostratigraphy, the facies scheme, sequence stratigraphic correlations, and subsidence history presented here can be combined to generate a more holistic view of the Katangan basin's tectonostratigraphic evolution.

The interpretations presented in the following sections are based predominantly on the synchronous Lower Roan Kafue rift model, on account of this model being based on higher-confidence surfaces than the model involving diachronous rifting across the traditional Zambian Copperbelt.

7.1.1 Lower Roan Group

The basal portions of the Lower Roan Group (e.g. Mindola clastics along the Kafue anticline) are interpreted to record the onset of terrestrial rifting in the Katangan basin after 883 $\pm$ 10 Ma. Though the exact onset of deposition is not known, and it was likely diachronous across the basin, it is inferred to have taken place $\sim$ 840 Ma, on account of the Nchanga granite having to be exhumed,

prior to Lower Roan sedimentation commencing. Poorly constrained detrital U-Pb and Rb-Sr age dates support a ∼ 840 Ma onset of deposition date, though these are treated with caution on account of large errors and small sample sizes (Cahen et al., 1970; Selley et al., 2018).

Based on regional geophysical surveys, structure, thickness of syn-rift fill, and stretching factors, the deepest parts of the Lower Roan terrestrial rift basin is interpreted to have extended along an arcuate central rift south of the current Domes region in Zambia (fig. 7.1) (Daly et al., 2024). This narrow, deep ($>$ 2.5 km at time of deposition), highly extended ($\beta >$1.5) rift zone was flanked by an extensive array of graben and half-graben structures (Selley et al., 2005; Williams and Nisbet, 2017; Selley et al., 2018) showing moderate stretching ($\beta <$ 1.5), extending to the margins of the Congo craton and eastern Kafue anticline. The Lower Roan syn-rift clastic sequence is interpreted to represent part of the 'stretching' tectonic sequence after (Chenin et al., 2022), based on β factors ($\leq$ 1.5). Lithospheric necking was likely not achieved, though this is not excluded to the SE (Porada and Berhorst, 2000; John et al., 2003). The central rift and much of the Domes region is interpreted to represent the 'stretching' domain, with much of the Kafue anticline and classical Congolese Copperbelt (excluding Kamoa) forming part of the 'proximal' stretching domain (Chenin et al., 2022). Syn-rift heatflow is therefore interpreted to have been highest near the deep central rift, becoming exponentially lower toward the basin margins.

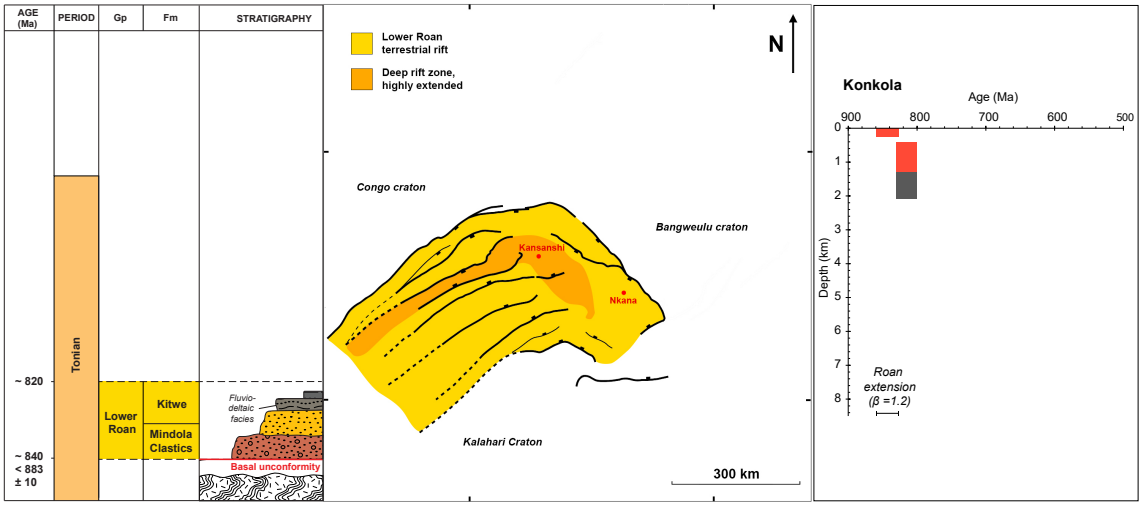

Figure 7.1: Palaeogeographic reconstruction of early-mid Lower Roan time, showing major normal faults (centre panel); chronostratigraphy and general stratigraphic trends (left panel); backstripped subsidence plot, using the Konkola type section as an illustrative example (right panel). Modified after Daly et al., (2024). The highly extended central rift zone is shown in orange against a backdrop of terrestrial Lower Roan deposition in yellow.

The KRX082 core in Solwezi stands out as being the deepest known drill core in the Zambian part of the Katangan basin, intersecting the thickest known succession of Lower Roan Group sediments in Zambia. The Lower Roan succession comprises continuously stacked aggradational siliciclastic successions in excess of 1.3 km thick, without the core reaching basement. $>$ 400 m of coarser siliciclastics are inferred between the end of the drill hole and the basement, by comparison to similar fluvial facies successions in RCB2, and paucity of coarser, conglomeratic facies at the base of the core. Such thicknesses of immature siliciclastic facies indicate greater accommodation space generation and sediment supply than has been observed anywhere else in the classical Copperbelt.

The conglomeratic $\rightarrow$ sandy $\rightarrow$ silty facies successions that fine upwards over 100's m known from the traditional Zambian Copperbelt (Mendelsohn, 1961; Eden, 1974; Binda and Mulgrew, 1974; Sweeney et al., 1986) are not evident in Solwezi, despite the Lower Roan Group's thickness in that location.

It is suggested that siliciclastic sediment supply, likely in the form of fluvial braidplain systems, was sufficiently high in Solwezi to balance significant basin subsidence (A $<$ S or A=S), with the Solwezi rift possibly representing an overfilled basin. Fairly monotonous, aggradational sandstone successions are characteristic of overfilled basins, where accommodation space is filled regardless of subsidence rate or degree of fault block rotation (Nottvedt et al., 1995). Though protracted rifting could also explain the thickness of siliciclastic facies, the lack of facies variation, and highly amplified aggradational successions, indicate that regardless of the rate or duration of accommodation space generation, sediment supply was sufficiently high to prevent significant lateral facies shifts. Conversely, the greater frequency of facies juxtaposition (in the order of 10's - 100's m), and variety of depositional settings (e.g. talus $\rightarrow$ fluvial $\rightarrow$ fan-delta/delta) in the traditional Copperbelt suggest that variation in sediment supply possibly exerted a greater control than in Solwezi, generating more pronounced low-order cyclicity in the transgressive and highstand systems tracts of the syn-rift succession.

The stratigraphic and subsidence data, combined with structural data from Daly et al. (2024) presented here provide an alternative to Selley at al.'s (2018) interpretation of the Katangan basin's evolution, which placed the 'depocentre maximum' in the D.R.C., west of Shinkolobwe. Few Lower Roan time-equivalent strata, e.g. Musonoi and Mines sub-Groups (Cailteux and De Put-

ter, 2019), are known to be exposed in the D.R.C., and their depositional thickness is difficult to determine, whereas in Solwezi and Konkola sub-basin Lower Roan thicknesses reach $>$ 1.3 km and $\sim$ 1 km, respectively.

The thickness of basal siliciclastics equivalent to the Lower Roan in the D.R.C. are estimates based on gravity inversion, and Gecamines 1:20,000 map sets (Selley et al., 2018). The gravity data permitting $>$ 3 km of compacted syn-rift fill assume thick sedimentary successions driving observed gravity anomalies instead of significant breccia volumes, or basement being near-surface. The low-density gravity signatures observed north of the 'Tenke window' could instead be attributable to breccias or basement being near-surface, as the basement inliers in the Zambian part of the basin show as strongly negative gravity anomalies. The apparent thickening of stratigraphy based on Gecamines maps could alternatively be accounted for by repetition of stratigraphy as a result of salt withdrawal-induced fault block rotation. This leaves open the possibility of the Congolese Copperbelt forming part of a stretched margin of the basin along-strike of the moderately extended (β 1.2) Zambian Copperbelt, instead of a central rift. The thick lower Roan succession observed in core KRX082 in Solwezi onlaps onto the Solwezi Dome to the South, and is also present on the southern margin of the Solwezi Dome. This suggests a basin south of the Domes region, now inverted along the most metamorphosed part of the basin, where the lithosphere was the most stretched and weakest. Basin inversion along the weakest portion of the crust south of the Domes region is interpreted to have caused the sheet of thrusted nappes to be emplaced in Solwezi, evident in core KRX082.

7.1.2 Upper Roan Group

The timing of the onset of Upper Roan deposition is not known, but can be cautiously approximated to commence 10 - 20 Myr after the onset of Lower Roan deposition, as the Upper Roan stratigraphy and structure indicate thermal subsidence taking over as the dominant subsidence mechanism following initial Lower Roan rifting (Veevers, 1981; Selley et al., 2005). During this time, basin subsidence began to exponentially reduce, with the basement in the traditional Zambian Copperbelt reaching depths of $\sim$2 - 3 km.

With Lower Roan fault networks shutting off, wide paralic zones prograded across Lower Roan structural highs as part of a lowstand systems tract, with siliciclastic sediment sources becoming more distal and topography flattening. This is evidenced by an abrupt switch from siliciclastic to

carbonate-dominated facies across much of the traditional Copperbelt, with mixed clastic-carbonate facies reducing in frequency and grain size upwards. This indicates the development shallow-dipping basin, with widening facies belts, covered by what is interpreted to be a large epicontinental sea. It is inferred that deeper water conditions prevailed along the central rift zone south of the domes (fig. 7.2).

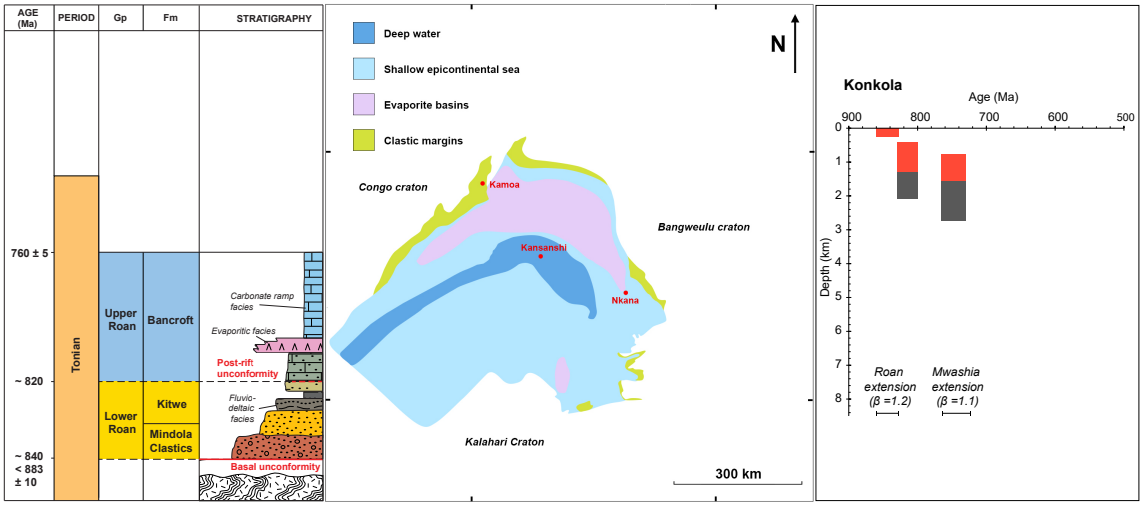

Figure 7.2: Palaeogeographic reconstruction of Upper Roan time, showing an extensive epicontinental sea and evaporitic basins covering the Lower Roan rift fill and onlapping basement as the basin thermally subsides (centre panel); chronostratigraphy and general stratigraphic trends (left panel); backstripped subsidence plot, using the Konkola type section as an illustrative example (right panel). Modified after Daly et al., (2024).

The apparent absence of prograding sandy facies across the Kafue anticline that could generate an erosional post-rift unconformity as part of the Upper Roan LST in the logged cores can be explained in several ways. The first is that the siliciclastic sources shifted sufficiently far toward the basin margins as the basin widened during the post-rift phase to not result in progradational terrestrial successions being recorded along much of the Kafue anticline. Paralic successions observed across the classical Zambian Copperbelt could therefore represent more basinal expressions of marginal fluvial systems, possibly forming a correlative conformity (Catuneanu et al., 2009). Additionally, if accommodation space generation exceeded sediment supply (either eustatically or tectonically), and sediment supply was restricted due to aridity (Selley et al., 2005; Hitzman et al., 2010), a clear basinward facies shift may be less well-developed, obscured, or absent (Bosence, 1998).

A combination of climate-change-induced reconfiguration of drainage networks and the basin widen-

ing is deemed the most plausible cause for the post-rift unconformity, SB2, not being well-developed across the Kafue anticline. This is based on abundant evidence for aridity, and stratigraphic evidence for the Upper Roan representing the post-rift phase following Lower Roan extension. The onset of arid conditions across much of the Katangan basin could possibly be used as a climate-based correlation surface that may warrant consideration given the paucity of chronological constraints in the Upper Roan (Glennie and Singhvi, 2002).

With the basin transitioning to flexure-driven thermal subsidence, the Upper Roan transgressive systems tract likely resulted in onlapping of marginal clastic facies onto the basin margins.

In the Congolese Copperbelt, the units equivalent in time to the Upper Roan (i.e. Fungurume sub-Group) appear to record a similar transition to more low-energy, carbonate-dominated deposition, interpreted as likely shallow marine and lagoonal sediments (Cailteux et al., 1994; Cailteux and De Putter, 2019; Mambwe et al., 2020). In both the Zambian and Congolese Copperbelts, the transgressive systems tract overlies the evaporite-carbonate successions of the Upper Roan, i.e Fungurume sub-Group (Mambwe et al., 2020).

Widespread evaporite and salt basins developed during the period of thermal subsidence, extending predominantly across the Congolese Copperbelt, and reducing towards the south-east across the Kafue anticline. The significant evaporite accumulations, likely in the order of 100's m (Selley et al., 2018), particularly in the Congolese part of the basin, suggests a prolonged phase of periodic restriction and evaporite deposition. This is inferred to be predominantly eustatically driven on account of reduced fault control on accommodation space generation. Though sabkhas were widespread and laterally extensive, they were likely not the source of the volumes of salt invoked in the basin, and indicate that deep salt basins must have existed throughout much of the Katangan basin during the Upper Roan (De Magnée and Francois, 1988; Jackson and Warin, 2003; Selley et al., 2018).

7.1.3 Mwashia Group

The timing of the onset of deposition of the Mwashia Group across the basin is not known, but has traditionally been broadly constrained by the ages of mafic suites to 765 $\pm$5 Ma - 735 $\pm$5 Ma (Key et al., 2001).

The Mwashia records renewed extension along major crustal fault systems that extend broadly lin-

early SW-NE along the margins of the Congo and Bangweulu craton (Daly et al., 2024). Though it is unclear to what extent Lower Roan faults were reactivated, the abundance of interpreted debris flow facies across the Kafue anticline suggest that Lower Roan fault networks were at least partially involved in generating new (sub-aqueous) topography and accommodation space during the Mwashia and early Nguba times. This is supported by the reintroduction of coarser siliciclastic facies above the carbonate-dominated Upper Roan successions.

The sub-parallel geometry of the main SE-NW-trending Mwashia fault systems on the western and eastern side of the Bangweulu craton, compared to the arcuate geometry of the Lower Roan rift, indicates a switch in extension polarity between the two rift phases, shown in fig. 7.3 (Key et al., 2001) (Daly et al., 2024). Such diachronous rifting has been invoked in the South China Sea (Ru and Pigott, 1986) and rift basins of Sudan (Schull, 1988), albeit at shorter timescales. Across much of the classical Zambian Copperbelt, the Mwashia Group represents a significant deepening and is delineated by a maximum flooding surface at its base. The increase in water depth results in a clear increase in the backstripped tectonic subsidence, though uncertainties in palaeo-bathymetry limit precise quantification of its magnitude. Additional stretching appears relatively minor ($\beta < 1.2$), but is again limited by uncertainty in palaeobathymetric estimates, possibly being an underestimate. Resumption of fault-control on stratigraphy appears to have resulted in rift-axial deepening, evidenced by debris flow facies in the Zambian Copperbelt, as well as basin widening, evidenced by coarse terrestrial siliciclastic successions observed in Kamoa as the 'Poudinge' (Schmandt et al., 2013; Kennedy et al., 2019), Chilonga, and Lusale. The basin expanding northwards is evidenced by Mwashia-age lavas, and diamictites occurring at Kibambale and Makonga (Master and Wendorff, 2011). Approximately E-W to SE-NW extension is inferred from the orientation of major crustal faults and N-S orientations of feeder dikes (Key et al., 2001). The Mwashia maximum flooding surface likely coincided with clastic sediment-starvation in more central parts of the basin, on account of clastic sources becoming more distal as part of a significant retrogradational facies shift stepping-out over the initial Roan basin.

Though generally more carbonate-rich, facies successions in the Mufufya syncline east of Fungurume in the D.R.C. show similar deepening into interpreted 4th-order maximum flooding surfaces in the Kansuki and Kamoya formations, forming part of an interpreted platform margin and barrier

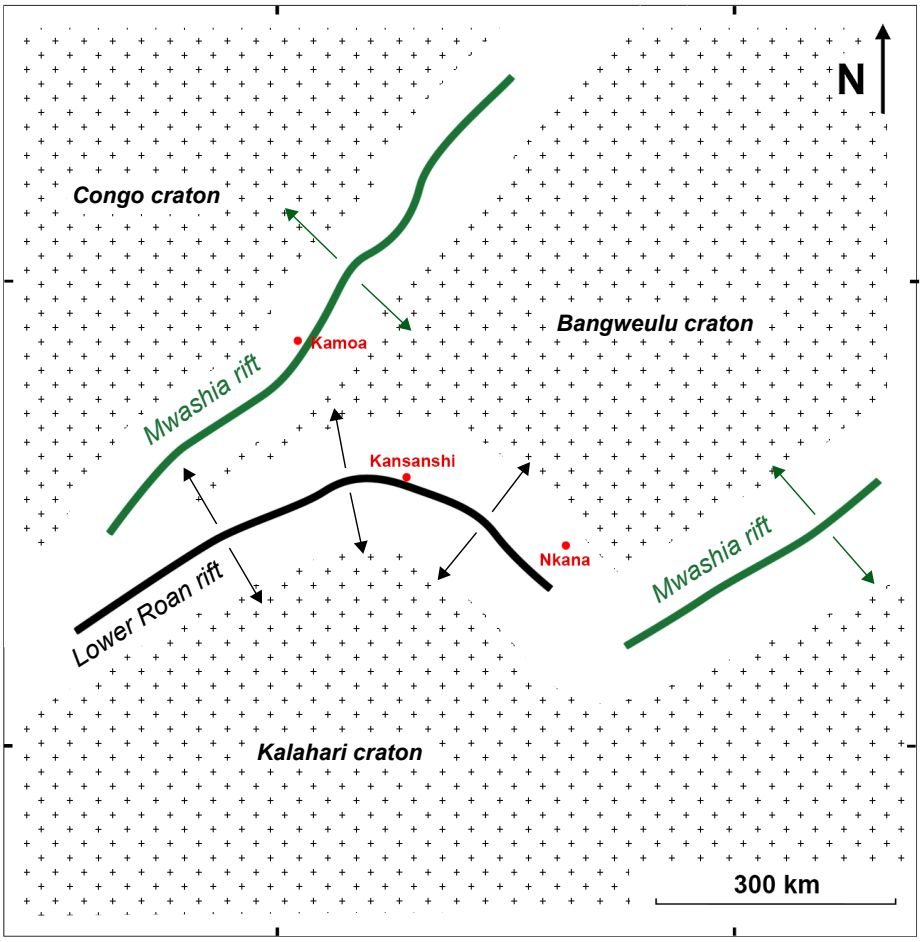

Figure 7.3: Tentative and simplified reconstruction of the two generations of rift systems forming the Katangan basin along the margins of the Congo, Bangweulu and Kalahari cratons: an arcuate Lower Roan rift, and a ∼ SE-NW trending sub-parallel Mwashia rifts. The Bangweulu craton underlying the traditional Zambian and Congolese Copperbelts is based on Bangweulu-age (∼1.8 Ga) basement extending from the Kafue anticline westwards across the Domes region to the Kabompo Dome (De Waele, Liégeois, Nemchin and Tembo, 2006). Modified after Daly et al. (2024).

shoals, respectively (Mambwe et al., 2020). However, the lack of independent chronological constraints, and uncertainty regarding the hierarchy (likely 2nd - 3rd order) of the Mwashia MFS2 in the Zambian Copperbelt, makes correlation of maximum flooding surfaces across the Zambian and Congolese Copperbelts difficult. Despite the Mwashia deepening being interpreted to be broadly coeval with magmatism, the precise timing of the deepening and MFS2 deposition with respect to mafic emplacement is unclear.

Extensive magmatism on the western margin of the basin (Key et al., 2001; Kennedy et al., 2019), in the eastern arm near Chilonga, and abundant low-volume intrusives across the Zambian and

Congolese Copperbelts (Mendelsohn, 1961; Lefebvre, 1975; Kampunzu et al., 1991; Binda, 1994) indicate that the second phase of rifting in the basin was magmatic. The Lwawu lavas in the western basin margin appear to have significant older dates $\sim$765 $\pm$5 Ma, with the oldest dated sample having an age of 784 $\pm$ 10 Ma, than the Luamata breccia ages (Key et al., 2001). The Luamata breccia and intrusive dates are significantly younger at $\sim$735 $\pm$ 5 Ma, with the youngest dated sample having an age of 707 $\pm$ 16 Ma (Key et al., 2001). This could suggest multiple episodes of both intrusive and extrusive magmatism over a prolonged period of reactivated extension in the Katangan basin, with the primary locus of extension shifting westwards towards the margins of the Congo craton, and the eastern arm of the basin opening broadly contemporaneously.

7.1.4 Nguba

The Nguba Group has traditionally been lithostratigraphically separated from the Mwashia Group by the first diamictite unit (i.e. Grand Conglomerat). Assuming the diamictite units were broadly synchronously deposited, the timing of onset of Grand Conglomerat deposition is constrained by mafic bodies to $<$735 Ma (Key et al., 2001), and by Re-Os dates in upper Mwashia shales to $<$727 Ma (Rooney et al., 2015). On account of these ages and evidence for glaciation (Stutzer, 1911; **?**; Wendorff and Key, 2009; Master and Wendorff, 2011), the Grand Conglomerat is associated with the Sturtian glaciation, despite the ages not clearly overlapping with globally accepted age ranges for the Sturtian glaciation at $\sim$717 - 660 Ma (Halverson et al., 2020).

Thick diamictite successions ($>$ 1.5 km) in Kamoa have been interpreted as debris flows (Kennedy et al., 2019), which supports the interpretation presented herein of many Nguba diamictites in Zambia likely being of debris flow origin. Taking into account the probability of at least some of the diamictite units being diachronous, either through ice-sheets not depositing glaciogenic diamictites synchronously, or not all debris flows being deposited synchronously, then distinguishing the upper parts of the Mwashia Group from the lower parts of the Nguba becomes more difficult, again due to limited independent chronostratigraphic constraints and broad range of Sturtian glaciation (Hoffman et al., 2017; Halverson et al., 2020).

The interpretation favoured here is that the Grand Conglomerat represents a period in the basin's history, possibly spanning 10's Myr, rather than a synchronous surface. It represents a phase of renewed tectonic control on basin fill, partially overlapping with the end of Mwashia magmatism,

and coinciding with widespread glaciation (Kampunzu et al., 2000; Eyles and Januszczak, 2004; McGee et al., 2012; Kennedy et al., 2019). These processes possibly interacted with each other, e.g. in the form of glacially derived debris flows (Kennedy et al., 2019; Tofaif et al., 2019). This would explain the possible ice-rafted debris in the clast-rich diamictite facies observed in core IT26.

The stratigraphic record generally was likely affected to some degree by widespread Sturtian glaciation (e.g. carbonate saturation, modified hydrological cycle), though to what degree remains unclear, as it depends on the extent and nature of glaciation: 'Snowball Earth' or simply more regionally extensive glaciation (Eyles and Januszczak, 2004, 2007; Hoffman et al., 2017). The interpreted Nguba MFS3 is a best-estimate at establishing a correlation between diamictite units, but in the proposed sequence stratigraphic correlations represents a 1st or 2nd order surface around which Sturtian diamictites diachronously cluster in time, assuming they are predominantly derived from rift-induced submarine topography. The thickness of diamictite units in Kamoa is interpreted to be the result of a favourable combination of the locus of extension switching westwards, generating significant amounts of accommodation space, large volumes of proximally sourced sediment, and glacial influence (Schmandt et al., 2013; Kennedy et al., 2019). It is estimated that Kamoa experienced a similar stretching factor during the Mwashia and Nguba as Solwezi did during the Lower Roan ($\sim$1.5), given the similar thicknesses in proximally-derived sediment.

What is notable in the Zambian Copperbelt is the relative thinness (100's m) and persistence of deep water successions that predominate in the Nguba Group, given the fact it spanned $\sim$80 - 100 Myr. Coarse siliciclastic facies appear absent above the diamictite units, with fine-grained siliciclastic and mixed or alternating clastic-carbonate facies predominating. The thickness of individual facies units and associations is significantly greater than during the Lower and Upper Roan, again indicating distal, likely deep, sedimentation. Even the basin margins in the West near Mwinilunga, and East in Mansa record deep water, possibly turbiditic facies. In both sequence stratigraphic correlations these were placed into a prolonged, HST on account of lack of facies variation. The rapid fault-controlled deepening during Mwashia and early Nguba times, and subsequent thermal subsidence during Nguba times, likely resulted in very deep and sediment-starved basin, with water depths well-below storm wave base, which further expanded over the Congo and Bangweulu cratons (fig. 7.4). The Katangan stratigraphy likely reached thicknesses of $\sim$4 km along the western Kafue anticline by the end of Nguba deposition.

As in the Zambia, the Nguba Group in the D.R.C. is interpreted as an initially deep water succession, comprising abundant dolomites, limestones and interbedded mudstones (Batumike et al., 2007; Cailteux and De Putter, 2019; Mambwe et al., 2020). These have been interpreted as possible platform carbonates in a proto-oceanic rift system (Cailteux and De Putter, 2019). In the middle to upper portions of the Nguba Group (e.g. Kaponda and Katete Formations in the D.R.C.), grain size increases, and siliciclastic proportions become greater, indicating shallowing in the northern parts of the Congolese Copperbelt, with the basin deepening southwards towards towards what is here interpreted as the central rift zone in Zambia (Batumike et al., 2007).

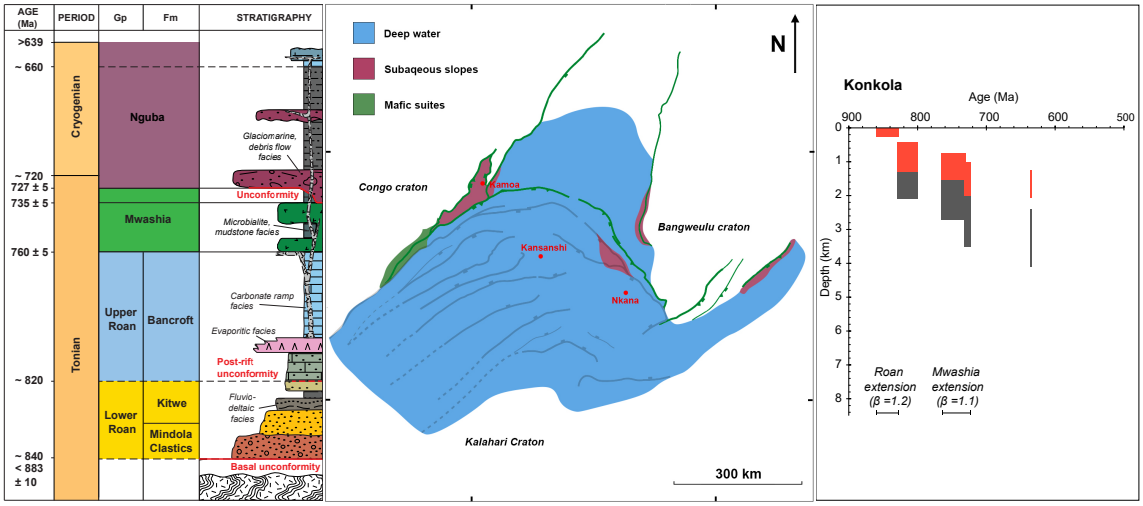

Figure 7.4: Palaeogeographic reconstruction of early to mid-Nguba time, showing major Mwashia normal faults and reactivated Lower Roan fault networks; the subaqueous slope deposits were likely much more numerous and widespread than illustrated on the map (centre panel); chronostratigraphy and general stratigraphic trends (left panel); backstripped subsidence plot, using Konkola type section as an illustrative example (right panel). Modified after Daly et al. (2024).

7.2 Kundelungu

The onset of deposition of the Kundelungu Group is based on the Petit Conglomerat diamictite at its base being interpreted as Marinoan in age, correlated with the Ghaub diamictite in Namibia at 635 $\pm$1.2 Ma (Hoffmann et al., 2004).

The subsidence history of the Kundelungu Group remains enigmatic. Apatite fission track thermochronology indicates $\geq$2 km of material were likely removed from the Kafue anticline since the Miocene (Daly et al., 2020), and the Kundelungu Group has been estimated to be $>$ 1 km thick

in the Congolese Copperbelt (Batumike et al., 2007). This suggests a pronounced increase in accommodation space generation prior to basin inversion. Southern provenance for clasts in the Petit Conglomerat, and muddier matrix (e.g. clast-poor diamictite facies), have been invoked to represent a switch from extensional to compressional regime in the Katangan (Batumike et al., 2006). With basin inversion commencing approximately 560 - 550 Ma (John et al., 2004; Naydenov et al., 2014), it is deemed most likely that accommodation space was generated via compression and flexure, rather than renewed extension, though whether this compressional basin took the form of a foreland basin or simply flexure of the basin between converging cratons is unclear (Cloetingh and Burov, 2011).

If Kundelungu tectonic subsidence was driven by flexure, then 'foreland' may not be the appropriate term to ascribe to the arcuate region north of the Domes (DeCelles and Giles, 1996; Porada and Berhorst, 2000; Cloetingh and Burov, 2011). What is termed the 'foreland' in the Katangan may more accurately be described as a retro-foreland (Dickinson, 1974; DeCelles and Giles, 1996). This is on account of interpreted northwards-directed deformation during basin inversion, and the degree of deformation reducing northwards from the highly deformed Domes region into the 'foreland' (Daly et al., 1984; Key et al., 2001; John et al., 2003; Broughton and Rogers, 2010). If a Kundelungu foreland basin existed, it would have formed south of the Domes on account of northward-directed movement. The possibility of an ocean existing in the southern part of the Katangan basin (John et al., 2003) raises the possibility of a forearc, as opposed to foreland, basin existing prior to complete basin inversion, though this remains speculative at this stage. Clearly, such fundamentally different interpretations of basin evolution during the latter half of the basin's history have significant implications for subsidence and thermal history, which in-turn affect the basin's mineral systems, and remain poorly resolved (Cloetingh and Burov, 2011).

The well-developed high-order (possibly 2nd to 3rd) SB4 unconformity and correlative conformity that marks the base of the prograding Kundelungu LST, and is expressed both on the western and eastern margins of the basin, arguably makes it more precisely correlatable than the Nguba MFS3. The drivers underpinning a fall in baselevel to generate this LST were possibly a combination of tectonism and glaciation (Hoffmann et al., 2004), similar to the Grand Conglomerat. In contrast to the Grand Conglomerat, there is clear evidence for baselevel fall prior to diamictite deposition, which could be interpreted as representing glaciation-induced baselevel fall. If the base-Kundelungu un-

conformity (SB4) in Mansa is predominantly tectonically driven, the it could be the result of flexural up-warping during compression, with the margin of the Bangweulu block at Mansa representing a flanking basin high (Cloetingh and Burov, 2011). Facies successions in the Kundelungu appear to be significantly shallower than in the Nguba, both in the Zambian and Congolese portions of the basin. Coarser siliciclastic facies appear in the basal Kundelungu successions in Zambia, followed by predominantly mixed clastic-carbonate successions. In the D.R.C. this trend appears to be mirrored, albeit with a northwards-increasing siliciclastic component, Batumike et al. (2007); Cailteux and De Putter (2019) interpreting epicontinental marine successions and marginal terrestrial successions. In the western part of the basin, facies successions in the Kundelungu appear to mimic those of the Upper Roan, and are interpreted as carbonate ramps, paralic zones and possible evaporitic facies.

The general tectonostratigraphic trends across the Katangan basin are summarised in a chronostratigraphic log shown in figure 7.5.

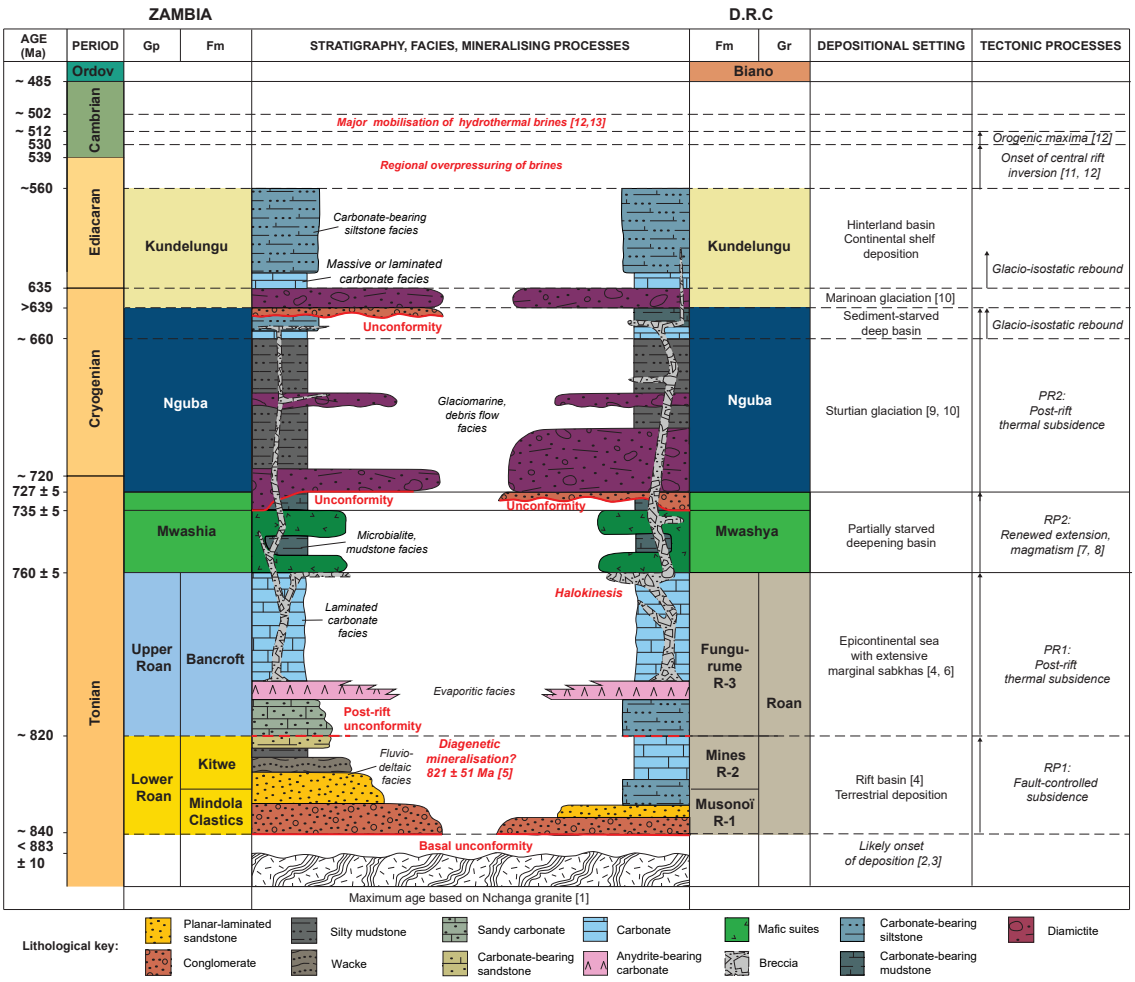

Figure 7.5: Chronostratigraphic log showing general stratigraphic evolution, depositional settings and tectonic processes operating in the katangan basin in Zambia and the D.R.C., based on facies analysis in this work as well as work by [1] Armstrong et al. (2005), [2] Selley et al. (2018), [3] Cahen et al. (1970), [4] Selley et al. (2005), [5] Muchez et al. (2015), [6] Binda (1994), [7] Key et al. (2001), [8] Kampunzu et al. (2000), [9] Rooney et al. (2015), [10] Halverson et al. (2020), [11] John et al. (2004), [12] Daly et al. (2020) *unpublished*, [13] Torrealday et al. (2000).

7.3 Mineralisation in a dynamic stratigraphic context

Oxidised siliciclastic sediments, derived from the Proterozoic basement underlying the Katangan basin, form a major source of copper (Hitzman et al., 2005, 2010; Parnell et al., 2021). The greatest thicknesses of oxidised sediment were deposited during Lower Roan and Mwashia rifting through a combination of sufficient sediment supply and accommodation space generation in fault-controlled basins and sub-basins (Selley et al., 2005). It is unclear how much copper the basement contributed to the overall source volume; however, given the long lifespan of the basin, it is plausible that fluids

circulated through the basement for prolonged periods and were able to leach a fraction of its metal budget. Total Cu-source would therefore be the sum of Cu contributed by oxidised siliciclastics and the Katangan basement. Modifying the source term for the mineralisation factor to take this into account would yield $S_{total} = S_{clastic} + S_{basement}$. It is postulated that basement Cu contributions become more important in thinner siliciclastic successions that alone may not represent a sufficiently large source, bringing Cu-concentrations above the critical threshold needed for a mineralised system.

Crude estimations of Cu source volumes for the Katangan basin have been made (Hitzman, 2000; Selley et al., 2018), but have not accounted for the increased Lower Roan thickness towards the interpreted central rift zone. Clearly, thicknesses of syn-rift clastic successions, and hence Cu source volume, vary significantly from the basin margins to the basin centre. However, this relationship is complicated by diachronous rifting in the Katangan basin. Lower Roan Group thicknesses are greatest in the interpreted central rift zone, decreasing towards the Lower Roan basin margins. Mwashia-age coarse siliciclastic successions appear to be greatest on the basin margins, where proximal clastic supply and accommodation space generation were greatest, whereas the basin centre was starved of coarse clastic facies. This is evidenced by the preponderance of fine-grained siliciclastic and plane-laminated carbonate facies across much of the Lower Roan basin during Mwashia times. This variable and diachronous distribution of clastic Cu source should be taken into account when quantifying clastic source volumes in the basin.

Though the mineralisation factor does not yet include a term describing salinity, it is clear that saline brines significantly enhanced the Katangan's mineral systems (Selley et al., 2005; Hitzman et al., 2010; Selley et al., 2018; Davey et al., 2020). Davey et al. (2020) proposed that residual bittern brines resulting from advanced evaporation, anomalously enriched in Cu and Co, benefited from long residence times under seals, increasing their potential for economic mineralisation. Stratigraphic or structural traps forming ideally hydrologically closed or partially closed systems appear to be crucial in enhancing mineralisation potential (Selley et al., 2005, 2018). Salt likely formed extensive seals, particularly in the D.R.C. (Jackson and Warin, 2003; Selley et al., 2018). For salt to form an effective seal over the basin's lifespan, significant thicknesses must have accumulated; most evidence points towards the Upper Roan being the salt source, which supports the proposed stratigraphic interpretation of the Congolese Copperbelt being more restricted and generally being able to accumulate greater salt thicknesses than the Zambian Copperbelt. In addition to the residual

brines, salt dissolution contributed a second-generation of syn to late-orogenic saline brines to the basin (Jackson and Warin, 2003; Selley et al., 2018). It is suggested the types of metasomatism are consistent with the proposed stratigraphic interpretation of the Congolese Copperbelt having been more restricted, accumulating greater volumes of evaporites compared to the central rift zone and along the Kafue anticline, as the Congolese Copperbelt is interpreted to show greater degrees of Mg-metasomatism compared to the Zambian Copperbelt, which is predominantly K-metasomatised (Selley et al., 2005, 2018). It could therefore be postulated that primary depositional environments exert a general, albeit diffuse, control on later alteration styles across the Katangan basin.

Depositional environments and their constituent facies had diverse geometries and played different roles in the Katangan mineral system at different times, including reductants and mineralisation sites, barriers to fluid flow, and possibly hydrocarbon sources (Mendelsohn, 1961; Clemmey, 1976; McGowan et al., 2003; Selley et al., 2005).

Elevated organic carbon concentrations were most likely in microbialite and mud-rich facies. Microbialite facies are interpreted to have been widespread between the late Lower Roan and early Upper Roan, whereas mud-rich units occur throughout the Katangan stratigraphy, but increase in frequency of occurrence in the Lower Roan, Mwashia, and Nguba Groups, coinciding with periods of rapid subsidence and/or sediment-starvation.

In the Lower Roan Group, around the Kafue anticline, reducing units are predominantly found in interpreted deltaic and fan-deltaic systems (e.g. fan-delta, delta slope, prodelta facies associations). It is difficult to determine with the data used in this work whether mud-rich units were deposited in a restricted marine or lacustrine setting. A lacustrine interpretation is cautiously favoured on account of MFS1 being correlatable between the ore shale along the Kafue anticline and onset of carbonate deposition in the deepest known part of the rift in Solwezi. Rapid fault-controlled subsidence resulted in reducing units being particularly well-developed in sharply regressive successions (e.g. MFS1 in the Lower Roan). Sharp mud-rich regressive surfaces likely exerted a significant permeability contrast on a sub-basin scale (Selley et al., 2005), possibly aiding in focussing fluids towards structural highs. Though lithostratigraphically correlatable, it is deemed unlikely that mud-rich units form continuous time-equivalent units on a regional scale, on account of facies shifts, and rifting on a regional scale likely being to some degree diachronous (White and McKenzie, 1988; Chenin et al., 2022).

In the Lower to Upper Roan transition and lower portions of the Upper Roan Group, microbialites and mud-rich units are interpreted as the main reductants. Mud-rich reductants tend to be restricted to paralic and sabkha successions (e.g. intertidal and sabkha facies associations), and at the Upper to Lower Roan transition co-occur with possible microbialite facies. Mud-rich reductants likely formed more disconnected units (Handford, 1981), with a greater degree of interbedding and lower total mud proportion per facies unit than early Lower Roan units, which are more commonly associated with sediment gravity flows and deep water sedimentation. The significantly greater proportion of carbonate in the Upper Roan generally limited the volume of mud-rich reductants. It is suggested that gentle progradational to retrogradational facies trends may affect mineralisation potential in mud-rich units by resulting in gentle redox and permeability contrasts, in which mineralisation might be dispersed at sub-economic grades over a larger stratigraphic interval. This is on account of reductants being too distributed, and fluid flow being insufficiently focused along impermeable units.

Mud-rich mineralisation sites become less common in the upper Lower Roan (e.g. the Lower Roan HST) and lower Upper Roan (e.g. Upper Roan LST). However, carbonate- and mixed siliciclastic-carbonate-hosted deposits are common both in the Zambian and Congolese Copperbelts at this stratigraphic level (Mendelsohn, 1961; Kampunzu et al., 2005; Selley et al., 2005). Many of what were possibly microbialite mats are now pervasively dolomitised and preclude precise interpretation. However, the abundance of mineralised dolomitic units could indicate that microbialite mats formed reducing sites of economic significance, and is supported by elevated TOC in some microbialites (Al-Siyabi, 2005; Grotzinger and Al-Rawahi, 2014). Microbial mats that formed on the denuded topography of Lower Roan rift highs and basin margins as the basin thermally subsided during the early Upper Roan TST were flooded during the late Upper Roan TST, possibly shifting their distribution towards the basin margins. Thus, two fundamentally different depositional settings in the Lower and Upper Roan Groups of Zambia and the D.R.C. could form viable sites of mineralisation, based on elevated TOC: sediment-starved or deep water mud-rich environments (e.g. restricted marine, pro-delta, lacustrine), and basin-marginal microbial mats (e.g. intertidal zones), the latter often associated with evaporites.

Mwashia reductants are more laterally extensive, particularly along the MFS2, where deep shelf settings are invoked to extend across much of the Kafue anticline. However, they appear less min-

eralised in the traditional Zambian Copperbelt, possibly as a result of clastic Cu sources being too distal, or fluids not being sufficiently focused in the deeper parts of the basin (e.g. western Kafue anticline to central rift zone) during Mwashia times. Lower Roan Cu-rich brines sealed under Upper Roan evaporite successions possibly prevented them from interacting with reductants higher in the stratigraphy (e.g. Mwashia, Nguba), with the basin being too connected at this stage for evaporites to be deposited in much of the basin during the Mwashia.

Nguba diamictites, silt- and mudstones form mineralised reductants on the basin margins, e.g. Fishtie, Kamoa (Schmandt et al., 2013; Hendrickson et al., 2015), likely on account of being underlain by marginal siliciclastic successions that form a proximal Cu-source, and that transition basinward into deeper marine facies. Much like the Lower Roan, mineralisation appears well-developed when thick siliciclastic successions are sharply overlain by mud-rich regressive successions, which appears to coincide with periods of fault-controlled subsidence in the basin's history (Mendelsohn, 1961; Binda and Mulgrew, 1974; Binda, 1994; Selley et al., 2005; Schmandt et al., 2013; Kennedy et al., 2019).

Flux of brine within basin domains will be controlled primarily by convection and compaction. With compaction tending to be exponential (Athy, 1930; Sclater and Christie, 1980), rapid initial porosity loss would have driven fluid expulsion during Lower Roan deposition, prior to 'sealing' of syn-rift successions by Upper Roan carbonate-evaporite successions in much of the Katangan basin. In the case of Solwezi, average bulk porosity would have reduced from ∼49% at the onset of Lower Roan deposition to 35 - 39% porosity by the end of Lower Roan deposition (see table 7.1).

KRX082, Solwezi	Bulk ϕ end Lower Roan	Bulk ϕ end Upper Roan	Bulk ϕ end Mwashia	Bulk ϕ end Nguba	Bulk ϕ end Kundelungu
Kundelungu					31 - 37
Nguba				42 - 48	13 - 22
Mwashia			41 - 44	26 - 35	12 - 21
Upper Roan		33 - 39	27 - 37	19 - 30	10 - 19
Lower Roan	35 - 39	18 - 28	16 - 27	12 - 23	7 - 15

Table 7.1: Table showing ranges of average bulk porosity (ϕ) values in the Solwezi type log derived from the KRX082 core for each stratigraphic Group throughout the basin's gross depositional history, based on the decompaction procedure used in Chapter 5.

A 10-14% reduction in pore fluid volume prior to evaporite deposition could have led to residual fluid volume (∼39-35% of bulk Lower Roan rock volume in the case of Solwezi) being more

concentrated in Cu, as there was less fluid volume but the siliciclastic Cu-source volume remained constant. Similar, though much less pronounced, trends in porosity loss can be observed at the Lower Roan basin margins near Ndola (table 7.2).

IT26, Ndola	Bulk ϕ end Lower Roan	Bulk ϕ end Upper Roan	Bulk ϕ end Mwashia	Bulk ϕ end Nguba	Bulk ϕ end Kundelungu
Kundelungu					31 - 37
Nguba				42 - 43	17 - 23
Mwashia			42	35 - 36	17 - 23
Upper Roan		40	38	32 - 34	17 - 22
Lower Roan	46 - 47	41 - 42	40	33 - 35	15 - 21

Table 7.2: Table showing ranges of average bulk porosity (ϕ) values in core IT26 near Ndola for each stratigraphic Group throughout the basin's gross depositional history, based on the decompaction procedure used in Chapter 5.

Heat flux exerts a major control on both fluid flow, driving convection, and Cu-solubility (Cathles and Adams, 2005; Yang et al., 2006). According to the McKenzie model, heat flux in rift systems increases sharply during stretching (e.g. Lower Roan fault-controlled subsidence), and decays exponentially as a function of time (McKenzie, 1978; White and McKenzie, 1988). Basal heat flux would therefore have been greatest in the most stretched parts of the basin, near the central rift zone, and lowest at the basin margins. As a result, strength of convection and efficiency of Cu-leaching in the Lower Roan siliciclastics would have been greatest towards the central rift zone (e.g. south of the Solwezi Dome), moderate in the northern and western Kafue anticline (e.g. Konkola sub-basin, Chambishi sub-basin), and low on the margins (e.g. Ndola) (fig. 7.6).

Basal heat flux varying as a function of time and stretching must be taken into account when quantifying the thermal history of the initial rift, as constant geotherms may be applicable to cratonic interiors, but do not account for variable thermal gradients along the stretched portions of lithosphere (McKenzie, 1978; White and McKenzie, 1988).

The McKenzie model can provide an initial first-order approximation of Roan heat flux. Quantifying heat flux for the Mwashia rift event is complicated by the diachronous emplacement of volumetrically variable extrusive mafic suites, and intrusives occurring at varying crustal levels, which would have generated localised thermal anomalies.

A crude calculation can be performed to estimate a range of plausible burial temperatures during Roan rifting by using a geotherm equation, taking into account changing basal heat flux and thermal

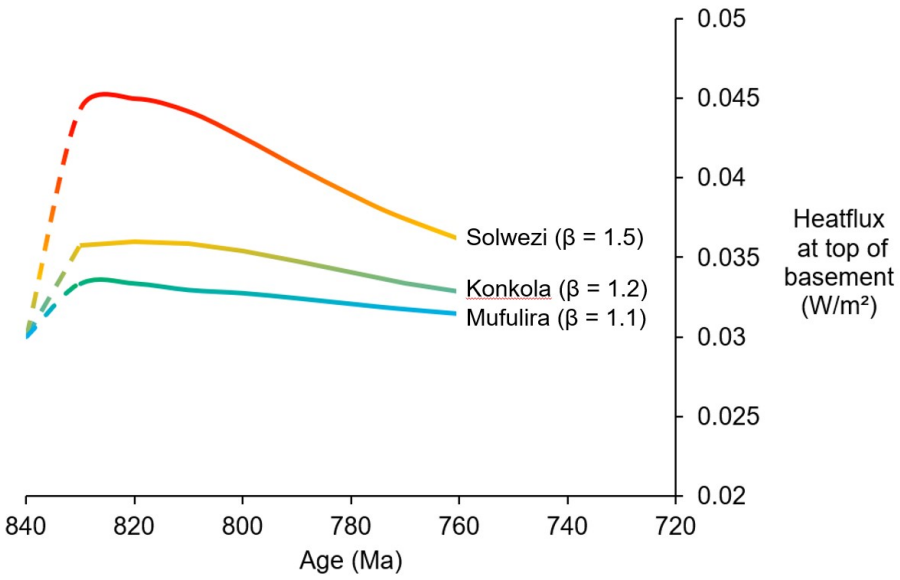

Figure 7.6: Heat flux at the basement-sediment interface over the course of Roan rifting and thermal subsidence, based on the McKenzie uniform extension model (McKenzie, 1978) in different parts of the basin. Though the absolute values come with significant uncertainty, the trend of increasing syn-rift heat flux with increasing stretching is evident. Dashed lines represent the fault-controlled subsidence phase.

conductivity from the end of the Lower Roan to the end of the Upper Roan (Sclater and Christie, 1980; Allen and Allen, 2013):

$$T(y) = T_0 + Q\left\{\frac{l_1}{K_1} + \frac{l_2}{K_2}\right\} \tag{7.1}$$

where

$T(y)$ is the temperature at depth y

T_0 is the surface temperature

Q is the basal heat flux (the sum of rift-induced heat flux and assumed radiogenic basement heat flux)

l_1 is the decompacted thickness of sediment layer 1 (i.e. Lower Roan)

K_1 is the bulk thermal conductivity of sediment layer 1

l_2 is the decompacted thickness of sediment layer 2 (i.e. Upper Roan)

K_2 is the bulk thermal conductivity of sediment layer 1

As sediment thermal conductivity is a function of porosity, and therefore burial, porosity values in table 7.1 were used, where $K_{bulk} = K_{sediment\,framework}(1-\theta) + K_{pore\,fluid}(\theta)$. Values of Q were derived from the Solwezi stretching factor computations (fig. 7.6), decompacted sediment thicknesses were based on the decompaction procedure in Chapter 5; further input values are shown in table 7.3.

Surface temperature	10 $^{\circ}C$
End Lower Roan rift-induced heat flux	0.045 mW^{-2}
End Upper Roan rift-induced heat flux	0.037 mW^{-2}
Radiogenic basement heat flux	0.03 mW^{-2}
Sediment framework thermal conductivity	5.5 $Wm^{-1}K^{-1}$
Pore fluid thermal conductivity	0.6 $Wm^{-1}K^{-1}$

Table 7.3: Table of values used to compute an estimates of Lower Roan temperatures in Solwezi, based on the KRX082 core, after computations in this work and Sclater and Christie (1980); Allen and Allen (2013).

An arbitrary $\pm 10\ ^{\circ}C$ uncertainty envelope was added to account for the many uncertainties and assumptions made in these computations (e.g. radiogenic heat input from sediments being omitted, and basement radiogenic heat flux remaining constant, uncertainties in the type logs and subsidence analysis). A range of plausible temperature estimates for the basement surface and Lower-Upper Roan contact throughout Roan rifting is provided in figure 7.7. Despite the Lower Roan rift being amagmatic, the relatively low geotherms indicated here, compared to modern rift systems, suggest that these values should be considered a plausible lower bound for burial temperatures (Allen and Allen, 2013).

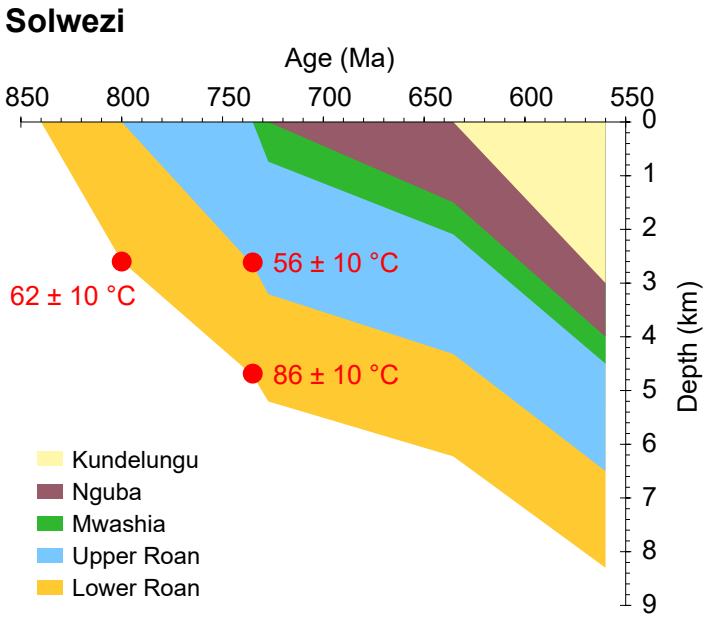

Figure 7.7: 1D burial-temperature plot of the Solwezi type log, derived from core KRX082, showing ranges of temperatures the Lower Roan could have achieved during Roan rifting, with a stretching factor of 1.5 .

The base of the Lower Roan Group could have reached temperatures $>62\ ^{\circ}C$ by the end of Lower Roan deposition, and $>86\ ^{\circ}C$ by the end of Upper Roan Group deposition. The Lower-Upper Roan contact could have reached $>56\ ^{\circ}$C by the end of Upper Roan Group deposition. These results provide a first-order approximation of basal brine temperatures throughout Lower and Upper Roan times.

These tentative temperature ranges have implications for diagenetic mineralisation in the Katangan, suggesting that framboidal pyrite could have crystallised during Lower and Upper Roan times

(De Waele, Muchez, Vets, Fernandez-Alonzo and Tack, 2006). Sweeney and Binda (1994)'s suggestion of biogenic fixation of sulphides occurring at temperatures < 100 °C could indicate sulphide formation during Upper Roan sedimentation in the deeper parts of the basin. Mineralisation temperatures >100 °C proposed by Annels (1989); El Desouky et al. (2010) were possibly only reached by the end of Upper Roan Group deposition, but almost certainly during Mwashia times, on account of widespread intrusive and extrusive magmatism elevating local temperature gradients on a regional scale. These broadly overlap with the Re-Os dates for diagenetic sulphide mineralisation of 787±26 Ma in Kamoto (Muchez et al., 2015), and Konkola deposit of 816±62 Ma (Barra et al., 2004).

Preliminary results for fission-track thermochronometry in Solwezi (see Appendix V) can provide insights into the second major mineralisation event in the basin associated with Lufilian metamorphism, between ∼540 - ∼473 Ma (Sillitoe et al., 2017; Saintilan et al., 2018). Thermal modelling of zircon and apatite fission track data from the KRX082 core indicate temperatures $\leq$ ∼250 °C, and hence uplift, from 500 Ma onwards (see fig. 7.8).

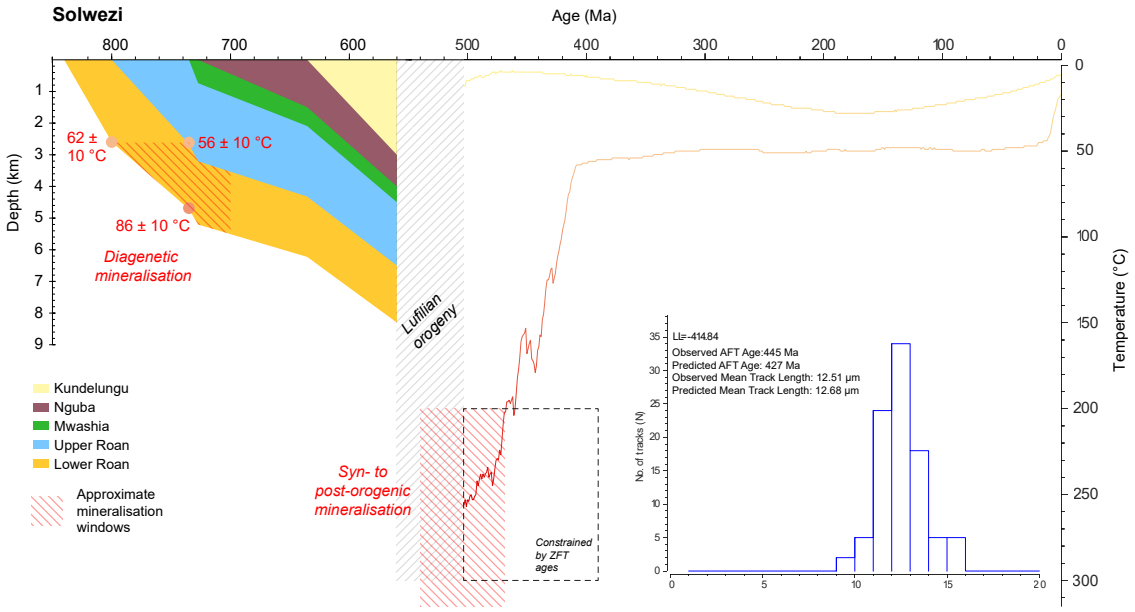

Figure 7.8: Composite lifetime burial-temperature plot for Solwezi showing burial and Roan temperature estimates prior to basin inversion, followed by a cooling/uplift model based on apatite and zircon fission track thermochronometry. The two main mineralisation events, Roan diagenetic, and Lufilian syn- to post-orogenic, are shown. The two lines in the thermal model are based on apatite fission tracks at a 95% confidence interval; the higher temperature bound is seen as a more reliable estimate of thermal evolution on account of being constrained by zircon fission tracks.

Multiple sulphide assemblages across the Zambian and Congolese Copperbelts (e.g. Kamoto,

Luiswishi, Mujimbeji, Chambishi, Lufubu) have been associated with basin inversion and metamorphism, with age and temperature estimates of $>$ 250 °C between $\sim$540 and $\sim$473 Ma (Richards et al., 1988; El Desouky et al., 2009; Turlin et al., 2016; Sillitoe et al., 2017; Saintilan et al., 2018). These data support what fission track data indicates was the peak of metamorphism ($>$ 250 °C pre-500 Ma) prior to the onset of rapid uplift post-500 Ma. Crucially, the results show one major phase of very rapid post-Lufilian cooling in Solwezi, lasting until $\sim$400 Ma, followed by prolonged residence at shallower crustal levels. Minor subsequent thermal events are likely, but the samples do not appear to have experienced temperature $>$50°C for durations for longer than 1 Myr.

Chapter 8

Conclusions

Though the Katangan basin of central Africa has been studied in detail for over a century, integrated basin-scale studies remain limited in quantity. This work has begun to provide a framework into which more detailed mine-scale studies can fit, achieving its aims of applying a basin analysis approach to improve our understanding of the stratigraphy, subsidence history and mineral systems of the Katangan basin.

Emphasis has been placed on proposing unified approaches using repeatable workflows that are sensitive to the constraints of the Neoproterozoic to generate a coherent picture of basin evolution. The techniques described are most applicable to parts of the basin that are least deformed and in which stratigraphy is best preserved, e.g. where tectonic fabrics and allochthonous salt breccias are minimal.

The facies scheme is adaptable and expandable, allowing for further subdivision and addition of facies not yet included. It also allows facies trends to be quantified and stratigraphic trends to be more clearly resolved. It has potential to be used for more sophisticated geo-statistical techniques (e.g. Markov chain analysis) in future. The facies scheme can be used in under-explored parts of the basin and aids more reliable, consistent and repeatable interpretations of depositional environments, which in-part control reductant compositions and geometries.

Several sequence stratigraphic correlations are possible on a basin-scale and expand on work that has been done previously. They represent a shift away from lithostratigraphy and allow for different stratigraphic hypotheses relying on the same fundamental approach to be tested, and an approximate relative chronological framework to be established in the absence of actual age dates. The

value of these lies in their predictive capability for stratal and facies successions, and hence aquifer connectivity and fluid pathways, reductants, lateral and vertical permeability contrasts, which exerted a significant control on the basin's initial diagenetic Cu-mineralisation. Sequence stratigraphy highlights the limitations of lithostratigraphy, by showing reductants and siliciclastic Cu-sources can be deposited contemporaneously in different parts of the basin. It also emphasises the need for independent chronostratigraphic constraints to evaluate the degree of diachroneity in mineralised mudstone units.

The quantified subsidence analysis allows for a first-order estimate of subsidence history and basin forming mechanisms to be made, which exerted a fundamental control on stratigraphic architecture, early basin heat flow, and development of hydrothermal systems in the basin. The central rift zone, interpreted to lie south of the Domes region, likely underwent $> 65\%$ stretching over the course of the basin's extensional history. Preliminary thermochronological work suggests the basin underwent one major phase of uplift and cooling during the Lufilian orogeny, coinciding with a second phase of mineralisation in the basin.

The abundance of continuous drill core from the Katangan basin provides an excellent database allowing for much more work to be done to better understand the basin, its evolution, and how it compares to other Neoproterozoic basins. Petrographic study of the various facies described herein would significantly enhance our understanding depositional systems, sediment sources, depositional and diagenetic history. Basin-wide geochronology and detrital zircon analysis could provide insights into sediment transport pathways through time, to complement the subsidence and sequence stratigraphic models proposed here. Building on Bull et al.'s (2011) work on isotope stratigraphy beyond the Kafue anticline, and performing it on cores across the basin, would be a valuable contribution allowing comparison to global isotope correlations (Halverson et al., 2020).

The paucity of precise age constraints remains a challenge, exerting a first-order uncertainty on our understanding of the Katangan basin's evolution. Further work on age dating (e.g. on the lamprophyres described in the classical Zambian Copperbelt, and the abundant Mwashia mafic suites across the basin) would be of great benefit in providing chronostratigraphic constraints in the basin. Further sequence stratigraphic correlations, on datasets with a greater spatial and structural resolution, taking into account the possibility of a base-Nguba lowstand systems tract, would allow for the effects of glaciation on Katangan stratigraphy and its subsidence history to be taken into account.

This thesis has highlighted some of the general considerations that need to be taken into account when interpreting the evolution of Precambrian basins. The limited – or absent – fossil record in Precambrian basins results in palaeobathymmetric constraints and gross depositional environmental interpretation relying almost exclusively on sedimentological interpretation. This, combined with poorly constrained Neoproterozoic sea level curves, results in backstripping being less suitable to determining basin forming mechanisms than in Phanerozoic basins. A priori constraints provided by the stratigraphy and geological context are therefore beneficial to inform subsidence analysis. Where chronological constraints are sufficient, subsidence analysis is still valuable in constraining burial history, however. Where biostratigraphy is absent, and chronostratigraphy is limited, reliance on facies analysis in drill core makes mis-correlation of higher and lower-order surface more likely. Seismic stratigraphy therefore becomes a valuable addition to core-based stratigraphic analysis, in addition to allowing stratal geometries in the subsurface to be imaged.

Palaeogeographic reconstructions remain under-utilised in mineral exploration, despite their value having been known for almost a century (Adams, 1943; Markwick, 2019). Facies analysis, sequence stratigraphy, and subsidence analysis can be combined in a mineral systems framework to complement existing techniques used in mineral exploration beyond the Katangan basin. Understanding the burial history, spatial distributions, and relationships between Cu sources, fluid pathways, and reductants through time would be of value in other sediment-hosted Cu deposits, such as the Phanerozoic Kupferschiefer and Proterozoic White Pine deposits.

Beyond sediment-hosted Cu deposits, several other mineral systems are interpreted to have benefited from favourable local stratigraphy, including the Bushveld Complex and Norilsk, via assimilation of evaporitic sediments into melts (Buchanan et al., 1981; Li et al., 2009). The utility of a basin analysis approach may therefore extend beyond sediment-hosted Cu deposits, and be worthy of consideration in any mineral system where sediments could have significantly affected ore forming processes.

Statement of Authorship for joint/multi-authored papers for PGR thesis

Title of Paper	Cratonic margin rifting, inversion tectonics, and diverse mineral systems: the Neoproterozoic Katangan basin of Africa
Publication Status	□Published □ Accepted for Publication □ Submitted for Publication × Unpublished and unsubmitted work written in a manuscript style (in preparation for publishing)
Publication Details	Daly, M.C., Zimba, M., Purkiss, M., Chibesakunda, F. (2024), 'Lithospheric Thickness, Rift and Inversion Tectonics: The Formation and Deformation of the Neoproterozoic Katangan Basin of Central Africa'.

Student Confirmation

Student Name:	Martin Purkiss		
Contribution to the Paper	Performed subsidence analysis and facies analysis, computed stretching factors, and contributed to manuscript.		
Signature		Date	30/09/2023

Supervisor Confirmation

By signing the Statement of Authorship, you are certifying that the candidate made a substantial contribution to the publication, and that the description described above is accurate.

Supervisor name and title: Michael C Daly, Visiting Professor.		
Supervisor comments The candidate has contributed substantial analytical work to a component of the publication in line with what he describes above.		
Signature 	Date	30th September 2023

Chapter 9

Appendix I – facies descriptions

Dark mudstone facies, dMs

The black mudstone facies comprises dark, mudstones containing $< 10\%$ silt. The facies may be fissile or shaley in parts. Continuous planar lamination is common. They are often carbonaceous (Selley et al., 2005). Bedding thickness is variable. Silt laminae are rare or absent. The facies units tend to be 10's m thick, with a median thickness of 15 m, approaching 100's m in the CHLDD001 core. The facies makes up 1.6% of the total measured facies thickness across all cores. Type examples can be found in the ZMSDD003 and CHLDD001 cores (fig. 9.1).

The uniformly fine grain size and ubiquity of planar lamination attests to a very low energy environment in which material settled out of suspension, with no evidence of oscillatory flow or wave reworking (Allen, 1970). Silt laminae indicate minor, periodic fluxes of silt into the system (Pickering et al., 1986; Zolitschka et al., 2015). Alternatively, this facies could also represent a moderate to low-energy environment starved of coarse terrigenous sediment (Trabucho-Alexandre, 2015).

Silty mudstone facies, SlMs

The silty mudstone facies comprises planar laminated mudstones punctuated by laminae or thin beds of silt or fine sand (10 - 50 % within a facies unit). Mudstones are frequently carbonaceous (Selley et al., 2005). Silty laminae are mostly thick and may occur in dm-scale laminae sets, forming laminites (fig. 9.2). Individual laminae frequently have sharp bases that fine upwards. The bases

of sandier laminae are often undulose and scoured. Laminae are mostly planar and occasionally continuous and wavy. Rarely, individual laminae may coarsen up into fine sands. Mud clasts up to 1 cm in size and intraclast conglomerates may be present. Sets of laminae rarely show clear cyclicity, often precluding them from being rhythmites. Bed thickness in the facies varies, but tends to be thin to medium. The facies occurs in units metres to 10's m thick, with a median thickness of 8 m. It comprises 1.7 % of total measured facies thickness, with core IT26 being containing type examples. The facies may form part of the Ore Shale and Hangingwall Argillite units in Binda and Mulgrew (1974) and Clemmey (1974).

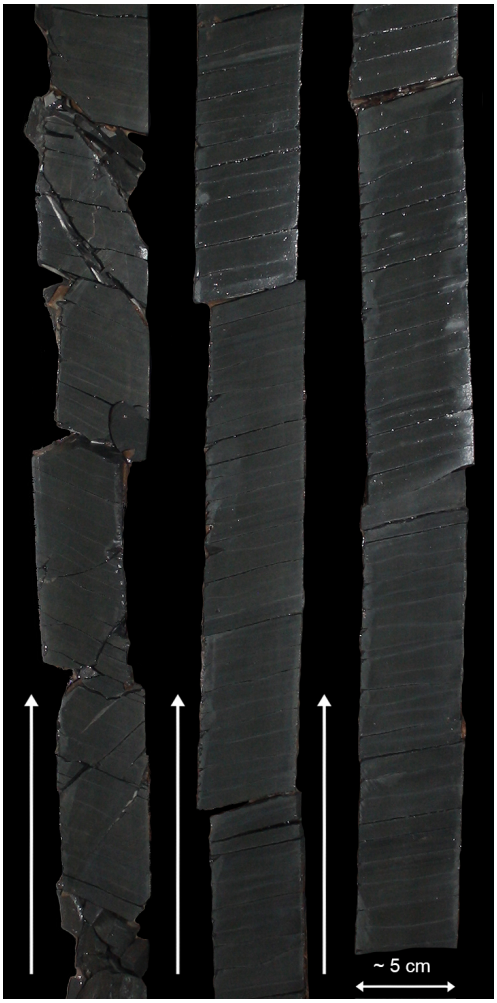

Figure 9.1: The dMs facies in the ZMSDD003 core, showing dark grey, fissile mudstone units with faint thin planar lamination. Arrows indicate way-up for the three cores.

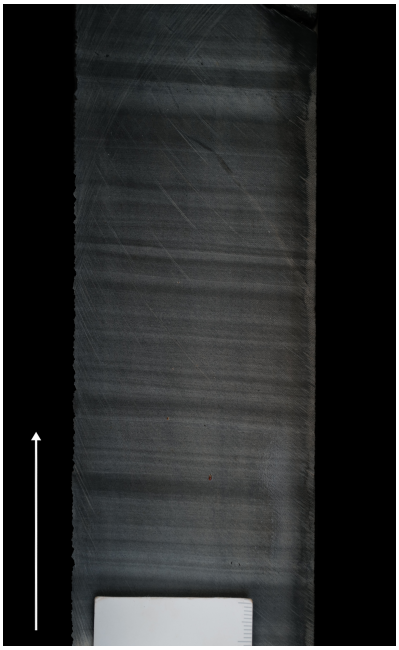

Figure 9.2: The SlMs facies in the CHLDD001 core. Laminites comprise thin planar laminated silts and mudstones. Arrow indicates way-up; mm-scale QP card for scale.

The facies represents a low-energy environment with deposition dominated by settling out of suspension, or one starved of coarse sediment. Thin wavy laminated units and scour marks suggest periodically elevated current or wave energy introducing coarser material, sufficient to disturb or erode into the substrate (Pickering et al., 1986; Myrow and Southard, 1996; Trabucho-Alexandre, 2015).

Laminated siltstone facies, LSl

The laminated siltstone facies comprises variably coloured siltstones and minor quantities of very fine to fine sands ($< 10\%$) with abundant primary structures (fig. 9.3). Thin and thick laminae are frequently arranged as laminites. This can give the facies a characteristic striped appearance, on account of colour changes or alternating redox between laminae. Laminae are continuous planar or wavy, with individual laminae and thin beds commonly fining upwards from a sharp base. The laminations can occur in pairs or triads, but their being slightly out-of-phase with respect to one another, as well as their non-uniform spacing, often precludes them from being true rhythmites (Reineck and Singh, 1980). Scour marks and small gutter casts may occur in isolation, with ripple cross-laminae sometimes forming dm-scale co-sets. Asymmetrical ripple laminae occur throughout beds, and are not restricted to the tops of units, nor to the tops of fining-up successions. Foresets of ripple laminae are generally concave. Hummocky cross-stratification may be present, though this is difficult to determine confidently in core. Soft-sediment deformation structures are isolated and rare. Clusters of rip-up clasts may be present. The facies tends to be thinly to medium-bedded, with thin units predominating. The facies occurs in packages 10's - 100's m thick, with a median thickness of 12 m, and is particularly well-expressed in cores ZMSDD003 and KADD04. It makes up 4.2% of total measured facies thickness.

The facies represents sediment fluxes periodically being introduced into a low-energy environment and settling out of suspension (Pickering et al., 1986). Occasional deposition from lower flow regimes generated ripple lamination (Allen, 1966; Jopling and Walker, 1968). Ripple marks occurring throughout units – not just at their tops – indicates persistent sediment agitation, as opposed to event beds deposited by steadily waning flows. Asymmetrical ripple marks may represent wave ripples or current ripples. Compaction and tectonic fabrics affect parameters such as the ripple in-

dex, making the two types difficult to distinguish in core (Reineck and Singh, 1980). Scour marks and gutter casts suggest sediment fluxes were energetic enough to erode and rework the tops of beds. Soft-sediment deformation, possibly load, structures indicate periods of elevated sediment accumulation rates, and hence reduced water expulsion (Stow and Shanmugam, 1980). Repeated thin fining-up units could represent deposition from very dilute turbulent flows such as distal turbidites (Stow and Shanmugam, 1980; Pickering et al., 1986).

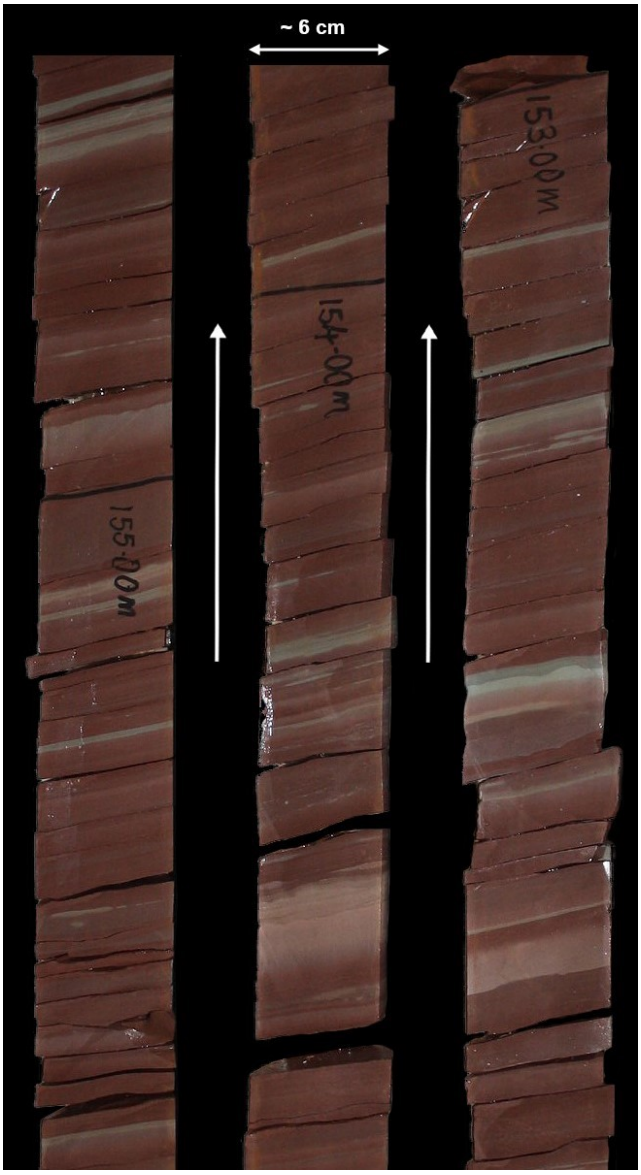

Figure 9.3: The LSl facies in the ZMSDD003 core, showing abundant laminites and thin graded beds. Some of the beds are grey and reduced; the majority are oxidised to a reddish-brown.

Sandy mudstone facies, SstMs

The sandy mudstone facies comprises laminated mudstones and siltstones punctuated by laminae and beds of sand and gravel (fig. 9.4). The facies is characteristically poorly sorted. Mudstone and siltstone comprise $\geq 50\%$ of the facies, with scattered granules outsized clasts up to fine gravel being common. It is distinguished from the wacke facies by having higher mud content, though the two facies may pass into one another.

Mudstones show abundant thin continuous and discontinuous wavy lamination. Mudstone beds appear thin to thickly bedded. Mud units may fine up from or coarsen into silts and fine sands.

Sandy beds tend to be arkosic and are very poorly sorted. Grains range in size from fine to gravel, are moderately to highly rounded, with low to high sphericity. Fining-up is absent in most units and restricted to thicker beds. The mud:sand ratio often increases towards the tops of units. Bed thickness is generally thin to medium, with bases often being undulose or scoured. Thinner beds are frequently discontinuous and in parts lenticular. Small apophyses of sand frequently penetrate muddy beds. Thin (cm-scale) sandy dikes penetrate mud-rich portions of the facies and locally disrupt muddy and silty laminae. Cm-scale sandy sills frequently branch off the main dike sub-perpendicularly. The sandstone dikes are as poorly sorted as their arkosic source beds, with no internal structure. Their geometry is sinuous and their edges sharp, but rarely straight. Poorly developed dish and water-escape structures are rare. That some sandy dikes may be infilled and compacted dessication cracks is not excluded, however, their length (dm-scale), branching into sills, and similar composition as the muddy sands they penetrate, make sandy dikes more likely in most cases.

Minor quantities ($< 5\%$ of a facies unit)of anhydrite may be present in thin beds or thick laminae that are concordant or discordant. The facies thickness ranges from metres to 10's m, with a median thickness of 15 m. The facies makes up 4.2% of total measured facies thickness. Type examples are found in cores KN192 and RCB2.

The sandy mudstone facies shares many similarities with the 'Shale with Grit' unit characterised by Binda and Mulgrew (1974) and the carbonaceous wacke described in Eden (1974), in that it is very poorly sorted and juxtaposes fine sediments with coarser sands and fine gravels. The facies is broadly equivalent to the poorly sorted arkose facies described by Bull et al. (2011). However, these authors used a broader compositional definition that incorporated anhydrite and dolomitic siltstones

in their facies, which are classified as separate facies in this scheme.

The facies is interpreted to have been deposited by sediment gravity flows. Where continuous lamination predominates in silts and mudstones, fine material likely settled out of suspension. Poorly sorted and undulose arkosic beds represent high-energy fluxes of coarse sediment. These arkosic beds likely represent deposition of bedload, either as traction carpets in high-density turbidity currents via frictional freezing (Lowe, 1982), or from muddy and sandy debris flows (Shanmugam, 2000, 2021). The paucity of fining-up indicates limited turbulence during deposition. Where bimodal grain size distribution is preserved and granular outsized clasts are present in discontinuously laminated fine-grained units, sediment fluxes were likely mud-rich cohesive flows deposited via cohesive freezing (Lowe, 1982; Dasgupta, 2003; Talling et al., 2012; Shanmugam, 2021). These flows were sufficiently competent to transport granule-sized clasts, but insufficiently turbulent to generate grading (Lowe, 1982; Lowe and Guy, 2000). These cohesive flows may be equivalent to the H3 division of hybrid event beds (Haughton et al., 2009). The abundance of discontinuous wavy lamination in coarser units suggests relatively high-energy emplacement of this facies (Mulder et al., 2003). Sandy apophyses into muddy substrate point to rapid deposition prior to de-watering.

Though rare, the presence of anhydrite is enigmatic, and could either be the result of secondary anhydrite precipitation, or sediment gravity flows being introduced into a deep water evaporitic setting (Fortuin and Krijgsman, 2003; Roveri et al., 2020).

Parts of the facies may appear similar to the heterolithic facies, with crude lenticular bedding. It could therefore be interpreted as having been deposited from bi-directional flows under fluctuating energy conditions, as has been suggested by Bull et al. (2011). However, the poor sorting, coarse grain size of sandy units, and outsized clasts, which require highly competent flows, make this interpretation seem unlikely in most cases.

Some sand-rich layers likely underwent complete particulate fluidisation post-deposition, on account of their lack of internal structure or sorting (Hurst et al., 2011). The sinuous geometry of sandy dikes suggests rapid post-depositional injection into mudstones with sufficient water content to preclude fully brittle fracture (Lowe, 1975; Reineck and Singh, 1980; Hurst et al., 2011). The dikes were likely injected quickly (in the order of cms^{-1}) due to the constituent granule-sized clasts having a high minimum-fluidisation velocity (Lowe, 1975). Possible generation mechanisms for the dikes include seismicity, fluid influx, and overpressure (Hurst et al., 2011). The latter two appear

implausible on account of the small scale of fluidisation structures, and due to the mudstones being wet enough to preclude brittle facture. This could suggest insufficient overburden to rapidly fluidise and inject dikes by overpressure (Hurst et al., 2011).

Wacke facies, Wck

The wacke facies is highly compositionally and texturally varied, characterised by poor sorting and variable mud content ranging from 15 to 50% in a facies unit. Grain sizes in coarser portions of the facies range from medium sand to gravel and isolated pebbles. Grains are angular to rounded with moderate to high sphericity. Mudstones and silts form a significant matrix component, and may form discrete thin to medium beds containing scattered granules and gravel. Coarser components of the facies tend to be arkosic and may be chaotically structured, crudely interbedded with more mud-rich units, graded, or massive (fig. 9.5).

In chaotically structured parts of the facies stratification is poorly developed. Bed contacts are often undulose or show scour. Fining-up is rare. Primary structures are abundant, but poorly developed on account of wide grain size distribution and poor sorting. Asymmetrical sand lenses, continuous and discontinuous planar and wavy laminae are ubiquitous. Sand lenses and discontinuous beds sometimes have serrated surfaces. Cm-scale lobate structures occur periodically, likely representing soft-sediment deformation.

Crudely interbedded parts of the facies tend to be less chaotic, with diffuse cm to dm-scale interbedding of muddier and sandier units. Sandier units show primitive planar and trough cross-lamination. Foresets are mostly concave and delineated by silt or fine sand. Cross bed sets are bounded by poorly developed planar or slightly undulose bedding surfaces.

Coarser units may fine upwards, often with concomitant upwards-reduction in clast quantity and transition to matrix-supported fabric on a dm-scale. Coarsening-up units are less common. Massive units are rare, but are more common with increasing grain size (up to gravel). Bed thickness in the facies tends to be medium. The facies occurs in packages metres - 10's m thick and has a median thickness of 12 m. It makes up 2.4% of total measured facies thickness and is well-expressed in cores KN192 and CHLDD001.

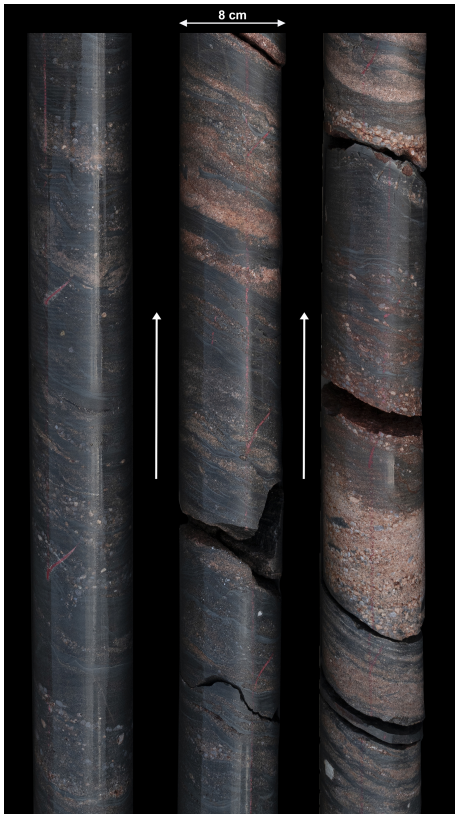

Figure 9.4: The SstMs facies in the KN192 core, showing wavy and lenticular arkose beds in laminated silt and mudstone. Small sand dikes are also visible. Arrows indicate way-up for the three cores.

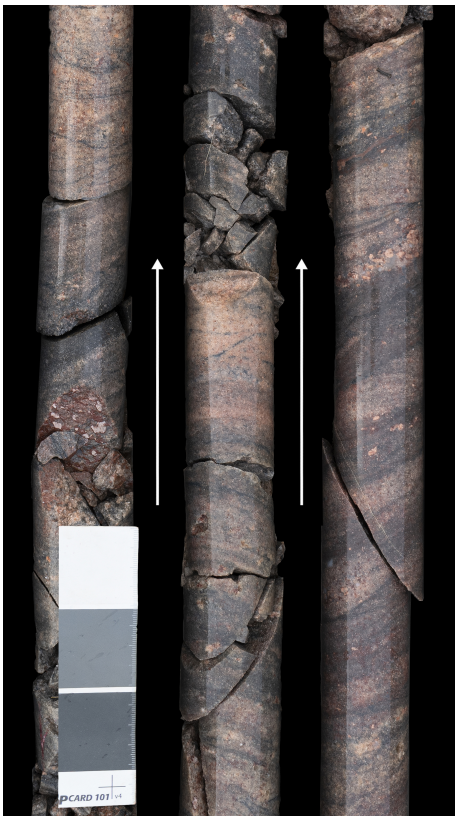

Figure 9.5: The Wck facies in the KN192 core, showing poor sorting, trough cross-lamination, granular outsized clasts and poorly developed structures. Arrows indicate way-up for the three cores. Mm-scale QP card for scale.

Due to the abundance and variety of structures, the facies could represent several depositional mechanisms from a variety of flow types. The combination of primary depositional processes and post-depositional reworking and loading are likely responsible for the facies's varied appearance. The facies is broadly interpreted to have been deposited very rapidly from sediment gravity flows (Pickering et al., 1986; Talling et al., 2012). The flows were predominantly sand-rich and sufficiently competent to transport gravel. The poor sorting, and variable grain size suggest that fluid turbulence was either dampened or restricted to certain parts of the flow (Lowe, 1982; Nemec and Steel, 1984; Shanmugam, 2000). More gravelly and poorly sorted portions of the facies were likely deposited as bedload in sandy debris flows, or, where there is evidence of fining-up or mud content is higher, traction carpets in high-density turbidites (Shanmugam, 2021; Talling et al., 2012; Shanmugam, 2000; Lowe, 1982). Lobate soft-sediment deformation structures indicate rapid deposition prior to

de-watering and post-depositional loading.

Where the facies is less chaotic and sand proportion is higher, the presence of cross-laminated units indicate deposition from the lower flow regime (Allen, 1970). This could represent periodic re-working by currents (Miall, 2013; Reineck and Singh, 1980), hyperpicnal input (Zavala, 2020), or deposition from a sediment gravity flow during periods of reduced sediment fallout rates (Talling et al., 2012).

Interbedded mudstone and sandstone facies, MsSst

The interbedded mudstone and sandstone facies comprises mudstones and sandstones interbedded in varying proportions. Sandstone units are generally arkosic or sub-arkosic. Laminated mudstones and siltstones make up finer units. Carbonate grains are rare, making up $< 10\%$ of the facies. The facies occurs in packages 10's m thick.

The interbedded mudstone and graded sandstone sub-facies can form part of the Ore Shale unit (Binda and Mulgrew, 1974; Selley et al., 2005)

Interbedded mudstone and graded sandstone sub-facies, MsgSst

The interbedded mudstone and graded sandstone sub-facies comprises distinctive repeated sets of graded sandstone units that are interbedded with laminated siltstones and mudstones (fig. 9.6).

Arkosic units are fine to coarse-grained and moderately to well-sorted. Grains are sub-rounded to rounded with moderate to high sphericity. Sandy units are thinly to thickly bedded, frequently fining upwards to a fine sand on a cm to dm-scale. Internal structures tend to comprise poorly developed planar lamination, convoluted lamination or may be unstructured in parts. Cm-scale ripple lamination is rare. The bases of arkosic units vary; they may be gradational, straight and sharp, undulose, or scoured.

Muddy and silty units are thinly to medium-bedded, in parts silty, comprising ≥ 50 % of the sub-facies. Lamination is abundant, with sets of laminae sometimes occurring as sets of thin laminites. Mm-scale laminae often fine upwards. Laminae are well-developed, predominantly planar and continuous. Wavy laminae are less common. Discontinuous wavy laminae may represent mud chips or

compacted mud clasts; it can be difficult to distinguish the two in narrow-diameter core. Muddy and silty beds can show isolated soft-sediment deformation structures and disrupted sets of laminites. The median thickness of the sub-facies is 12 m. It makes up 0.2% of total measured facies thickness. The sub-facies is interpreted to have been deposited by sediment gravity flows or, deposition under fluctuating energy conditions of sediment flux. Higher energy input of sandy units is supported by sharp bases and scouring into muddier units. The repetition of units showing well-developed fining-up indicates significant flow turbulence (Pickering et al., 1986; Talling et al., 2012). The interbedding of graded arkosic beds with muddy and silty beds appears to represent a primitive Bouma sequence (Bouma et al., 1962). Sandier units likely represent bedload, and muddy beds the lofted portion of the flow which settles out of suspension (Lowe, 1982; Garcia, 1994; Haughton et al., 2009). The low sand:mud ratio and well-developed grading suggest this sub-facies was deposited from low-density, highly turbulent flows (Talling et al., 2012; Shanmugam, 2021).

Alternatively, where sandy units do no show pronounced grading, have diffuse bases or where Bouma sequences are not clearly distinguishable, the facies could result from suspension settling in a low energy or sediment-starved environment, with massive sands with gradational contacts being introduced periodically from bottom currents when sediment supply or higher energy conditions allowed (Trabucho-Alexandre, 2015; Stow and Smillie, 2020). Reworking by periodic currents or oscillatory flows may then be responsible for convoluted or wavy bedding (Myrow and Southard, 1996).

Interbedded thin mudstone and sandstone sub-facies, tMsSst

The interbedded thin mudstone and sandstone sub-facies comprises repeated units of predominantly arkose and thin intercalated mudstone or siltstone beds that make up $< 10\%$ of the facies (fig. 9.7). Arkosic units are medium to coarse, moderately poorly to moderately well-sorted, with granules of feldspar often scattered throughout. Grains are angular to sub-rounded with moderate to high sphericity. Beds sometimes fine upwards rapidly at their tops, and may be massive or structured. Internal structures are often poorly developed, but tend to comprise silty or fine mm-scale planar and wavy lamination. Cm-scale to dm-scale cross-stratification can be present, as may cm-scale soft-sediment deformation structures. Mud clasts (mm to cm-scale) of varying roundness and angularity may be present. Beds are medium to thick, with sharp bases.

Thin, poorly stratified, conglomeratic units may be present at the bases of sandy units, comprising angular to rounded, moderate to high spericity clasts or varying composition.

Muddy units are thin to medium bedded. They are sometimes silty, with abundant planar or wavy lamination. Their spacing appears non-uniform and varies from dm - 10's m. Wavy lamination is sometimes discontinuous. Shorter discontinuous wavy laminae could represent highly flattened mud clasts. Cm-scale fine sand lenses may occur in isolation, and may show internal cross-lamination. Mud accounts for $< 10\%$, a feature that distinguishes it from other interbedded mud and sandstone sub-facies. The sub-facies has a median thickness of 34.5 m, and makes up 2.2% of total measured facies thickness.

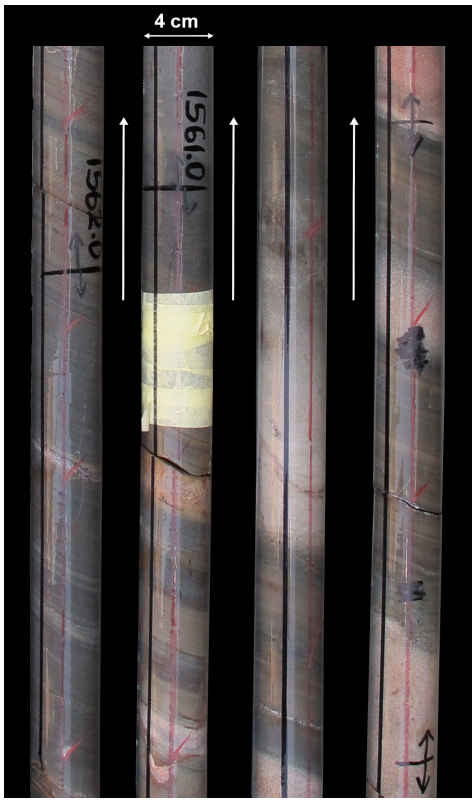

Figure 9.6: The MsgSst sub-facies in the KN192 core, showing sandstones grading into planar laminated siltstone and mudstones. Arrows indicate way-up for the four cores.



Figure 9.7: The tMsSst sub-facies in the KN192 core showing sharp interbedding of thinly bedded laminated mud- and siltstone units with arkosic sandstones.

The sub-facies's bimodal grain size distribution, with well-developed lamination in muddy interbeds, suggest coarse sediment input, followed by periods of quiescence with material settling out

of suspension. Coarse material was likely transported as bedload, on account of larger grain size and moderate to poor sorting (Miall, 2013). Where cross-lamination and soft-sediment deformation structures are prevalent, deposition was likely rapid and from currents in the lower flow regime (Allen, 1966). Where current-generated structures are absent, deposition from sand flows may be invoked (Shanmugam, 1996). Muds and silts were deposited out of suspension, prior to renewed coarse siliciclastic input (Jopling and Walker, 1968; Allen, 1970). The predominance and thickness of sand relative to mud units, indicates that deposition from currents predominated, and was only occasionally punctuated by periods of lower energy.

Interbedded mudstone and clean sandstone sub-facies, MscSst

The interbedded mudstone and clean sandstone sub-facies is characterised by disorderly interbedding of sandstones, predominantly of sub-arkosic composition, and mudstones (fig. 9.8). Mudstones make up $\leq$ 50% of the sub-facies. The sub-arkosic composition and clean appearance of sandy units shows a greater compositional maturity, which differentiates it from other mixed mudstone-sandstone facies (e.g. SstMs, Wck).

Sub-arkosic units are quartz-rich and mud-poor ($<$ 5 %), giving them a light-coloured, clean appearance. Grain size ranges from medium to very coarse, with scattered granules of feldspar; grains are sub-rounded to well-rounded and of moderate to high sphericity. Matrix mud is mostly absent. Minor quantities ($<$ 10 %) of medium to coarse sub-rounded carbonate grains are rare. Sub-arkosic units range from very thin to thickly bedded; grading is rare, and contacts are commonly sharp. They are mostly well-sorted, but may be poorly sorted in dm-thick intervals. Planar lamination and ripple cross lamination are common, the latter often delineated by thin mud-rich foresets. Ripple cross laminae may show a degree of bi-directionality in parts, though it is often not very clear to distinguish in core.

Some interstitial cm-scale sandy beds have a higher mud content ($<$ 50 %), are more poorly sorted, and show discontinuous wavy laminae. Granule-sized clasts within these poorly sorted units are often aligned, and crudely fine upwards, often capped by continuously laminated mudstones and siltstones. Rarely, these poorly sorted sandy units show coarsening up on a cm-scale.

Muddier units show abundant continuous and discontinuous planar lamination, and may contain

both symmetrical and asymmetrical soft-sediment deformation, representing load structures or poorly developed flame structures. They tend to be thinly to medium-bedded. Sandstone dikes are abundant, resulting in a chaotic, but sharply defined penetration of sand into muddy units. Interbedding of clean sand and muddier units may be sharp and planar, or more commonly chaotic, often forming alternating coarsening-fining-up cycles. The sub-facies has a median thickness of 17.5 m and makes up 1.4% of total measured facies thickness.

The interbedded mudstone and clean sandstone sub-facies may form part of the Argillaceous Quartzite unit referred to by Binda (1994).

The interpretation of this sub-facies depends on the symmetry of soft-sediment deformation, orderliness of interbedding between sandy and muddy units, and degree to which ripple lamination is preserved. Asymmetrical soft-sediment deformation, absent or poorly developed ripple lamination, chaotic interbedding of muddy and sandy units, and poor sorting are more indicative of deposition on a slope from high-density turbulent flows – equivalent to S1 units of the Lowe sequence (Lowe, 1982) – or from sandy debris flows (Shanmugam, 1996, 2000). Where soft-sediment deformation structures are asymmetrical, they are interpreted to have formed autokinetically, due to their small scale and restriction to thin and medium-bedded units (Leeder, 1987).

Where the sub-facies is more clearly stratified, better sorted, and current-generated structures are more evident, it is interpreted to have formed by periodic introduction of sand as bedload into a low-energy setting. Ripple cross-lamination in clean sandy units indicate deposition from currents in the lower flow regime (Allen, 1966). During deposition of bi-directionally ripple laminated clean sands, oscillatory flows likely predominated (Allen, 1966; Miall, 2013). The interstitial silt and mudstone beds record suspension settling between periods of sand input. In such a case, soft sediment deformation would be driven by sediment loading, rather than slope instability.

In both interpretations, soft-sediment deformation structures indicate that de-watering had not occurred yet and deposition was very rapid (Owen, 1996). Rapid deposition is also supported by the absence of grading, indicating that suspension settling was restricted to laminated mudstone and siltstone units.

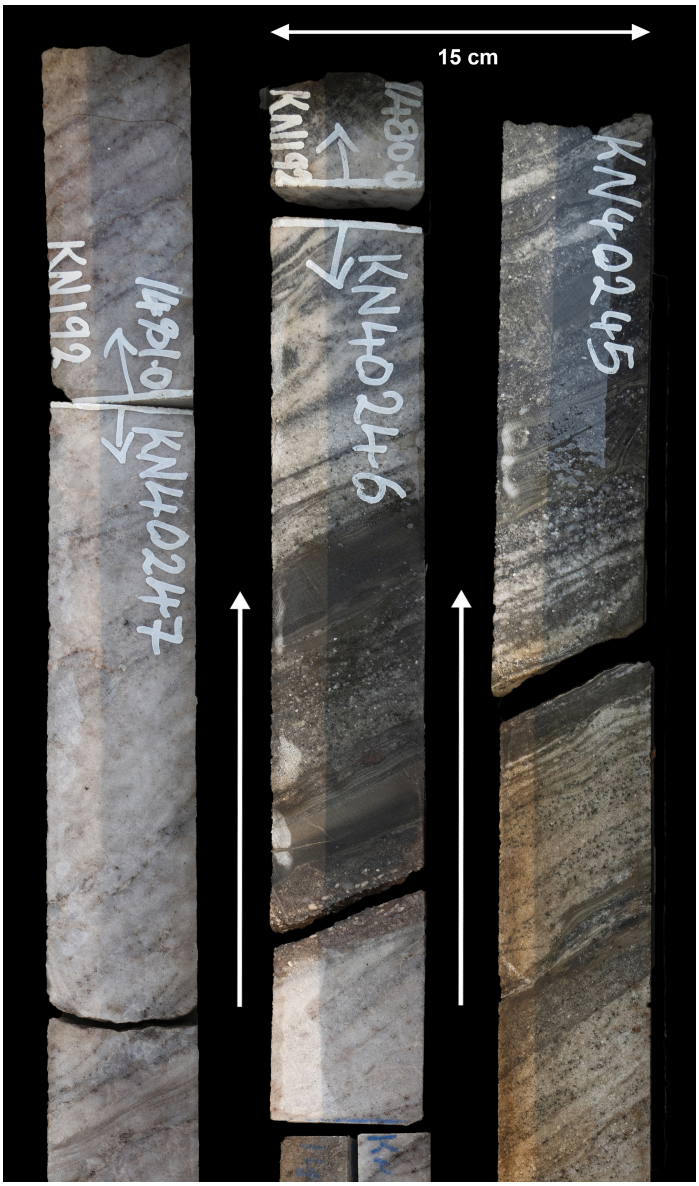

Figure 9.8: The MscSst sub-facies in the KN192 core, showing subarkosic units crudely interbedded with siltstones. Soft-sediment deformation is visible, as are abundant scattered granules. Arrows indicate way-up for the three cores.

Heterolithic facies, Het

The heterolithic facies comprises laminated and thinly interbedded sandstones and silt or mudstones, with characteristic wavy, lenticular or flaser lamination.

Sand is arkosic to sub-arkosic in composition, and fine to coarse in grain size. It ranges from moderately well-sorted to poorly sorted. Grains are round to sub-angular, with low to high sphericity.

Fining-up may occur on a cm-scale.

Mud content ranges from 10 % to 50 %, distinguishing it from the sandy mudstone and interbedded thin mudstone and sandstone facies. Mud units may be silty in parts. Wavy, flaser, and lenticular lamination (Reineck and Wunderlich, 1968) are common – often occurring together on a dm-scale – with wavy lamination being the most common. Wavy lamination may be continuous or discontinuous, the former being more frequent. Cm-scale ripple lamination may be present. Thickness of lamination ranges from thin to thick. The mud:sand ratio typically stays constant on a dm-scale. The facies occurs in packages metres - 10's m thick, with a median facies thickness of 9 m. It comprises 2.8 % of total measured facies thickness and is well-expressed in cores IT26 and KN192.

The facies is interpreted as having been deposited in a setting with cyclically variable current strength or sediment supply, e.g. where there is alternation of slack water and current or wave influence (Martin, 2000). As wavy lamination predominates, conditions must have been favourable for both sand and mud deposition and preservation. Where flaser and lenticular lamination occur, conditions were more favourable for either sand or mud deposition, respectively (Reineck and Wunderlich, 1968; Reineck and Singh, 1980).

Planar laminated sandstone facies, LSst

The planar laminated sandstone facies is composed of variably sorted arkose and sub-arkose. The grain size is generally coarse, but ranges from fine to granular; the facies tends to not be interbedded. The facies is characterised by an abundance of thin planar parallel and sub-parallel lamination. This facies can form part of what Binda and Mulgrew (1974) described as the Footwall Quartzite. The facies thickness ranges from metres to 100's m, with type examples in cores RCB2 and IT26. Three sub-facies are recognised:

Well-sorted planar laminated sandstone sub-facies, wLSst

The well-sorted laminated sandstone sub-facies is generally sub-arkosic in composition, or arkosic with $< 50\%$ feldspar, with minor lithic component. The grain size ranges from fine to coarse, but is generally coarser; grains tend to be sub-angular to sub-rounded, with high sphericity. Very gra-

dational fining-up within beds is common. The facies is mostly well-sorted, occasionally becoming moderately sorted with increasing grain size. Thin planar lamination is common, with coarser portions of the facies becoming more massive. Laminae horizontal or sub-horizontal, thin ($<$ 2 mm) and range in grain size from mud to fine sand. Bed thickness is variable, but tends to be thin to medium. The sub-facies has a median thickness of 8 m, making up 0.8% of total measured facies thickness.

The well-sorted planar laminated sandstone sub-facies shares some compositional characteristics and abundance of planar lamination with the well-sorted arkose facies described by Bull et al. (2011). However, the facies definition used by Bull et al. (2011) is broader, encompassing a greater range of sedimentary structures, which in this facies scheme have been used to divide sub-facies. This sub-facies also shares some visual similarities with the Glassy Quartzite unit mentioned by Binda (1994) and Selley et al. (2005) (e.g. low mud content, high quartz proportion), though primary structures are often sufficiently well-preserved to preclude it from being a true quarzite.

The sub-facies is interpreted to have deposited from unidirectional currents. Deposition from the upper flow regime likely predominated, on account of abundant planar lamination associated with coarser beds (Allen, 1966; Ashley, 1990). The well-sorted nature and compositional maturity of the facies indicates substantial winnowing of lithics and muds. The facies is the result of deposited material being continually reworked, and/or the fines being transported in suspension during deposition of coarser bedload material (Reineck and Singh, 1980; Ashley, 1990).

Poorly sorted laminated sandstone sub-facies, pLSst

The poorly sorted laminated sandstone sub-facies comprises moderately to poorly sorted arkose and sub-arkose (fig. 9.9). The facies can be micaceous, containing $\leq$ 15% muscovite or biotite mica. The grain size is variable, ranging from fine to very coarse, but is mostly coarse with scattered granules. Clasts tend to be sub-angular to sub-rounded with moderate to high sphericity. The bedding thickness is variable, ranging from thin to thick, with beds sometimes fining up. The coarser portions of the facies tend to be more massive, with finer portions showing more well-developed structures. Thin and thick planar laminae are common, in parts becoming slightly wavy. Scour marks are rare. The sub-facies often contains very thinly bedded mud-rich units ($<$ 10%

per facies unit), which can show well-developed thin planar and wavy laminae. The sub-facies is abundant, forming 9.5% of total measured facies thickness, with a median thickness of 35 m.

The facies is interpreted to have been deposited from the upper flow regime, on account of abundant planar lamination (Ashley, 1990; Miall, 2013). The relative textural and compositional immaturity suggests that sediment was likely transported as bedload and deposited more proximally (Allen, 1970; Reineck and Singh, 1980). Thin mud-rich laminae suggest periodic waning of flow strength to deposit finer material. The poorer sorting and greater proportion of mica suggest less reworking and/or more proximal deposition, or a different provenance compared to the well-sorted laminated sandstone sub-facies.

Cross-stratified sandstone facies, XSst

The cross-stratified sandstone facies comprises ripple-laminated and cross-bedded sandstones, commonly arkose and sub-arkose (fig. 9.10). The facies tends to be moderately sorted, fine to coarse-grained, with sub-angular to sub-rounded clasts of moderate to high sphericity. The facies is characterised by cm to dm-scale cross stratification.

Ripple cross-lamination predominates in finer sands. Ripple marks are asymmetric and occur in isolation or sets on a dm-scale. Sets of ripple cross-laminated sand may be separated by dm to m-scale sets of plane-bedded sand. Foresets of ripples vary in geometry. Climbing ripples may be present. Cm-scale gutter casts occur but are rare. Bounding surfaces of the ripple cosets tend to be bed-parallel, sharp and straight or slightly undulose. Mm-scale to cm-scale mud clasts of varying roundness and angularity may be scattered throughout the facies. Bed thickness is commonly thin or medium.

In cross-bedded portions of the facies, trough and planar cross-bed sets are generally well-developed, with co-sets being $<$ 1 m thick. As far as could be determined in core, the cross-bedding appears to be predominantly simple. Foresets are planar to concave, and frequently delineated by very thin laminae of fine sands and silts. Co-sets of planar cross-beds tend to be bounded by planar, sub-parallel bedding surfaces. Herringbone cross-stratification may be present, though often more difficult to discern in narrow-diameter core. Bedding thickness tends to be medium. The facies occurs in packages of metres - 10's m in thickness, with a median thickness of 25 m. It makes up

4.8% of total measured facies thickness. RCB2 is the type core for the facies.

The cross-stratified sandstone facies shares some compositional and structural similarities with well-sorted arkose facies defined by Bull et al. (2011). However, the facies definition used by Bull et al. (2011) is broader than the one proposed here. The cross-stratified sandstone facies described here is also characterised predominantly by its primary structures, as opposed to the degree of sorting. The cross-stratified sandstone facies may comprise the Footwall Quartzite described by Binda and Mulgrew (1974).

The cross-stratified sandstone facies is interpreted to have formed as a result of sub-aqueous ripple and dune migration in the lower flow regime (Ashley, 1990). Where ripple marks show trough cross-lamination, ripples were possibly undulatory and where ripple cross-lamination is planar, ripples were likely straight-crested (Allen, 1966). Deposition of bedload predominated when foresets are planar, whereas simultaneous settling from bedload and suspension is more likely when foresets are more asymptotical; the presence of climbing ripples indicates periods of increased accumulation rate (Ashley et al., 1982). Planar and trough cross-bedding indicates migration of 2-D and 3-D dunes, respectively (Ashley, 1990). Where there is an absence of clear direction reversal of cross-beds, unidirectional sediment transport and deposition from currents – as opposed to oscillatory or bi-directional flows – is inferred (Reineck and Singh, 1980).

Clast-supported conglomerate facies, CCgm

The clast supported conglomerate facies comprises granular, gravel and cobble size conglomerates with predominantly clast-supported fabric. Composition of the facies varies, ranging from arkose to lithic-arenite. Clast shape is variable, ranging from angular to rounded. Matrix mud content is $< 25\%$. Minor, thin mud-rich beds may be present. Well-stratified units commonly show primary structures. The facies occurs in packages of variable thickness, which increase with increasing grain size, from metres (e.g. core KN192) to 100's m (e.g. core RCB2).

The clast-supported conglomerate facies and its sub-facies comprise what Binda and Mulgrew (1974) described as the Basal (Boulder) Conglomerate, Second Conglomerate, and Footwall Conglomerate and Sandstone.

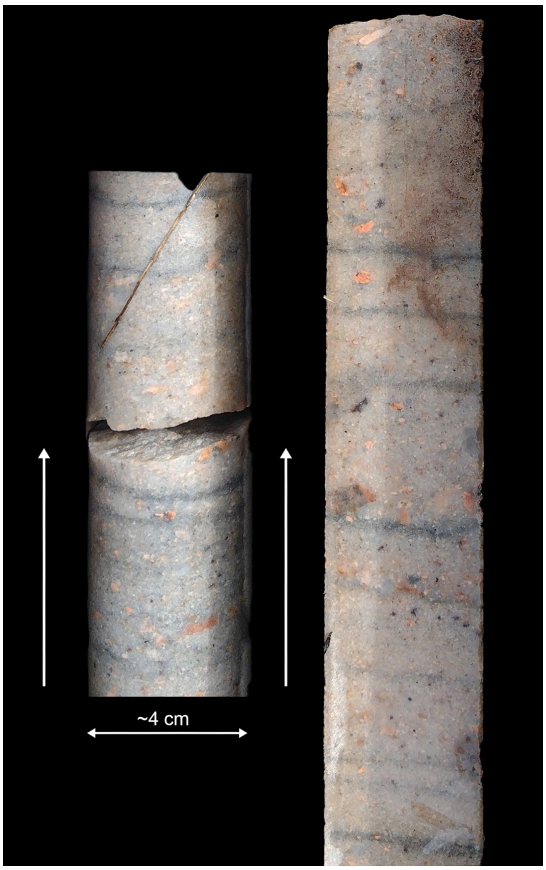

Figure 9.9: The pLSst sub-facies in the IT26 core displaying characteristic poor sorting, with granule-sized feldspar clasts dispersed in a poorly laminated arkose. Arrows indicate way-up.



Figure 9.10: The XSst facies in the IT26 core showing trough cross-stratification, with silty laminae delineating foresets. Arrow indicates the way up.

Fine stratified clast-supported conglomerate sub-facies, fCCgm

The fine clast-supported conglomerate sub-facies comprises granular, and in parts pebbly, oligomicts of sub-arkose to lithic arenite composition (fig. 9.11). $\sim 75\%$ of clasts are > 1 mm in diameter; the maximum clast size is < 15 mm (medium pebble). Mud and silt content is $< 10\%$.

Clasts are predominantly sub-rounded with moderate sphericity. The sub-facies is uniformly poorly sorted. Planar lamination is abundant. Cm to dm-scale cross-beds are common; their foresets are tabular or concave and delineated by fine sands or mud drapes. Bed contacts are straight, but often diffuse. Beds frequently fine upwards. Bedding thickness ranges from thin to medium. The sub-facies has a median thickness of 2 m and makes up 0.2% of total measured facies thickness.

The sub-facies is interpreted to have been deposited from bed load in unidirectional currents, on ac-

count of a lack of bi-directional current indicators (Nemec and Steel, 1984; Todd, 1989). Fining-up units are interpreted as the result of waning current strength. Crude planar lamination in very coarse, granular and pebbly intervals likely represents upper plane bed sedimentation (Allen, 1970). Poorly developed cross-bedding suggests movement of dunes (Allen, 1970), and makes deposition from sandy debris flows or high density turbidites less likely (Lowe, 1982; Shanmugam, 2000, 2021).

Coarse stratified clast-supported conglomerate sub-facies, sCCgm

The stratified clast-supported conglomerate sub-facies comprises polymict gravel to cobble-conglomerates. Clasts are round to sub-angular; their sphericity is moderate to high. The minimum clast size is $<$ 15 mm (medium pebble).

The matrix is mostly arkosic sand, with grain size ranging from coarse to granular. Imbrication, where present, is poor. Planar lamination is most common in sandy interbeds, where poorly developed planar and trough cross-lamination may also be present. The sub-facies becomes more clearly stratified with finer grain size, and more diffusely stratified with increasing grain size (pebble or larger). Bedding thickness is medium to thick, where discernible in core. Beds and bed sets sometimes fine upwards, with finer units often delineating bed contacts. Bedding planes, where apparent, are frequently undulose. Internal erosion surfaces tend to be poorly developed. Occasionally, clast-supported and more matrix-supported units are juxtaposed (the matrix can range from muddy to sandy). The clast:matrix ratio can sometimes reduce, with the matrix becoming more muddy ($\leq$ 50 %), towards the tops of units. The sub-facies has a median thickness of 8 m and comprises 5.4% of total measured facies thickness

The stratified clast-supported conglomerate sub-facies could be the result of several depositional processes. Where the sub-facies is clearly stratified, with units repeatedly fining-up, and clasts are more rounded, it is interpreted to be streamflow or current-generated and deposited from bedload (Nemec and Steel, 1984; Todd, 1989). Sandy interbeds which are are laminated or cross-stratified were likely deposited from the lower flow regime (Allen, 1966). Where the facies is better sorted and mud content is lower, particularly in units that fine upwards, fluid turbulence likely predominated to allow for settling of coarser clasts, and mud being carried away in suspension (Miall, 2013). Where mud content increases significantly towards the tops of beds, the sub-facies may represent a

debris flow deposit. In these cases, flows were likely more cohesive, deposited via frictional freezing, with sandy cross-stratified units representing streamflow between periods of coarser mass flow input (Lowe, 1982; Nemec and Steel, 1984; Todd, 1989).

Disorganised clast-supported conglomerate sub-facies, dCCgm

The disorganised clast-supported conglomerate sub-facies comprises gravel and cobble, typically oligomict, conglomerates (fig. 9.12). The sub-facies is predominantly arkosic. Clasts vary from round to highly angular, frequently within the same bed. The sphericity of clasts ranges from very low to high. The matrix is muddy to sandy. Imbrication, where present, is poorly developed. The sub-facies does not tend to show clear stratification and is at best diffusely stratified. Stratification is often delineated by abrupt variation in clast:matrix ratios, rather than changes in grain size. Beds, where discernible, occur on a dm to m-scale. The very poor sorting, grain shape variation and poor or absent stratification give the sub-facies its disorganised appearance. The fabric is predominantly clast-supported; however, subordinate, dm-scale intervals that are matrix-supported are not uncommon. These latter units comprise $\leq$ 25 % of the sub-facies and have a sandy, and less commonly a mud-rich, matrix. The sub-facies has a median thickness of 14 m and makes up 0.4 % of total measured facies thickness.

With few primary structures and poor stratification, the exact nature of the depositing flows is difficult to determine. Paucity of fining-up sections and the textural immaturity indicate that turbulence was limited during deposition. The sub-facies likely represents cohesive debris flows deposited via cohesive freezing (Lowe, 1982; Nemec and Steel, 1984; Shanmugam, 2021). In the matrix-poor portions of the sub-facies the matrix possibly acted as a lubricant for movement, rather than fully supporting the larger clasts (Lowe, 1982). In units where clast angularity is very high, sphericity is lower, and matrix mud content is higher, inter-granular dispersive pressure was likely reduced and the flow more cohesive, limiting grain interactions (Lowe, 1982; Todd, 1989). Alternatively, the angularity and low sphericity of clasts might be the result of proximal deposition, and less indicative of flow process, whether cohesive or non-cohesive (Lowe, 1982; Shanmugam, 2021).

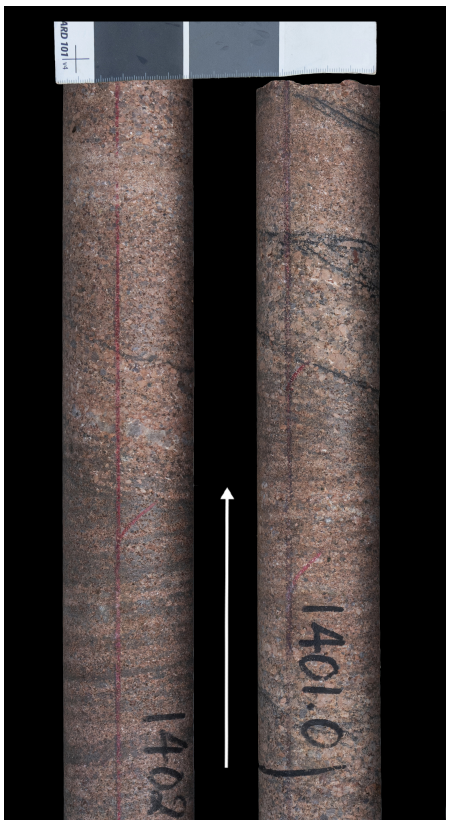

Figure 9.11: The fCCgm sub-facies in the KN192 core, showing clear cross-stratification. Arrows indicate way-up for the cores. Mm-scale QP card for scale.



Figure 9.12: Sub-facies dCCgm in the KN192 core. Note the range of clast angularity and sphericity. Arrows indicate way-up for the cores. Mm-scale QP card for scale.

Diamictite facies, Dia

The diamictite facies comprises matrix-supported polymict conglomerates. Clast compositions are varied, e.g. quartzite, granite, schist (Robert, 1940). Striated clasts and dropstones have been documented by numerous authors, and are widespread across the basin (Stutzer, 1911; Binda and Van Eden, 1972; Master and Wendorff, 2011). The matrix tends to be very fine, clay-rich, and often admixed with $<$ 1 mm clasts of quartz, feldspar, and muscovite, and fragments of granite and quartz porphyry (Master and Wendorff, 2011).

Binda and Van Eden (1972) divided the Grand Conglomerat into three main facies: the 'pebbly mudstone', 'layered siltstone and argillite', and 'isolated pebbles in finely layered beds'. The 'pebbly mudstone' facies and the 'isolated pebbles in finely layered beds' facies broadly correspond to the clast-poor diamictite sub-facies in this scheme. If the clasts are predominantly dolomitic in the 'peb-

bly mudstone' facies, they are assigned to the carbonate diamictite sub-facies in this facies scheme. The clast-rich diamictite sub-facies described herein likely falls between the 'pebbly mudstone' facies and 'minor conglomeratic beds within diamictites' described by Binda and Van Eden (1972). Wendorff and Key (2009) described diamictites across the Zambian copperbelt, noting many characteristics which correspond to depositional interpretations of the three diamictite sub-facies in this scheme (e.g. evidence of glacial clast rain-out, debris flows, and carbonate-bearing conglomerates). The two predominant sub-facies proposed in this scheme are clast-rich and clast-poor diamictites, differentiated by their clast proportion (> 20 % or ≤ 20 %, respectively, figs 9.13,9.14). The diamictite facies occurs in packages 10's m thick; the type core for the facies is L83, in which both the Grand and Petit Conglomerat are expressed, and KN192.

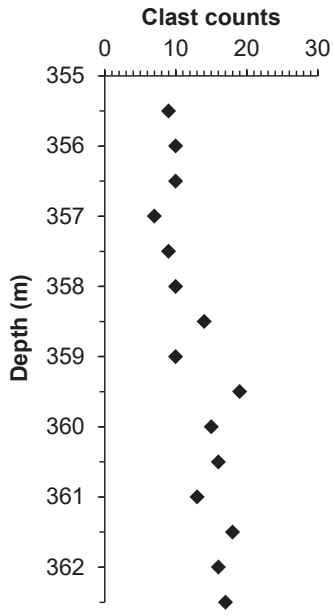

Figure 9.13: Clast counts for the crDia sub-facies in the ZMSDD003 core, measured at 0.5 m intervals, showing higher clast proportion and tendency for upwards clast quantity reduction.

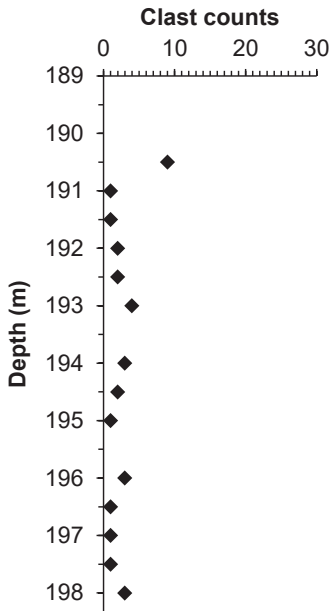

Figure 9.14: Clast counts for the cpDia sub-facies in the ZMSDD003 core, measured at 0.5 m intervals, showing significantly lower clast counts (< 10 clasts / 0.5 m).

Clast-rich diamictite sub-facies, crDia

The clast rich diamictite facies is characterised by poorly sorted matrix-supported polymict conglomerate, containing > 20 % clasts (fig. 9.15). Clasts range in size from granules to cobbles. They

are angular to rounded, and of low to high sphericity. Clast composition is varied; the sub-facies may contain clasts of quartzite, gneiss, mica schist, granite, andesite or chert. Clasts sometimes show 'wrap-around' fabrics, with smaller grains arranged around a larger clast, which may vary in composition with respect to the central clast. Imbrication of clasts can occur in the most clast-rich portions of the sub-facies. Rarely, isolated cm-scale clusters of sub-angular to rounded sand and gravel-sized grains stand out in a finer, silty or muddy matrix. The clusters often have a moderately rounded shape.

The matrix is predominantly muddy or silty, often massive, and occasionally shows continuous – mostly planar – laminae. These laminae can occur in small sets, forming laminites. Rarely the matrix is sandy, showing poorly developed wavy lamination. The sub-facies is occasionally punctuated by thin sandy interbeds, which may fine upwards. Stratification tends to be indistinct, but the facies appears medium to very thickly bedded, where discernible. The median thickness of the sub-facies is 23 m. It makes up 1.6% of total measured facies thickness.

The sub-facies is interpreted to have been generated by debris flows. The abundance of muddy matrix, absence of fining-up and poor sorting suggests a lack of fluid turbulence and makes deposition from cohesive flows via cohesive freezing more likely (Lowe, 1982; Dasgupta, 2003; Shanmugam, 2021). Sandy interbeds likely separate individual debris flow units. Their frequent fining-up indicates that they were deposited from turbulent flows. They possibly represent lofted portions on top of debris flows (Talling et al., 2012; Shanmugam, 2021), turbidity currents or sandy debris flows (Talling et al., 2012; Shanmugam, 2000). The presence of isolated rounded clusters of grains surrounded by a finer matrix may be interpreted as ice-rafted debris, potentially indicating a weak glacial influence (Bennett et al., 1996).

Alternatively, this facies may represent sub-aerial debris flow freezing at the terminus of a glacier. Varying degrees of liquefaction and fluid turbulence may result in crude stratification of grading similar to what is observed in this sub-facies (Lawson, 1982).

Clast-poor diamictite sub-facies, cpDia

The clast-poor diamictite is a matrix-supported polymict conglomerate, containing $\leq$ 20 % clasts (fig. 9.16). Clasts rarely exceed pebble size, but are as compositionally varied as in the clast-rich

diamictite sub-facies. Clasts also tend to have a higher sphericity, and be more rounded. The matrix is uniformly muddy or silty. It is predominantly unstructured, rarely showing planar lamination, which may be deformed around clasts. Lonestones are common. Thin sandy interbeds are rare. Stratification is unclear or absent, but bedding appears to be thick or very thick. The median thickness of the sub-facies is 40 m. It makes up 2.1% of total measured facies thickness.

The facies is interpreted to have formed by settling out of suspension in a low-energy setting, as opposed to mass flows (Reineck and Singh, 1980). This is supported by the abundance of fine-grained matrix, presence of undisturbed planar lamination, and deformation of laminae around the base of some clasts. Clasts that deform underlying laminae are interpreted as dropstones that settled out of suspension following ice rafting (Bennett et al., 1996; Hoffmann et al., 2004). As the observed clasts did not appear to represent pyroclastic material, a volcanic origin of outsized clasts is excluded for now (Bennett et al., 1996).



Figure 9.15: The crDia sub-facies in the ZMSDD003 core, showing variation in clast size and composition (e.g. andesite, mica schist). Arrows indicate way-up for the two cores.



Figure 9.16: The cpDia sub-facies in the ZMSDD003 core, showing a lower clast count and average size. Grey patches are reduction spots. Arrows indicate way-up for the three cores.

Carbonate diamictite sub-facies, CaDia

The carbonate diamictite sub-facies shares characteristics of both the clast-rich and clast-poor diamictite sub-facies, with the difference that > 20 % of clasts are composed of carbonate. Clast range in size from granules to coarse pebbles and tend to be sub-rounded to rounded; sphericity ranges from low to high. The sub-facies is predominantly matrix-supported with isolated cm- to dm-scale intervals that are clast-supported (fig. 9.17).

The matrix is muddy to silty, and may contain variable quantities of carbonate, frequently dolomite. Lamination is rare, and may in isolated cases be deformed around clasts. The clast-rich portions of the facies can show well-developed imbrication and sub-horizontal to horizontal alignment. The sub-facies is poorly stratified or unstratified, with stratification being slightly clearer in clast-supported intervals. The facies appears predominantly thickly bedded, with clast-supported intervals being thinly to medium-bedded. The median thickness of the sub-facies is 6 m. It makes up 0.5% of total measured facies thickness.

The sub-facies is interpreted to have been deposited mainly by debris flows. This is on account of lack of fining-up, poor sorting and abundance of matrix mud. Flow during deposition appears to have been predominantly laminar, due to common horizontal clast alignment and abundance of low sphericity clasts, suggesting grain-to-grain interactions were limited (Lowe, 1982; Shanmugam, 1996). The flows were therefore likely to be cohesive, with matrix strength supporting outsized clasts, and deposited via cohesive freezing (Lowe, 1982; Shanmugam, 2021). Where clasts clearly deform underlying laminae, they may be interpreted as dropstones, suggesting weak glacial influence (Bennett et al., 1996).



Figure 9.17: The CaDia sub-facies in the KN192 core with variably angular, mostly low sphericity, clasts embedded in a dolomitic, silty matrix. Arrow indicates the way up for both cores.

Interbedded carbonate-mudstone facies, CaMs

The carbonate-bearing mudstone facies comprises silty mudstones interbedded with thin to medium-bedded carbonates ($<$ 50 % within a facies unit), which are commonly dolomitised (fig. 9.18). Lamination in the mudstones is predominantly continuous and planar. Carbonates occur as laminae and beds. Thin carbonate laminae occur in isolation or small cm to dm-scale sets, often showing continuous wavy lamination. They show little to no internal structure, and appear micritic. In rare cases they are deformed and/or discontinuous. Beds of carbonate are thin to medium-bedded. Interbedded mudstone-carbonate packages can have thicknesses of 10's m. Carbonate may rarely be disseminated throughout the mudstone. Asymmetrical shear structures and soft-sediment deformation within the mudstones are rare, as are isolated edgewise conglomerates and scour marks. Thin beds of silt or fine sand may occur in minor quantities ($<$ 10 %), often with sharp bases and fining upwards. Thickness of mudstone beds varies, from medium to very thick. The facies occurs in packages that are 10's m thick, with a median thickness of 20.5 m. It makes up 4.8% of total measured facies thickness and is well-expressed in cores ZMSDD003 and KN192.

The facies is interpreted as having been deposited out of suspension in a low energy environment, in the absence of significant oscillatory flow (Reineck and Singh, 1980). Coarser material was periodically introduced with sufficient energy to rework and scour the substrate. Edgewise conglomerates indicate periodic agitation of sediment and proximal or in-situ re-deposition (Sepkoski, 1982). The source of the carbonate is difficult to constrain, but may be the result of precipitation, or ooid shoals that were dolomitised post-deposition (Hood et al., 2015; Hood and Wallace, 2018). Deposition on a gentle slope appears likely where there is evidence for asymmetrical soft-sediment deformation and shearing.

Carbonate-bearing siltstone facies, CaSl

The carbonate-bearing siltstone facies comprises siltstones with $>$ 10 % carbonate component. The carbonate is frequently dolomitised. Thin mudstone and fine sandstone beds may occur in minor ($<$ 10 %) quantities. Carbonate may be disseminated, finely laminated, or – rarely – thinly interbedded.

Lamination tends to be planar and is less commonly wavy. Scour marks, soft-sediment deformation structures and edgewise conglomerates are rare. Bed contacts are mostly sharp, rarely erosional. Carbonate tends to be disseminated or may be concentrated in lighter laminae. These laminae may be thick or thin. Bedding thickness varies, but tends to be thin or medium. The amount of primary structures tends to decrease with increasing bed thickness, with thick and very thick beds often being unstructured. The facies ranges in thickness from 10's to 100's m. The facies has a median thickness of 18 m and is common, making up 12.7% of total measured facies thickness. Type examples are found in cores KN192 and L83.

Sediment settling out of suspension in a low-energy, carbonate producing environment is the likely depositional mechanism for this facies (James and Dalrymple, 2010). Energy conditions were periodically sufficient to generate wavy lamination and scour the substrate. Where soft-sediment deformation is present, elevated accumulation rates were likely. Massive intervals of carbonate-bearing siltstone are enigmatic, and preclude detailed interpretation at this stage. However, the lack of evidence for wave-reworking suggests low-energy deposition. Where carbonate forms discrete beds, it may represent direct precipitation, or dolomitised ooids (Hood et al., 2015).

Laminated silty carbonate facies, lSlCa

The laminated silty carbonate facies has a conspicuous striped appearance showing tight interbedding and alternating lamination of carbonate and silt or mudstone (fig. 9.19). Carbonate accounts for 50 - 75 % of the facies, occurring in thin or very thin beds, or as individual laminae. Beds are densely laminated, thin and thick laminae being abundant. Lamination is continuous and frequently wavy, sometimes irregularly lobate along the length of laminae and tends to be parallel or sub-parallel. Thicker laminae may be compositionally graded or compositionally inversely graded on a mm-scale.

Muddy and silty units are commonly planar laminated, and are thinly or very thinly bedded, rarely occurring as individual laminae. They frequently grade into or out of carbonate beds and laminae. Contacts with carbonate beds and laminae are rarely straight. The interbedded and interlaminated carbonates and silts are arranged in dm to m-scale packages of rhythmites and laminites (the former mainly characterised by equidistance between repeating laminae), often resembling varves. The

facies occurs in units 10's m thick; it has a median thickness of 18 m and makes up 1.1% of total measured facies thickness. The type core for the facies is ZMSDD003.

The laminated silty carbonate facies is comparable to the Calcaire Rose unit, with Alvarez and Maurin (1991) noting similarly rhythmic lamination in silts and carbonates. The facies shares some similarities with the 'finely layered facies' described by Binda and Van Eden (1972), showing a varved appearance.

The facies is interpreted to have formed via suspension settling in a low-energy setting that may be periodically agitated by oscillatory flows to generate undulation in laminae. Compositional grading within laminae indicates gradual changes in siliciclastic sediment supply during deposition Zolitschka et al. (2015). Siliciclastic sediment supply was reduced or attenuated to form carbonate units, with minor siliciclastic input generating fine laminae. The repetition of carbonate and silty laminae and beds suggest cyclical processes exerted a significant control on deposition (Reineck and Singh, 1980; Zolitschka et al., 2015).

Carbonate-bearing heterolithic facies, CaHet

The carbonate-bearing heterolithic facies is composed of finely inter-bedded and laminated carbonate-bearing mud-, silt- and sandstones. It is similar to the heterolithic facies (Het), but is distinguished by a significant ($>$ 10 %) carbonate content, with carbonate commonly being dolomitised (fig. 9.20). Minor anhydrite ($<$ 10 %) may be present.

Mudstones occur mostly as thin to thick laminae, which may coarsen-up into silts or very fine sands. Muddy or silty flasers occasionally bifurcate. Sand ranges in grain size from very fine to coarse, and may occur as laminae or thin to medium beds with sharp bases. Lenses of fine to medium sand tend to be symmetrical. Continuous and discontinuous lamination are ubiquitous. Thin and thick wavy lamination is abundant, with laminae often fining upwards. Scour marks and soft-sediment deformation structures may be present at the base of sandier units.

Carbonate tends to occur in the matrix and as thin to thick micritic lamination, or as thin to beds with sharp contacts. Laminae of carbonate may be planar and straight, but are commonly wavy or can bifurcate as flasers. Mudstone, sandstone and carbonate units are interbedded on a cm-scale, forming thin to medium-bedded heterolithic beds. The facies ranges in thickness from 10's to 100's

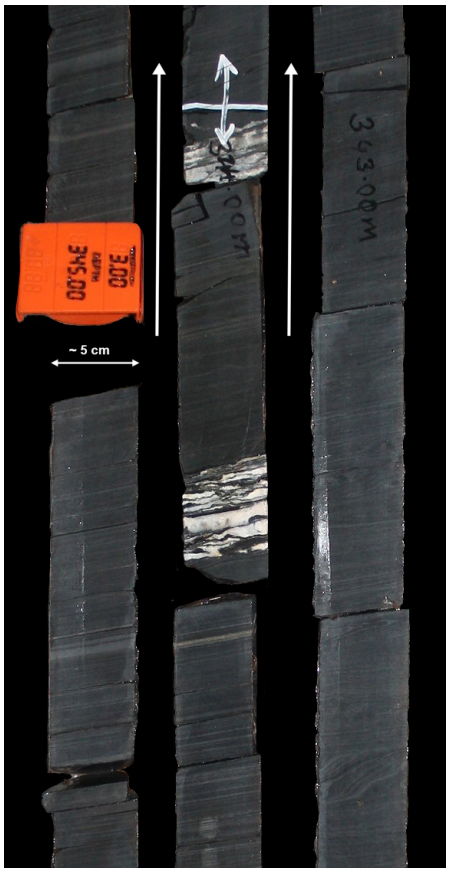

Figure 9.18: The CaMs facies in the ZMSDD003 core, showing planar lamination, shear structures, and thin carbonate beds. Arrows indicate way-up for the three cores.

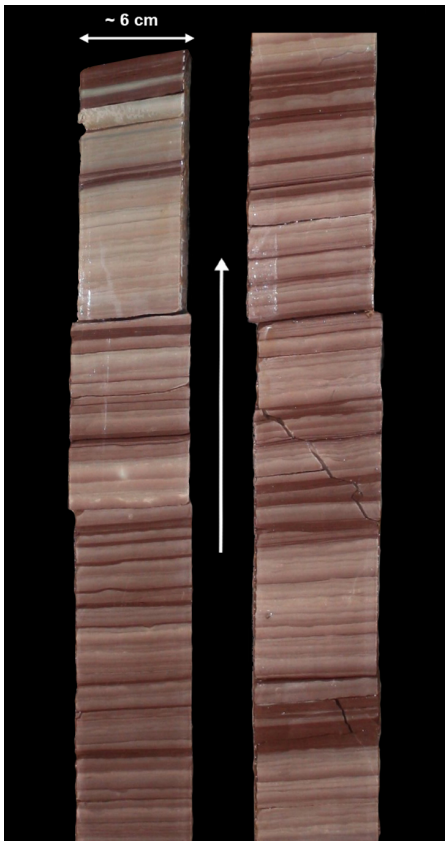

Figure 9.19: The lSlCa facies in the ZMSDD003 core, showing abundant rhythmic graded laminites in carbonate and siltstone. The arrow indicates way-up for the two cores.

m, with a median facies thickness of 17 m. It makes up 3.5% of the total measured facies thickness. KN192 is the type core for this facies. The facies shares some similarities with the description of the South Ore Body Shale by Clemmey (1974) where flaser bedding occurs in conjunction with dolomitic siltstones.

The facies is interpreted to have been deposited sub-aqueously under fluctuating, bi-directional, or oscillatory flow in a mixed clastic-carbonate system (Reineck and Wunderlich, 1968; Siahi et al., 2016). Energy conditions were high enough to generate discontinuous bedding, but insufficiently high to transport grains coarser than medium sand. Conditions allowing both mud and sand deposition and preservation are inferred (Reineck and Wunderlich, 1968).

Carbonate-bearing sandstone facies, CaSst

The carbonate-bearing sandstone facies comprises sub-arkoses and sub-litharenites with < 50 % carbonate, which may occur as discrete grains or in the matrix. Both siliciclastic and carbonate clasts are fine to very coarse grained, and may rarely reach fine gravel size (fig. 9.21). Clasts are generally sub-angular to sub-rounded with moderate to high sphericity. The facies is well-sorted, showing well-developed primary structures. It may be interbedded with thinly bedded mudstones and siltstones, or show mud-rich laminae. Continuous planar lamination is common, as is ripple cross-lamination, dm-scale planar and trough cross-stratification, and herringbone cross-stratification. Cross-bed sets tend to be bounded by planar, horizontal bedding surfaces. Laminae and ripple foresets are often delineated by darker muds to fine sands. The carbonate components of the facies tend to be pervasively dolomitised. Bedding thickness ranges from thin to thick. Facies units are 10's m thick, with a median thickness of 8 m. The facies makes up 0.6% of total measured facies thickness and is expressed well in core IT26.

The carbonate-bearing sandstone facies is interpreted to have been deposited by currents in a moderate to high-energy marine setting. Ripple marks and cross-bedding indicate ripple and dune migration, respectively (Allen, 1966). Abundant primary structures indicate deposition took place from currents that were oscillatory, bi-directional or uni-directional (Allen, 1970; Ashley, 1990). The low mud fraction suggests either a lack of mud at source, or finer material being winnowed. The presence of dunes, a carbonate component, textural and compositional maturity suggest sediment was being continuously re-worked in a higher-energy marine setting, with proximal siliciclastic source (Siahi et al., 2016).

Sandy carbonate facies, SstCa

The sandy carbonate facies is varied in composition and structure, but is characterised by > 50 % carbonate and interbedded – often carbonate-bearing – sand or mudstone. The facies tends to be pervasively dolomitised and may comprise thin to thick beds of crystalline carbonate, packstone or ruddstone, up to pebble size, with rounded, high sphericity grains in thin to thick beds.

Medium-grained sub-arkose and sub-litharenite may occur as a minor component within carbonate

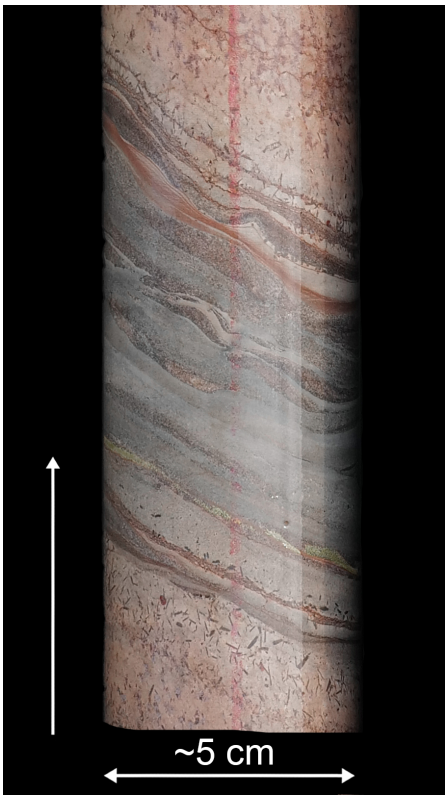

Figure 9.20: The CaHet facies in the KN192 core, showing discontinuous wavy sand laminae interbedded with silty, carbonate-bearing mudstone and carbonate. Arrow indicates way-up.

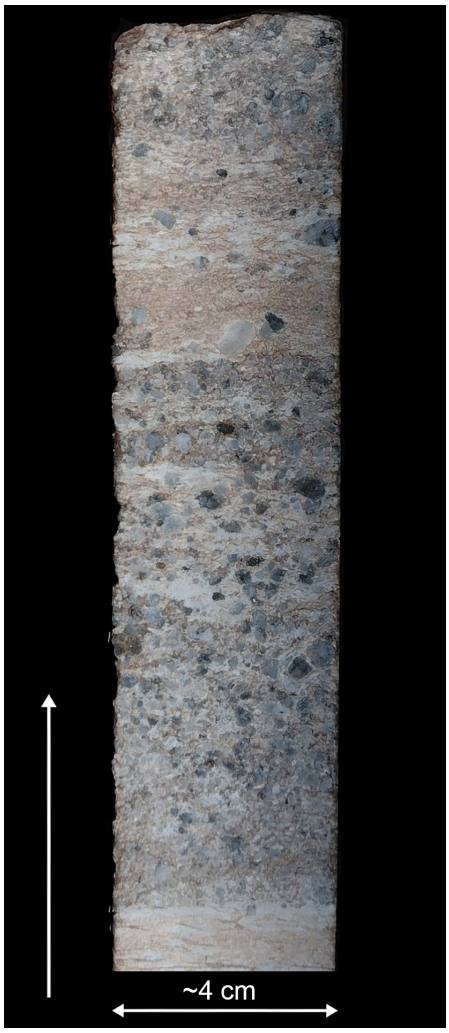

Figure 9.21: Facies CaSst in the IT26 core with very coarse to fine gravel-sized sublitharenite with dolomitic matrix. The arrow indicates way-up.

units, or in discrete thin interbeds. Thin mudstone and siltstone beds, sometimes forming dm-scale groups of laminites, can punctuate carbonate units.

Planar lamination, continuous and discontinuous wavy lamination are common; cross-lamination is rare. Carbonate units may co-occur with heterolithic units, creating mixed sets of densely interlaminated carbonate, sandstone and mudstone. The facies occurs in packages metres to 10's m thick, with a median thickness of 18 m, making up 1.5% of total measured facies thickness. It is expressed well in cores L83 and RCB2.

Depositional mechanisms of the sandy carbonate facies are varied. Carbonate-rich units with a

lower mud content were likely deposited in a high-energy shallow marine setting, on account of minor siliciclastic input and rounded grains in packstones and ruddstones (Siahi et al., 2016). Where facies composition is more mixed, the proportion of siliciclastics is higher and lamination is more abundant, bi-directional flows and rapid fluctuations in energy likely predominated (James and Dalrymple, 2010; Siahi et al., 2016).

Clast-supported carbonate conglomerate, CaCgm

The clast-supported carbonate conglomerate facies is similar to the disorganised clast-supported conglomerate sub-facies, with the difference that it contains $>$ 20 % carbonate clasts (fig. 9.22). Clasts show variable roundness and commonly low sphericity, ranging in size from gravel to pebbles, and may be imbricated. The matrix is predominantly granular and sandy, with interstitial carbonate mud. Matrix-supported intervals are rare. It is sometimes interbedded with dm-scale sandy units of variable composition, often lithic arenites or lithic greywackes. The facies is diffusely stratified or unstratified, but appears thickly bedded. Soft-sediment deformation and water-escape structures are isolated, and may form discordant cm to dm-scale pipe-like structures in which muds and sands are mixed in swirled textures. The facies occurs in units metres to 10's m thick, with a median thickness of 4 m. It comprises 0.6% of total measured facies thickness, and is well-expressed in KN192.

The facies appears similar to the 'carbonate clast conglomerate' at the Mushishima River described by Wendorff and Key (2009), on account of mixed carbonate-clastic composition and dolomitic cement.

The facies is interpreted to have been deposited from subaqueous debris flows. The absence of clear stratification and grading suggests limited turbulence during transport (Lowe, 1982; Miall, 2013). The facies was likely deposited from cohesive debris flows via cohesive freezing (Lowe, 1982; Shanmugam, 2021). This is evidenced by the low sphericity of many clasts, suggesting limited inter-granular dispersive pressure, with micritic mud in the matrix possibly acting as a lubricant during movement (Lowe, 1982). This could suggest predominantly laminar flow (Shanmugam, 1996). However, the facies could also be interpreted as representing a sandy debris flow, on the basis of relatively low mud content in a detrital matrix and abundance of granule-sized material

(Shanmugam, 1996). De-watering structures and soft sediment deformation could have resulted from the reversal of density gradients (Lowe, 1975). Fluidisation is likely the cause of pipe-like de-watering structures, where they are discordant (Lowe, 1975). Where clasts are tabular in shape and strongly imbricated, they may represent rip-up clasts redeposited with minimal transport from the sites of erosion (Sepkoski, 1982).

Massive carbonate facies, MCa

The massive carbonate facies comprises predominantly dolomitic crystalline carbonate with little discernible primary structure. Laminae are rare, but tend to be mud-rich. The facies may contain disseminated silt or mud (< 20 %). Minor (< 5 %) anhydrite is occasionally present, occurring as variably-orientated seams and infilling void spaces. Bedding is poorly developed, and bed contacts often unclear. Where discernible, the facies appears medium to thickly bedded. Contacts may be sharp or diffuse. Mm to cm-scale stylolites are preserved in parts. The facies occurs in units 10's m thick, with a median thickness of 14 m. It makes up 4.8% of total measured facies thickness and is well-expressed in core L83.

The massive carbonate facies shares the characteristics of Chingola Dolomite units (and local variations thereof) mentioned by Binda and Mulgrew (1974) and Bull et al. (2011). It is equivalent in part to the 'massive white dolomite facies' described by Bull et al. (2011), though the scheme proposed here has further sub-divided the massive white dolomite facies described by these authors on the basis of microbialites and anhydrite content.

Interpretation of this facies is difficult on account of limited diagnostic sedimentary structures. The paucity or lack of siliciclastic material suggests clastic supply was restricted or distal. It is unclear, however, whether massive carbonates originally were syn-sedimentary precipitates (e.g. ooid shoals), or to what extent they were biotically mediated and represent carbonate reefs (Hood et al., 2015; Hood and Wallace, 2018).

Laminated carbonate facies, LCa

The laminated carbonate facies comprises crystalline, predominantly dolomitic, carbonate. The facies is characterised by abundant lamination. Silt and mud content varies; anhydrite and fine sand may occur in minor quantities. The facies occurs in units 10's m thick; type cores are ZMSDD003 and L83.

Planar laminated carbonate sub-facies, pLCa

The planar laminated carbonate sub-facies comprises mostly dolomitised crystalline carbonate (fig. 9.23). Mud and silt content is low (< 10 %), making up abundant thin planar laminae. Wavy thin laminae are rare. Lamination is parallel, sometimes showing slight grading. Mm-scale stylolites may be present. Bedding thickness is difficult to discern on account of abundant of lamination, but appears thin to medium. The sub-facies has a median thickness of 10 m, and makes up 1.1% of total measured facies thickness.

The sub-facies is interpreted to have formed in a low-energy environment, with little to no oscillatory flow agitating the substrate. The minor siliciclastic component suggests a distal or restricted clastic sediment supply (Hood et al., 2015; Siahi et al., 2016).

Variably laminated carbonate sub-facies, vLCa

The variably laminated carbonate sub-facies comprises crystalline, commonly dolomitised, carbonate. It has a higher siliciclastic content (< 50 %) of fine sand, silt, and mud than the planar laminated carbonate sub-facies, proportions of which vary. The sub-facies can also contain minor anhydrite (< 10 %). Disseminated phlogopite may also be present (Bull et al., 2011).

Lamination is abundant and ranges from thick to thin, planar to wavy. Cross-lamination is rare and difficult to discern on account of pervasive recrystallisation. Thin muddy and silty beds may be variably laminated and interbedded, with clastic:carbonate rations varying within interbedded sections. The facies is thinly to medium-bedded, with bed contacts commonly being sharp. The median thickness of the sub-facies is 25.5 m; it makes up 11.8% of total measured facies thickness.



Figure 9.22: Facies CaCgm in the KN192 core, showing poor sorting and clast-supported texture with minor sulphide mineralisation. The arrow indicates way-up for both cores.

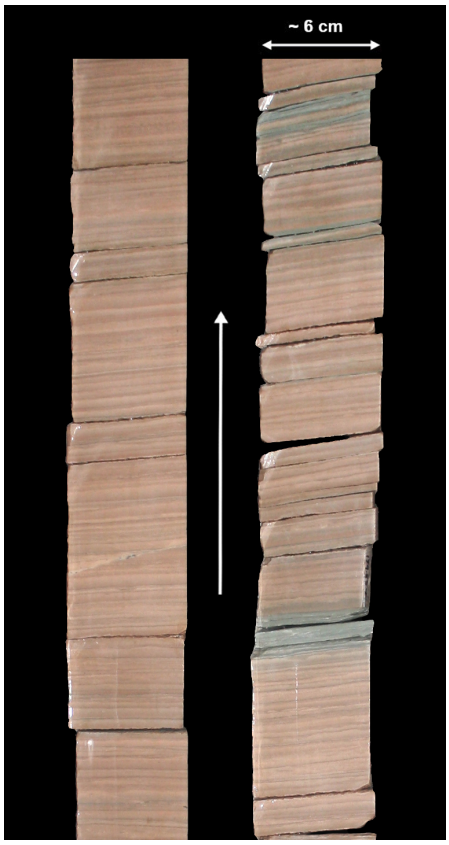

Figure 9.23: The pLCa sub-facies in the ZMSDD003 core, showing ubiquitous parallel planar lamination and low silt-content. The arrow indicates way-up for both cores.

The sub-facies shares many of the characteristics of the 'dolomitic siltstone facies' and 'bedded grey dolomite facies' described by Bull et al. (2011). Similarities include the presence of planar lamination, thin interbedding of units and silt component. Depositional mechanisms are difficult to constrain on account of recrystallisation convoluting abundant primary structures. A low-energy carbonate-producing environment with fluctuating amounts of siliciclastic sediment input likely predominated (Siahi et al., 2016). Abundance of wavy lamination suggests continuous reworking of beds; where present, cross-lamination could indicate either deposition from currents or oscillatory flows (Allen, 1966).

Red karst facies, Rk

The red karst facies comprises predominantly dolomitic carbonate with distinctive red or orange colouration, and may show brecciated tops. Dissolution textures are varied and abundant. Remnant carbonate often shows cauliflower or nodular textures with abundant interstitial red-brown clay seams. Clay is preferentially concentrated in the most porous portions of carbonate, which frequently show sponge-like dissolution textures and fenestral fabrics. Fenestrae and void spaces are may be filled with calcite. Remnant carbonate sometimes preserves planar and wavy laminae. Red karst facies units tend to have sharp, sometimes irregular, bounding surfaces.

The facies occurs in units that are metres - 10's m thick. Its median thickness is 2 m. It makes up 0.5% of total measured facies thickness. Type examples are found in the KN192 and L83 cores.

The facies is interpreted to record the dissolution of primary carbonates, leaving residual haematite-rich clays and fenestral fabrics (Kenny and Knauth, 2001). The calcite-filled vugs may be the result of seawater percolating through void spaces (James and Dalrymple, 2010).

Anhydrite-rich carbonate facies, AnCa

The anhydrite-rich carbonate facies comprises carbonates containing > 10 % anhydrite. Carbonates are predominantly dolomitic. They occur either as crystalline units with a paucity of primary structures and often sugary texture, or as poorly laminated units with < 25 % silt or mud component. Cm-scale nodular textures are common. Thin and very thin beds of laminated fine sand, silt and mud may occur periodically between carbonate units. Abundant primary, often bedding-parallel, anhydrite characterises this facies. Chickenwire and enterolithic textures, as well as displacive anhydrite nodules are common (fig. 9.24). Secondary anhydrite frequently occurs in void spaces or as veins. Bed contacts tend to be sharp. Bedding thickness varies from thin to thick. The facies thickness ranges from metres to 10's m, with a median thickness of 10 m. It comprises 5.2% of total measured facies thickness, with type examples in the L83 core.

The anhydrite-rich carbonate facies shares many similarities with the dolomitic siltstone facies described by Bull et al. (2011), which also notes anhydrite nodules and casts after gypsum. The facies is interpreted to have formed under evaporitic conditions, with displacive anhydrite textures being

the result of early diagenesis (James and Dalrymple, 2010; Christeleit et al., 2015).

Microbialite facies, Mic

The microbialite facies consists of sandy and minor silty carbonates, showing what may be interpreted as stromatolitic structures.

As the identification of microbially induced sedimentary structures (MISS) is difficult in core, identifaction was based mainly on Noffke (2009). Microbialites are only interpreted 1.) in cores that did not show strong tectonic fabrics 2.) in portions of the stratigraphy that were interpreted to be transgressive 3.) where mud proportion was low 4.) where facies formed part of intertidal or shallow marine facies associations 5.) where the geometry of MISS matches that of known ancient and modern examples.

Stromatolitic structures show mixed clastic-carbonate layering, with repeating mm-scale fine sandy laminae (fig. 9.25). Primary lamination may also be delineated by very thin haematite laminae. Stromatolitic structures may be domal and rounded, or columnar, sometimes with serrated textures. They occur on a cm-dm scale and at a variety of orientations, commonly upright or inclined. Domal geometry varies in height and radius of curvature. Cm-scale rounded relief can be superimposed on top of laminae sets. Bedding thickness is difficult to discern but tends to be an order of magnitude larger than the microbial structures themselves, in the order of metres - 10s m. The facies thickness ranges from 10's to 100's m and is well-expressed in cores IT26 and KN192, with a median thickness of 49.5 m. It makes up 5.6% of total measured facies thickness. The facies is shown in figure 9.25.

The facies encompasses several units described by other authors, including the Algal Dolomite unit (Annels, 1974), reef dolomite (Cailteux et al., 1994; Binda, 1994) and biohermal reef dolomite (Fleischer, 1984).

The variable orientation and geometry of the microbial structures suggests formation in either intertidal and sub-tidal zones (Beukes and Lowe, 1989; Hood et al., 2015). The degree of linkage between microbial structures is difficult to ascertain due to the diameter constraints of drill core.

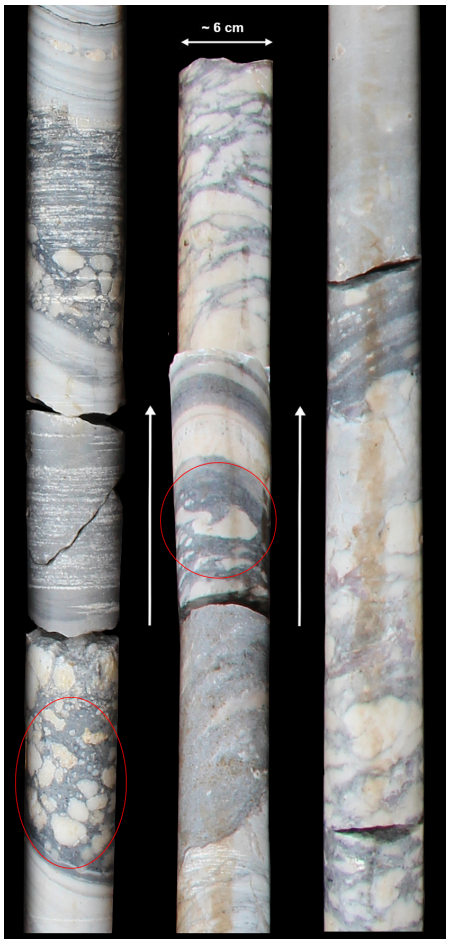

Figure 9.24: The AnCa facies in the L83 core, characteristic of the sabkha facies association. Nodular anhydrite and enterolithic structures (circled red) embedded in grey silty dolomite are abundant. Arrows indicate way-up for the three cores. The core begins in the lower left-hand corner.

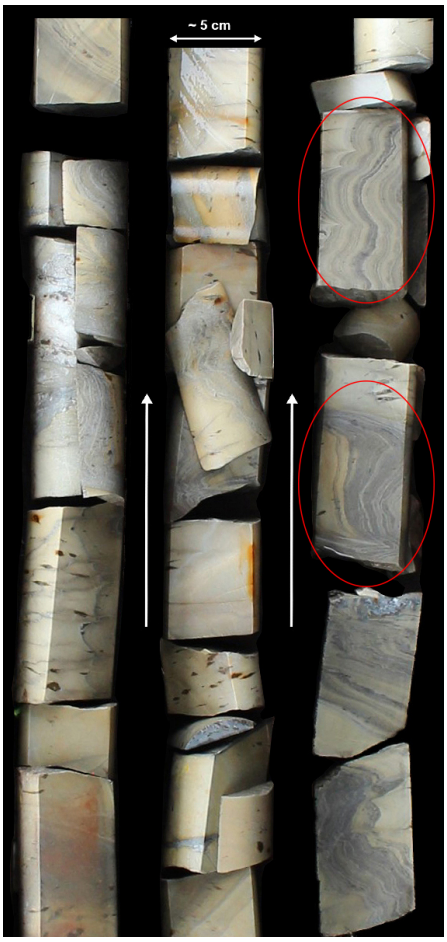

Figure 9.25: The StMic facies in the IT26 core, showing microbially induced sedimentary structures that characterise the facies (circled red), which are interpreted as domal and columnar stromatolites. Arrows indicate way-up for the three cores. The core begins in the lower left-hand corner.

Appendix II – Stratigraphic logs

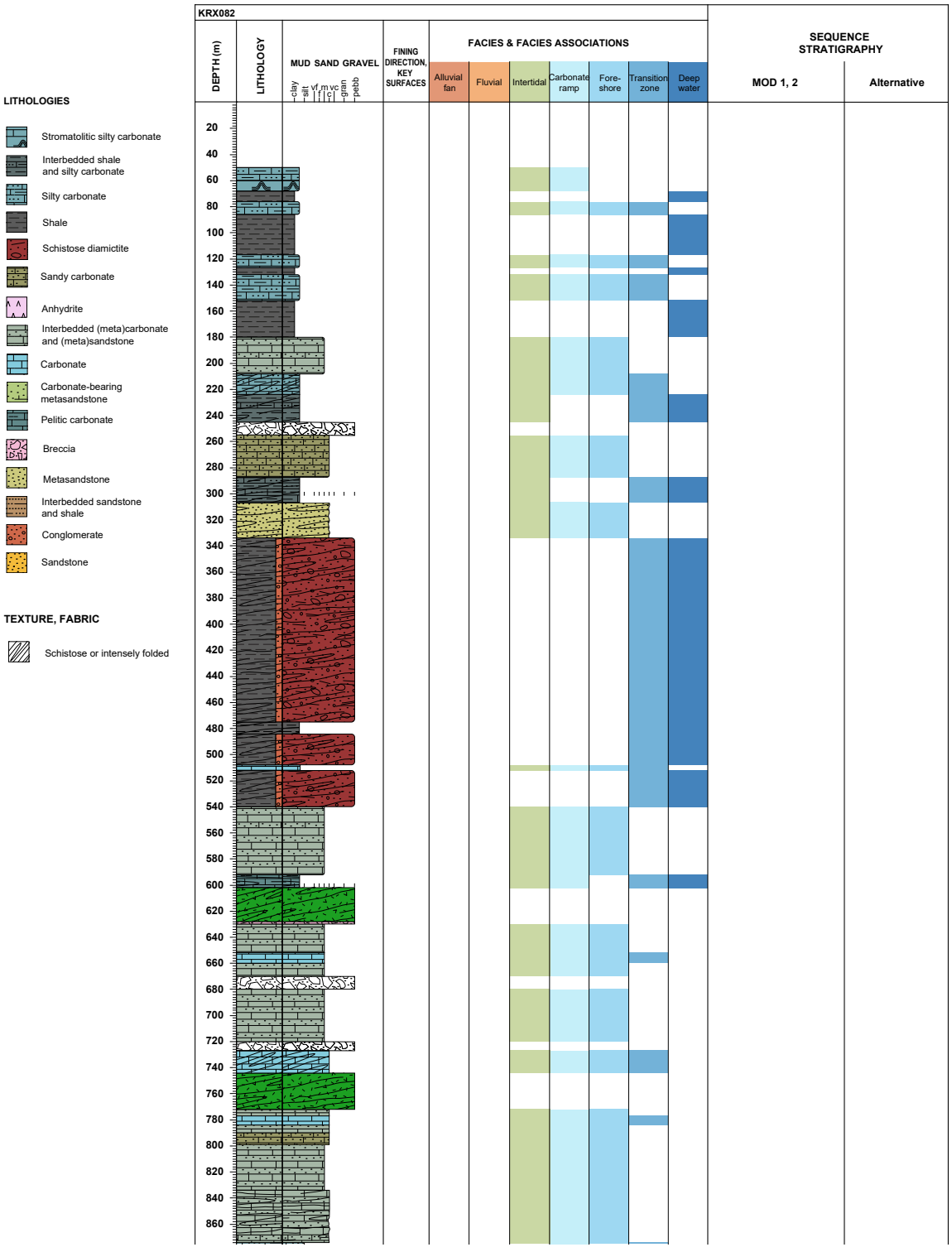

Figure 9.26: KRX082 (Solwezi) stratigraphic log

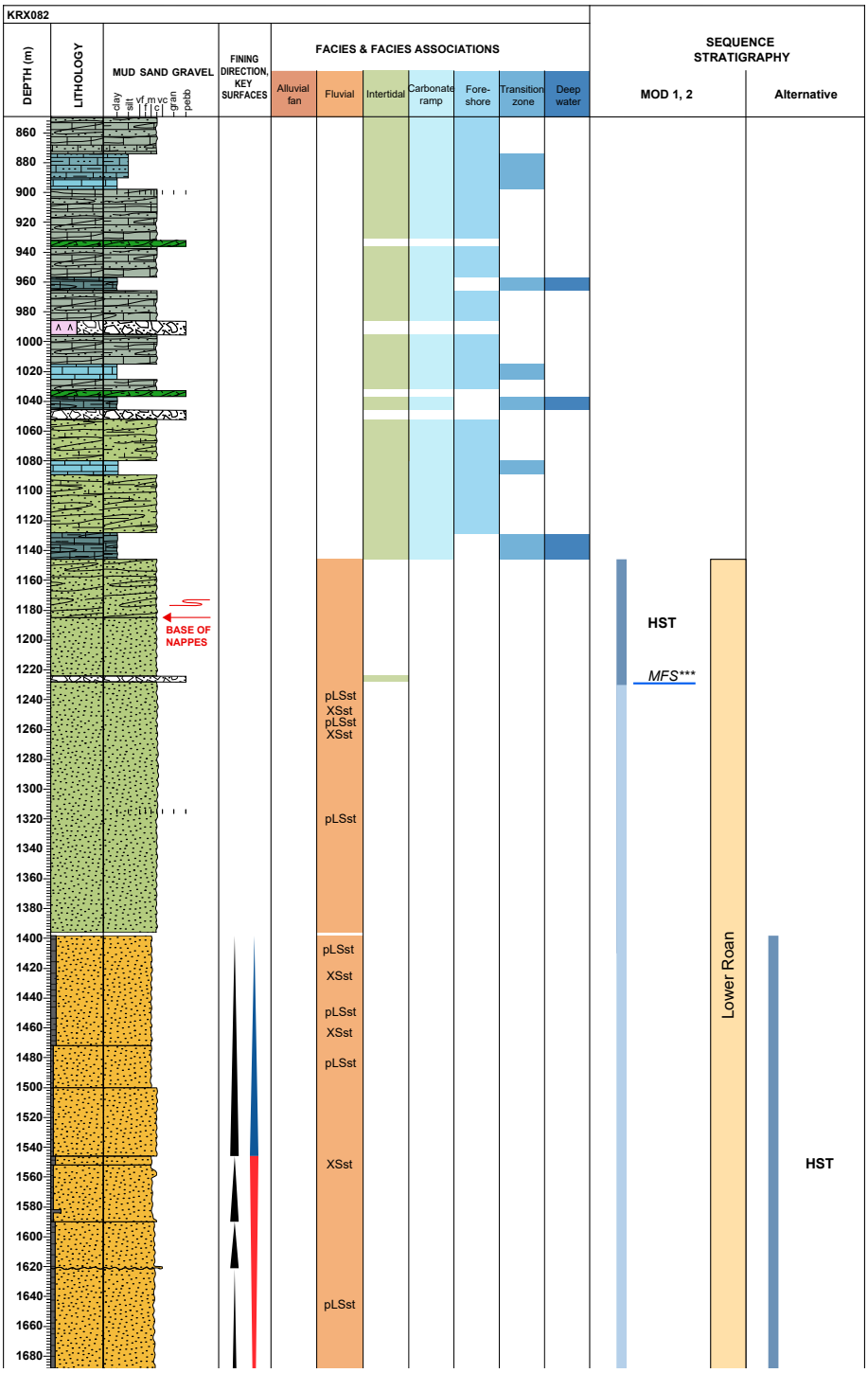

Figure 9.27: KRX082 (Solwezi) stratigraphic log, continued

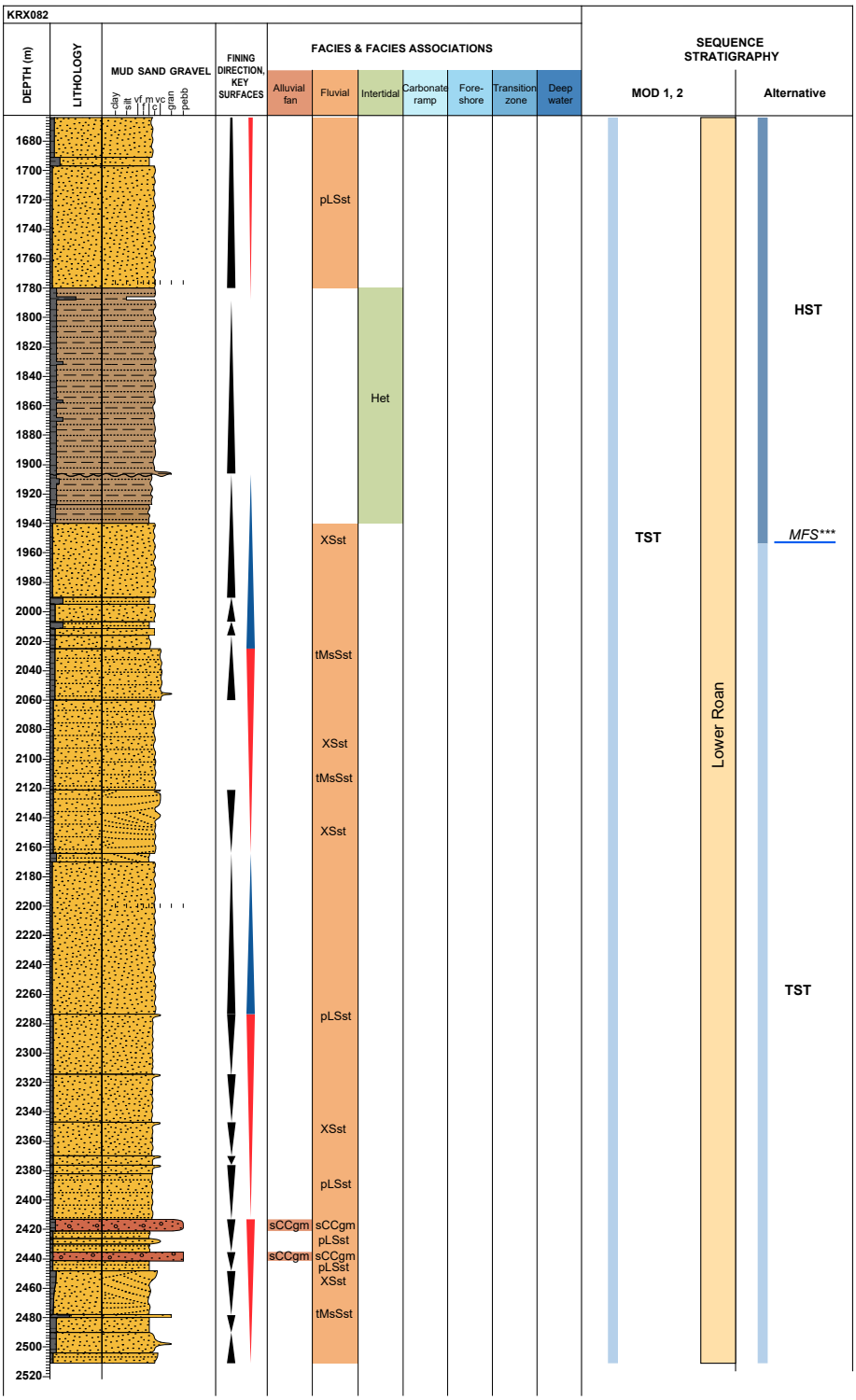

Figure 9.28: KRX082 (Solwezi) stratigraphic log, continued

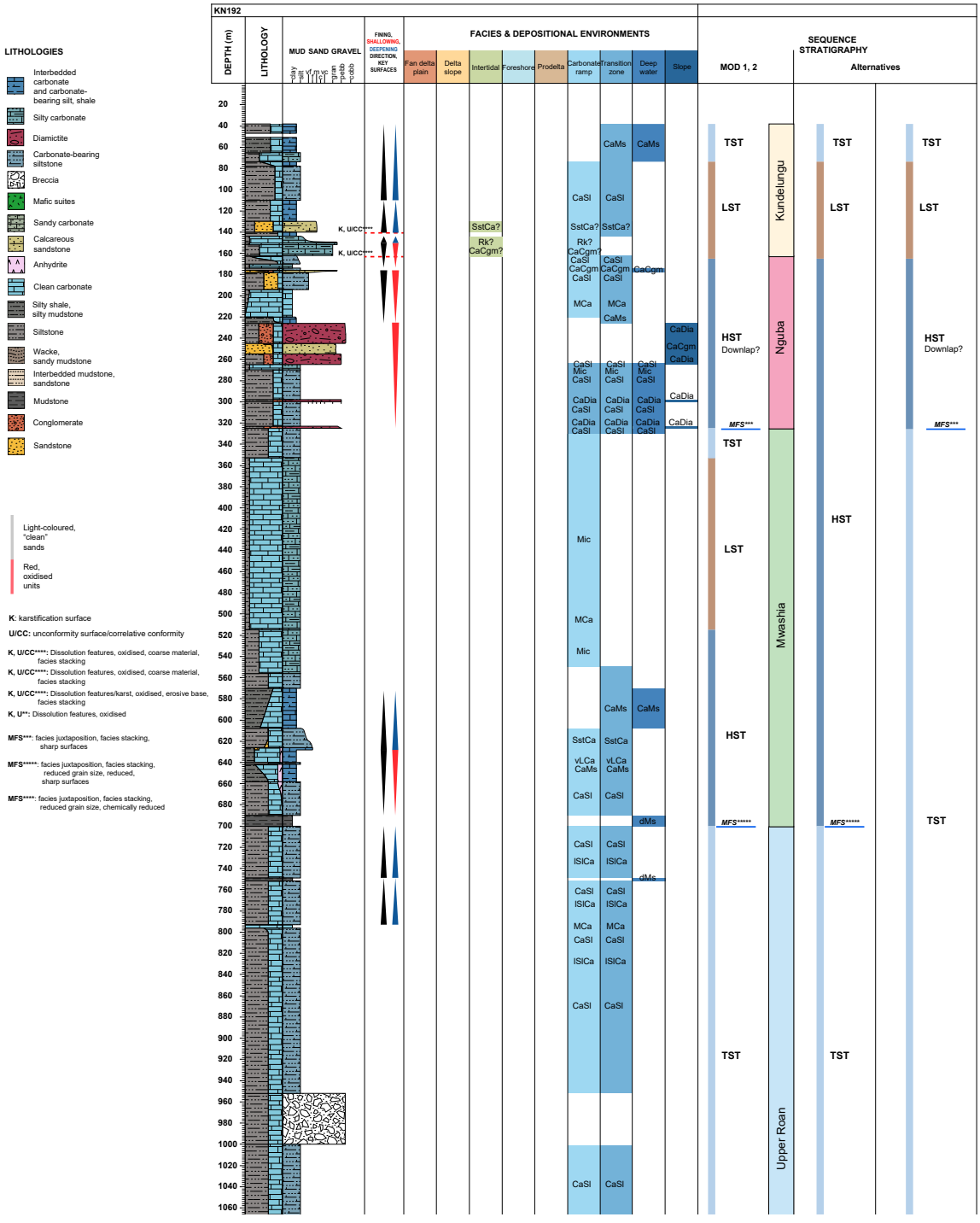

Figure 9.29: KN192 (Lubambe) stratigraphic log

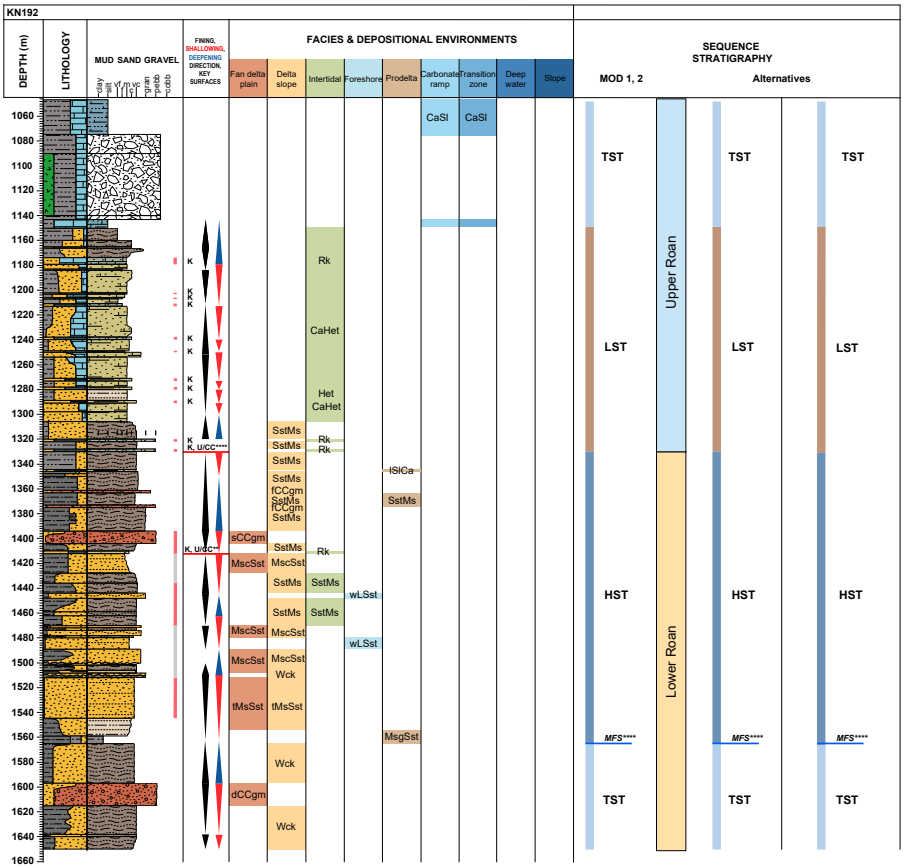

Figure 9.30: KN192 (Lubambe) stratigraphic log, continued

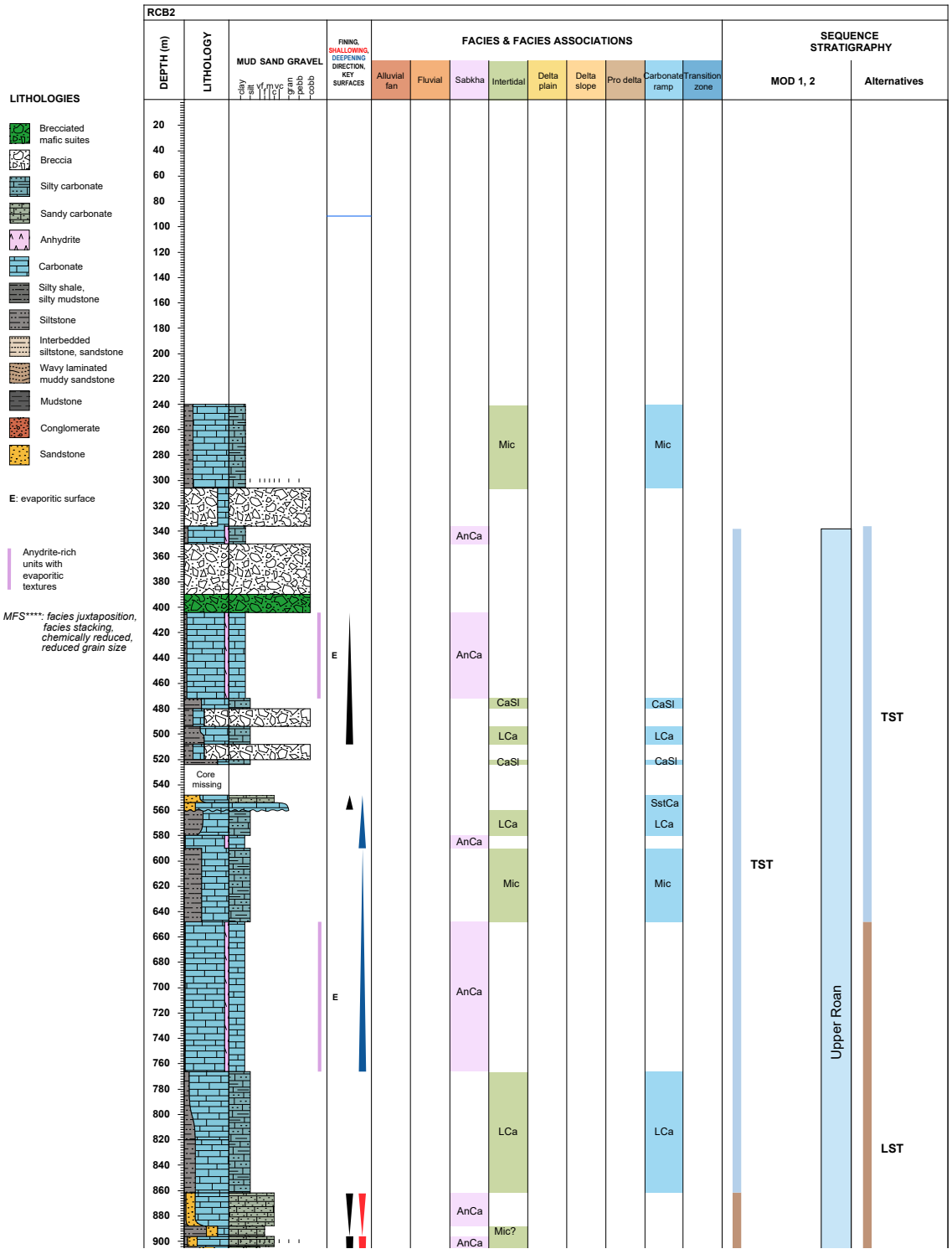

Figure 9.31: RCB2 (Chambishi) stratigraphic log

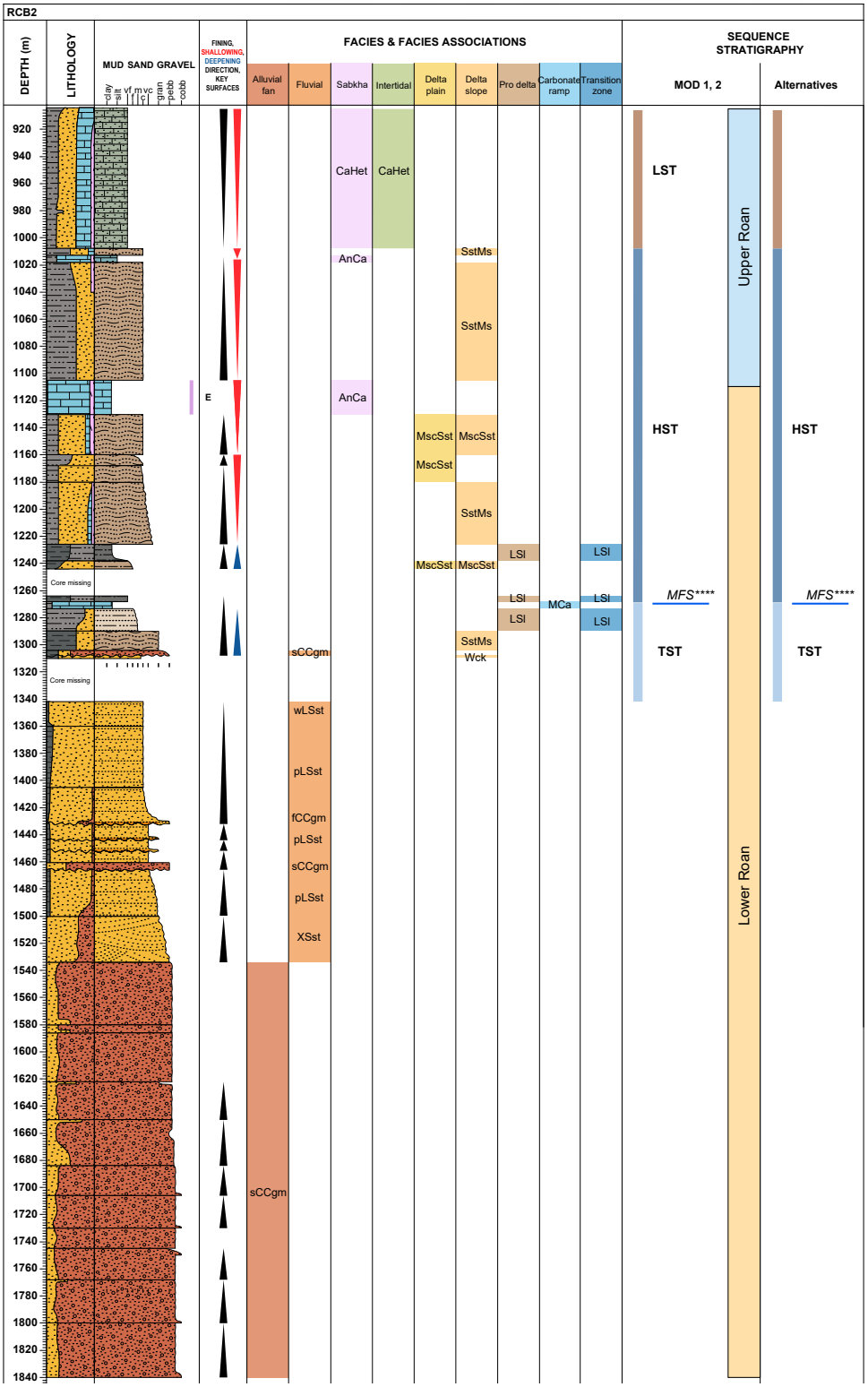

Figure 9.32: RCB2 (Chambishi) stratigraphic log, continued

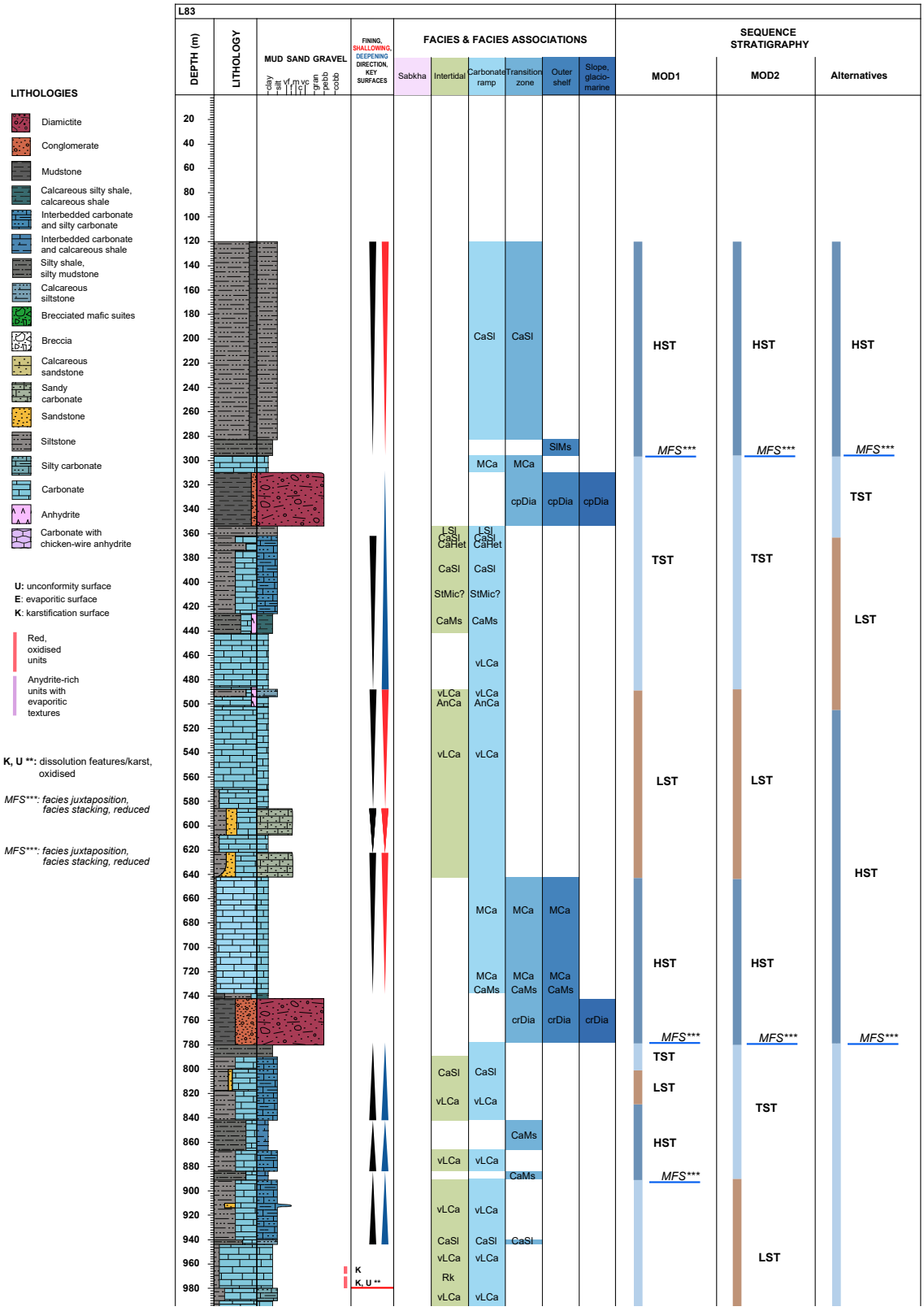
LITHOLOGIES
Diamictite
Conglomerate
Mudstone
Calcareous silty shale, calcareous shale
Interbedded carbonate and silty carbonate
Interbedded carbonate and calcareous shale
Silty shale, silty mudstone
Calcareous siltstone
Brecciated mafic suites
Breccia
Calcareous sandstone
Sandy carbonate
Sandstone
Siltstone
Silty carbonate
Carbonate
Anhydrite
Carbonate with chicken-wire anhydrite
U: unconformity surface
E: evaporitic surface
K: karstification surface
Red, oxidised units
Anydrite-rich units with evaporitic textures
K, U **: dissolution features/karst, oxidised
MFS***: facies juxtaposition, facies stacking, reduced
MFS***: facies juxtaposition, facies stacking, reduced
L83
DEPTH (m)
LITHOLOGY
MUD SAND GRAVEL
clay
silt
vf
f
m
c
vc
gran
pebb
cobb
FINING, SHALLOWING, DEEPENING DIRECTION, KEY SURFACES
FACIES & FACIES ASSOCIATIONS
Sabkha
Intertidal
Carbonate ramp
Transition zone
Outer shelf
Slope, glacio-marine
SEQUENCE STRATIGRAPHY
MOD1
MOD2
Alternatives
HST
MFS***
TST
LST
HST
MFS***
TST
LST
HST
MFS***
TST
LST

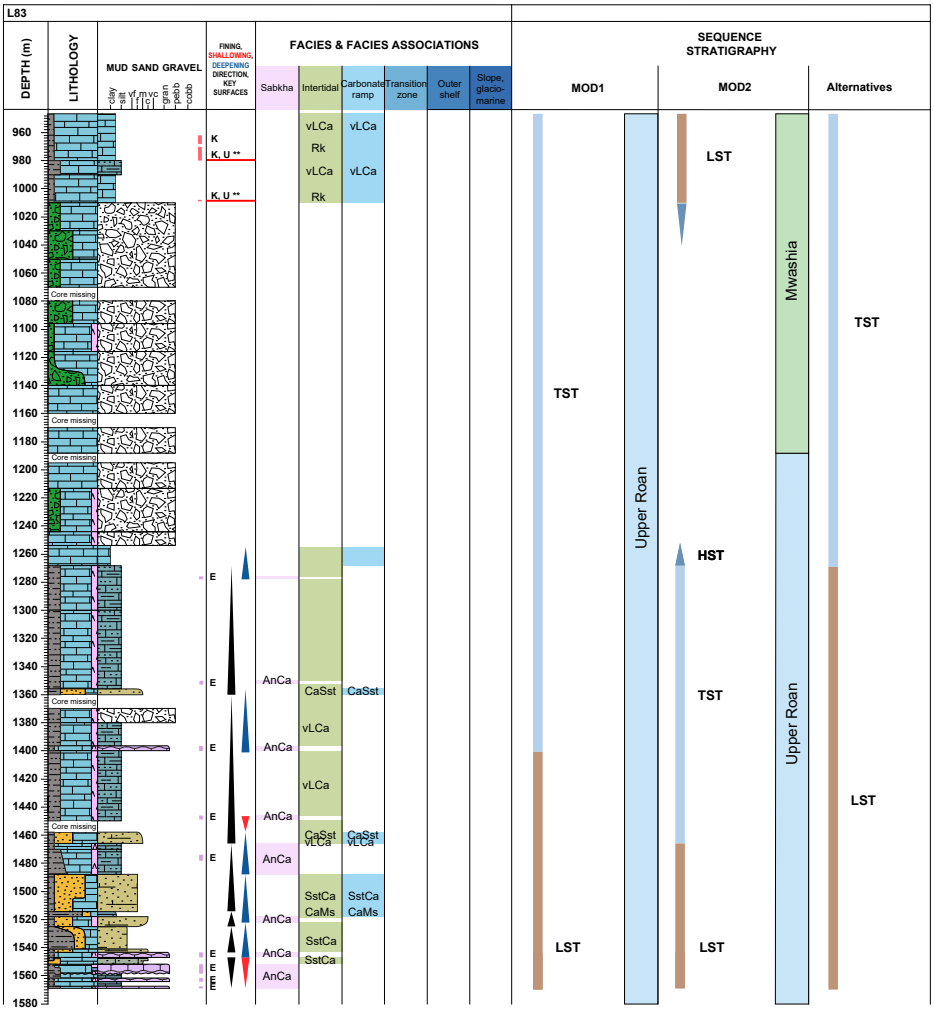

Figure 9.34: L83 (Mufulira) stratigraphic log, continued

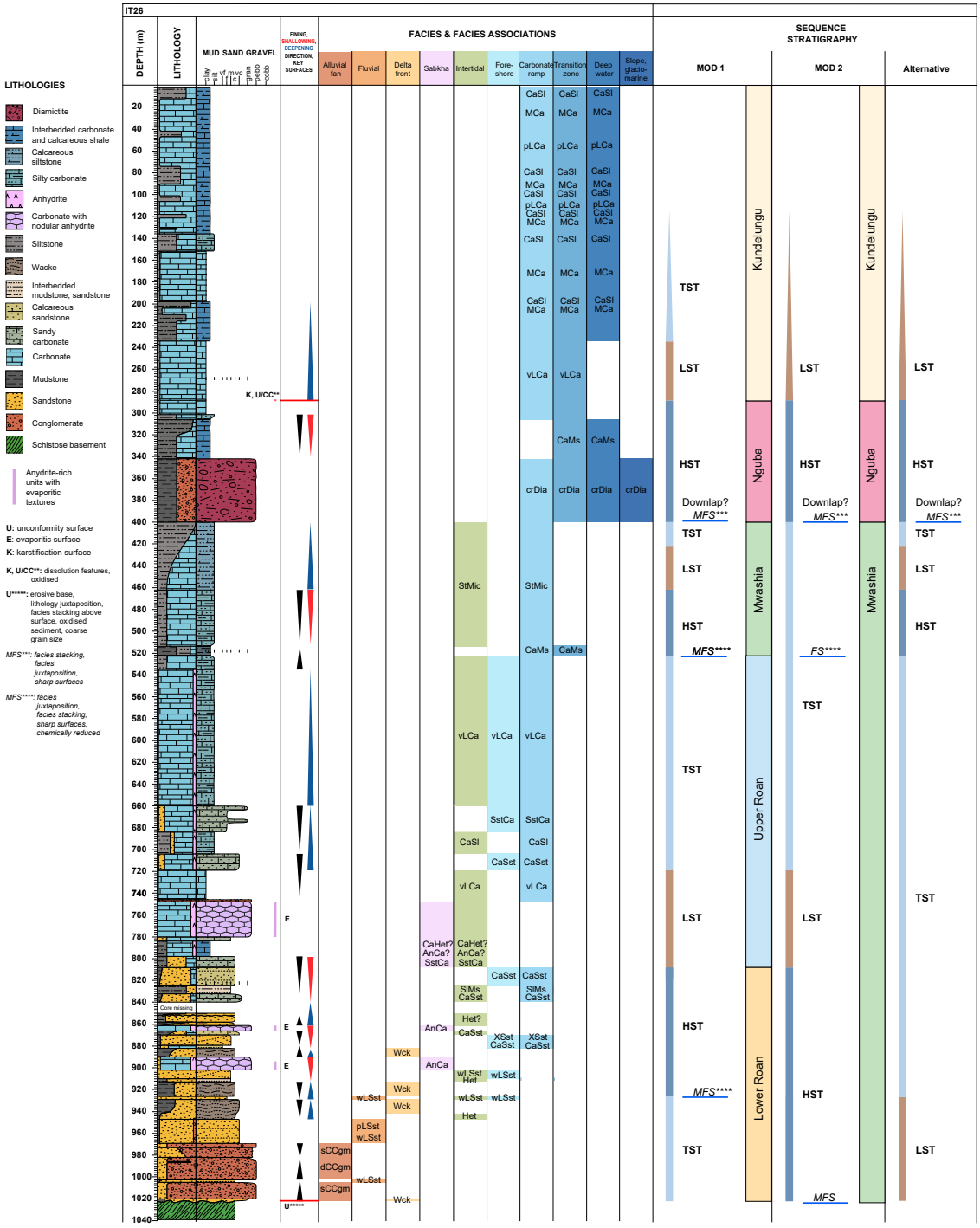

Figure 9.35: IT26 (Ndola) stratigraphic log, continued

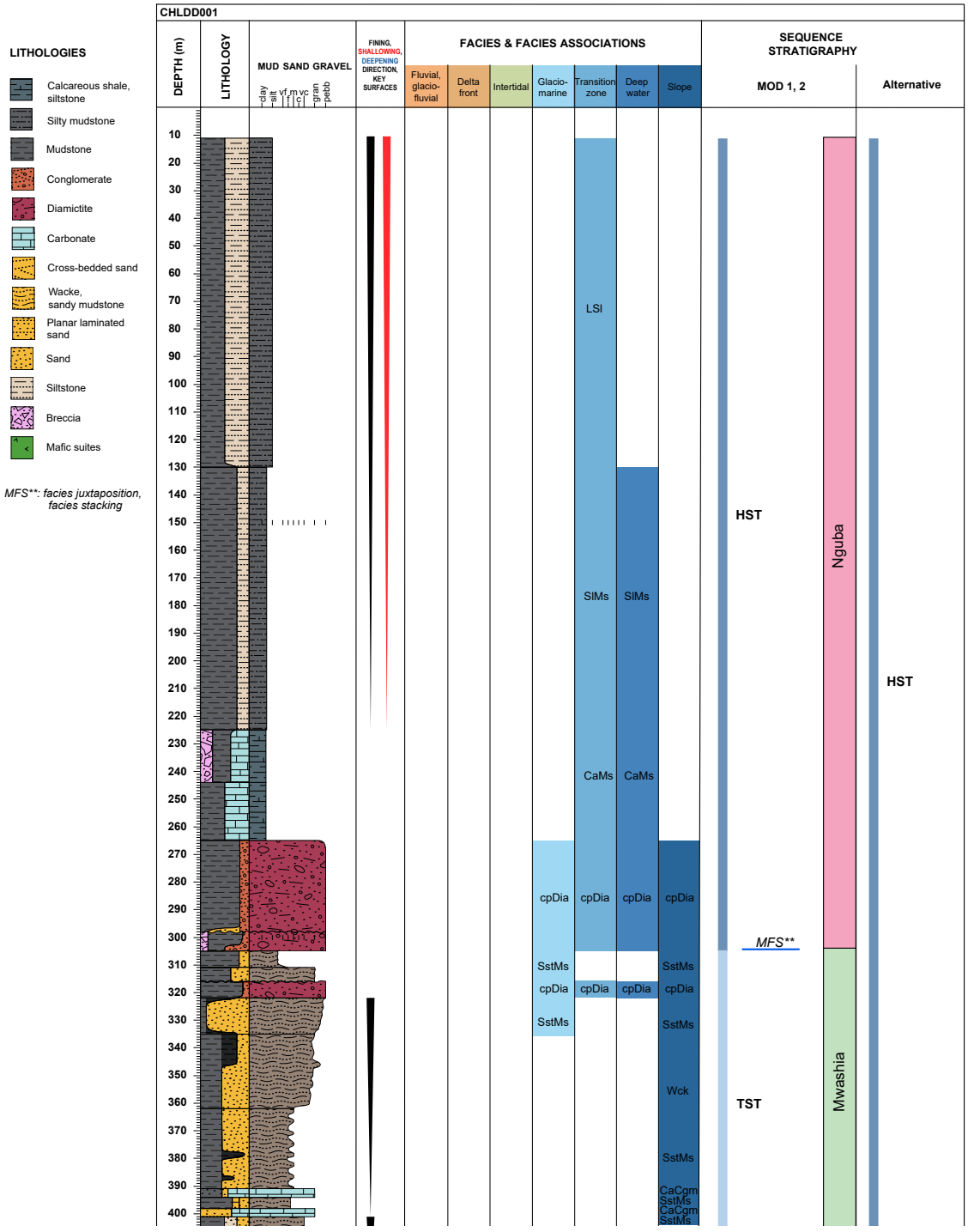

Figure 9.36: CHLDD001 (Chilonga) stratigraphic log

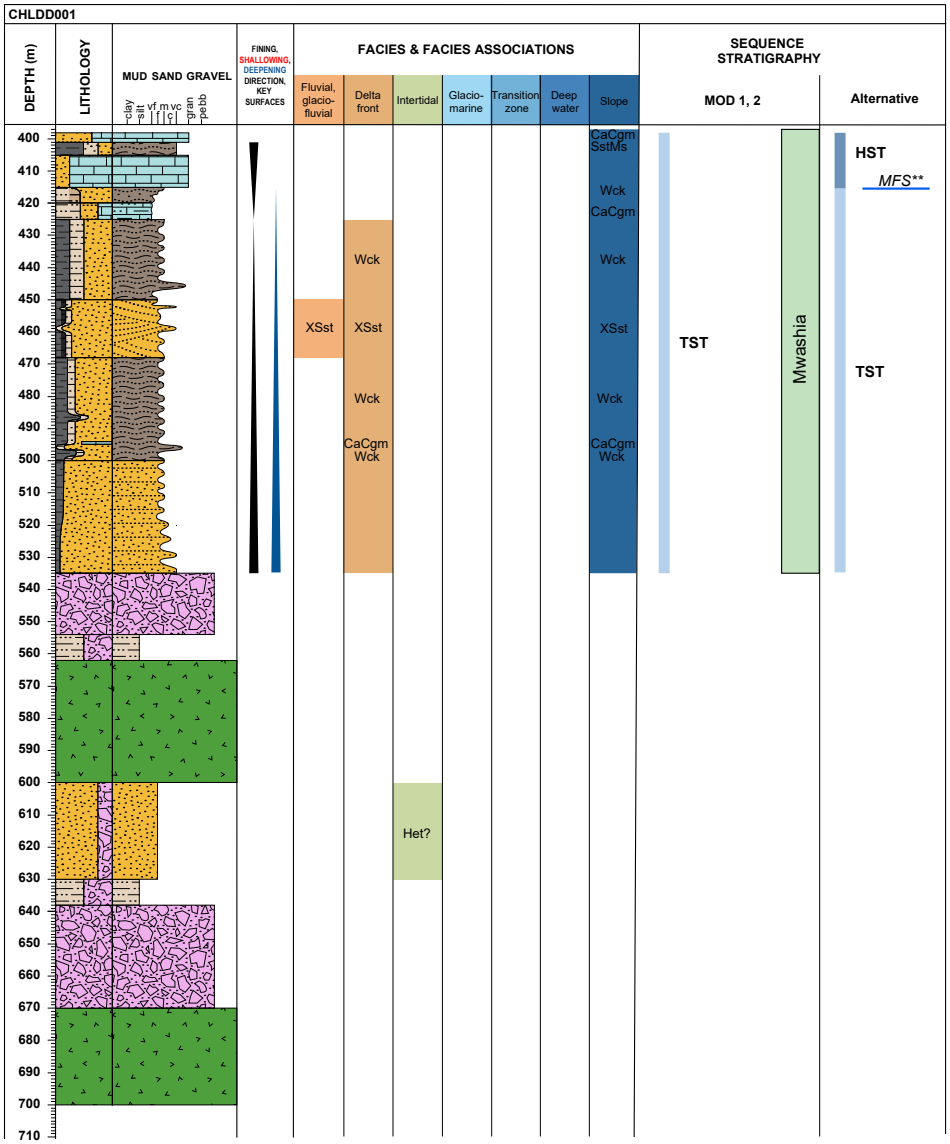

Figure 9.37: CHLDD001 (Chilonga) stratigraphic log, continued

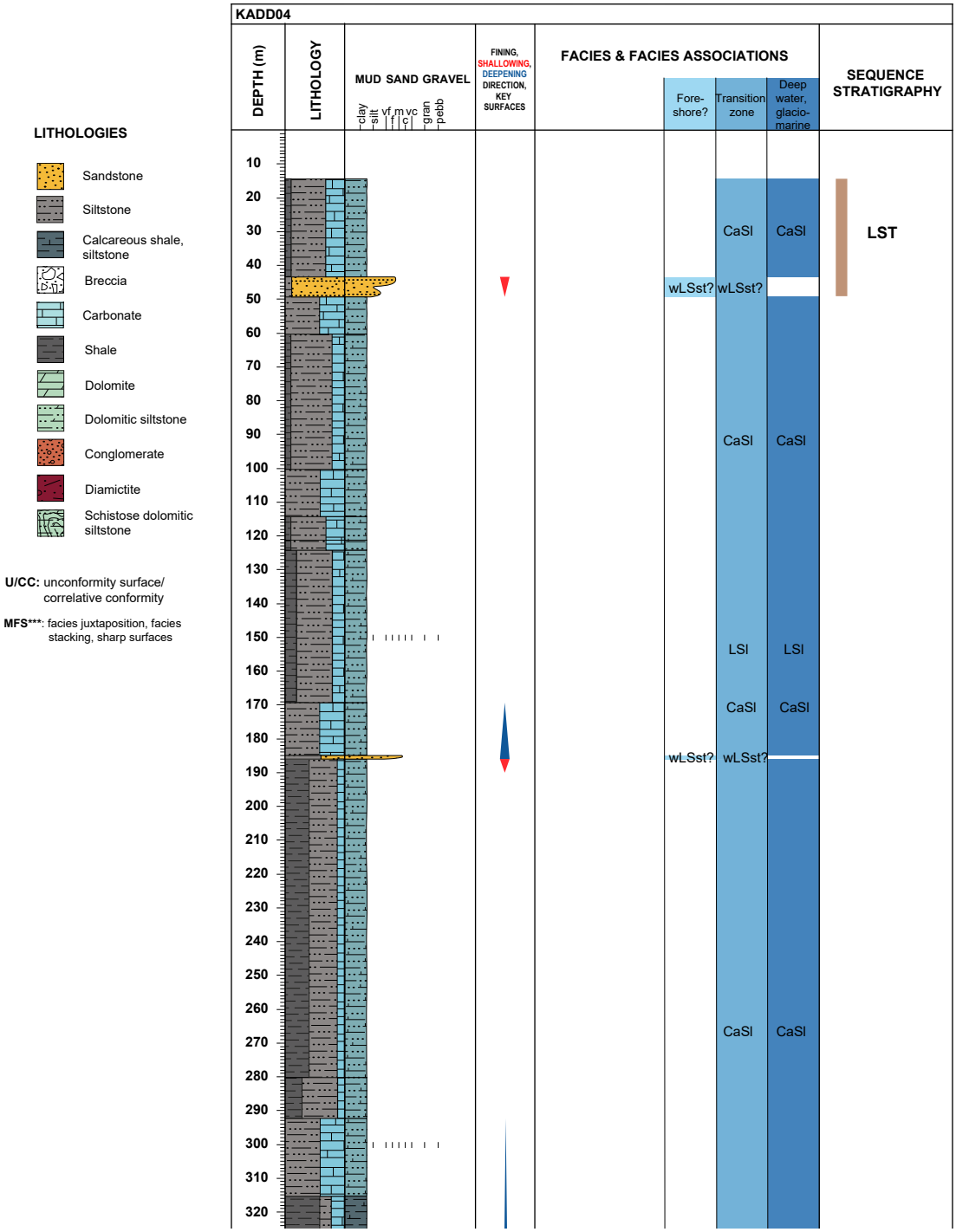

Figure 9.38: KADD04 (Lusale) stratigraphic log

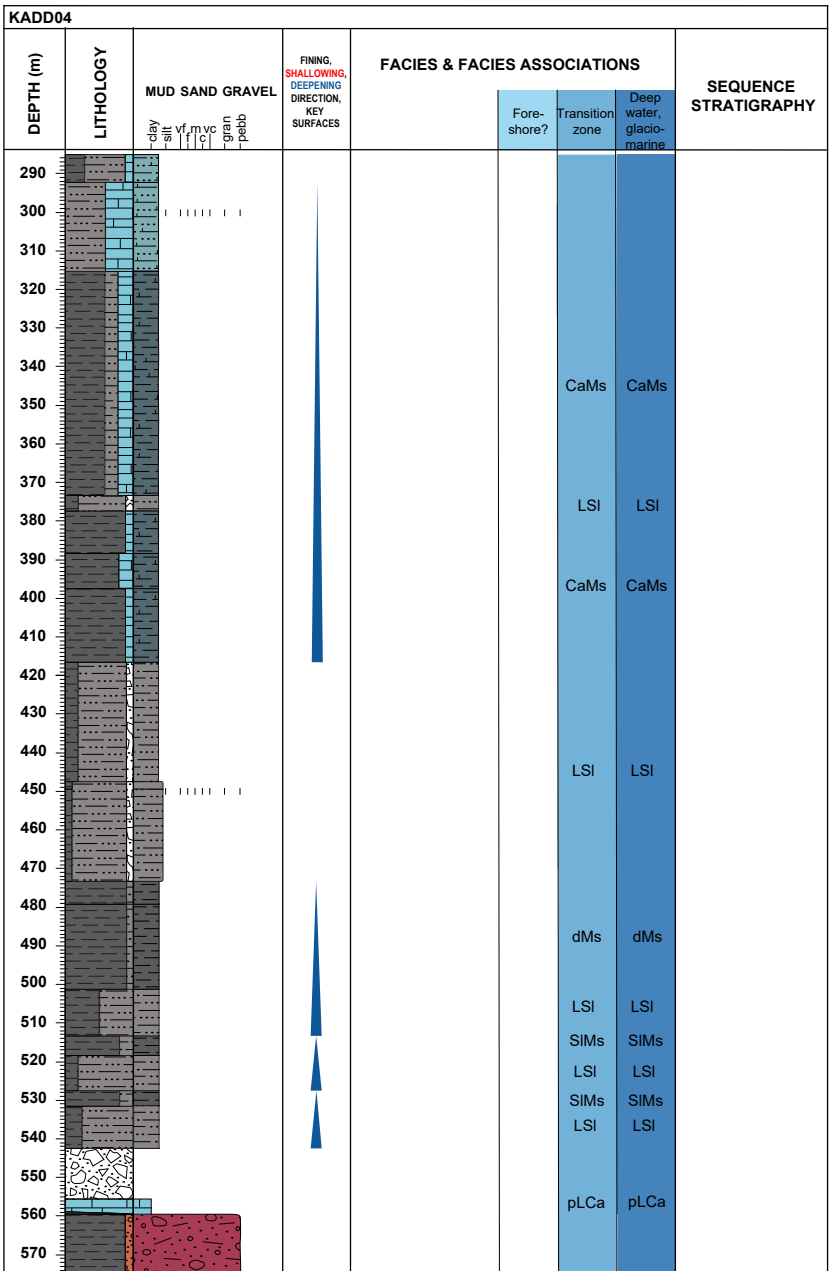

Figure 9.39: KADD04 (Lusale) stratigraphic log, continued

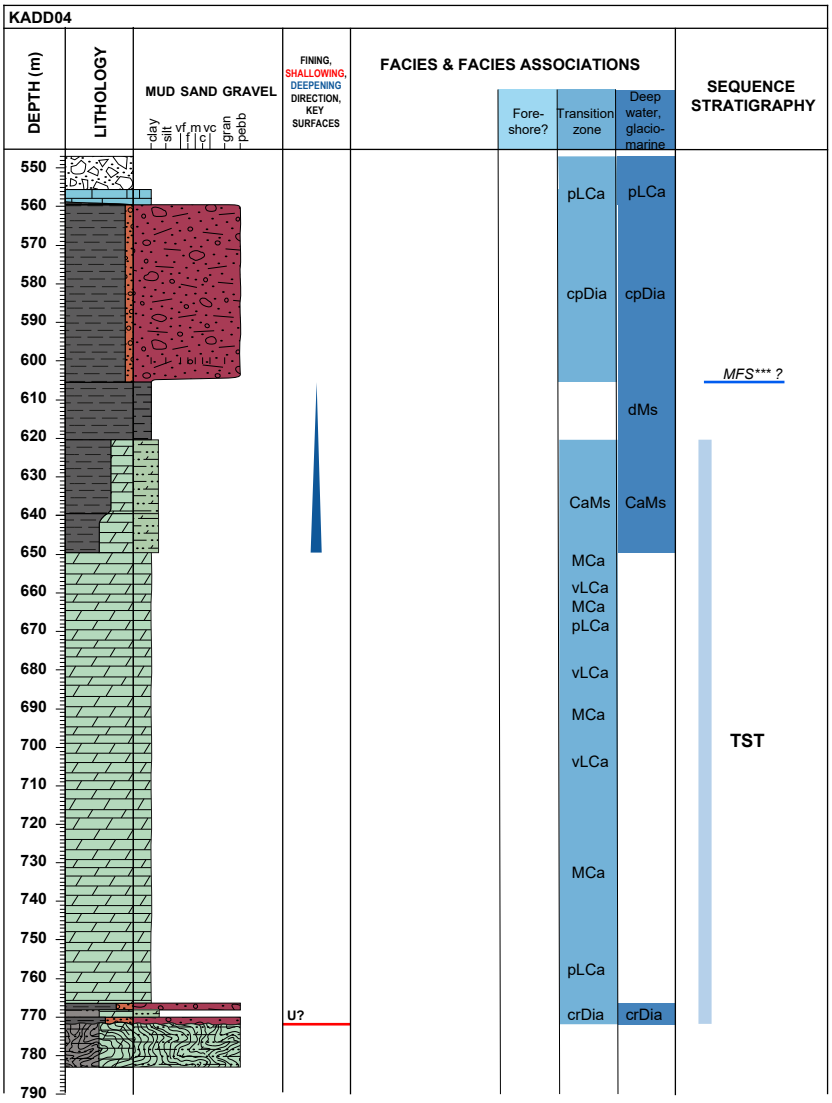

Figure 9.40: KADD04 (Lusale) stratigraphic log, continued

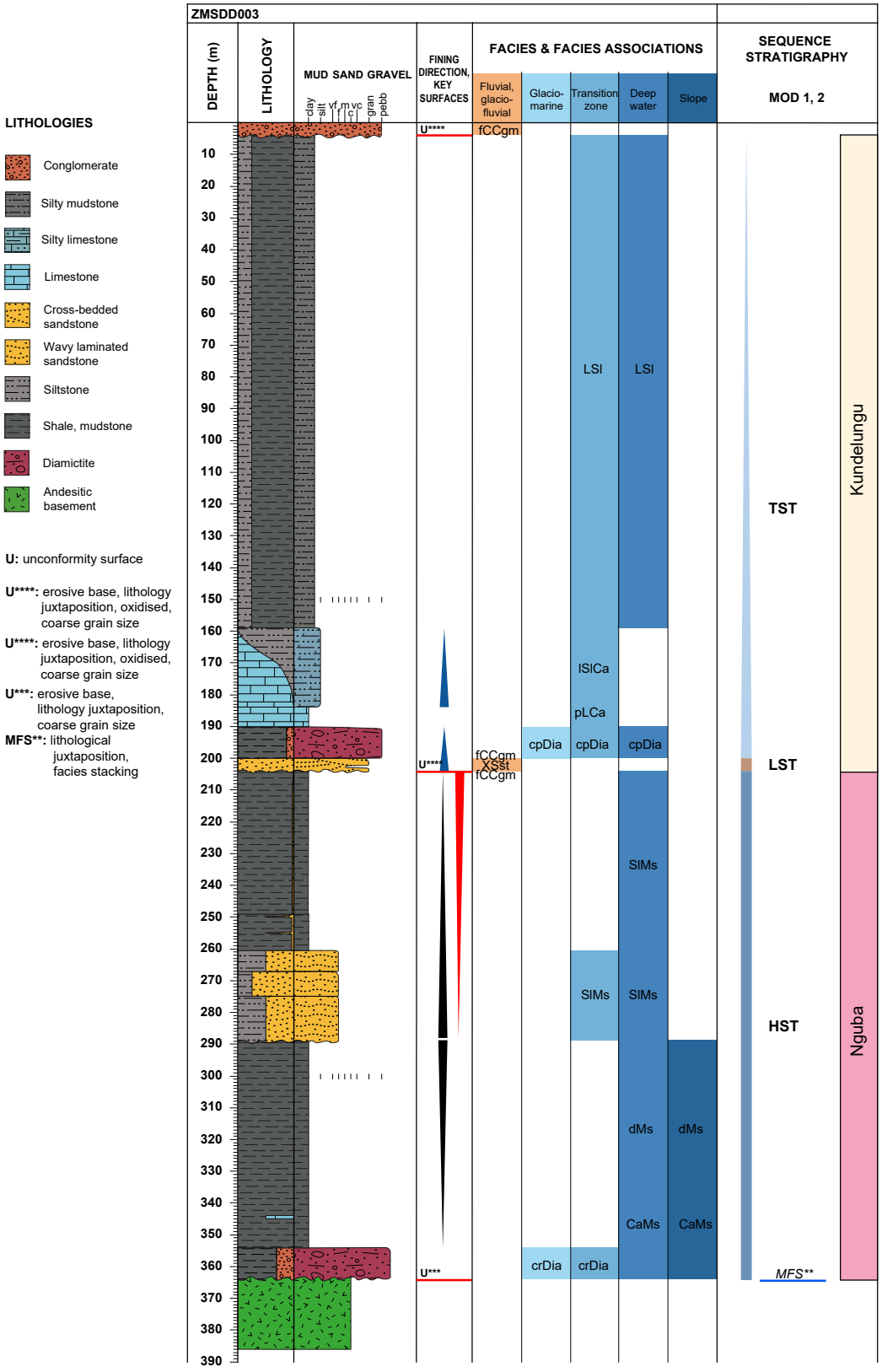

Figure 9.41: ZMSDD003 (Mansa) stratigraphic log

Appendix III – Type logs

The following are the tabulated type logs for each of the 8 backstripped cores, showing best-estimates of thickness and palaeobathymmetry as ranges to account at least in-part for uncertainties in the stratigraphic record.

KRX082

Group	Thickness (m)	Palaeo water depth range	Comments	Sources for thickness estimates
Kundelungu	2000 - 3000	50 - 250	Inferred thickness based on apatite fission track analysis; water depth inferred from Kundelungu facies in L83 and KADD04	> 2 km of stratigraphy removed since the Miocene (Daly et al., 2020); > 1km Kundelungu thickness in DRC (Batumike et al., 2007)
Nguba	500 - 1000	10 - 500	Inferred thickness based on Nguba thickness in L83, sheared clast proportions, and increased Nguba thickness northwards into the D.R.C. Water depth inferred from facies in L83	Based on core logging and comparison with L83; Selley et al. (2018)
Mwashia	150 - 500	10 - 250	Inferred thickness based on thickness increases of Mwashia and Nguba units to the NW from IT26 to KN192 Water depth inferred from facies in L83 and KN192	Based on core logging and comparison with IT26, L83, KN192
Upper Roan	1000 - 2000	0 - 50	Inferred thickness based on Upper Roan thickness in RCB2; water depth inferred from RCB2	Based on core logging, comparison with RCB2;
Lower Roan	1330 - 1800	0 - 10	Up to 470 m of Lower Roan sediments added based on facies analysis and thickness of conglomerates in RCB2	Based on core logging, facies analysis, core logging of RCB2 and facies

KN192

Group	Thickness (m)	Palaeo water depth range	Comments	Sources for thickness estimates
Kundelungu	2000 - 3000	50 - 250	Inferred thickness based on apatite fission track analysis; water depth inferred from Kundelungu facies in L83 and KADD04	> 2 km of stratigraphy removed since the Miocene (Daly et al., 2020); > 1km Kundelungu thickness in DRC (Batumike et al., 2007)
Nguba	400 - 800	10 - 500	140 – 240 m of Nguba sediments added to account for missing top of Nguba	Based on core correlation with L83 and IT26, and comparison with Kipushi (Van Wilderode et al., 2013)
Mwashia	487	10 - 250		Based on core logging
Upper Roan	578	0 - 250		Based on core logging
Lower Roan	400 - 1200	0 - 250	80 m of Lower Roan sediments inferred to account for erosion; Up to 800 m of Lower Roan sediments inferred to account for missing base of Lower Roan, based on Lower Roan thicknesses in the Konkola Basin	Based on core logging; Sweeney et al. (1986), Torremans et al. (2013) Max. water depth of Lower Roan mudstones estimated to be 250 m, based on an approximate mean depth of East African Rift Valley lakes

RCB2

Group	Thickness (m)	Palaeo water depth range	Comments	Sources for thickness estimates
Kundelungu	2000 - 3000	50 - 250	Inferred thickness based on apatite fission track analysis; water depth inferred from Kundelungu facies in L83 and KADD04	> 2 km of stratigraphy removed since the Miocene (Daly et al., 2020); > 1km Kundelungu thickness in DRC (Batumike et al., 2007)
Nguba	400 - 500	10 - 500	Water depth inferred from Nguba facies in L83	Based on correlation with L83 and IT26
Mwashia	150 - 500	10 - 250	Water depth inferred from Mwashia facies in L83, KN192	Based on correlation with L83 and KN192
Upper Roan	918 - 1200	0 - 250	Up to 282 m of Upper Roan inferred to account for missing top of Upper Roan	Based on core logging and correlation with KN192
Lower Roan	832 - 900	0 - 250	Up to 68 m of Lower Roan sediments inferred to account for missing base of Lower Roan, based on facies trends and Lower Roan thickness in the Konkola Basin	Based on core logging; Sweeney et al. (1986) Max. water depth of Lower Roan mudstones estimated to be 250 m, based on approximate mean depth of East African Rift lakes

L83

Group	Thickness (m)	Palaeo water depth range	Comments	Sources for thickness estimates
Kundelungu	2000 - 3000	50 - 250	Inferred thickness based on apatite fission track analysis	> 2 km of stratigraphy removed since the Miocene (Daly et al., 2020); > 1km Kundelungu thickness in DRC (Batumike et al., 2007)
Nguba	420	10 – 500		Based on core logging
Mwashia	112	10 - 250		Based on core logging
Upper Roan	680 – 900	0 - 250	Up to 220 m of sediment added to account for missing base of Upper Roan	Based on core logging and correlation with RCB2
Lower Roan	120 - 500	0 - 30	Inferred based on sub-regional Lower Roan thickness ranges (< 500 m) and local stratigraphy at the Mufulira mine, water depths inferred from IT26	Binda & Mulgrew (1974); Wendorff (2005); AMIRA Report P544

IT26

Group	Thickness (m)	Palaeo water depth range	Comments	Sources for thickness estimates
Kundelungu	2000 - 3000	50 - 250	Inferred thickness based on apatite fission track analysis; water depth inferred from Kundelungu facies in L83 and KADD04	> 2 km of stratigraphy removed since the Miocene (Daly et al., 2020); > 1km Kundelungu thickness in DRC (Batumike et al., 2007)
Nguba	400 - 500	10 - 500	Up to 100 m of Nguba sediment inferred, to account for missing top of Nguba	Based on core correlation with L83
Mwashia	122	10 - 250		Based on core logging
Upper Roan	276	0-30		Based on core logging
Lower Roan	224	0 - 30		Based on core logging

CHLDD001

Group	Thickness (m)	Palaeo water depth range	Comments	Sources for thickness estimates
Kundelungu	2000 - 3000	50 - 250	Inferred thickness based on apatite fission track analysis; water depth inferred from Kundelungu facies in L83 and KADD04	> 2 km of stratigraphy removed since the Miocene (Daly et al., 2020); > 1km Kundelungu thickness in DRC (Batumike et al., 2007)
Nguba	400 - 500	30 - 250	Up to 178 m of Nguba sediment inferred to account for missing top of Nguba Lower water depth limit on account of ripple x-lam and laminites	Based on core correlation with L83
Mwashia	348	30 - 100		Based on core logging

KADD04

Group	Thickness (m)	Palaeo water depth range	Comments	Sources for thickness estimates
Kundelungu	2000 - 3000	30 - 250	Inferred thickness based on apatite fission track analysis	> 2 km of stratigraphy removed since the Miocene (Daly et al., 2020); > 1km Kundelungu thickness in DRC (Batumike et al., 2007)
Nguba	165	10 - 500		Based on core logging

Figure 9.42

ZMSDD003

Group	Thickness (m)	Palaeo water depth range	Comments	Sources for thickness estimates
Kundelungu	2000 - 3000	10 - 250	Inferred thickness based on apatite fission track analysis	> 2 km of stratigraphy removed since the Miocene (Daly et al., 2020); > 1km Kundelungu thickness in DRC (Batumike et al., 2007)
Nguba	165 - 250	10 - 500	Up to 85 m of sediment added to account for erosion surface at top of Nguba	Based on core logging

Appendix IV – Decompaction and backstripping procedure

Decompaction

Sedimentary rocks are porous media composed of framework grains and void space. This void space can be occupied by fluid or interstitial secondary minerals (Allen and Allen, 2013). Porosity (ϕ) is the fraction volume of void space in the medium, whereas the void ratio (e) is the ratio of void space to solid volume (Allen and Allen, 2013).

ϕ and e are related by equation 9.1:

$$\phi = \frac{e}{e+1} \tag{9.1}$$

where

e = 1 if ϕ = 0.50

As porosity tends to scale inversely with depth, the two can be related by a negative exponential, first proposed by Athy (1930):

$$\phi(y) = \phi_0^{-y/y_0} \tag{9.2}$$

where

ϕ_0 is the porosity at the surface,

y is depth,

y_0 is the depth at which ϕ has reduced to $(1/e)(\phi_0)$.

Progressive burial of sediments results in compaction and porosity loss. Compaction represents a uniaxial, vertical strain in sediments. It is the result of overburden causing a reduction in pore volume, and the compression of the solid framework (Athy, 1930). Porosity loss can include compaction and volumetric strain, but may also occur as a result of other mechanisms, such as precipitation of secondary phases. Secondary minerals infilling pore space may therefore reduce porosity, without any change in total volume of the rock. Porosity loss (and compaction) are driven by three groups of processes: mechanical compaction, physio-chemical compaction, and cementation (Allen and Allen, 2013).

Porosity change with depth is highly dependent on lithology, and hence, mineralogy. Generally, ductile or mechanically weaker sediments will experience greater degrees of compaction than mechanically stronger sediments (Allen and Allen, 2013). Several factors determine porosity depth relationships:

Lithology: different rock types tend to exhibit different porosity-depth trends as a function of bulk composition, e.g. shales will compact relatively easily compared to quartz-arenites (Sclater and Christie, 1980; Turer and Maynard, 2003).

Facies: individual facies will have characteristic grain size distributions, clay contents and ϕ_0 values. Facies will therefore have characteristic porosity-depth relationships (Sclater and Christie, 1980).

Framework: framework composition determines the degree to which the lithology undergoes volumetric strain and deformation. Lithologies with higher quartz content will tend to compact less easily over a given depth interval than lithologies with higher clay or lithic content (Allen and Allen, 2013).

Temperature: temperature exerts a strong control on reactions and kinetics. It therefore affects diagenetic processes, e.g. dissolution, dehydration reactions and cementation (Allen and Allen, 2013).

Time: Compaction of sediments takes time. The longer the period of compaction lasts, the greater the porosity loss experienced within a formation (Sclater and Christie, 1980; Allen and Allen, 2013).

At shallow depths, or within individual stratigraphic units, a linear relationship between porosity and depth can be observed (Allen and Allen, 2013). These linear trends follow the form:

$$\phi = \phi_0 - ay \tag{9.3}$$

where

ϕ_0 is initial porosity of the lithology

y is depth

a is the coefficient of porosity change with depth

At greater depths: negative exponential trends predominate, following a form based on Athy's equation (9.2) (Athy, 1930).

$$\phi(y) = \phi_0^{-cy} \tag{9.4}$$

where

ϕ_0 is initial porosity of the lithology

y is depth

c is a coefficient controlling the rate of change of porosity with depth

Understanding how porosity changes with depth allows for sediment layers to be decompacted to their original thicknesses. Decompaction involves bringing up the lowest sediment layer to where its top is at a depth of 0 (relative to a datum) and calculating its porosity according to its porosity-depth curve (see equation 9.4). This is can be performed sequentially for multiple stratigraphic units, by taking the next lowest unit, bringing it to the surface, decompacting it, and partially re-compacting the unit below it, then bringing up the next lowest unit, compacting all the units below it, and so on. Decompaction is performed using equation 9.5 (Sclater and Christie, 1980; Müller et al., 2018):

$$y_2' - y_1' = y_2 - y_1 - \frac{\phi_0}{c}[e^{-cy_1} - e^{-cy_2}] + \frac{\phi_0}{c}[e^{-cy_1'} - e^{-cy_2'}] \tag{9.5}$$

where

y_1 is the top of the stratigraphic unit at its current depth

y_2 is the base of the stratigraphic unit at its current depth

y'_1 is the top of the stratigraphic unit at the decompacted or partially re-compacted depth

y'_2 is the base of the stratigraphic unit at the decompacted or partially re-compacted depth

ϕ_0 is initial porosity

c is the exponential decay constant controlling the rate of change of porosity with depth

Backstripping

What follows is the derivation of the backstripping equation, based on Watts and Ryan (1976) and Allen and Allen (2013).

Basement subsidence is determined by three variables: sediment load $y(t)$, water depth $W_d(t)$, and eustasy $\Delta_{SL}(t)$

Figure 9.43 shows two 1D sections through the lithosphere, one decompacted, the other backstripped, in isostatic balance with one another.

The isostatic balance at compensation depth is given by equation 9.6.

$$\rho_w g W_d(t) + \bar{\rho}_b g y(t) + \rho_c g y_c + \rho_m g a_1 = \rho_w g Y(t) + \rho_c g y_c + \rho_m g a_2 \tag{9.6}$$

where

ρ_w is the density of water

$\bar{\rho}_b$ is the bulk density of sediment

ρ_c is the density of the crust

ρ_m is the density of the underlying mantle

g is the Earth's gravitational constant

$W_d(t)$ is water depth at at time t

$y(t)$ is thickness of sediment deposited at time t

y_c is crustal thickness

a_1 is initial lithospheric mantle thickness

a_2 is lithospheric mantle thickness after removal of sediment

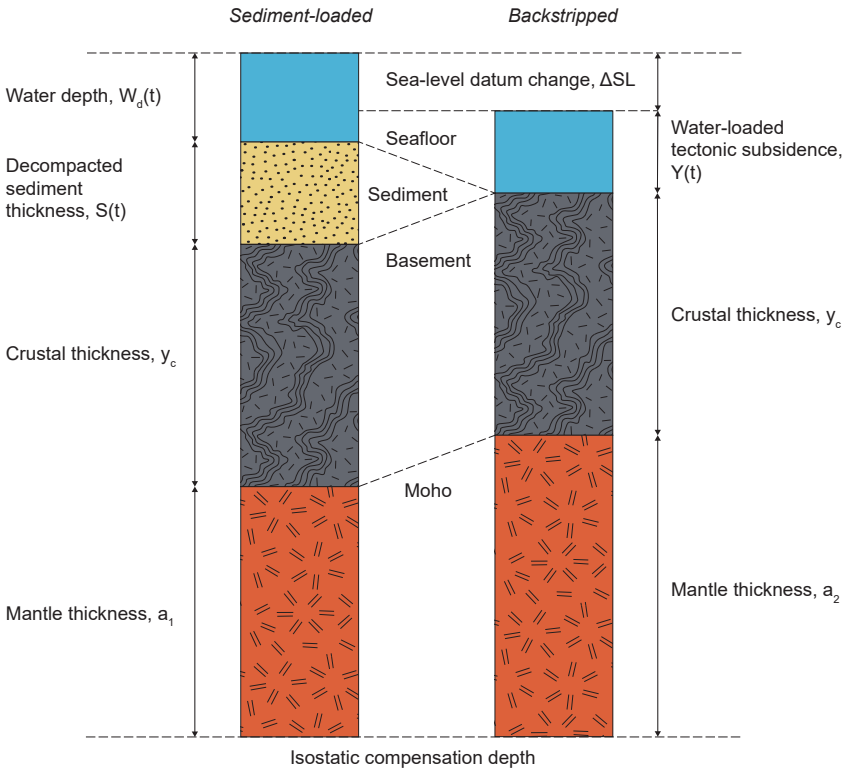

Figure 9.43: Example of two columns in isostatic balance assuming Airy isostasy, the left being loaded with a thickness of sediment (decompacted), the right backstripped showing commensurate isostatic adjustment, after Allen and Allen (2013).

$Y(t)$ is tectonic subsidence at time t

Equating the thicknesses of both these columns, and removing common terms (g, y_c), and adding a term to account for eustatic sea level change (Δ_{SL}), gives equation 9.7.

$$W_d(t) - \Delta_{SL} + y(t) + a_1 = Y(t) + a_2 \tag{9.7}$$

where

$W_d(t)$ is water depth at time t

$y(t)$ is thickness of sediment deposited at time t

Δ_{SL} is eustatic change

a_1 is initial lithospheric mantle thickness

a_2 is lithospheric mantle thickness after removal of sediment

$Y(t)$ is tectonic subsidence at time t

The solution for tectonic subsidence, is found by combining equations 9.6 and 9.7.

$$Y(t) = W_d(t) + y(t)\left(\frac{\rho_m - \bar{\rho}_b(t)}{\rho_m - \rho_w}\right) - \frac{\rho_m}{\rho_m - \rho_w}\Delta_{SL}(t) \tag{9.8}$$

where $Y(t)$ is the tectonic subsidence at time t

ρ_w is the density of water

$\bar{\rho}_b$ is the bulk density of sediment

ρ_c is the density of the crust

ρ_m is the density of the underlying mantle

$W_d(t)$ is water depth at time t

$y(t)$ is thickness of sediment deposited at time t

Δ_{SL} is eustatic change

a_1 is initial lithospheric mantle thickness

a_2 is lithospheric mantle thickness after removal of sediment

$Y(t)$ is tectonic subsidence at time t

The bulk density of an individual stratigraphic unit is given by equation 9.9.

$$\rho_{b,i}(t) = \phi_i(t)\rho_w + (1 - \phi_i(t))\rho_{s,i} \tag{9.9}$$

where

$\rho_{b,i}$ is the bulk density of a stratigraphic unit

ρ_w is the density of water

$\rho_{s,i}$ is the density of solid phases (grains + cements), over i units

$\rho_{b,i}$ is the combined bulk density of pore fluid and density of solid phases, over i units

ϕ_i is the porosity, over i units

The average bulk density of the sediment fill in a basin is hence a sum of the bulk densities of the stratigraphic units within it, given by equation 9.10:

$$\bar{\rho}_b(t) = \frac{\sum_i \rho_{b,i}(t)\Delta y_i(t)}{\sum_i \Delta y_i(t)} \tag{9.10}$$

where

$\bar{\rho}_b(t)$ is the average bulk density of the sediment fill

$\rho_{b,i}$ is the combined bulk density of pore fluid and density of solid phases, over i units

y_i is sediment layer thickness, over i units

Palaeobathymetry, or water depth, controls accumulation space in a basin over time. Estimates of past water depths are provided by palaeontology, facies analysis and geochemistry (Watts and Ryan, 1976; Roberts et al., 1998; Allen and Allen, 2013). Fossil assemblages characteristic of different settings, from paralic to abyssal, can be used as indicators of bathymmetry (Ekdale, 1988; Allen and Allen, 2013). The use of fossil assemblages to constrain palaeobathymmetry is of course of limited or no use in the Neoproterozoic sedimentary successions, and one must instead rely on facies analysis.

Sedimentary facies are an imperfect, albeit useful indicator of past water depths, allowing broad first-order estimates of water depth to be constrained (e.g. terrestrial, intertidal, above or below storm wave base etc.) (Immenhauser, 2009). Eustatic corrections can be made, as sea level change affects palaeobathymmetry and any increases in water volume within a basin must be isostatically compensated (Steckler and Watts, 1978). This is shown in equation 9.11:

$$\Delta_{SL} = \left(\frac{\rho_m - \rho_w}{\rho_m}\right)(h_2 - h_1) \tag{9.11}$$

where

Δ_{SL} is the change in sea level

ρ_m is the density of the mantle (assuming thin oceanic crust)

ρ_w is the density of water

h_1 is the initial water depth

h_2 is the new water depth after sea level change

Global, or large-scale, sea level change is measured relative to a datum; the difference between

the new sea level and datum is termed 'freeboard' (f) (Allen and Allen, 2013).

$$f = \frac{(\rho_m - \rho_w)h}{\rho_m} \tag{9.12}$$

where

f is the freeboard ρ_m is the density of the mantle (assuming thin oceanic crust)

ρ_w is the density of water

h is the eustatic sea level change

McKenzie Uniform Extension model

Initial fault controlled subsidence is given by equation 9.13.

$$y_s = \frac{y_L\left[(\rho_m^* - \rho_c^*)\frac{y_c}{y_L}(1 - \alpha_v\frac{T_m y_c}{2y_L}) - \frac{\alpha_v T_m \rho_m^*}{2}\right](1 - \frac{1}{\beta})}{\rho_m^*(1 - \alpha_v T_m) - \rho_s} \tag{9.13}$$

where

y_s is the thickness of basin fill (sediment, water, air)

y_c is the thickness of the crust

y_L is the thickness of the lithosphere

T_m is the temperature of the mantle

ρ_m^* is the density of the mantle at 0 °C

ρ_c^* is the density of the crust at 0 °C

ρ_s is the density of the basin fill (water, sediment, air)

α_v is the volumetric coefficient of thermal expansion

β is the stretch factor

The subsequent thermal subsidence is given by equation 9.14.

$$S(t) = E_0\frac{\beta}{\pi}sin\left(\frac{\pi}{\beta}\right)(1 - e^{\frac{-t}{\tau}}) \tag{9.14}$$

where

$S(t)$ is the thermal subsidence

β is stretch factor

τ is the thermal time constant of the lithosphere

and

$$E_0 = \frac{4 y_L \rho_m^* \alpha_v T_m}{\pi^2 (\rho_m^* - \rho_s)} \tag{9.15}$$

where

y_L is the thickness of the lithosphere

T_m is the temperature of the mantle

ρ_m^* is the density of the mantle at 0 °C

ρ_s is the density of the basin fill (water, sediment, air)

α_v is the volumetric coefficient of thermal expansion

The thermal time constant of the lithosphere is given by equation 9.16.

$$\tau = \frac{y_L^2}{\pi^2 \kappa} \tag{9.16}$$

where

τ is the thermal time constant of the lithosphere

κ is the thermal diffusivity

Appendix V – Lufilian uplift and thermal history: preliminary results from apatite and zircon fission-track analysis

Samples were collected for fission track analysis and geochronology at the London Geochronology Centre at University College London to begin to constrain the thermal and uplift history of the basin post-inversion. Work is on-going, and preliminary results are shown here.

Fission track analysis was developed in the 1960's, and allows for the thermal history of a mineral sample to be constrained (Price and Walker, 1962, 1963). Fission tracks in minerals are the result of nuclear fission generating linear damage trails in a crystal lattices. Fission tracks anneal over time when a sample is exposed to temperatures in excess of a minerals closure temperature. The number of preserved fission tracks in a sample corresponds to the concentration of daughter isotopes, and their length to the amount of time below their closure temperature (Price and Walker, 1963; Allen and Allen, 2013; Riley et al., 2023).

Fission tracks are generally low-temperature thermochronometers; however, different minerals have different closure temperatures, and can hence resolve different portions of a region's uplift history. Apatite and zircon, the two minerals analysed here, have closure temperatures of 110 $\pm$10 °C and 240 $\pm$20 °C, respectively (Allen and Allen, 2013).

Methodology

Samples for apatite and zircon fission track analysis were collected from a range of depths from sandy facies in the KRX082, KN192, CHLDD001, and KADD04 cores. Samples were crushed, milled, and underwent standard separation procedures (e.g. density separation in bromoform, followed by magnetic separation for apatites and zircons, followed by a second density separation using diiodemethane for zircons.) Samples were then mounted for LA-ICP-MS analysis, in epoxy resin for apatites, in teflon for zircons.

For apatite fission track analysis a LA-ICP-MS a New Wave UP 193 nm laser ablation system, coupled to an Agilent 7900 quadrupole mass spectrometer was used. Laser ablation used a fluence of 2.3 Jcm^{-2}, a repetition rate of 7 Hz, with a 50 μm spot ablating for 30 seconds.

For zircon fission track analysis the laser ablation used a repetition rate of 9 Hz, with a 35μm spot ablating for 40 seconds.

Spontaneous fission tracks were counted in samples where uranium concentration was sufficiently high, and track densities sufficiently low, using a Zeiss axioplan microscope at 1250x magnification. Age calculation and plotting was performed using IsoplotR (Vermeesch, 2018). The thermal history was modelled in QtQt (http://iearth.edu.au/codes/QTQt/).

Results

Preliminary apatite fission track results are shown in table 9.1, and figure 9.44 below:

	ns	*A* (μm^{-2})	^{238}U	$S(^{238}U)$	*Age (Ma)*	± *2s*
KN192 1345 m						
	26	4834	3.82	0.33	313	132
	15	3453	2.00	0.07	476	250
	71	13810	2.47	0.08	452	113
	28	6905	1.94	0.05	468	184
	29	4834	1.96	0.08	648	249
	55	13810	2.07	0.08	417	119
	28	6767	2.49	0.19	366	150
	19	5524	2.12	0.07	362	170
	31	6905	2.25	0.06	429	159
	18	4143	1.33	0.04	719	339
	38	6905	3.27	0.12	369	122
	50	8286	1.98	0.07	652	196
	51	11048	2.37	0.07	423	124
	29	4834	3.17	0.08	413	155
	19	3453	2.07	0.06	570	267
	54	13810	2.41	0.10	360	103
	37	6767	3.22	0.12	377	126
	34	6905	1.84	0.07	594	214
	25	6905	2.59	0.08	309	126
	64	13810	2.31	0.08	443	117
	73	13810	2.58	0.09	447	110
KRX082 2204 m						
	30	8286	1.64	0.06	483	180
	25	6905	2.99	0.18	270	113
	27	8286	1.33	0.04	534	208
	30	6905	3.04	0.08	317	117
	42	8286	2.68	0.08	416	131
	21	6905	2.06	0.06	327	144
	32	8286	1.53	0.06	550	199
	22	6905	1.61	0.05	435	187
	34	8286	2.15	0.06	420	146
	40	11048	1.31	0.05	600	195
	22	6905	1.18	0.04	587	253
	27	6767	1.64	0.05	531	207
	34	11048	1.35	0.05	499	175
	23	6905	1.93	0.06	381	161
	48	11048	1.62	0.07	583	176
	36	6905	2.46	0.06	465	157
	35	6905	2.78	0.07	402	137

Table 9.1: Apatite fission track data from cores KN192 and KRX082.

Where

Session zeta: 454855 ± 58047

^{238}U decay constant: 0.000155125± 8.3e-8 Myr^{-1} (Jaffey et al., 1971)

Ns: Number of spontaneous tracks

A: Counting area (in μm^2)

^{238}U: Uranium concentration (in ppm and based on ^{43}Ca/^{238}U of NIST 612)

S(^{238}U): standard error of U concentration

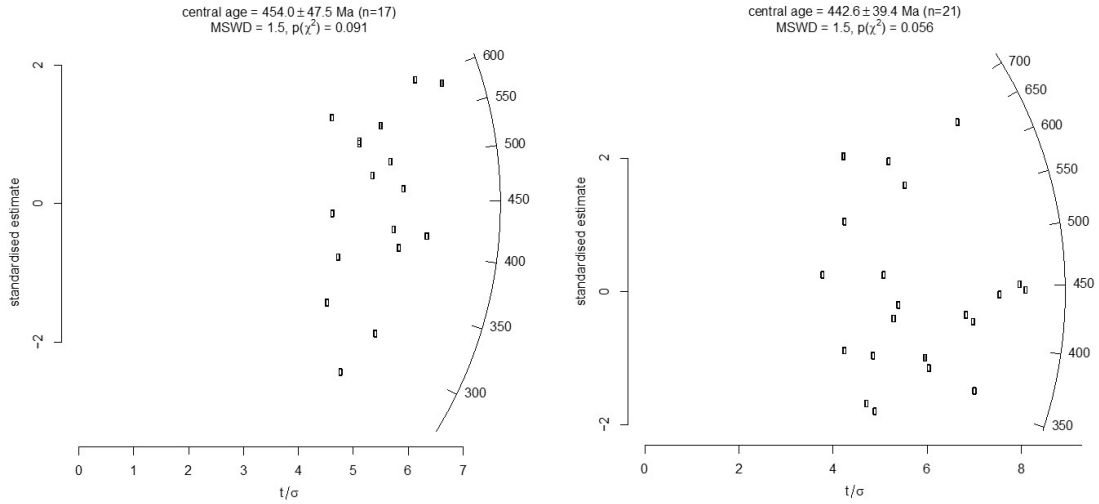

Figure 9.44: Radial plots of apatite fission-track ages for KRX082 (left) and KN192 (right), with central ages of 454 ± 48 Ma, and 443 ±39 Ma, respectively.

Preliminary zircon fission track results are shown table 9.2, and figure 9.45 below:

	ns	*A* (μm^{-2})	^{238}U	$S(^{238}U)$	*Age (Ma)*	$\pm$ *2s*
KRX082 2506 m						
	284	2762	52.0	3.5	416.6	74.8
	128	2209.6	39.7	2.1	310	63.9
	170	1657.2	54.1	2.6	400	72.4
	312	2071.5	56.6	4.4	554.6	106.7
	851	3452.5	40.1	2.4	1215.6	167.7
	169	2071.5	44.9	2.1	383.8	69.1
	224	2209.6	52.7	2.4	405.6	65.6
KRX082 2409 m						
	714	2900.1	100.3	3.7	513.2	53.9
	326	2209.6	78.4	2.6	397.1	51.3
	295	1242.9	111.4	3.4	447.8	58.9
	222	3314.4	34.6	1.3	408.1	62.8
	251	2209.6	50.2	2.7	474.6	78.7
	302	2209.6	65.1	2.4	441.5	60.3
	129	2071.5	25.6	1.2	508.8	101.5
	149	1242.9	62.5	2.3	404.5	72.7
KN192 1646 m						
	171	1242.9	46.5	1.3	613.8	99.9
	210	1104.8	75.1	1.4	528.6	75.6
	152	1104.8	82.2	1.8	354.3	59.5
	164	1104.8	85.8	1.6	365.9	58.8
	164	1242.9	62.3	2.5	445.2	78.2
	144	1104.8	85.9	1.4	322	54.7
KN192 1409 m						
	219	1381	98.9	2.0	339.8	47.9

Table 9.2: Zircon fission track data from cores KN192 and KRX082.

Where

Session zeta: 435268±18869

^{238}U decay constant: 0.000155125± 8.3e-8 Myr^{-1} (Jaffey et al., 1971)

Ns: Number of spontaneous tracks

A: Counting area (in μm^2)

^{238}U: Uranium concentration (in ppm and based on Si/U of NIST 612)

S(^{238}U): standard error of U concentration

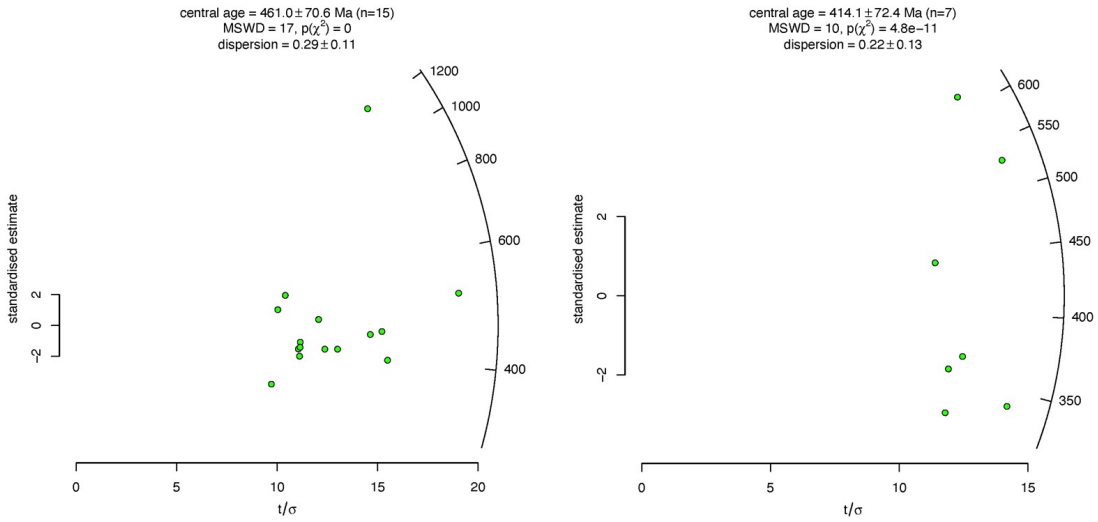

Figure 9.45: Radial plots of zircon fission-track ages for KRX082 (left) and KN192 (right), showing considerable dispersion in sample ages, with central ages of 461 ± 71 Ma, and 414 ±72 Ma, respectively.

A preliminary thermal model is shown in figure 9.46, constrained by both zircon, and apatite fission track data. It shows one major uplift event, expressed as a rapid cooling throughout the Ordovician. It is followed by a prolonged residence at shallower crustal levels without major reburial, though smaller thermal events are not excluded.

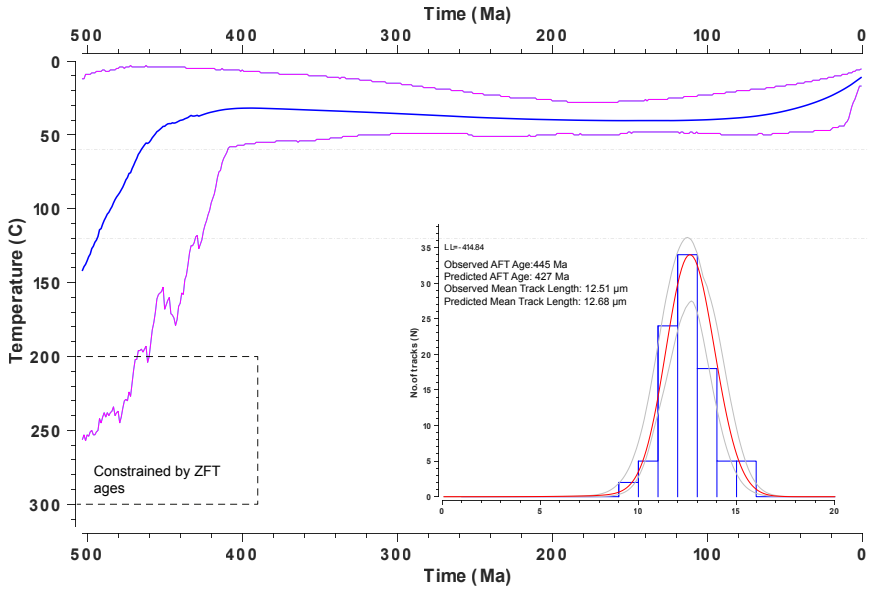

Figure 9.46: Preliminary thermal model for samples at a depth of 2204 m in the KRX082 core, with pink lines indicating a 95% confidence interval, and box showing zircon fission track constraints.

Considerations

Preliminary fission-track analyses provide a adequate initial estimate of cooling history as a baseline that can be expanded upon.

The quantity of apatite samples amenable to fission track analysis was limited by abundant inclusions, crystal defects, and uranium heterogeneity. Additionally, uranium contents tended to be low ($\sim$1-3 ppm), limiting spontaneous fission track density.

A significant amount of zircons were sufficiently old to have too uncountably large numbers of fission tracks, and/or had abundant defects and inclusions. The zircons used for the cooling model are therefore a biased sub-set of the total zircon population.

Bibliography

Adams, J. E. (1943), 'Paleogeography and petroleum exploration', *Journal of Sedimentary Research* **13**(3), 108–111.

Aitken, J. F. (1998), 'Sedimentology of Late Devensian glaciofluvial outwash in the Don Valley, Grampian Region', *Scottish Journal of Geology* **34**(2), 97–117.

Al-Siyabi, H. A. (2005), 'Exploration history of the Ara intrasalt carbonate stringers in the South Oman Salt Basin', *GeoArabia* **10**(4), 39–72.

Allen, J. R. L. (1966), 'On bedforms and palaeocurrents', *Sedimentology* **6**(3), 153–190.

Allen, J. R. L. (1970), *Physical Processes of Sedimentation*, Unwin, London.

Allen, P. A. and Allen, J. R. L. (2013), *Basin Analysis: Principles and Application to Petroleum Play Assessment*.

Alvarez, P. and Maurin, J.-C. (1991), 'Evolution sédimentaire et tectonique du bassin protérozoïque supérieur de Comba (Congo) : Stratigraphie séquentielle du Supergroupe Ouest-Congolien et modèle d'amortissement sur décrochements dans le contexte de la tectogénèse panafricaine', *Precambrian Research* **50**(1), 137–171.

Andersen, L. and Unrug, R. (1984), 'Geodynamic evolution of the Bangweulu Block, northern Zambia', *Precambrian Research* **25**(1-3), 187–212.

Anderton, R. (1985), 'Clastic facies models and facies analysis', *Geological Society, London, Special Publications* **18**(1), 31–47.

Annels, A. (1989), 'Ore genesis in the Zambian Copperbelt with particular reference to the northern sector of the Chambishi basin', *Geological Association of Canada, Special Paper* **36**, 427–452.

Annels, A. E. (1974), 'Some aspects of the stratiform ore deposits of the Zambian Copperbelt and their genetic significance', *Annales de la Société géologique de Belgique* .

Annels, A. E. (1984), 'The geotectonic environment of Zambian copper-cobalt mineralization', *Journal of the Geological Society* **141**(2), 279–289.

Antia, E., Flemming, B. and Wefer, G. (1994), 'Transgressive facies sequence of a high energy, wave-tide-storm-influenced shoreface: A case study of the east Frisian Barrier Islands (Southern North Sea)', *Facies* **30**(1), 15–23.

Armstrong, R., Master, S. and Robb, L. (2005), 'Geochronology of the Nchanga Granite, and constraints on the maximum age of the Katanga Supergroup, Zambian Copperbelt', *Journal of African Earth Sciences* **42**(1-5), 32–40.

Ashley, G. M. (1990), 'Classification of Large-Scale Subaqueous Bedforms: A New Look at an Old Problem-SEPM Bedforms and Bedding Structures', *SEPM Journal of Sedimentary Research* **Vol. 60**.

Ashley, G. M., Southard, J. B. and Boothroyd, J. C. (1982), 'Deposition of climbing-ripple beds: a flume simulation', *Sedimentology* **29**(1), 67–79.

Athy, L. F. (1930), 'Density, Porosity, and Compaction of Sedimentary Rocks', *AAPG Bulletin* **14**(1), 1–24.

Barr, M. W. C., Cahen, L. and Ledent, D. (1978), 'Geochronology of syntectonic granites from Central Zambia: Lusaka Granite and granite NE of Rufunsa', *Annales de la Société géologique de Belgique* .

Barra, F., Broughton, D. W., Ruiz, M. and Hitzman, M. W. (2004), 'Multi-stage mineralization in the Zambian Copperbelt based on Re-Os isotope constraints.', *Geological Society of America Abstracts with Programs* **36**(5), 516.

Barton, P. and Wood, R. (1984), 'Tectonic evolution of the North Sea basin: crustal stretching and subsidence', *Geophysical Journal International* **79**(3), 987–1022.

Basson, I. J., McCall, M.-J., Koegelenberg, C. K. and Jakaitė, L. (2023), 'Emplacement and preservation of mineralized écaille within Roan Breccia of the Lufilian Arc, Central African Copperbelt: the Thrust Belt Boudinage model', *Mineralium Deposita* **58**(3), 511–529.

Batumike, M., Cailteux, J. and Kampunzu, A. (2007), 'Lithostratigraphy, basin development, base metal deposits, and regional correlations of the Neoproterozoic Nguba and Kundelungu rock successions, central African Copperbelt', *Gondwana Research* **11**(3), 432–447.

Batumike, M., Kampunzu, A. and Cailteux, J. (2006), 'Petrology and geochemistry of the Neoproterozoic Nguba and Kundelungu Groups, Katangan Supergroup, southeast Congo: Implications for provenance, paleoweathering and geotectonic setting', *Journal of African Earth Sciences* **44**(1), 97–115.

Bennett, M. R., Doyle, P. and Mather, A. E. (1996), 'Dropstones: their origin and significance', *Palaeogeography, Palaeoclimatology, Palaeoecology* **121**(3), 331–339.

Beukes, N. J. and Lowe, D. R. (1989), 'Environmental control on diverse stromatolite morphologies in the 3000 Myr Pongola Supergroup, South Africa', *Sedimentology* **36**(3), 383–397.

Binda, P. L. (1994), 'Stratigraphy of Zambian copperbelt orebodies', *Journal of African Earth Sciences* **19**(4), 251–264.

Binda, P. L. and Mulgrew, J. R. (1974), 'Stratigraphy of copper occurrences in the Zambian Copperbelt', *Annales de la Société géologique de Belgique* .

Binda, P. L. and Van Eden, J. G. (1972), 'Sedimentological evidence on the origin of the Precambrian Great Conglomerate (Kundelungu Tillite), Zambia', *Palaeogeography, Palaeoclimatology, Palaeoecology* **12**(3), 151–168.

Bodiselitsch, B., Koeberl, C., Master, S. and Reimold, W. U. (2005), 'Estimating Duration and Intensity of Neoproterozoic Snowball Glaciations from Ir Anomalies', *Science* **308**(5719), 239–242.

Bosence, D., Procter, E., Aurell, M., Bel Kahla, A., Boudagher-Fadel, M., Casaglia, F., Cirilli, S., Mehdie, M., Nieto, L., Rey, J., Scherreiks, R., Soussi, M. and Waltham, D. (2009), 'A Dominant Tectonic Signal in High-Frequency, Peritidal Carbonate Cycles? A Regional Analysis of Liassic Platforms from Western Tethys', *Journal of Sedimentary Research* **79**(6), 389–415.

Bosence, D. W. J. (1998), Stratigraphic and sedimentological models of rift basins, *in* B. H. Purser and D. W. J. Bosence, eds, 'Sedimentation and Tectonics in Rift Basins: Red Sea - Gulf of Aden', Springer Netherlands, Dordrecht, pp. 9–25.

Bouma, A. H., Kuenen, P. H. and Shepard, F. P. (1962), *Sedimentology of some Flysch deposits: a graphic approach to facies interpretation*, Elsevier Pub. Co., Amsterdam; New York.

Brookfield, M. E. (1977), 'The origin of bounding surfaces in ancient aeolian sandstones', *Sedimentology* **24**(3), 303–332.

Broughton, D. W., Hitzman, M. W. and Stephens, A. J. (2002), Exploration History and Geology of the Kansanshi Cu(-Au) Deposit, Zambia, *in* R. J. Goldfarb and R. L. Nielsen, eds, 'Integrated Methods for Discovery: Global Exploration in the Twenty-First Century', Vol. 9, Society of Economic Geologists.

Broughton, D. W. and Rogers, T. (2010), Discovery of the Kamoa Copper Deposit, Central African Copperbelt, D.R.C., *in* R. J. Goldfarb, E. E. Marsh and T. Monecke, eds, 'The Challenge of Finding New Mineral Resources: Global Metallogeny, Innovative Exploration, and New Discoveries', Vol. 15 (1), Society of Economic Geologists.

Buchanan, D. L., Nolan, J., Suddaby, P., Rouse, J. E., Viljoen, M. J. and Davenport, J. W. J. (1981), 'The genesis of sulfide mineralization in a portion of the Potgietersrus Limb of the Bushveld Complex', *Economic Geology* **76**(3), 568–579.

Bull, S., Selley, D., Broughton, D., Hitzman, M., Cailteux, J., Large, R. and McGoldrick, P. (2011), 'Sequence and carbon isotopic stratigraphy of the Neoproterozoic Roan Group strata of the Zambian copperbelt', *Precambrian Research* **190**(1-4), 70–89.

Bull, W. B. (1977), 'The alluvial-fan environment', *Progress in Physical Geography: Earth and Environment* **1**(2), 222–270.

Cahen, L. (1984), *The geochronology and evolution of Africa*, Clarendon Press, Oxford.

Cahen, L., J, D. and D, L. (1970), 'On the age and petrogenesis of the microcline-bearing pegmatite veins at Roan Antelope and at Musoshi (Copperbelt of Zambia and S-E Katanga)', *Annales Musée royale de l'Afrique Centrale, Sci. géol.* **65**, 43–68.

Cailteux, J., Binda, P., Katekesha, W., Kampunzu, A., Intiomale, M., Kapenda, D., Kaunda, C., Ngongo, K., Tshiauka, T. and Wendorff, M. (1994), 'Lithostratigraphical correlation of the Neoproterozoic Roan Supergroup from Shaba (Zaire) and Zambia, in the central African copper-cobalt metallogenic province', *Journal of African Earth Sciences* **19**(4), 265–278.

Cailteux, J. L. and De Putter, T. (2019), 'The Neoproterozoic Katanga Supergroup (D. R. Congo): State-of-the-art and revisions of the lithostratigraphy, sedimentary basin and geodynamic evolution', *Journal of African Earth Sciences* **150**, 522–531.

Cathles, III, L. M. and Adams, J. J. (2005), Fluid Flow and Petroleum and Mineral Resources in the Upper (<20-km) Continental Crust, *in* J. W. Hedenquist, J. F. H. Thompson, R. J. Goldfarb and J. P. Richards, eds, 'One Hundredth Anniversary Volume', Society of Economic Geologists.

Catuneanu, O. (2017), Chapter One - Sequence Stratigraphy: Guidelines for a Standard Methodology, *in* M. Montenari, ed., 'Stratigraphy & Timescales', Vol. 2 of *Advances in Sequence Stratigraphy*, Academic Press, pp. 1–57.

Catuneanu, O., Abreu, V., Bhattacharya, J., Blum, M., Dalrymple, R., Eriksson, P., Fielding, C., Fisher, W., Galloway, W., Gibling, M., Giles, K., Holbrook, J., Jordan, R., Kendall, C., Macurda, B., Martinsen, O., Miall, A., Neal, J., Nummedal, D., Pomar, L., Posamentier, H., Pratt, B., Sarg, J., Shanley, K., Steel, R., Strasser, A., Tucker, M. and Winker, C. (2009), 'Towards the standardization of sequence stratigraphy', *Earth-Science Reviews* **92**(1-2), 1–33.

Chenin, P., Manatschal, G., Ghienne, J.-F. and Chao, P. (2022), 'The syn-rift tectono-stratigraphic record of rifted margins (Part II): A new model to break through the proximal/distal interpretation frontier', *Basin Research* **34**(2), 489–532.

Christeleit, E. C., Brandon, M. T. and Zhuang, G. (2015), 'Evidence for deep-water deposition

of abyssal Mediterranean evaporites during the Messinian salinity crisis', *Earth and Planetary Science Letters* **427**, 226–235.

Clemmey, H. (1974), 'Sedimentary geology of a late Precambrian copper deposit at Kitwe, Zambia', *Annales de la Société géologique de Belgique* .

Clemmey, H. (1976), Aspects of stratigraphy, sedimentology and ore genesis on the Zambian Copperbelt., PhD thesis, University of Leeds, Leeds.

Cloetingh, S. and Burov, E. (2011), 'Lithospheric folding and sedimentary basin evolution: a review and analysis of formation mechanisms: Lithospheric folding and sedimentary basin evolution', *Basin Research* **23**(3), 257–290.

Cook, H. E., McDaniel, P. N., Mountjoy, E. W. and Pray, L. C. (1972), 'Allochthonous carbonate debris flows at Devonian bank ('reef') margins Alberta, Canada', *Bulletin of Canadian Petroleum Geology* **20**(3), 439–497.

Cosi, M., De Bonis, A., Gosso, G., Hunziker, J., Martinotti, G., Moratto, S., Robert, J. and Ruhlman, F. (1992), 'Late proterozoic thrust tectonics, high-pressure metamorphism and uranium mineralization in the Domes Area, Lufilian Arc, Northwestern Zambia', *Precambrian Research* **58**(1-4), 215–240.

Coward, M. and Daly, M. (1984), 'Crustal lineaments and shear zones in Africa: Their relationship to plate movements', *Precambrian Research* **24**(1), 27–45.

Creveling, J. R. and Mitrovica, J. X. (2014), 'The sea-level fingerprint of a Snowball Earth deglaciation', *Earth and Planetary Science Letters* **399**, 74–85.

Daly, M. C. (1986*a*), 'Crustal shear zones and thrust belts: their geometry and continuity in Central Africa', *Philosophical Transactions of the Royal Society of London. Series A, Mathematical and Physical Sciences* **317**(1539), 111–128.

Daly, M. C. (1986*b*), 'The intracratonic Irumide Belt of Zambia and its bearing on collision orogeny during the Proterozoic of Africa', *Geological Society, London, Special Publications* **19**(1), 321–328.

Daly, M. C. (1988), 'Crustal Shear Zones in Central Africa: a Kinematic Approach to Proterozoic Tectonics', *Episodes* **11**(1), 5–11.

Daly, M. C., Chorowicz, J. and Fairhead, J. D. (1989), 'Rift basin evolution in Africa: the influence of reactivated steep basement shear zones', *Geological Society, London, Special Publications* **44**(1), 309–334.

Daly, M. C., Green, P., Watts, A. B., Davies, O., Chibesakunda, F. and Walker, R. (2020), 'Tectonics and Landscape of the Central African Plateau and their Implications for a Propagating Southwestern Rift in Africa', *Geochemistry, Geophysics, Geosystems* **21**(6).

Daly, M., Chakraborty, S., Kasolo, P., Musiwa, M., Mumba, P., Naidu, B., Namateba, C., Ngambi, O. and Coward, M. (1984), 'The Lufilian arc and Irumide belt of Zambia: Results of a geotraverse across their intersection', *Journal of African Earth Sciences (1983)* **2**(4), 311–318.

Daly, M. and Unrug, R. (1982), 'The Muva Supergroup of northern Zambia: a craton to mobile belt sedimentary sequence', *South African Journal of Geology* **85**(3), 155–165.

Dasgupta, P. (2003), 'Sediment gravity flow—the conceptual problems', *Earth-Science Reviews* **62**(3-4), 265–281.

Davey, J., Roberts, S. and Wilkinson, J. J. (2020), 'Copper- and cobalt-rich, ultrapotassic bittern brines responsible for the formation of the Nkana-Mindola deposits, Zambian Copperbelt', *Geology* **49**(3), 341–345.

Davidson, D. M. (1931), 'The geology and ore deposits of Chambishi, Northern Rhodesia', *Economic Geology* **26**(2), 131–152.

Davies, N. S. and Gibling, M. R. (2010), 'Cambrian to Devonian evolution of alluvial systems: The sedimentological impact of the earliest land plants', *Earth-Science Reviews* **98**(3), 171–200.

De Magnée, I. and Francois, A. (1988), The Origin of the Kipushi (Cu, Zn, Pb) Deposit in Direct Relation with a Proterozoic Salt Diapir. Copperbelt of Central Africa, Shaba, Republic of Zaire, *in* G. H. Friedrich and P. M. Herzig, eds, 'Base Metal Sulfide Deposits in Sedimentary and Volcanic Environments', Special Publication of the Society for Geology Applied to Mineral Deposits, Springer, Berlin, Heidelberg, pp. 74–93.

De Waele, B. and Fitzsimons, I. (2007), 'The nature and timing of Palaeoproterozoic sedimentation at the southeastern margin of the Congo Craton; zircon U–Pb geochronology of plutonic, volcanic and clastic units in northern Zambia', *Precambrian Research* **159**(1-2), 95–116.

De Waele, B., Johnson, S. and Pisarevsky, S. (2008), 'Palaeoproterozoic to Neoproterozoic growth and evolution of the eastern Congo Craton: Its role in the Rodinia puzzle', *Precambrian Research* **160**(1-2), 127–141.

De Waele, B., Kampunzu, A. B., Mapani, B. S. E. and Tembo, F. (2006), 'The Mesoproterozoic Irumide belt of Zambia', *Journal of African Earth Sciences* **46**(1), 36–70.

De Waele, B., Liégeois, J.-P., Nemchin, A. A. and Tembo, F. (2006), 'Isotopic and geochemical evidence of proterozoic episodic crustal reworking within the irumide belt of south-central Africa, the southern metacratonic boundary of an Archaean Bangweulu Craton', *Precambrian Research* **148**(3-4), 225–256.

De Waele, S., Muchez, P., Vets, J., Fernandez-Alonzo, M. and Tack, L. (2006), 'Multiphase origin of the Cu–Co ore deposits in the western part of the Lufilian fold-and-thrust belt, Katanga (Democratic Republic of Congo)', *Journal of African Earth Sciences* **46**(5), 455–469.

DeCelles, P. G. and Giles, K. A. (1996), 'Foreland basin systems', *Basin Research* **8**(2), 105–123.

Delpomdor, F., Callec, Y., Bailly, L., Mashigiro, E. H., Ilunga, S., Sebagenzi, S., Mupande, J. F., Kampata, D. and Cailteux, J. (2020), 'Sedimentary evolution and chemostratigraphy of the post-Sturtian cap carbonate-like Dolomie Tigrée Formation (Katanga Supergroup) in the Democratic Republic of the Congo', *Journal of African Earth Sciences* **162**, 103727.

Dickinson, W. R. (1974), Plate Tectonics And Sedimentation, *in* W. R. Dickinson, ed., 'Tectonics and Sedimentation', Vol. 22, SEPM Society for Sedimentary Geology.

Dunham, R. J. (1962), 'Classification of Carbonate Rocks According to Depositional Textures', **38**, 108–121.

Eden, J. G. v. (1974), 'Depositional and Diagenetic Environment Related to Sulfide Mineralization, Mufulira, Zambia', *Economic Geology* **69**(1), 59–79.

Eisbacher, G. (1985), 'Late proterozoic rifting, glacial sedimentation, and sedimentary cycles in the light of windermere deposition, Western Canada', *Palaeogeography, Palaeoclimatology, Palaeoecology* **51**(1-4), 231–254.

Ekdale, A. A. (1988), 'Pitfalls of Paleobathymetric Interpretations Based on Trace Fossil Assemblages', *PALAIOS* **3**(5), 464–472.

El Desouky, H. A., Muchez, P., Boyce, A. J., Schneider, J., Cailteux, J. L. H., Dewaele, S. and von Quadt, A. (2010), 'Genesis of sediment-hosted stratiform copper–cobalt mineralization at Luiswishi and Kamoto, Katanga Copperbelt (Democratic Republic of Congo)', *Mineralium Deposita* **45**(8), 735–763.

El Desouky, H. A., Muchez, P. and Cailteux, J. (2009), 'Two Cu–Co sulfide phases and contrasting fluid systems in the Katanga Copperbelt, Democratic Republic of Congo', *Ore Geology Reviews* **36**(4), 315–332.

Embry, A. F. (1993), 'Transgressive–regressive (T–R) sequence analysis of the Jurassic succession of the Sverdrup Basin, Canadian Arctic Archipelago', *Canadian Journal of Earth Sciences* **30**(2), 301–320.

Eriksson, P., Condie, K., Tirsgaard, H., Mueller, W., Altermann, W., Miall, A., Aspler, L., Catuneanu, O. and Chiarenzelli, J. (1998), 'Precambrian clastic sedimentation systems', *Sedimentary Geology* **120**(1-4), 5–53.

Eyles, N., Eyles, C. H. and Miall, A. D. (1983), 'Lithofacies types and vertical profile models; an alternative approach to the description and environmental interpretation of glacial diamict and diamictite sequences', *Sedimentology* **30**(3), 393–410.

Eyles, N. and Januszczak, N. (2004), "Zipper-rift': a tectonic model for Neoproterozoic glaciations during the breakup of Rodinia after 750 Ma', *Earth-Science Reviews* **65**(1-2), 1–73.

Eyles, N. and Januszczak, N. (2007), 'Syntectonic subaqueous mass flows of the Neoproterozoic Otavi Group, Namibia: where is the evidence of global glaciation?', *Basin Research* **19**(2), 179–198.

Fleischer, V. (1984), 'Discovery, geology and genesis of copper—cobalt mineralisation at Chambishi Southeast prospect, Zambia', *Precambrian Research* **25**(1-3), 119–133.

Fortuin, A. and Krijgsman, W. (2003), 'The Messinian of the Nijar Basin (SE Spain): sedimentation, depositional environments and paleogeographic evolution', *Sedimentary Geology* **160**(1-3), 213–242.

Freeze, R. A. and Cherry, J. A. (1979), *Groundwater*, Prentice-Hall.

Frey, R. W. and Howard, J. D. (1988), 'Beaches and beach-related facies, Holocene barrier islands of Georgia', *Geological Magazine* **125**(6), 621–640.

Frimmel, H. E., Basei, M. S. and Gaucher, C. (2011), 'Neoproterozoic geodynamic evolution of SW-Gondwana: a southern African perspective', *International Journal of Earth Sciences* **100**(2-3), 323–354.

Frimmel, H. E., Klötzli, U. S. and Siegfried, P. R. (1996), 'New Pb-Pb Single Zircon Age Constraints on the Timing of Neoproterozoic Glaciation and Continental Break-up in Namibia', *The Journal of Geology* **104**(4), 459–469.

Fromhold, T. A. and Wallace, M. W. (2012), 'Regional recognition of the Neoproterozoic Sturtian–Marinoan boundary, Northern and Central Adelaide Geosyncline, South Australia', *Australian Journal of Earth Sciences* **59**(4), 527–546.

Ganne, J. and Feng, X. (2017), 'Primary magmas and mantle temperatures through time', *Geochemistry, Geophysics, Geosystems* **18**(3), 872–888.

Garcia, M. H. (1994), 'Depositional Turbidity Currents Laden with Poorly Sorted Sediment', *Journal of Hydraulic Engineering* **120**(11), 1240–1263.

Garlick, W. G. (1964), 'Association of mineralization and algal reef structures on Northern Rhodesian copper-belt, Katanga, and Australia', *Economic Geology* **59**(3), 416–427.

Garlick, W. G. (1981), 'Sabkhas, slumping, and compaction at Mufulira, Zambia', *Economic Geology* **76**(7), 1817–1847.

Garlick, W. G. and Fleischer, V. (1972), 'Sedimentary environment of Zambian copper deposition.', *Geologie en Mijnbouw* **51**, 271–299.

Gawthorpe, R. L. and Leeder, M. R. (2000), 'Tectono-sedimentary evolution of active extensional basins', *Basin Research* **12**(3-4), 195–218.

Glennie, K. W. and Singhvi, A. K. (2002), 'Event stratigraphy, paleoenvironment and chronology of SE Arabian deserts', *Quaternary Science Reviews* **21**(7), 853–869.

Goscombe, B., Armstrong, R. and Barton, J. M. (2000), 'Geology of the Chewore Inliers, Zimbabwe: constraining the Mesoproterozoic to Palæozoic evolution of the Zambezi Belt', *Journal of African Earth Sciences* **30**(3), 589–627.

Goscombe, B., Foster, D. A., Gray, D. and Wade, B. (2020), 'Assembly of central Gondwana along the Zambezi Belt: Metamorphic response and basement reactivation during the Kuunga Orogeny', *Gondwana Research* **80**, 410–465.

Gressly, A. (1838), 'Observations géologiques sur le Jura Soleurois', *Neue Denkschriften der allgemeinen Schweizerischen Gesellschaft für die gesammten Naturwissenschaften* **2**, 1–112.

Grotzinger, J. and Al-Rawahi, Z. (2014), 'Depositional facies and platform architecture of microbialite-dominated carbonate reservoirs, Ediacaran–Cambrian Ara Group, Sultante of Om', *AAPG Bulletin* **98**(8), 1453–1494.

Haines, P. W., Jago, J. B. and Gum, J. C. (2010), 'Turbidite deposition in the Cambrian Kanmantoo Group, South Australia', *Australian Journal of Earth Sciences* .

Halverson, G., Porter, S. and Shields, G. (2020), The Tonian and Cryogenian Periods, *in* 'Geologic Time Scale 2020', Elsevier, pp. 495–519.

Hamilton, S. (1967), 'Copper mineralization in the upper part of the Copper Harbor Conglomerate at White Pine, Michigan', *Economic Geology* **62**(7).

Handford, C. (1981), 'A process-sedimentary framework for characterizing recent and ancient sabkhas', *Sedimentary Geology* **30**(4), 255–265.

Hanson, R. E. (2003), 'Proterozoic geochronology and tectonic evolution of southern Africa', *Geological Society, London, Special Publications* **206**(1), 427–463.

Hanson, R. E., Wardlaw, M. S., Wilson, T. J. and Mwale, G. (1993), 'U-Pb zircon ages from the Hook granite massif and Mwembeshi dislocation: constraints on Pan-African deformation, plutonism, and transcurrent shearing in Central Zambia', *Precambrian Research* **63**(3-4), 189–209.

Hanson, R. E., Wilson, T. J. and Munyanyiwa, H. (1994), 'Geologic evolution of the neoproterozoic Zambezi orogenic belt in Zambia', *Journal of African Earth Sciences* **18**(2), 135–150.

Haq, B. U. and Schutter, S. R. (2008), 'A Chronology of Paleozoic Sea-Level Changes', *Science* **322**(5898), 64–68.

Hatch, J. and Leventhal, J. (1992), 'Relationship between inferred redox potential of the depositional environment and geochemistry of the Upper Pennsylvanian (Missourian) Stark Shale Member of the Dennis Limestone, Wabaunsee County, Kansas, U.S.A.', *Chemical Geology* **99**(1-3), 65–82.

Haughton, P., Davis, C., McCaffrey, W. and Barker, S. (2009), 'Hybrid sediment gravity flow deposits – Classification, origin and significance', *Marine and Petroleum Geology* **26**(10), 1900–1918.

Hendrickson, M. D., Hitzman, M. W., Wood, D., Humphrey, J. D. and Wendlandt, R. F. (2015), 'Geology of the Fishtie deposit, Central Province, Zambia: iron oxide and copper mineralization in Nguba Group metasedimentary rocks', *Mineralium Deposita* **50**(6), 717–737.

Hitzman, M. (2000), 'Source basins for sediment-hosted stratiform Cu deposits: implications for the structure of the Zambian Copperbelt', *Journal of African Earth Sciences* **30**(4), 855–863.

Hitzman, M., Kirkham, R., Broughton, D., Thorson, J. and Selley, D. (2005), The Sediment-Hosted Stratiform Copper Ore System, *in* 'One Hundredth Anniversary Volume', Society of Economic Geologists.

Hitzman, M. W. and Broughton, D. W. (2017), 'Discussion: "Age of the Zambian Copperbelt" by Sillitoe et al. (2017) Mineralium Deposita', *Mineralium Deposita* **52**(8), 1273–1275.

Hitzman, M. W., Selley, D. and Bull, S. (2010), 'Formation of Sedimentary Rock-Hosted Stratiform Copper Deposits through Earth History', *Economic Geology* **105**(3), 627–639.

Hoffman, P. F., Abbot, D. S., Ashkenazy, Y., Benn, D. I., Brocks, J. J., Cohen, P. A., Cox, G. M., Creveling, J. R., Donnadieu, Y., Erwin, D. H., Fairchild, I. J., Ferreira, D., Goodman, J. C., Halverson, G. P., Jansen, M. F., Le Hir, G., Love, G. D., Macdonald, F. A., Maloof, A. C., Partin, C. A., Ramstein, G., Rose, B. E. J., Rose, C. V., Sadler, P. M., Tziperman, E., Voigt, A. and Warren, S. G. (2017), 'Snowball Earth climate dynamics and Cryogenian geology-geobiology', *Science Advances* **3**(11), e1600983.

Hoffmann, K.-H., Condon, D. J., Bowring, S. A. and Crowley, J. L. (2004), 'U-Pb zircon date from the Neoproterozoic Ghaub Formation, Namibia: Constraints on Marinoan glaciation', *Geology* **32**(9), 817–820.

Holz, M., Vilas-Boas, D. B., Troccoli, E. B., Santana, V. C. and Vidigal-Souza, P. A. (2017), Conceptual Models for Sequence Stratigraphy of Continental Rift Successions, *in* 'Stratigraphy & Timescales', Vol. 2, Elsevier, pp. 119–186.

Hood, A. v. S. and Wallace, M. W. (2018), 'Neoproterozoic marine carbonates and their paleoceanographic significance', *Global and Planetary Change* **160**, 28–45.

Hood, A. v. S., Wallace, M. W., Reed, C. P., Hoffmann, K. H. and Freyer, E. E. (2015), 'Enigmatic carbonates of the Ombombo Subgroup, Otavi Fold Belt, Namibia: A prelude to extreme Cryogenian anoxia?', *Sedimentary Geology* **324**, 12–31.

Hou, B., Keeling, J. and Li, Z. (2017), 'Paleovalley-related uranium deposits in Australia and China: A review of geological and exploration models and methods', *Ore Geology Reviews* **88**, 201–234. **URL:** *https://www.sciencedirect.com/science/article/pii/S0169136817300665*

Huismans, R. S., Podladchikov, Y. Y. and Cloetingh, S. (2001), 'Transition from passive to active rifting: Relative importance of asthenospheric doming and passive extension of the lithosphere', *Journal of Geophysical Research: Solid Earth* **106**(B6), 11271–11291.

Hunt, D. and Tucker, M. E. (1992), 'Stranded parasequences and the forced regressive wedge systems tract: deposition during base-level fall', *Sedimentary Geology* **81**(1-2), 1–9.

Hurst, A., Scott, A. and Vigorito, M. (2011), 'Physical characteristics of sand injectites', *Earth-Science Reviews* **106**(3-4), 215–246.

Immenhauser, A. (2009), 'Estimating palaeo-water depth from the physical rock record', *Earth-Science Reviews* **96**(1-2), 107–139.

Ingram, R. L. (1954), 'Terminology for the thickness of stratification and parting units in sedimentary rocks', *Geological Society of America Bulletin* **65**(9), 937.

Jackson, G. C. A. (1932), 'The Geology of the N'Changa District, Northern Rhodesia', *Quarterly Journal of the Geological Society* **88**(1-4), 443–515.

Jackson, M. P. A. and Warin, O. N. (2003), 'Neoproterozoic allochthonous salt tectonics during the Lufilian orogeny in the Katangan Copperbelt, central Africa', *Geological Society of America Bulletin* p. 17.

Jacobs, J., Pisarevsky, S., Thomas, R. J. and Becker, T. (2008), 'The Kalahari Craton during the assembly and dispersal of Rodinia', *Precambrian Research* **160**(1), 142–158.

Jaffey, A., Flynn, K., Glendenin, L., Bentley, W. and Essling, A. (1971), 'Precision Measurement of Half-Lives and Specific Activities of 235U and 238U', *Physical review C* **4**(5).

James, N. P. and Dalrymple, R. W., eds (2010), *Facies Models 4*, GEOtext 6, Geological Association of Canada c/o Department of Earth Sciences Memorial University of Newfoundland St. John's, Newfoundland & Labrador.

John, T., Schenk, V., Haase, K., Scherer, E. and Tembo, F. (2003), 'Evidence for a Neoproterozoic ocean in south-central Africa from mid-oceanic-ridge–type geochemical signatures and pressure-temperature estimates of Zambian eclogites', *Geology* **31**(3), 243–246.

John, T., Schenk, V., Mezger, K. and Tembo, F. (2004), 'Timing and PT Evolution of Whiteschist Metamorphism in the Lufilian Arc–Zambezi Belt Orogen (Zambia): Implications for the Assembly of Gondwana', *The Journal of Geology* **112**(1), 71–90.

Johnson, S., De Waele, B., Evans, D., Banda, W., Tembo, F., Milton, J. and Tani, K. (2007), 'Geochronology of the Zambezi Supracrustal Sequence, Southern Zambia: A Record of Neo-

proterozoic Divergent Processes along the Southern Margin of the Congo Craton', *The Journal of Geology* **115**(3), 355–374.

Jopling, A. V. and Walker, R. G. (1968), 'Morphology and origin of ripple-drift cross-lamination, with examples from the Pleistocene of Massachusetts', *Journal of Sedimentary Research* **38**(4), 971–984.

Jordaan, J. (1961), Nkana, *in* F. Mendelsohn, ed., 'The geology of the Northern Rhodesian copperbelt', MacDonald, London, pp. p. 297–328.

Kampunzu, A. and Cailteux, J. (1999), 'Tectonic Evolution of the Lufilian Arc (Central Africa Copper Belt) During Neoproterozoic Pan African Orogenesis', *Gondwana Research* **2**(3), 401–421.

Kampunzu, A., Cailteux, J., Kamona, A., Intiomale, M. and Melcher, F. (2009), 'Sediment-hosted Zn–Pb–Cu deposits in the Central African Copperbelt', *Ore Geology Reviews* **35**(3-4), 263–297.

Kampunzu, A., Cailteux, J., Moine, B. and Loris, H. (2005), 'Geochemical characterisation, provenance, source and depositional environment of 'Roches Argilo-Talqueuses' (RAT) and Mines Subgroups sedimentary rocks in the Neoproterozoic Katangan Belt (Congo): Lithostratigraphic implications', *Journal of African Earth Sciences* **42**(1-5), 119–133.

Kampunzu, A., Kapenda, D. and Manteka, B. (1991), 'Basic magmatism and geotectonic evolution of the Pan African belt in central Africa: Evidence from the Katangan and West Congolian segments', *Tectonophysics* **190**(2-4), 363–371.

Kampunzu, A., Tembo, F., Matheis, G., Kapenda, D. and Huntsman-Mapila, P. (2000), 'Geochemistry and Tectonic Setting of Mafic Igneous Units in the Neoproterozoic Katangan Basin, Central Africa: Implications for Rodinia Break-up', *Gondwana Research* **3**(2), 125–153.

Kennedy, K., Eyles, N. and Broughton, D. (2019), 'Basinal setting and origin of thick (1·8 km) mass-flow dominated Grand Conglomérat diamictites, Kamoa, Democratic Republic of Congo: Resolving climate and tectonic controls during Neoproterozoic glaciations', *Sedimentology* **66**(2), 556–589.

Kenny, R. and Knauth, L. P. (2001), 'Stable isotope variations in the Neoproterozoic Beck Spring Dolomite and Mesoproterozoic Mescal Limestone paleokarst: Implications for life on land in the Precambrian', *GSA Bulletin* **113**(5), 650–658.

Key, R., Liyungu, A., Njamu, F., Somwe, V., Banda, J., Mosley, P. and Armstrong, R. (2001), 'The western arm of the Lufilian Arc in NW Zambia and its potential for copper mineralization', *Journal of African Earth Sciences* **33**(3-4), 503–528.

Kiefer, C., Oswald, P., Moernaut, J., Fabbri, S. C., Mayr, C., Strasser, M. and Krautblatter, M. (2021), 'A 4,000 year debris-flow record based on amphibious investigations of fan delta activity in Plansee (Austria, Eastern Alps)'.

Krivolutskaya, N., Makvandi, S., Gongalsky, B., Kubrakova, I. and Svirskaya, N. (2021), 'Chemical Characteristics of Ore-Bearing Intrusions and the Origin of PGE–Cu–Ni Mineralization in the Norilsk Area', *Minerals* **11**(8), 819. Number: 8 Publisher: Multidisciplinary Digital Publishing Institute.
URL: *https://www.mdpi.com/2075-163X/11/8/819*

Krumbein, W. C. and Garrels, R. M. (1952), 'Origin and Classification of Chemical Sediments in Terms of pH and Oxidation-Reduction Potentials', *The Journal of Geology* **60**(1), 1–33.

Kunzmann, M., Crombez, V., Catuneanu, O., Blaikie, T. N., Barth, G. and Collins, A. S. (2020), 'Sequence stratigraphy of the ca. 1730 Ma Wollogorang Formation, McArthur Basin, Australia', *Marine and Petroleum Geology* **116**, 104297.

Lawson, D. E. (1982), 'Mobilization, Movement and Deposition of Active Subaerial Sediment Flows, Matanuska Glacier, Alaska', *The Journal of Geology* **90**(3), 279–300.

Leeder, M. (1987), 'Sediment deformation structures and the palaeotectonic analysis of sedimentary basins, with a case-study from the Carboniferous of northern England', *Geological Society, London, Special Publications* **29**(1), 137–146.

Lefebvre, J. J. (1975), 'Les roches ignées dans le Katangien du Shaba (Zaïre), le district du cuivre', *Annales de la Société géologique de Belgique* .

Lefebvre, J. J. (1977), 'Le contact entre le Kundelungu et le Roan à Mulungwishi, Shaba, Zaïre', *Annales de la Société géologique de Belgique* .

Li, C., Ripley, E. M. and Naldrett, A. J. (2009), 'A new genetic model for the giant Ni-Cu-PGE sulfide deposits associated with the Siberian flood basalts', *Economic Geology* **104**(2), 291–301.

Liu, Y. and Richard Peltier, W. (2013), 'Sea level variations during snowball Earth formation: 1. A preliminary analysis', *Journal of Geophysical Research: Solid Earth* **118**(8), 4410–4424.

Lowe, D. R. (1975), 'Water escape structures in coarse-grained sediments', *Sedimentology* **22**(2), 157–204.

Lowe, D. R. (1982), 'Sediment Gravity Flows: II Depositional Models with Special Reference to the Deposits of High-Density Turbidity Currents', *SEPM Journal of Sedimentary Research* **Vol. 52**.

Lowe, D. R. and Guy, M. (2000), 'Slurry-flow deposits in the Britannia Formation (Lower Cretaceous), North Sea: a new perspective on the turbidity current and debris flow problem', *Sedimentology* **47**(1), 31–70.

Lønne, I. and Nemec, W. (2004), 'High-arctic fan delta recording deglaciation and environment disequilibrium: High-arctic fan delta recording deglaciation', *Sedimentology* **51**(3), 553–589.

MacIntyre, T. J. (2019), Geology and geochemistry of the Kansanshi Cu-(Au) deposit, North-Western Province, Zambia, PhD thesis, Colorado School of Mines.

Mambwe, P., Delpomdor, F., Lavoie, S., Mukonki, P., Batumike, J. and Muchez, P. (2020), 'Sedimentary evolution and stratigraphy of the ˜765–740 Ma Kansuki-Mwashya platform succession in the Tenke-Fungurume Mining District, Democratic Republic of the Congo', *Geologica Belgica* **23**(1-2), 69–85.

Markwick, P. J. (2019), 'Palaeogeography in exploration', *Geological Magazine* **156**(2), 366–407.

Martin, A. J. (2000), 'Flaser and wavy bedding in ephemeral streams: a modern and an ancient example', *Sedimentary Geology* **136**(1), 1–5.

Martins-Neto, M. and Catuneanu, O. (2010), 'Rift sequence stratigraphy', *Marine and Petroleum Geology* **27**(1), 247–253.

Martinsen, O. J. (1989), 'Styles of soft-sediment deformation on a Namurian (Carboniferous) delta slope, Western Irish Namurian Basin, Ireland', *Geological Society, London, Special Publications* **41**(1), 167–177.

Mastalerz, K. (1995), 'Deposits of high-density turbidity currents on fan-delta slopes: an example from the upper Visean Szczawno formation, Intrasudetic Basin, Poland', *Sedimentary Geology* **98**(1-4), 121–146.

Master, S. and Wendorff, M. (2011), 'Chapter 12 Neoproterozoic glaciogenic diamictites of the Katanga Supergroup, Central Africa', *Geological Society, London, Memoirs* **36**(1), 173–184.

McCuaig, T., Scarselli, S., O'Connor, T., Busuttil, S. and McCormack, N. (2018), The Power of a Systems Approach to Mineral and Petroleum Exploration in Sedimentary Basins.

McGee, B., Halverson, G. P. and Collins, A. S. (2012), 'Cryogenian rift-related magmatism and sedimentation: South-western Congo Craton, Namibia', *Journal of African Earth Sciences* **76**, 34–49.

McGowan, R. R., Roberts, S. and Boyce, A. J. (2006), 'Origin of the Nchanga copper–cobalt deposits of the Zambian Copperbelt', *Mineralium Deposita* **40**(6-7), 617–638.

McGowan, R. R., Roberts, S., Foster, R. P., Boyce, A. J. and Coller, D. (2003), 'Origin of the copper-cobalt deposits of the Zambian Copperbelt: An epigenetic view from Nchanga', *Geology* **31**(6), 497.

McKenzie, D. (1978), 'Some remarks on the development of sedimentary basins', *Earth and Planetary Science Letters* **40**(1), 25–32.

Melvin, J. (1986), 'Upper Carboniferous fine-grained turbiditic sandstones from Southwest England; a model for growth in an ancient, delta-fed subsea fan', *Journal of Sedimentary Research* **56**(1), 19–34.

Mendelsohn, F., ed. (1961), *The geology of the Northern Rhodesian copperbelt*, MacDonald, London.

Miall, A. D. (1985), 'Architectural-element analysis: A new method of facies analysis applied to fluvial deposits', *Earth-Science Reviews* **22**(4), 261–308.

Miall, A. D. (2013), *The Geology of Fluvial Deposits: Sedimentary Facies, Basin Analysis, and Petroleum Geology*, Springer.

Miall, A. D. (2022), Stratigraphy: The Modern Synthesis, *in* A. D. Miall, ed., 'Stratigraphy: A Modern Synthesis', Springer Textbooks in Earth Sciences, Geography and Environment, Springer International Publishing, pp. 341–417.

Muchez, P., André-Mayer, A.-S., El Desouky, H. A. and Reisberg, L. (2015), 'Diagenetic origin of the stratiform Cu–Co deposit at Kamoto in the Central African Copperbelt', *Mineralium Deposita* **50**(4), 437–447.

Mulder, T., Syvitski, J. P., Migeon, S., Faugères, J.-C. and Savoye, B. (2003), 'Marine hyperpycnal flows: initiation, behavior and related deposits. A review', *Marine and Petroleum Geology* **20**(6-8), 861–882.

Myrow, P. M. and Southard, J. B. (1996), 'Tempestite deposition', *Journal of Sedimentary Research* **66**, 875–887.

Müller, R. D., Cannon, J., Williams, S. and Dutkiewicz, A. (2018), 'PyBacktrack 1.0: A Tool for Reconstructing Paleobathymetry on Oceanic and Continental Crust', *Geochemistry, Geophysics, Geosystems* **19**(6), 1898–1909.

Naydenov, K. V., Lehmann, J., Saalmann, K., Milani, L., Kinnaird, J. A., Charlesworth, G., Frei, D. and Rankin, W. (2014), 'New constraints on the Pan-African Orogeny in Central Zambia: A structural and geochronological study of the Hook Batholith and the Mwembeshi Zone', *Tectonophysics* **637**, 80–105.

Nemec, W. and Steel, R. J. (1984), 'Alluvial and Coastal Conglomerates: Their Significant Features and Some Comments on Gravelly Mass-Flow Deposits', pp. 1–31. CSPG Special Publications.

Nichols, G. and Fisher, J. (2007), 'Processes, facies and architecture of fluvial distributary system deposits', *Sedimentary Geology* **195**(1-2), 75–90.

Noffke, N. (2009), 'The criteria for the biogeneicity of microbially induced sedimentary structures (MISS) in Archean and younger, sandy deposits', *Earth-Science Reviews* **96**(3), 173–180.

Nottvedt, A., Gabrielsen, R. and Steel, R. (1995), 'Tectonostratigraphy and sedimentary architecture of rift basins, with reference to the northern North Sea', *Marine and Petroleum Geology* **12**(8), 881–901.

Owen, G. (1996), 'Experimental soft-sediment deformation: structures formed by the liquefaction of unconsolidated sands and some ancient examples', *Sedimentology* **43**(2), 279–293.

Parnell, J., Wang, X., Raab, A., Feldmann, J., Brolly, C., Michie, R. and Armstrong, J. (2021), 'Metal Flux from Dissolution of Iron Oxide Grain Coatings in Sandstones', *Geofluids* **2021**, 1–14.

Patranabis-Deb, S. and Chaudhuri, A. K. (2007), 'A retreating fan-delta system in the Neoproterozoic Chattisgarh rift basin, central India: Major controls on its evolution', *AAPG Bulletin* **91**(6), 785–808.

Payton, C. E. (1977), *Seismic Stratigraphy — Applications to Hydrocarbon Exploration*, American Association of Petroleum Geologists.

Pettijohn, F., Potter, P. and Siever, R. (1987), *Sand and Sandstone*, Springer New York, NY.

Pickering, K., Stow, D., Watson, M. and Hiscott, R. (1986), 'Deep-water facies, processes and models: a review and classification scheme for modern and ancient sediments', *Earth-Science Reviews* **23**(2), 75–174.

Plint, A. G. and Nummedal, D. (2000), 'The falling stage systems tract: recognition and importance in sequence stratigraphic analysis', *Geological Society, London, Special Publications* **172**(1), 1–17.

Pontén, A. and Plink-Björklund, P. (2007), 'Depositional environments in an extensive tide-influenced delta plain, Middle Devonian Gauja Formation, Devonian Baltic Basin', *Sedimentology* **54**(5), 969–1006.

Porada, H. (1989), 'Pan-African rifting and orogenesis in southern to equatorial Africa and eastern Brazil', *Precambrian Research* **44**(2), 103–136.

Porada, H. and Berhorst, V. (2000), 'Towards a new understanding of the Neoproterozoic-early palæozoic Lufilian and northern Zambezi belts in Zambia and the Democratic Republic of Congo', *Journal of African Earth Sciences* **30**(3), 727–771.

Posamentier, H. W. and Allen, G. P. (1999), *Siliciclastic Sequence Stratigraphy—Concepts and Applications*, SEPM Society for Sedimentary Geology.

Posamentier, H. W., Jervey, M. T. and Vail, P. R. (1988), 'Eustatic Controls on Clastic Deposition I—conceptual Framework'.

Posamentier, H. W. and Vail, P. R. (1988), Eustatic Controls on Clastic Deposition II—sequence and Systems Tract Models, *in* 'Sea-Level Changes: An Integrated Approach', SEPM (Society for Sedimentary Geology).

Price, P. B. and Walker, R. M. (1962), 'Chemical Etching of Charged-Particle Tracks in Solids', *Journal of Applied Physics* **33**(12), 3407–3412.
URL: *https://doi.org/10.1063/1.1702421*

Price, P. B. and Walker, R. M. (1963), 'Fossil tracks of charged particles in mica and the age of minerals', *Journal of Geophysical Research (1896-1977)* **68**(16), 4847–4862. _eprint: https://onlinelibrary.wiley.com/doi/pdf/10.1029/JZ068i016p04847.
URL: *https://onlinelibrary.wiley.com/doi/abs/10.1029/JZ068i016p04847*

Rainaud, C., Master, S., Armstrong, R. and Robb, L. (2005), 'Geochronology and nature of the Palaeoproterozoic basement in the Central African Copperbelt (Zambia and the Democratic Republic of Congo), with regional implications', *Journal of African Earth Sciences* **42**(1-5), 1–31.

Raji, M., Gröcke, D. R., Greenwell, H. C., Gluyas, J. G. and Cornford, C. (2015), 'The effect of interbedding on shale reservoir properties', *Marine and Petroleum Geology* **67**, 154–169.

Ramli, M. T. L., Amijaya, H. and Akmaluddin (2021), 'The Lithofacies of Pandua Formation Shale in the Andowia Area, North Konawe, Southeast Sulawesi and Its potential as Petroleum source rock', *E3S Web of Conferences* **325**, 08013.
URL: *https://www.e3s-conferences.org/10.1051/e3sconf/202132508013*

Reading, B. G. (1978), *Sedimentary environments and facies*, Blackwell Scientific Publication.

Reineck, H.-E. and Singh, I. B. (1980), *Depositional Sedimentary Environments*, 2 edn, Springer Berlin, Heidelberg.

Reineck, H.-E. and Wunderlich, F. (1968), 'Classification and Origin of Flaser and Lenticular Bedding', *Sedimentology* **11**(1-2), 99–104.

Richards, J. P., Krogh, T. E. and Spooner, E. T. C. (1988), 'Fluid inclusion characteristics and U-Pb rutile age of late hydrothermal alteration and veining at the Musoshi stratiform copper deposit, Central African copper belt, Zaire', *Economic Geology* **83**(1), 118–139.
URL: *http://pubs.geoscienceworld.org/economicgeology/article/83/1/118/20439/Fluid-inclusion-characteristics-and-UPb-rutile-age*

Riley, T. R., Millar, I. L., Carter, A., Flowerdew, M. J., Burton-Johnson, A., Bastias, J., Storey, C. D., Castillo, P., Chew, D. and Whitehouse, M. J. (2023), 'Evolution of an Accretionary Complex (LeMay Group) and Terrane Translation in the Antarctic Peninsula', *Tectonics* **42**(2), e2022TC007578.

Robert, M. (1933), 'Le système du Kundelungu au Katanga', *Bulletin des séances de l'Institut royal colonial belge* **4**(2), 436–440.

Robert, M. (1940), 'Contribution à la géologie du Katanga: Le système du Kundelungu et le système schisto-dolomitique', *Mémoires - Institut royal colonial belge. Section des sciences naturelles et médicales. Collection in 8* **6**, 1–108.

Roberts, A. M., Kusznir, N. J., Yielding, G. and Styles, P. (1998), '2D flexural backstripping of extensional basins; the need for a sideways glance', *Petroleum Geoscience* **4**(4), 327–338.

Rooney, A. D., Strauss, J. V., Brandon, A. D. and Macdonald, F. A. (2015), 'A Cryogenian chronology: Two long-lasting synchronous Neoproterozoic glaciations', *Geology* **43**(5), 459–462.

Roveri, M., Lugli, S., Manzi, V., Reghizzi, M. and Rossi, F. (2020), 'Stratigraphic relationships between shallow-water carbonates and primary gypsum: insights from the Messinian succession of the Sorbas Basin (Betic Cordillera, Southern Spain)', *Sedimentary Geology* **404**, 105678.

Ru, K. and Pigott, J. D. (1986), 'Episodic Rifting and Subsidence in the South China Sea', *AAPG Bulletin* **70**(9), 1136–1155.

Ruffell, A., Moles, N. and Parnell, J. (1998), 'Characterisation and prediction of sediment-hosted ore deposits using sequence stratigraphy', *Ore Geology Reviews* **12**(4), 207–223.

Saintilan, N. J., Selby, D., Creaser, R. A. and Dewaele, S. (2018), 'Sulphide Re-Os geochronology links orogenesis, salt and Cu-Co ores in the Central African Copperbelt', *Scientific Reports* **8**(1), 14946.

Sanders, D. (2010), 'Sedimentary facies and progradational style of a Pleistocene talus-slope succession, Northern Calcareous Alps, Austria', *Sedimentary Geology* **228**(3), 271–283.

Sarafian, E., Evans, R. L., Abdelsalam, M. G., Atekwana, E., Elsenbeck, J., Jones, A. G. and Chikambwe, E. (2018), 'Imaging Precambrian lithospheric structure in Zambia using electromagnetic methods', *Gondwana Research* **54**, 38–49.

Schlager, W. (1993), 'Accommodation and supply—a dual control on stratigraphic sequences', *Sedimentary Geology* **86**(1-2), 111–136.

Schlager, W., Reijmer, J. J. G. and Droxler, A. (1994), 'Highstand shedding of carbonate platforms', *Journal of Sedimentary Research* **64**(3b), 270–281.

Schmandt, D., Broughton, D., Hitzman, M. W., Plink-Bjorklund, P., Edwards, D. and Humphrey, J. (2013), 'The Kamoa Copper Deposit, Democratic Republic of Congo: Stratigraphy, Diagenetic and Hydrothermal Alteration, and Mineralization', *Economic Geology* **108**(6), 1301–1324.

Schneiderhöhn, H. (1932), 'The geology of the copperbelt, Northern Rhodesia', *Mining Magazine* **46**, 241–245.

Schull, T. J. (1988), 'Rift Basins of Interior Sudan: Petroleum Exploration and Discovery1', *AAPG Bulletin* **72**(10), 1128–1142.

Sclater, J. G. and Christie, P. A. F. (1980), 'Continental stretching: An explanation of the Post-Mid-Cretaceous subsidence of the central North Sea Basin', *Journal of Geophysical Research: Solid Earth* **85**(B7), 3711–3739.

Selley, D., Broughton, D., Scott, R., Hitzman, M., Bull, S., Large, R., McGoldrick, P., Croaker, M., Pollington, N. and Barra, F. (2005), A New Look at the Geology of the Zambian Copperbelt, *in* 'One Hundredth Anniversary Volume', Society of Economic Geologists.

Selley, D., Scott, R., Emsbo, P., Koziy, L., Hitzman, M. W., Bull, S. W., Duffett, M., Sebagenzi, S., Halpin, J. and Broughton, D. W. (2018), Structural Configuration of the Central African Copperbelt: Roles of Evaporites in Structural Evolution, Basin Hydrology, and Ore Location, *in* 'Metals, Minerals, and Society', Society of Economic Geologists.

Sepkoski, J. J. (1982), Flat-Pebble Conglomerates, Storm Deposits, and the Cambrian Bottom Fauna, *in* G. Einsele and A. Seilacher, eds, 'Cyclic and Event Stratification', Springer, Berlin, Heidelberg, pp. 371–385.

Shanmugam, G. (1996), 'High-density turbidity currents; are they sandy debris flows?', *Journal of Sedimentary Research* **66**(1), 2–10.

Shanmugam, G. (2000), '50 years of the turbidite paradigm (1950s—1990s): deep-water processes and facies models—a critical perspective', *Marine and Petroleum Geology* **17**(2), 285–342.

Shanmugam, G. (2021), Gravity flows: debris flows, grain flows, liquefied/fluidized flows, turbidity currents, hyperpycnal flows, and contour currents, *in* 'Mass Transport, Gravity Flows, and Bottom Currents', Elsevier, pp. 89–148.

Shultz, A. W. (1984), 'Subaerial Debris-Flow Deposition in the Upper Paleozoic Cutler Formation, Western Colorado', *SEPM Journal of Sedimentary Research* **54**(3), 759–772.

Siahi, M., Hofmann, A., Hegner, E. and Master, S. (2016), 'Sedimentology and facies analysis of Mesoarchaean stromatolitic carbonate rocks of the Pongola Supergroup, South Africa', *Precambrian Research* **278**, 244–264.

Sillitoe, R. H., Perelló, J., Creaser, R. A., Wilton, J., Wilson, A. J. and Dawborn, T. (2017), 'Age of the Zambian Copperbelt', *Mineralium Deposita* **52**(8), 1245–1268.

Sloss, L. L. (1962), 'Stratigraphic Models in Exploration 1', *AAPG Bulletin* **46**(7), 1050–1057.

Steckler, M. and Watts, A. (1978), 'Subsidence of the Atlantic-type continental margin off New York', *Earth and Planetary Science Letters* **41**(1), 1–13.

Stow, D. A. V. and Shanmugam, G. (1980), 'Sequence of structures in fine-grained turbidites: Comparison of recent deep-sea and ancient flysch sediments', *Sedimentary Geology* **25**(1), 23–42.

Stow, D. and Smillie, Z. (2020), 'Distinguishing between Deep-Water Sediment Facies: Turbidites, Contourites and Hemipelagites', *Geosciences* **10**(2).

Studt, F. E. (1913), 'The geology of Katanga and Northern Rhodesia : an outline of the geology of South Central Africa', *South African Journal of Geology* **16**(1), 44–80.

Stutzer, O. (1911), 'Über Dwykakonglomerat im Lande Katanga, Belgisch-Kongo.', *Zeitschrift der Deutschen Geologischen Gesellschaft* pp. 626–629.

Sweeney, M. and Binda, P. (1994), 'Some constraints on the formation of the Zambian Copperbelt deposits', *Journal of African Earth Sciences* **19**(4), 303–313.

Sweeney, M., Binda, P. and Vaughan, D. (1991), 'Genesis of the ores of the Zambian Copperbelt', *Ore Geology Reviews* **6**(1), 51–76.

Sweeney, M., Turner, P. and Vaughan, D. J. (1986), 'Stable isotope and geochemical studies in the role of early diagenesis in ore formation, Konkola Basin, Zambian copper belt', *Economic Geology* **81**(8), 1838–1852.

Talling, P. J., Masson, D. G., Sumner, E. J. and Malgesini, G. (2012), 'Subaqueous sediment density flows: Depositional processes and deposit types', *Sedimentology* **59**(7), 1937–2003.

Teichert, C. (1958), 'Concepts of Facies', *AAPG Bulletin* **42**(11), 2718–2744.

Tembo, F., Kampunzu, A. and Porada, H. (1999), 'Tholeiitic magmatism associated with continental rifting in the Lufilian Fold Belt of Zambia', *Journal of African Earth Sciences* **28**(2), 403–425.

Todd, S. P. (1989), 'Stream-driven, high-density gravelly traction carpets: possible deposits in the Trabeg Conglomerate Formation, SW Ireland and some theoretical considerations of their origin', *Sedimentology* **36**(4), 513–530.

Tofaif, S., Vandyk, T. M., Le Heron, D. P. and Melvin, J. (2019), 'Glaciers, flows, and fans: Origins of a Neoproterozoic diamictite in the Saratoga Hills, Death Valley, California', *Sedimentary Geology* **385**, 79–95.

Torrealday, H. I., Hitzman, M. W., Stein, H. J., Markley, R. J., Armstrong, R. and Broughton, D. (2000), 'Re-Os and U-Pb dating of the vein-hosted mineralisation at the Kansanshi copper deposit, northern Zambia', *Economic Geology* **95**(5), 1165–1170.

Trabucho-Alexandre, J. (2015), Organic Matter-Rich Shale Depositional Environments, *in* 'Fundamentals of Gas Shale Reservoirs', John Wiley & Sons, Ltd, pp. 21–45.

Tshiauka, T., Katekesha, W., Cailteux, J., Intiomale, M., Kampunzu, A., Kapenda, D., Chabu, M., Ngongo, K., Mutombo, K. and Nkanika, W. (1995), 'Sedimentary sequences in the Musoshi Copper District (SE Shaba, Zaire) and incidences on copper and cobalt.', *Annales de la Société géologique de Belgique* **101**, 29–48.

Tucker, M. E. (1985), 'Shallow-marine carbonate facies and facies models', *Geological Society, London, Special Publications* **18**(1), 147–169.

Turer, D. and Maynard, J. B. (2003), 'Combining Subsidence Analysis and Detrital Modes of Sandstones to Constrain Basin History: An Example from the Eastern Pontides of Turkey', *International Geology Review* **45**(4), 329–345.

Turlin, F., Eglinger, A., Vanderhaeghe, O., André-Mayer, A.-S., Poujol, M., Mercadier, J. and Bartlett, R. (2016), 'Synmetamorphic Cu remobilization during the Pan-African orogeny: Microstructural, petrological and geochronological data on the kyanite-micaschists hosting the Cu(–U) Lumwana deposit in the Western Zambian Copperbelt of the Lufilian belt', *Ore Geology Reviews* **75**, 52–75.

Turner, E. C., James, N. L. P. and Narbonne, G. M. (2000), 'Taphonomic Control on Microstructure in Early Neoproterozoic Reefal Stromatolites and Thrombolites', *Palaios* **15**(2), 87–111.

Turner, S. A. (2010), 'Sedimentary record of Late Neoproterozoic rifting in the NW Tarim Basin, China', *Precambrian Research* **181**(1-4), 85–96.

Twite, F., Broughton, D., Nex, P., Kinnaird, J., Gilchrist, G. and Edwards, D. (2019), 'Lithostratigraphic and structural controls on sulphide mineralisation at the Kamoa copper deposit, Democratic Republic of Congo', *Journal of African Earth Sciences* **151**, 212–224.

Udden, J. A. (1912), Geology and mineral resources of the Peoria quadrangle, Illinois, Technical Report, Washington: Government Printing Office.

Unrug, R. (1983), 'The Lufilian Arc: a microplate in the Pan-African collision zone of the Congo and the Kalahari cratons', *Precambrian Research* **21**(3-4), 181–196.

USGS (2023), Mineral commodity summaries 2023, USGS Numbered Series 2023, U.S. Geological Survey, Reston, VA.

Vail, P. R. (1991), The stratigraphic signatures of tectonics, eustasy and sedimentation: an overview, *in* G. Eisele, W. Rieken and A. Seilacher, eds, 'Cycles and Events in Stratigraphy', Springer Berlin, pp. 617–659.

Veevers, J. J. (1981), 'Morphotectonics of Rifted Continental Margins in Embryo (East Africa), Youth (Africa-Arabia), and Maturity (Australia)', *The Journal of Geology* **89**(1), 57–82.

Vermeesch, P. (2018), 'IsoplotR: A free and open toolbox for geochronology', *Geoscience Frontiers* **9**(5), 1479–1493.

Wagoner, J. C. V., Mitchum, R. M., Campion, K. M. and Rahmanian, V. D. (1990), 'Siliciclastic Sequence Stratigraphy in Well Logs, Cores, and Outcrops: Concepts for High-Resolution Correlation of Time and Facies', **174**, 3–55.

Wagoner, J. C. V., Posamentier, H. W., Mitchum, R. M., Vail, P. R., Sarg, J. F., Loutit, T. S. and Hardenbol, J. (1988), 'An Overview of the Fundamentals of Sequence Stratigraphy and Key Definitions'.

Walker, R. G. (1966), 'Shale Grit and Grindslow Shales: Transition from Turbidite to Shallow Water Sediments in the Upper Carboniferous of Northern England', *SEPM Journal of Sedimentary Research* **36**(1), 90–114.

Walther, J. (1894), *Einleitung in die geologie als historische wissenschaft: Beobachtungen über die bildung der gesteine und ihrer organischen einschlüsse*, G. Fischer.

Wanless, H. and Weller, J. (1932), 'Correlation and Extent of Pennsylvanian Cyclothems 12', *GSA Bulletin* **43**(4), 1003–1016.

Watts, A. B. and Ryan, W. B. F. (1976), Flexure of the Lithosphere and Continental Margin Basins, *in* M. H. P. Bott, ed., 'Developments in Geotectonics', Vol. 12 of *Sedimentary Basins of Continental Margins and Cratons*, Elsevier, pp. 25–44.

Wendorff, M. (2000), 'Genetic aspects of the Katangan megabreccias: Neoproterozoic of Central Africa', *Journal of African Earth Sciences* **30**(3), 703–715.

Wendorff, M. (2003), 'Stratigraphy of the Fungurume Group - evolving foreland basin succession in the Lufilian fold-thrust belt, Neoproterozoic-Lower Palaeozoic, Democratic Republic of Congo', *South African Journal of Geology* **106**(1), 17–34.

Wendorff, M. (2005), 'Sedimentary genesis and lithostratigraphy of Neoproterozoic megabreccia from Mufulira, Copperbelt of Zambia', *Journal of African Earth Sciences* **42**(1-5), 61–81.

Wendorff, M. and Key, R. (2009), 'The relevance of the sedimentary history of the Grand Conglomerat Formation (Central Africa) to the interpretation of the climate during a major Cryogenian glacial event', *Precambrian Research* **172**(1-2), 127–142.

Went, D. J. (2005), 'Pre-vegetation alluvial fan facies and processes: an example from the Cambro-Ordovician Rozel Conglomerate Formation, Jersey, Channel Islands', *Sedimentology* **52**(4), 693–713.

Wentworth, C. K. (1922), 'A Scale of Grade and Class Terms for Clastic Sediments', *The Journal of Geology* **30**(5), 377–392.

Wheeler, H. E. (1958), 'Time-Stratigraphy1', *AAPG Bulletin* **42**(5), 1047–1063.

White, N. and McKenzie, D. (1988), 'Formation of the "steer's head" geometry of sedimentary basins by differential stretching of the crust and mantle', *Geology* **16**(3), 250–253.

Wilgus, C. K., Hastings, B. S., Posamentier, H., Van Wagoner, J., Ross, C. A. and Kendall, C. G. S. C., eds (1988), *Sea-Level Changes: An Integrated Approach*, SEPM (Society for Sedimentary Geology).

Williams, P. R. and Nisbet, B. W. (2017), 'Structural framework of the Lufilian Fold Belt in the Domes region of North Western Province, Zambia from interpretation of geophysical data', *Journal of African Earth Sciences* **129**, 542–557.

Woodhead, J. A. (2013), The Neoproterozoic Roan Group in the Zambian Copperbelt: sequence stratigraphy, alteration and mineralization, PhD thesis, Colorado School of Mines.

Xiao, S. and Narbonne, G. (2020), The Ediacaran Period, *in* 'Geologic Time Scale 2020', Elsevier, pp. 521–561.

Xie, X. and Heller, P. L. (2009), 'Plate tectonics and basin subsidence history', *GSA Bulletin* **121**(1-2), 55–64.

Xu, K.-k., Xie, W., Sun, K., Ren, J.-p., Gong, P.-h., He, S.-f., Lu, Y.-g. and Zhang, H. (2022), 'Geochronology, geochemistry, and petrogenesis of I- and A-type granites in the Solwezi Dome of the Lufilian Arc: implications for the late-Mesoproterozoic magmatic and geodynamic evolution in northern Zambia', *Arabian Journal of Geosciences* **15**(23), 1729.

Yang, J., Large, R. R., Bull, S. and Scott, D. L. (2006), 'Basin-Scale Numerical Modeling to Test the Role of Buoyancy-Driven Fluid Flow and Heat Transfer in the Formation of Stratiform Zn-Pb-Ag Deposits in the Northern Mount Isa Basin', *Economic Geology* **101**(6), 1275–1292.

Zavala, C. (2020), 'Hyperpycnal (over density) flows and deposits', *Journal of Palaeogeography* **9**(1), 1–21.

Zolitschka, B., Francus, P., Ojala, A. E. K. and Schimmelmann, A. (2015), 'Varves in lake sediments – a review', *Quaternary Science Reviews* **117**, 1–41.